DISSERTATION

submitted to the

Combined Faculty of Mathematics, Engineering and
Natural Sciences of Heidelberg University, Germany

for the degree of

Doctor of Natural Sciences

Put forward by:

Karla Maria Tame Narvaez

born in:

Puebla, Mexico

Oral examination: July 27th, 2022

New physics searches in extended scalar sectors

ii

Abstract

This thesis investigates minimal extensions to the standard model (SM) scalar sector. These are separated into two parts: renormalizable and non-renormalizable. The second one is strongly motivated by dark matter while both of them get motivated by the fermion mass hierarchies. In particular, the smallness of the first fermion family masses, the dominance of the top-quark mass, or the dominance of the third fermion family masses. Additionally, the discovery of a fundamentally looking scalar particle, in agreement with the SM particle spectrum, serves as a strong reason to consider a multiscalar scenario. In the first part, we extend the SM with a second scalar doublet and consider it with the same quantum numbers as the SM Higgs. Two new models are proposed and called Type-A and B, where either the top quark alone or all third-generation fermions couple to the doublet with a larger vacuum-expectation-value (vev). This distinction becomes possible after implementing a parity symmetry and introducing the *singular alignment ansatz*. As a consequence, the remaining fermions exclusively acquire their masses through the small vev of the other doublet. Simultaneously, we avoid undesirable flavor-changing-neutral-currents at tree-level. We study the main differences between the proposed new models and conventional ones and include a discussion of their structure and phenomenological consequences. In the second part of this thesis, we extend the SM with a scalar singlet and a dark matter (DM) fermion. We embed this into a hybrid framework in the form of an effective completion of simplified models called extended dark matter effective field theory (eDMEFT). The phenomenology of the dimension five operators connecting the SM fermions with the dark sector is explored in the form of missing energy at several colliders in a restricted case scenario. Here we address the smallness of first-generation fermion masses via suppressed Z_2 breaking effects. The theoretical matching of the eDMEFT is performed with more-UV-complete theories such as two Higgs doublets plus a (pseudo-)scalar mediator and the inclusion of new vector-like quarks. In addition, we explore their collider signatures. Finally, we use the same framework to scrutinize the XENON1T electron recoil excess. We confront it with various astrophysical and laboratory constraints both in a general setup and in the one presented in the mentioned case scenario. We find that the excess can be explained by modified neutrino–electron interactions, linked with the neutrino and electron masses, while DM–electron scattering does not lead to statistically significant improvement. We analyze the parameter space preferred by the anomaly and find severe constraints that can only be avoided in certain corners of the parameter space. In particular, problematic bounds on electron couplings from Big-Bang Nucleosynthesis can be circumvented via a late phase transition in the new scalar sector.

Zusammenfassung

In dieser Arbeit werden minimale Erweiterungen des skalaren Sektors des Standard-
modells (SM) untersucht. Diese sind in zwei Teile unterteilt: renormierbare und nicht
renormierbare. Der zweite ist stark durch dunkle Materie motiviert, während beide
durch die Massenhierarchie der Fermionen motiviert werden, insbesondere durch die
kleinen Massen der ersten Fermionenfamilie, die Dominanz der Topquarkmasse, oder
die Dominanz der Massen in der dritten Fermionenfamilie. Die Entdeckung eines el-
ementar aussehenden skalaren Teilchens, dem Higgs, die mit dem SM- Teilchenspek-
trum übereinstimmt, ist ebenfalls ein starker Grund, ein multiskalares Szenario in Be-
tracht zu ziehen. Im ersten Teil dieser Arbeit erweitern wir das SM um ein zweites
skalares Dublett, für welches wir die gleichen Quantenzahlen annehmen wie für das
SM-Higgs. Es werden zwei neue Modelle vorgeschlagen, Typ A und Typ B, in de-
nen entweder nur das Top-Quark oder alle Fermionen der dritten Generation an das
Dublett mit dem größeren Vakuum-Erwartungswert (VEV) koppeln. Diese Unterschei-
dung wird möglich, nachdem eine Paritätssymmetrie eingeführt und der singuläre
Alignment-Ansatz angewandt wird. Infolgedessen erhalten die übrigen Fermionen
ihre Masse ausschließlich durch den kleinen VEV des anderen Dubletts. Zugleich
vermeiden wir unerwünschte flavourverändernde neutrale Ströme (FCNCs) auf Tree-
Level. Wir untersuchen die Hauptunterschiede zwischen den vorgestellten neuen Mod-
ellen und konventionellen Modellen und diskutieren ihre Strukturen und die phäno-
nologischen Konsequenzen. Im zweiten Teil dieser Arbeit, erweitern wir das SM um ein
skalares Singulett und ein Dunkle Materie (DM) Fermion. Wir betrachten dies in einem
hybriden Framework in Form einer effektiven Vervollständigung der vereinfachten
Modelle, der erweiterten effektiven Feldtheorie der dunklen Materie (eDMEFT). Die
Phänomenologie der Operatoren der fünften Dimension, die die SM-Fermionen mit
dem dunklen Sektor verbinden, wird in einem eingeschränkten Szenario in Form von
Suchen nach fehlender Energie an mehreren Teilchenbeschleunigern erforscht. Zusät-
zlich behandeln wir die Kleinheit der Fermionenmassen der ersten Generation als un-
terdrückten Effekt der Brechung einer Z_2 Symmetrie. Das theoretische Matching an
die eDMEFT wird mit weiteren UV-vollständigen Theorien ansgeführt, wie ein Mod-
ell mit zwei zusätzlichen Higgs-Dubletts sowie einem (pseudo-)skalaren Teilchen oder
eines mit neuen vektorartigen Quarks. Darüber hinaus erforschen wir ihre Collider-
Signaturen. Schließlich verwenden wir das gleiche Framework, um den Überschuss an
Events im XENON1T Elektronenrückstoß-Experiment zu untersuchen. Wir konfron-
tieren ihn mit verschiedenen astrophysikalischen und experimentellen Einschränkun-
gen, sowohl in einem allgemeinen als auch in dem erwähnten Szenario. Wir stellen
fest, dass der Überschuss durch modifizierte Neutrino-Elektronen- Wechselwirkungen
erklärt werden kann, die mit den Neutrino- und Elektronenmassen verbunden sind,
während die DM-Elektron-Streuung nicht zu einer statistisch signifikanten Verbesserung
führt. Wir analysieren den Parameterraum der von der Anomalie bevorzugt wird,
und finden starke Einschränkungen, die nur in bestimmten Ecken des Parameterraums
vermieden werden können. Insbesondere problematische Einschränkungen für Elek-
tronenkopplungen aus der primordialen Nukleosynthese können durch einen späten
Phasenübergang im neuen skalaren Sektor umgangen werden.

Contents

viii

A ti, tía Ana, donde quiera que estés . . .

Te prometí que iba a ser doctora, he aquí el final de mi promesa.

Publications

A major part of the results presented in this thesis is based on the author's publications listed below:

I. **Natural 2HDMs without FCNCs** *J.L. Diaz-Cruz (Puebla U., Mexico), U.J. Saldana-Salazar, K.M. Tame-Narvaez, V.T. Tenorth (Heidelberg, Max Planck Inst.)* Published in: Phys.Rev.D 104 (2021) 3, 035018 • e-Print: 2010.05923 [hep-ph]

II. **EFT interpretation of XENON1T electron recoil excess: Neutrinos and dark matter** *Giorgio Arcadi(Rome III U. and INFN, Rome3), Andreas Bally, Florian Goertz Karla Tame-Narvaez, Valentin Tenorth (Heidelberg, Max Planck Inst.) Stefan Vogl (Munich, Max Planck Inst.)* Published in: Phys.Rev.D 103 (2021) 2, 023024 • e-Print: 2007.08500 [hep-ph]

Another publication from the author, relevant for this thesis is:

I. **Di-jet/e^+e^- + MET to probe Z_2-odd Mediators to the Dark Sector** *Florian Goertz, Karla Tame-Narvaez, Valentin Titus Tenorth (Heidelberg, Max Planck Inst.)* Published in: Eur.Phys.J.C 79 (2019) 10, 860 • e-Print: 1906.08007 [hep-ph]

Unpublished work

I. **Matching the eDMEFT to More-UV-Complete Theories** *Florian Goertz, Karla Tame-Narvaez, Valentin Titus Tenorth, Stefan Vogl* (Heidelberg, Max Planck Inst. and Munich, Max Planck Inst.)
  Preliminary results of the aforementioned work derived here by the author for the first time are shown in Sec. 3.5 and Sec. 3.6.

The following works were started in the last year of the author's Ph.D., however, they are not relevant for this thesis.

II. **Scalar-Mediated VBF-like Higgs Production using Machine Learning** *Florian Goertz, Karla Tame-Narvaez* (Heidelberg, Max Planck Inst.)

III. **Self-Supervised Anomaly Detection for Jets** *Barry Dillon, Tilman Plehn, Karla Tame-Narvaez* (Institut für Theoretische Physik der Universität Heidelberg and Heidelberg, Max Planck Inst.)

Chapter 1

Introduction

With the discovery of the Higgs boson, announced in 2012 by the CMS [1] and AT-LAS [2] collaborations, the predicted particle spectrum of the Standard Model (SM) was fully confirmed. All the observed particles can be organized through the symmetrical properties of the theory. First, due to Lorentz-invariance, the spectrum can be separated into two types of particles: half-integer ($s = 1/2$) and integer ($s = 0, 1$) spin. In the former case, there are twelve elementary particles [1] called fermions giving place to ordinary matter. These twelve may be further divided into two sectors: quarks and leptons. The first sector is composed of two types of quarks: those with electric charge, $q = 2/3$, called up-type quarks (u, c, t) and those with electric charge, $q = -1/3$, called down-type quarks (d, s, b). The second sector consists of two types of leptons: those with electric charge, $q = -1$, called charged leptons (e, μ, τ) and those with $q = 0$ called neutrinos (ν_e, ν_μ, ν_τ). On the other hand, the SM particle content with integer spin ($s = 0, 1$) consists of four kind of vector bosons ($s = 1$), carriers of the fundamental forces (except for gravity): the gluons G_μ^a ($a = 1, 2, ..., 8$), which mediate the strong interactions; the weak bosons, $W_\mu^\pm$ and Z_μ^0, which mediate the weak interactions; and the photon, γ_μ, which mediates the electromagnetic interactions. These vector bosons can be called gauge bosons as they are a consequence of the SM local (or gauge) symmetry group, $\mathcal{G}_{\text{SM}}$:

$$\mathcal{G}_{\text{SM}} = SU(3)_c \times SU(2)_L \times U(1)_Y \,, \tag{1.1}$$

where Y denotes the hypercharge, L means that only the left-handed fermionic parts will non-trivially transform under the weak isospin group and c denotes the colour symmetry group. For more details about the non-trivial transformations of the fermions under the SM gauge group, see Appendix A. For last, the SM theory has one scalar ($s = 0$) field called the Higgs boson. It is a doublet under $SU(2)_L$ and it is required in order to spontaneously break the electroweak symmetry, $SU(2)_L \times U(1)_Y \to U(1)_{\text{EM}}$, in agreement with observation, where EM stands for electromagnetism. This breaking happens through the Higgs mechanism, i.e. the neutral component of the Higgs boson acquires a vacuum expectation value (vev) different than zero and as a consequence the corresponding fields of the three broken generators of the initial symmetry group,

---

[1]Note that every charged fermion has also its corresponding anti-particle. Additionally, all fermions (except neutrinos) have a right-handed and left-handed chirality, which is the projection of total angular momentum on the direction of motion in the massless limit.

become massive and one preserved Abelian generator field remains massless. Furthermore, by virtue of the Yukawa interactions, between the fermions and the Higgs boson, the non-zero vev will give rise to the fermion mass terms.

In relation to the previous discussion, the SM theoretical framework possesses eighteen physical and arbitrary parameters which must be determined by experiments: nine charged-fermions masses, four mixing parameters, three gauge couplings, and the Higgs' vev as well as its mass. Due to historical reasons, the SM considered neutrinos as massless particles. Now, that we know they have mass, their massive nature can be incorporated either by assuming them Dirac or Majorana (their own antiparticles) fermions. Once this is done, the free parameters can increase respectively up to twenty-five or twenty-seven, depending on their massive nature.

The SM has achieved tremendous success both in the theoretical and experimental points of view. However, there is a clear lack of understanding of certain emergent patterns in various measured parameters. One example of this is the flavour puzzle, which consists of a single, but rather precise question: Why do the fermion masses and mixing parameters in the SM take the values they have? In principle, they are arbitrary, nonetheless, by taking a closer look to the experimental values, we start noticing some hierarchies between groups with similar masses, which may suggest an underlying mechanism.

The measured fermion masses show the following hierarchy:

$$
\begin{array}{ccccc}
& & \text{intergeneration} & & \\
& & \longrightarrow & & \\
m_t & \gg & m_c & \gg & m_u \\
\Downarrow & & \Downarrow & & \wedge \\
m_b & \gg & m_s & \gg & m_d \\
\vee & & \wedge & & \vee \\
m_\tau & \gg & m_\mu & \gg & m_e \\
\Downarrow & & \Downarrow & & \Downarrow \\
m_{\nu 3(2)} & ? & m_{\nu 2(1)} & ? & m_{\nu 1(3)}
\end{array}
$$

From here, several intriguing features can be identified such as: i) the dominance of the top-quark mass among all the fermion masses, $m_t \sim$ EW scale and $m_t \gg m_f$; the intergenerational hierarchy, $m_3 \gg m_2 \gg m_1$; ii) how the down-type quarks and charged leptons have similar masses, $m_{d_i} \sim m_{e_i}$ ($d_{1,2,3} = d, s, b$ and $e_{1,2,3} = e, \mu, \tau$); iii) and the smallness of the neutrino masses, $m_\nu \ll m_e$. These unsolved questions, among others, are commonly referred to as the problem of mass [3].

We find another interesting set of patterns in the observed quark mixing as described by the Cabibbo-Kobayashi-Maskawa (CKM) matrix. This unitary matrix contains all the information on the strength of flavour-changing weak decays mediated by the charged $W^\pm$ bosons. The CKM matrix happens to be approximately close to the unit matrix $\mathbf{V}_{\text{CKM}} \sim \mathbf{1}$; showing that flavour transitions between members of the same family are more likely to happen, $|V_{ud}| \simeq |V_{cs}| \simeq |V_{tb}| \simeq 1$, when compared to those from

different ones which are strongly suppressed, $|V_{cd}| \simeq |V_{us}| \simeq 0.23$, $|V_{ts}| \simeq |V_{cb}| \simeq 0.04$ and $|V_{td}| \sim |V_{ub}| \sim \mathcal{O}(10^{-3})$. When the massive nature of neutrinos is considered, their observed mixing is described by the Pontecorvo–Maki–Nakagawa–Sakata (PMNS) matrix. Unlike the quark mixing matrix, the PMNS shows a completely different behaviour with a more anarchic structure. For more information about the flavour mixing in the SM, please see Appendix A.

Besides the puzzle represented by the SM parameters, there are *new* observables that cannot be explained with the SM current framework. In the last decades, we have discovered, by several means, evidence on the existence of another kind of (non-baryonic) matter. This points towards a new cold, weakly-interacting and electrically-neutral particle, called dark matter (DM). In Sec. 3.2, we introduce and discuss in detail the current evidence of DM as well as the experimental efforts for detecting it.

As previously mentioned, there are many motivations to suspect on the existence of new, undetected particles, that could be responsible of one or more of these phenomena. Thus, the urge of extending the SM, and include all new possible interactions between the SM fermions and the new physics (NP) sector.

There are two approaches to incorporate new particles and extend the SM theory while still keeping it gauge and Lorentz invariant: via renormalizable ($D \leq 4$ operators) or "non-renormalizable" ($D > 4$ operators) models. The second approach corresponds to the concept of Effective field theories (EFT). These theories provide a modern perspective on renormalization, going beyond the pure systematic cancellations of infinities. Here, the higher-dimensional interactions, often called non-renormalizable by historic reasons, parameterize the effects of NP in the low energy theory and are suppressed by an energy scale Λ^N with $N = D - 4$ and D the operator's dimension. This kind of operators contribute at some precision level and its coefficients, known as *Wilson Coefficients*, capture the physics of the high energy (or UV) theory. The effects of the higher-dimensional operators are numerically suppressed if the cutoff scale Λ is much larger than the typical energies achieved in experiments. Hence, by default, EFTs are renormalizable order by order in operator dimension as long as the cutoff scale is large.

When speaking about DM, EFTs are generally a valid description of its interactions with the SM as long as the mass of a heavy mediator, that could induce the operators, lies out of the kinematic reach of the collider. In this regard, since LHC limits on DM usually correspond to mass-suppression scales that are lower than the energy of the process, the validity of the EFT approximation becomes questionable and an active mediator particle would need to be included instead. This simple point requires a careful and consistent use of the effective approach, checking its range of validity, in the context of DM searches at the LHC. Now, unlike EFTs, simplified models which are made of renormalizable operators, are valid to arbitrary high energies as they capture the on-shell effects of the mediators. A downside of such models is that the structure of the couplings does not always respect gauge invariance. In addition, they are not as model independent as EFTs, since the mediator is explicitly present in the operators, no additional new physics is allowed, and they often do not capture realistic UV scenarios. A comparison of the advantages and disadvantages of EFTs and simplified models in a DM context is discussed in Ref. [4]. It is the combination of these two approaches that

is of special interest in this thesis and will be explored through a hybrid framework and to be later discussed.

After building any new beyond the SM (BSM) model, it is necessary to study their phenomenology and verify that the parameters in the proposed theory are not ruled out by current experimental limits. To this end, we normally perform Monte Carlo simulations followed by an extensive analysis of signal vs background. The latter can be done through conventional methods like *cut and count* or by studying the Likelihood ratio. However, as technology evolves, the amount of available data increases dramatically. Only the ATLAS and CMS experiments at the LHC generate petabytes ($\sim 10^9$ Mb) of data per year. This together with the continuous quest for more precision have brought the need of implementing new methods to perform the analysis of our models. Machine learning (ML), is nowadays the most efficient tool for the analysis of "big data". Several ML algorithms can be easily adapted to physics analysis, some of them are decision trees, decision forest, linear regression, logistic regression and neural networks. For more information, on the relation between physics and ML please see Ref. [5] and for a broad overview with practical examples/exercises refer to Ref. [6]. The implementation of such techniques is not the main scope of this work and therefore will only be mentioned as complementary information.

This thesis is divided into two independent parts: the first one in which two renormalizable extensions of the SM are built (Chapter 2) and the second one where a non-renormalizable approach is considered (Chapters 3 and 4). The overarching idea being to understand the puzzles mentioned in the beginning. More explicitly, the content of the present document goes as follows. In Chapter 2, we study the flavour puzzle by extending the SM content with a second scalar in a two-Higgs doublet model (2HDM) scenario [7]. Dirac's and 't Hooft's naturalness criteria are discussed in Sec. 2.1. We motivate such scalar extensions in Sec. 2.2 and introduce the 2HDM formalism in Sec. 2.3. We explore the origin for the observed difference between the SM fermion masses by linking the energy scale of a given set of fermions to a unique Higgs doublet. To avoid the unwanted appearance of flavour changing neutral currents (FCNC) we employ the singular alignment ansatz [8] in Sec. 2.7. We then explicitly construct two models called Type-A and B, in Sec. 2.8, where either the top quark alone or the heaviest fermion generation couples to the Higgs doublet with the largest vev, while the other fermions couple to the second scalar doublet. The main differences between the new proposed models and conventional ones are discussed together with their phenomenological consequences, like possible tests at the LHC, in Secs. 2.9–2.11. Additional information on the flavour in the SM is found in Appendix A.

The following two chapters compose the second part of the thesis and deal with non-renormalizable scalar extensions. In Chapter 3 we explore a model where not only the problem of mass is considered but also DM. We first introduce the concept of effective field theories (EFTs) from a top-down and bottom-up approach in Sec. 3.1, giving further explicit examples in Appendix B. Then, a brief overview of DM and simplified models is given in Sec. 3.2 which is followed by their combination in a framework

called extended dark matter EFT [9] in Sec. 3.3. This framework addresses drawbacks regarding validity at high energies and/or generality that conventional DM effective field theories or simplified models suffer of. Here, the advantages of model independence of effective theories are taken but also the dark matter states and a new scalar mediator are kept as propagating degrees of freedom. The presence of the latter, which properly connects the dark sector to the fields with the help of dimension five operators, increases the consistently testable parameter space at colliders. Afterwards, in Sec. 3.4, we present an eDMEFT case scenario [10] where we explored the possibility of DM coupling to the first generation of the SM fermions via a scalar mediator, $\mathcal{S}$, odd under a parity symmetry. We can then address the small nature of the first generation fermion masses together with a prominent di-jet/lepton plus missing transverse energy (MET) signal at the (HL-)LHC and the future e^+e^- Compact Linear Collider (CLIC) [11]. To finalize, in Sect. 3.5 we match concrete models of DM to the mentioned framework. This allows us to translate the experimental constraints derived in Ref. [12] to more-UV-complete scenarios. To achieve this, we considered three setups: two Higgs doublets plus a pseudoscalar or a scalar mediator and another one with heavy vector-like quarks plus a scalar mediator. Both models also contain fermionic DM. With this, we want to show that the eDMEFT can be used as a convenient standard interface between experiment and concrete DM models. Lastly, in Sec. 3.6, we study the collider signatures in the eDMEFT and translate the exclusion limits into the more-UV-complete parameters by using the matching relations obtained in the previous section. In particular, we focus in mono-jet searches where the signal is characterized by a jet plus large missing energy. A more complete study on the matching of these theories is new, unpublished work and partially presented in this thesis, and will be extended to a paper [13].

In Chapter 4, we present an EFT interpretation of the reported XENON1T Electron Recoil Excess [14]. We start by introducing the observed excess in Sec. 4.1 and continue by detailing the setup in Sec. 4.2, which is a slightly extended version of the eDMEFT. We continue by fitting the excess in Sec. 4.3 and confront several astrophysical and laboratory constraints for the previous framework in Sec. 4.4. Our findings are the following two: i) the excess can be explained by neutrino/electron interactions, while a DM-electron scattering does not lead to statistically significant improvement; ii) additionally, severe constraints are obtained in the parameter space preferred by the anomaly, where it can only be avoided in certain small regions. In Sec. 4.5, we realize how the potential problematic bounds on electron couplings from Big-Bang Nucleosynthesis can be circumvented via a late phase transition in the new scalar sector. Lastly, in Sec. 4.6 we discuss the current status of the XENON1T excess and what should we expect for the future DM experiments.

Finally, in Chapter 5, we summarize our findings and conclude. Additionally, three appendices have been added where we give details on the SM flavour sector (Appendix A), three of the most common EFTs (Appendix B) and a brief discussion on the required procedures for the statistical analyses done in Sec. 3.4 (Appendix C).

Part I

Renormalizable Extensions of the Scalar Sector

Chapter 2

Natural 2HDMs without FCNCs

The discovery of the Higgs particle not only represented a validation of the SM theory but it also opened the door to the possibility of having more than one fundamental scalar in Nature. Hence, we focus here on a minimal renormalizable extension of the SM by going beyond the simplest choice of introducing a weak singlet scalar and instead, consider a weak doublet scalar with the same quantum numbers as the SM Higgs. The reason behind this choice is to not only extend the scalar spectrum but simultaneously address the hierarchy in the fermion masses, as this inclusion doubles the amount of Yukawa terms, providing an additional freedom to study the origin of the fermion masses.

The outlook of the chapter is as follows. In Sec. 2.1, we discuss Dirac and 't Hooft's naturalness criteria, and evaluate under which conditions the SM fermions could be called natural. We find that multi-scalar theories with suitable vevs, could fulfill both naturalness criteria in the SM fermionic sector. In Sec 2.2, we explore possible extensions to the SM scalar sector and discuss the minimal scenario where only a second $SU(2)$ doublet is added to the SM content. Here we also present several theoretical constraints on the CP-even potential parameters. In Sec. 2.3, we discuss the general aspects of the 2HDM models. We continue in Sec. 2.4 with ways to avoid problematic flavour-changing-neutral-currents and motivate the need for a Z_2 symmetry. Here we also present the four conventional types of 2HDMs with natural flavour conservation [15,16]. The soft-breaking of the latter symmetry and how to produce hierarchical vevs are discussed in Sec. 2.5. We discuss the scalar potential and the theoretical constraints in Sec. 2.6. In Sec. 2.7, we study in detail the generalization of the Yukawa alignment called singular alignment [8]. Moving forward, in Sec. 2.8, we present the setup of two new natural 2HDM types (Type-A and Type-B). In both types, we address either the heaviness of the top or of the third fermion family compared with the other SM fermions. We continue in Sec. 2.9, with the study of the corresponding scalar couplings and the branching ratios of the SM-like scalar h in Type-A and B. Furthermore, in Sec. 2.10 we list all the experimental constraints that are relevant for the phenomenological study and defining convenient benchmarks. To finalize, in Sec 2.11 we present and discuss the phenomenological results. Complementary information on flavour physics in the SM can be found in Appendix A.

2.1   Naturalness as a Motivation to Multiscalar Theories

The concept of naturalness has played an important role in particle physics, for recent discussions see Refs. [17–21]. It gives rise to the *hierarchy problem*. The latter can be seen as an unnatural separation between the Planck scale, as defined by the Planck mass $M_p \sim 10^{19}$ GeV, and the EW scale, as defined by the SM Higgs' vev, $v \sim 10^2$ GeV. This particular situation originates because the loop-effects or quantum corrections to the Higgs mass are way larger than the tree level effects. From the symmetry point of view, we understand the lightness of the fermions as they are protected by the chiral symmetry, also the gauge bosons become massive only after the electroweak symmetry breaking and therefore their mass is naturally expected at $\mathcal{O}(100)$ GeV. However, the Higgs mass has no symmetry protecting it and therefore nothing prevents the appearance of large quantum corrections in this parameter, thus making unnatural to have a light mass. We will not elaborate further as it is not the focus of this thesis and rather move to another issue with hierarchical numbers, while referring the reader to the previous references.

As mentioned in the introduction in Chapter 1, the SM fermion masses have among them very well defined patterns and they cannot be explained by the SM current framework. We are interested in studying these patterns that, as a whole, do not represent a problem from the viewpoint of the aforementioned discussion. However, the fact that the top-quark is the only one with coupling $y_t = 1$, in accordance to the EW scale, triggers the question of how *naturally* small, when compared to the top-quark, are the other Yukawa parameters in the fermionic sector. That is, how expected can small quantities be in a given theory. As *natural* is a subjective concept one must stick to a mathematical (or at least to a conventional) definition that could help us to distinguish when the parameter's value may be considered natural.

Dirac and 't Hooft proposed two pioneering criteria to be capable of clearly defining naturalness, Ref. [22] and [23], respectively. Dirac's naturalness criterion [22] requires all dimensionless couplings of a giving theory to be of order one in order to be called natural. On the other hand, 't Hooft's criterion [23] states that a smaller than one parameter is natural if the theory, where it is contained, acquires a symmetry when this parameter is set to zero. For extended reviews on naturalness, see Refs. [24–27].

Applying Dirac's criterion to the SM would then demand the observation of all the fermion masses to be around the electroweak scale, i.e. $m_f = y_f v$ with $y_f \sim \mathcal{O}(1)$ and $v = 174$ GeV the SM Higgs vev; which, as mentioned before, is only satisfied by the top quark. The unnaturalness of the SM lighter fermions can then be described as:

$$y_t \sim 1 \gg y_f \qquad (f = c, b, s, u, d, \tau, \mu, e) . \tag{2.1}$$

However, the smallness in this set of small Yukawas could still be called natural according to 't Hooft's criterion. In fact, if we take the limit where all SM Yukawa couplings are taken to zero, we recover a $U(3)^5$ flavour symmetry. This corresponds to a $U(3)$ symmetry for each type of right- and left-handed fermion

$$U(3)_{Q_L} \times U(3)_{L_L} \times U(3)_{d_R} \times U(3)_{u_R} \times U(3)_{e_R} . \tag{2.2}$$

A caveat still exists: there is no common parameter among this set of masses that could simultaneously bring all of them to zero. Although this is a subjective choice, it brings many benefits. The main one is that the lightness of the whole set of fermion masses is related to a single parameter in a minimalist approach. Note that the intricacies also appearing within the set itself would require additional parameters but at the expense of further complexities in the theory. As we are interested in the minimalist approach we do not consider them here. Now, there are two ways to solve the aforementioned caveat: 1) with a common Yukawa that would point to a symmetry or 2) the appearance of other vevs which would be used to make the distinction between mass scales. Here, we consider the second approach.

A theory with multiple Higgs doublets with all of them acquiring a vev would imply for the fermion mass matrices

$$\mathbf{M}_f = \sum_i \mathbf{Y}_f^i v_i \tag{2.3}$$

where $f = u, d, e$ and $\sum_i v_i^2 = v^2 = (174 \text{GeV})^2$. In general, when moving to the mass basis, one would expect the fermion masses to be given by a linear combination of Yukawa parameters and vevs

$$m_f = \sum_i y_f^i v_i \,. \tag{2.4}$$

It is only through the introduction of symmetries that a given vev could be made responsible for the masses in a certain fermion sector. In Sec. 2.8, we discuss such a mechanism.

2.2 Scalar Extensions

The fact of having already observed a neutral scalar particle points towards the possibility of a richer scalar sector. These new scalars could then be used to tackle some of the SM downsides, as the problem of mass or DM, as we will see in the upcoming sections. Nevertheless, multi-scalar theories should satisfy severe constraints imposed by the measured 125 GeV scalar.

There are several types of scalar multiplets, that could belong to the electroweak symmetry breaking sector. In particular, scalar singlets and doublets under $SU(2)_L$ are among the safest options[1]. This because they do not spoil, at tree level, the well precise measurement of $\rho = M_W/(\cos(\theta_w)M_Z) = 1$. New contributions to this parameter are constrained by the maximum allowed deviations from the SM-expectation [32], the experimental value of the rho parameter is:

$$\rho_{exp} = 1.00040 \pm 0.00024 \,. \tag{2.5}$$

---

[1]The inclusion of larger $SU(2)_L$ representations is possible under the right choice of hypercharges. In general, these type of models have a richer scalar sector, e.g. adding a Higgs triplet with $Y = 2$ to the SM one has doubly charged scalars apart from the known single charged ones which may give unique phenomenology like the possibility of explaining the smallness of the neutrino masses, accommodating DM candidates, and providing an interesting search channel for collider searches, as a recent example see Ref. [28]. Nevertheless, they also bring up more subtleties into play [29–31].

The tree-level contributions produced from a theory with N number of scalar multiplets is [33]

$$\rho_{tree} = \frac{\sum\limits_{i=0}^{N} [T_i(T_i + 1) - Y_i^2] v_i}{2 \sum\limits_{i=0}^{N} Y_i^2 v_i} \, , \tag{2.6}$$

where T denote the weak isospin and Y the hypercharge, i stands for the i-th scalar multiplet respectively. Lastly, v_i is the vev acquired by the neutral component of the corresponding multiplet. At this point, is easy to note that if the scalar sector contains only $SU(2)$ singlets and doublets i.e. $T_i = 0$ and $T_i = 1/2$ with $Y_i = 0$ and $\pm 1/2$, respectively, then the requirement $\rho = 1$ at tree level is automatically fulfilled without the need of any fine-tuning among the vevs.

Note that a clear disadvantage of extending the SM scalar sector with additional scalar singlets is that they do not contribute to the flavour structure of the theory, as scalar singlets do not couple to fermions (in a renormalizable theory) due to gauge invariance. Their only contributions are in the scalar sector. On the contrary, Higgs weak doublets enrich the Yukawa sector of the theory. Hence, adding additional doublets turns out to be the most compelling option, as they allow the study of an origin for the mass hierarchies.

As the two dominant aspects in the fermion mass hierarchies are: i) top-quark dominance, $m_t \gg m_f$, and ii) the third fermion family mass being much larger than the first two, $m_3 \gg m_{1(2)}$, then we only consider the introduction of one Higgs doublet that could help us make the distinction between the two different energy scales. Therefore, in the following, we focus on a minimal extension of the SM scalar sector with only one additional scalar doublet with the same quantum numbers as the SM one called two-Higgs-doublet model (2HDM).

2.3 The General 2HDM

We have introduced a second Higgs doublet to the SM framework with hypercharge[2] $Y = \frac{1}{2}$,

$$\Phi_j = \begin{pmatrix} \phi_j^+ \\ v_j + \phi_j^0 \end{pmatrix} \qquad (j = 1, 2) \, , \tag{2.7}$$

where v_j represents the corresponding vev[3] and ϕ_j^0 can be decomposed as $\phi_j^0 = \Re(\phi_j^0) + i\Im(\phi_j^0)$. Note that we have doubled the amount of scalar fields, and so, the scalar spectra is now made of two electrically charged scalars and four neutral ones. After EWSB,

---

[2]We are employing the following definition for the electric charge operator, $\mathbf{Q} = \mathbf{1}Y + \frac{\sigma_3}{2}$ where σ_3 is the diagonal Pauli matrix with the two eigenvalues ± 1.

[3]In general, v_j can be complex, e.g. in a Charge-Parity (CP) violating potential [34].

it is necessary to ensure that three of them remain massless (Goldstone bosons) and become the longitudinal degrees of freedom of the weak gauge bosons ($W^{\pm}$ and Z^0), thus making us end up with five physical Higgs bosons to be later discussed in more detail.

The most general scalar potential for two scalar doublets, Φ_1 and Φ_2, is written as follows [34]

$$
\begin{aligned}
V_{2\text{HDM}} = \sum_{x=1,2} & \left[m_{xx}^2 (\Phi_x^\dagger \Phi_x) + \frac{\lambda_x}{2} (\Phi_x^\dagger \Phi_x)^2 \right] - (m_{12}^2 \Phi_1^\dagger \Phi_2 + \text{h.c.}) \\
& + \lambda_3 (\Phi_1^\dagger \Phi_1)(\Phi_2^\dagger \Phi_2) + \lambda_4 (\Phi_1^\dagger \Phi_2)(\Phi_2^\dagger \Phi_1) \\
& + \left[\frac{1}{2} \lambda_5 (\Phi_1^\dagger \Phi_2)^2 + \lambda_6 (\Phi_1^\dagger \Phi_1)(\Phi_1^\dagger \Phi_2) + \lambda_7 (\Phi_2^\dagger \Phi_2)(\Phi_1^\dagger \Phi_2) + \text{h.c.} \right] .
\end{aligned}
\tag{2.8}
$$

The physical or nonphysical nature of the parameters can be deduced from the following counting. First, as the potential should be real, the two mass parameters m_{11}, m_{22} are required to be real while the third one m_{12} can be, in general, complex. On the other hand, $\{\lambda_1, \lambda_2, \lambda_3, \lambda_4\}$ are required to be real while $\{\lambda_5, \lambda_6, \lambda_7\}$ can also be, in general, complex. That is, we have fourteen parameters (ten magnitudes and four complex phases). To finally determine which of them is physical, we take into account the fact that there is a nonphysical freedom in rotating the Higgs basis,

$$
\begin{pmatrix} \widetilde{\Phi}_1 \\ \widetilde{\Phi}_2 \end{pmatrix} = \mathbf{U} \begin{pmatrix} \Phi_1 \\ \Phi_2 \end{pmatrix} ,
\tag{2.9}
$$

where $\mathbf{U}$ is a two-dimensional unitary matrix, $\mathbf{U}^\dagger \mathbf{U} = \mathbf{U} \mathbf{U}^\dagger = \mathbf{I}_{2\times 2}$. This unitary matrix can be re-expressed as $\mathbf{U} = e^{i\alpha} \widetilde{\mathbf{U}}$ where $\widetilde{\mathbf{U}}$ is a special unitary matrix. The complex phase gets automatically cancel out in the scalar potential, offering no reduction in the number of parameters, while the three parameters implied by the remaining rotating freedom, $\widetilde{\mathbf{U}}$, translates into the fact that, when moving to the mass basis or any other special basis, there are $11 = 14 - 3$ physical parameters.

There exists several conditions that the scalar potential should satisfy. The ones required for minimizing the potential in Eq. (2.8) are

$$
m_{11}^2 = m_{12}^2 \tan \beta - v^2 [\lambda_1 \cos^2 \beta + \lambda_{345} \sin^2 \beta + 3\lambda_6 \sin \beta \cos \beta + \lambda_7 \sin^2 \beta \tan \beta] \tag{2.10}
$$
$$
m_{22}^2 = m_{12}^2 \tan^{-1} \beta - v^2 [\lambda_2 \sin^2 \beta + \lambda_{345} \cos^2 \beta + \lambda_6 \cos^2 \beta \tan^{-1} \beta + 3\lambda_7 \sin \beta \cos \beta]
$$

where $\lambda_{345} = \lambda_3 + \lambda_4 + \lambda_5$, $\tan \beta = v_2/v_1$ and $v^2 = v_1^2 + v_2^2$. On the other hand, the scalar potential should be bounded from below (BFB), that is we require that there should not be any directions in the field space in which the Higgs potential grows infinitely negative, $V_{2\text{HDM}} \to -\infty$. To this end, the lambda parameters should meet certain requirements as

$$
\lambda_{1,2} \geq 0 , \qquad \lambda_3 \geq -\sqrt{\lambda_1 \lambda_2} , \qquad \lambda_3 + \lambda_4 - |\lambda_5| \geq -\sqrt{\lambda_1 \lambda_2} .
\tag{2.11}
$$

It has been shown in Refs. [35,36] that these are actually necessary and sufficient conditions when $\lambda_6 = \lambda_7 = 0$. However, when assuming these couplings as complex the additional requirements do not follow a simple analytic formula. For simpler scenarios, like when assumed real, one may find other necessary conditions like [37,38],

$$2|\lambda_6 + \lambda_7| < \lambda_1 + \lambda_2 + \lambda_3 + \lambda_4 + \lambda_5 . \tag{2.12}$$

Further details on the constraints for the general 2HDM are out of the scope of this work and instead, we refer the interested reader to Ref. [34].

2.4   FCNCs and the Introduction of a Z_2 Symmetry

Adding a second scalar doublet to the SM brings its own challenges. One of them is the dangerous presence of flavour-changing-neutral-currents (FCNCs) at tree-level[4]. The latter are interactions that change the flavour of fermions through a neutral mediator. These interactions do not show up in the SM at tree level and get suppressed at the loop level. This happens because the Z and γ bosons couple only diagonally in flavour space. Additionally, the FCNCs present at the loop level have been experimentally observed to be strongly suppressed [39,40]. The smallness of the FCNCs in the SM has long been understood through the Glashow–Iliopoulos–Maiani (GIM) mechanism [41]. However, its simplicity requires only considering one Higgs doublet; once two scalar doublets are assumed, the fermion mass matrix

$$\mathbf{M}_f = v_1 \mathbf{Y}_1 + v_2 \mathbf{Y}_2 , \tag{2.13}$$

has more than one contribution. As a consequence, the diagonalization of the mass matrix, $\mathbf{M}_f$, does not guarantee that any of the two Yukawa matrices conforming it also become diagonal. Hence, there is nothing that may prevent potential flavour transitions at the tree level. These FCNCs get mediated by the linear combination of the neutral components of the doublets. Note that this undesirable aspect, in general, is a common feature of multiscalar theories that have no clear mechanism to suppress FCNCs. To overcome this situation, one must call for further assumptions.

A typical approach to avoid tree-level FCNCs, departing from the general 2HDM, is to introduce a Z_2 symmetry under which both the scalar doublets and the fermions get non-trivial charges [15,16]. Conventionally, the Z_2-parities are assigned as

$$\Phi_2 \to +\Phi_2 \qquad \text{and} \qquad \Phi_1 \to -\Phi_1 . \tag{2.14}$$

Note how this allows the separation into two different set of fermions, those which *only* interact with Φ_1 and those which *only* interact with Φ_2. This distinction reduces the contribution of the Yukawa matrices to a single one per fermion-type, i.e the mass matrix in Eq. (2.13) becomes $\mathbf{M}_f = v_i \mathbf{Y}_i$, where $i = 1, 2$ depending on the assigned Z_2

---

[4]The only kind of flavour-changing transitions occurring at tree level are those mediated by the charged $W^\pm$ bosons.

charge of the given fermion type. Then the diagonalization of the mass matrix ensures the diagonalization of the Yukawa matrix, preventing FCNCs at tree-level.

There are four common types of distributing the Z_2 charges and therefore four conventional 2HDMs:

- **Type I**: Here all quarks and leptons couple to only one scalar doublet Φ_2.

- **Type II**: Here Φ_2 couples to up-type quarks, while Φ_1 couples to down-type quarks and charged leptons.

- **Type X** (or lepton-specific): Here Φ_2 couples to all quarks, while Φ_1 couples to all leptons.

- **Type Y** (or flipped): Here Φ_2 couples to up-type quarks and leptons, while Φ_1 couples to down-type quarks.

A summary of the Z_2 charge distribution for each of the aforementioned 2HDM types is shown in Table 2.1. For a thorough assessment of 2HDMs please refer to [34] and for more recent reviews to [33, 42]. Note that, when introducing the Z_2 symmetry in the 2HDM, this is usually applied *only* to the right-handed (RH) fermions. As an example, let us consider the Type-II scenario, where the Z_2 assignments for the fermions are,

$$d_{i,R} \to - d_{i,R} , \qquad e_{i,R} \to - e_{i,R} ,$$
$$u_{i,R} \to + u_{i,R} , \tag{2.15}$$

with $i = 1, 2, 3$. Here, all left-handed fermions are even under the parity symmetry. Then, Φ_2 can only couple to up-type quarks, while Φ_1 couples to down-type quarks and charged leptons, shown in the second column of Table 2.1.

The introduction of the parity symmetry reduces the number of parameters in the scalar potential, $m_{12}^2, \lambda_{6,7} = 0$. Then, the most general Z_2-invariant scalar potential is expressed as

$$V_{2\text{HDM}}^{Z_2} = \sum_{x=1,2} \left[m_{xx}^2 (\Phi_x^\dagger \Phi_x) + \frac{\lambda_x}{2} (\Phi_x^\dagger \Phi_x)^2 \right] + \lambda_3 (\Phi_1^\dagger \Phi_1)(\Phi_2^\dagger \Phi_2)$$
$$+ \lambda_4 (\Phi_1^\dagger \Phi_2)(\Phi_2^\dagger \Phi_1) + \frac{1}{2} \left[\lambda_5 (\Phi_1^\dagger \Phi_2)^2 + \lambda_5^* (\Phi_2^\dagger \Phi_1)^2 \right] . \tag{2.16}$$

Note that after demanding hermiticity, λ_5 remains as the only complex parameter in the potential, while m_{11}^2, m_{22}^2, and $\lambda_{1,2,3,4}$ are real. However, performing the now allowed phase redefinition[5] the complex phase of λ_5 can be turned to zero without loss of generality. Therefore, as all parameters are real we conclude that the potential is CP-symmetric and only has seven physical parameters.

---

[5]The parity distinction between the two Higgses brings the complex phase back.

Type-	I	II	X	Y
$u_{i,R}$	Φ_2	Φ_2	Φ_2	Φ_2
$d_{i,R}$	Φ_2	Φ_1	Φ_2	Φ_1
$\ell_{i,R}$	Φ_2	Φ_1	Φ_1	Φ_2

TABLE 2.1: The four different types of 2HDMs without tree-level FC-NCs. The allowed couplings between each fermion and a certain Higgs doublet are imposed by a group symmetry, e.g. a Z_2. Note that only the right-handed components obtain a non-trivial charge assignment.

Another set of options to evade FCNCs include, next to arranging the additional scalar particles to be very heavy, suppressing dangerous Yukawa couplings [43], separating the Yukawa matrices, by introducing a Z_2 symmetry, such that only one scalar doublet couples to a given right-handed fermion field [15, 16], or Yukawa alignment [44, 45], in which the different Yukawa matrices are proportional to each other. In particular, the new models proposed in this chapter, assume a generalized version of the Yukawa alignment, where their parameters are assumed to be in a certain region of flavour space. There, both Yukawa matrices become diagonal in the mass basis, irrespective of the fact that they were initially not proportional to the mass matrix. The simplest case assumption is known as the Yukawa alignment anzat [44] while the flavour non-universal realization of the latter is called singular alignment [8, 45] and it is explained in detail in Sec. 2.7.

2.5 Soft-Breaking Z_2 and Hierarchical vevs

The problem of mass has many facets as aforementioned in Chapter 1. To understand them all, within a renormalizable approach, would actually require having more than two Higgs doublets, e.g. the most extreme case would require a nine Higgs doublet model [46] while the minimal one, requires only four Higgs doublets [8]. With two scalar doublets there are only two vevs, allowing a single split in the fermion mass spectrum. This split can be either use as a way to understand the top-dominance aspect, where $m_t \gg m_f$ (f stands for all other fermions except the top quark), or the third-generation-dominance where $m_3 \gg m_{1,2}$ where the sub-index indicates the fermion generation.

Now, there are two requirements that are necessary in order to guarantee the separation of the fermion masses into two energy scales: i) to be able to express a given set of eigenmasses in terms of a chosen vev regardless of the fermion type, for example:

$$m_t = y_t v_2 \qquad \text{and} \qquad m_{c(u)} = y_{c(u)} v_1 \, , \qquad (2.17)$$

and ii) to be able to produce and control the hierarchy between the vevs, $v_2 \gg v_1$. To this end, singular aligning the Yukawa matrices with the right Z_2 assignments will guarantee the first condition. However, the second requirement is not a conventional procedure in 2HDMs. In the following, we discuss the subtleties and details on the mechanism.

We want the following two scales:

$$v_2 \sim \mathcal{O}(100)\,\text{GeV} \qquad \text{and} \qquad v_1 \sim \mathcal{O}(1)\,\text{GeV} . \tag{2.18}$$

The energy scale of each vev should correspond to the heaviest mass of the set of fermions with which they are coupled. In order to create such a hierarchy, we then guarantee that in the first stage only Φ_2 develops a vev by assuming

$$m_{22}^2 < 0 \qquad \text{and} \qquad m_{11}^2 > 0 . \tag{2.19}$$

Therefore, the Z_2 symmetry is preserved, and

$$v_2 = \sqrt{\frac{-m_{22}^2}{\lambda_2}} , \tag{2.20}$$

while $v_1 = 0$. The second stage then requires to softly-break the Z_2 symmetry by adding the term

$$- m_{12}^2(\Phi_1^\dagger \Phi_2 + \Phi_2^\dagger \Phi_1) \tag{2.21}$$

to the potential in Eq. (2.16). Choosing m_{12}^2 to be real ensures that these terms preserve CP. If the condition $m_{12}^2 t_\beta \gg \lambda_1 v_1^2$ with $t_\beta = v_2/v_1$ is met, then Φ_2 induces a small vev to Φ_1 of the form

$$v_1 \simeq \frac{m_{12}^2 v_2}{m_{11}^2 + \lambda_{345} v_2^2} , \tag{2.22}$$

where $\lambda_{345} \equiv \lambda_3 + \lambda_4 + \lambda_5$. One can show that in this case the heavy scalar masses are above the EW scale. The two minimization conditions from which Eqs. (2.20) and (2.22) were derived are:

$$\begin{aligned} m_{22}^2 v_2 &= m_{12}^2 v_1 - \lambda_2 v_2^3 - \lambda_{345} v_2 v_1^2 , \\ m_{11}^2 v_1 &= m_{12}^2 v_2 - \lambda_1 v_1^3 - \lambda_{345} v_1 v_2^2 . \end{aligned} \tag{2.23}$$

Note that, in the limit where $v_1 \to 0$ and $m_{12}^2 \to 0$ we recover the vev in Eq. (2.20). For the sake of illustration, we can simplify the expression for v_1 by assuming $\lambda_{345} \sim \mathcal{O}(1)$ and $m_{11} \sim v_2$, thus obtaining

$$v_1 \sim \frac{m_{12}^2}{v} . \tag{2.24}$$

Hence, if $m_{12} \sim \mathcal{O}(10\,\text{GeV})$ then $v_1 \sim \mathcal{O}(1\,\text{GeV})$, as expected. Realize that the smallness of v_1 is natural regarding 't Hooft's criterion, as if setting it to zero we recover the initial Z_2 symmetry. Now, as both vevs contribute to the W-boson mass, they satisfy the condition

$$v^2 = v_1^2 + v_2^2 = (174\,\text{GeV})^2 . \tag{2.25}$$

As we still need one of the scalars to be responsible for the top-quark mass, it is straightforward to realize that the large vev will be close to the EW scale, i.e. $v_2 \approx v$. The latter is a direct consequence of taking the hierarchical nature between the vevs, $v_2 \gg v_1$.

2.6   The Scalar Potential and its Theoretical Constraints

The physical states of the CP-symmetric potential are: two CP-even (h, H) and one CP-odd (A) in the neutral scalar sector, and a pair of scalars ($H^\pm$) in the charged sector. The transition from the interaction to the mass basis, i.e. from

$$(\mathrm{Re}(\phi^0_{1,2}),\ \mathrm{Im}(\phi^0_{1,2}),\ \phi^\pm_{1,2}) \to (h, H, A, H^\pm, G^0, G^\pm)$$

depends on only two mixing angles (α, β), and is parametrized as follows:

$$\begin{pmatrix} h \\ H \end{pmatrix} = \begin{pmatrix} \cos\alpha & -\sin\alpha \\ \sin\alpha & \cos\alpha \end{pmatrix} \begin{pmatrix} \mathrm{Re}(\phi^0_2) \\ \mathrm{Re}(\phi^0_1) \end{pmatrix},$$
$$\begin{pmatrix} A \\ G^0 \end{pmatrix} = \begin{pmatrix} \cos\beta & -\sin\beta \\ \sin\beta & \cos\beta \end{pmatrix} \begin{pmatrix} \mathrm{Im}(\phi^0_2) \\ \mathrm{Im}(\phi^0_1) \end{pmatrix}, \tag{2.26}$$
$$\begin{pmatrix} H^+ \\ G^+ \end{pmatrix} = \begin{pmatrix} \cos\beta & -\sin\beta \\ \sin\beta & \cos\beta \end{pmatrix} \begin{pmatrix} \phi^+_2 \\ \phi^+_1 \end{pmatrix},$$

where G^0 and G^+ denote the required two massless SM Goldstone bosons. In the following, we refer to h as the SM-like Higgs with mass $m_h = 125$ GeV. Furthermore we know that $\tan(\beta) = v_2/v_1$, therefore, $v_2 = v\sin(\beta)$ and $v_1 = v\cos(\beta)$. Through the invariants of the scalar mass matrices and

$$t_{2\alpha} = \frac{2(v^2\lambda_{345}\, s_{2\beta} - m^2_{12})}{m^2_{12}(t_\beta - t_\beta^{-1}) + 2v^2(c^2_\beta\lambda_1 - s^2_\beta\lambda_2)}, \tag{2.27}$$

the quartic couplings of the scalar potential in Eq. (2.16) can be expressed in terms of the Higgs mass eigenvalues [47–49]

$$\lambda_1 = \frac{1}{2v^2 c^2_\beta}\left(m^2_h c^2_\alpha + m^2_H s^2_\alpha - M^2 s^2_\beta \right),$$
$$\lambda_2 = \frac{1}{2v^2 s^2_\beta}\left(m^2_h s^2_\alpha + m^2_H c^2_\alpha - M^2 c^2_\beta \right),$$
$$\lambda_3 = \frac{1}{2v^2}\left[\frac{s_{2\alpha}}{s_{2\beta}}(m^2_H - m^2_h) + 2m_{H^\pm} - M^2 \right], \tag{2.28}$$
$$\lambda_4 = \frac{1}{2v^2}\left(M^2 + m^2_A - 2m^2_{H^\pm} \right),$$
$$\lambda_5 = \frac{1}{2v^2}\left(M^2 - m^2_A \right),$$

where $M^2 \equiv 2m^2_{12}/s_{2\beta}$, m_A, $m_{H^\pm}$ are the masses for the neutral CP-odd and charged scalars and m_h, m_H are the masses of the SM-like and heavy Higgs, correspondingly. We note that $\lambda_{345} = [M^2 + (m^2_H - m^2_h)s_{2\alpha}/s_{2\beta}]/(2v^2)$.

For the scalar potential to be bounded from below, the quartic couplings should

fulfil the conditions in Eq. (2.11) [35,50] Moreover, from imposing unitarity and perturbativity conditions, the coefficients have to satisfy the following relations [33,51]

$$
\begin{aligned}
|\lambda_3 + 2\lambda_4 \pm 3\lambda_5| &\leq 16\pi \,, \\
|\lambda_3 \pm \lambda_4| \leq 16\pi \,, \qquad |\lambda_3 \pm \lambda_5| &\leq 16\pi \,, \\
\left| \frac{1}{2} \left(\lambda_1 + \lambda_2 \pm \sqrt{(\lambda_1 - \lambda_2)^2 + 4\lambda_4^2} \right) \right| &\leq 16\pi \,, \\
\left| \frac{1}{2} \left(\lambda_1 + \lambda_2 \pm \sqrt{(\lambda_1 - \lambda_2)^2 + 4\lambda_5^2} \right) \right| &\leq 16\pi \,, \\
\left| \frac{1}{2} \left(3\lambda_1 + 3\lambda_2 \pm \sqrt{9(\lambda_1 - \lambda_2)^2 + 4(2\lambda_3 + \lambda_4)^2} \right) \right| &\leq 16\pi \,.
\end{aligned}
\tag{2.29}
$$

These constraints indirectly ensure that the potential remains perturbative up to very high scales. Any additional constraint on the sizes of the λ_i will make the analysis more restrictive.

For last, in order to guarantee a global minimum, we need to fulfill the constraint [52]

$$
m_{12}^2 \left(m_{11}^2 - m_{22}^2 \sqrt{\frac{\lambda_1}{\lambda_2}} \right) \left(t_\beta - \sqrt[4]{\frac{\lambda_1}{\lambda_2}} \right) > 0 \,.
\tag{2.30}
$$

2.7 Singular Alignment

The right implementation of the parity symmetry Z_2, starting from a general 2HDM, avoided the appearance of tree-level FCNCs and produced four types. This class of theories, in which symmetries are adequately used to complement the GIM mechanism when going beyond the SM, are said to possess Natural Flavour Conservation (NFC) [15,16].

Interestingly, the four conventional models can actually be contained as particular cases of an ansatz called Yukawa alignment [44]. It is a generalized approach to prohibit FCNCs at tree level, without choosing a particular type, and consistent with NFC theories. The ansatz states that the two Yukawa matrices, contributing to a given mass matrix, should be proportional to each other

$$
\mathbf{Y}_1 \propto \mathbf{Y}_2 \,,
\tag{2.31}
$$

guaranteeing the simultaneous diagonalization of both Yukawa matrices, $\mathbf{Y}_{1(2)}$, when moving to the mass basis.

Realize how the Yukawa alignment and the four models it may represent, are flavour universal regarding how the parity symmetry was employed. A flavour non-universal approach has been already proposed [8,45]. This kind of alignment in flavour space does not have any specific symmetry protection at the Lagrangian level. Therefore, one-loop quantum corrections may induce misalignment in the Yukawa matrices and

bring about FCNCs at the loop level. In Ref. [45], it was shown that the induced misalignment is a quite small effect, as the initial alignment in the multi-Higgs Lagrangian has some residual flavour symmetries, which tightly limit the type of FCNC operators that can be generated at higher orders. This can be easily understood as both the flavour universal Yukawa alignment and its generalization are a linear realization of the minimal flavour violation hypothesis [53] and could be derived from it [54]. This hypothesis states that the only source of flavour breaking should come from the Yukawa matrices, even in the presence of new particles and interactions [55–57]. Lastly, this kind of apparently adhoc ansatz could originate from a family symmetry as shown in Ref. [58] or from an effective approach with additional hidden scalars [59].

In order to explain the singular alignment ansatz, let us first introduce a key concept: the Singular Value Decomposition (SVD). In general, a complex matrix $\mathbf{M}$ can be decomposed as

$$\mathbf{M} = \mathbf{L}^\dagger \mathbf{\Sigma} \mathbf{R} \,, \tag{2.32}$$

where $\mathbf{\Sigma} = \mathrm{diag}(m_1, m_2, m_3)$ with $m_i > 0$ and $\mathbf{L}$ and $\mathbf{R}$ are unitary matrices which rotate independently the left and right-handed fermion fields. Notice how the SVD in Eq. (2.32) can also be written as a sum of three rank 1 matrices,

$$\mathbf{M} = \sum_i m_i \mathbf{L}^\dagger \mathbf{P}_i \mathbf{R} \,, \tag{2.33}$$

where $\mathbf{P}_i$ are three projector operators, $\mathbf{P}_i^2 = \mathbf{P}_i$ and $\sum_i \mathbf{P}_i = \mathbb{1}_{3\times3}$. Here each $\mathbf{P}_i$ reads

$$\mathbf{P}_1 = \begin{pmatrix} 1 & 0 & 0 \\ 0 & 0 & 0 \\ 0 & 0 & 0 \end{pmatrix} \,, \quad \mathbf{P}_2 = \begin{pmatrix} 0 & 0 & 0 \\ 0 & 1 & 0 \\ 0 & 0 & 0 \end{pmatrix} \,, \quad \mathbf{P}_3 = \begin{pmatrix} 0 & 0 & 0 \\ 0 & 0 & 0 \\ 0 & 0 & 1 \end{pmatrix} \,. \tag{2.34}$$

In the following, we denote each rank 1 matrix by

$$\mathbf{\Delta}_i = \mathbf{L}^\dagger \mathbf{P}_i \mathbf{R} \,, \tag{2.35}$$

and we refer to it as a *singular matrix*.

Now, let us apply the aforementioned and continue with the discussion on the singular alignment ansatz. The latter takes, as starting point, the singular value decomposition in Eq. (2.32) and apply it to Eq. (2.13). The mass matrix then takes the form

$$\mathbf{L}^\dagger \mathbf{M}_{\mathrm{diag}} \mathbf{R} = v_1 \mathbf{Y}_1 + v_2 \mathbf{Y}_2 \,. \tag{2.36}$$

Note that $\mathbf{M}_{\mathrm{diag}}$ can be expressed in terms of the projection operators as

$$\mathbf{M}_{\mathrm{diag}} = \sum_i m_i \mathbf{P}_i \quad \text{with} \quad [\mathbf{P}_i]_{jk} = \delta_{ij}\delta_{ik} \quad (i,j,k = 1,2,3) \tag{2.37}$$

then, it is possible to redefine the l.h.s of Eq. (2.36) as

$$\sum_i m_i \mathbf{\Delta}_i = v_1 \mathbf{Y}_1 + v_2 \mathbf{Y}_2 \,, \tag{2.38}$$

where recall $\mathbf{\Delta}_i = \mathbf{L}^\dagger \mathbf{P}_i \mathbf{R}$.

Now the ansatz of singular alignment is defined by demanding that each Yukawa matrix satisfies

$$\mathbf{Y}_k = \alpha_k \mathbf{\Delta}_1 + \beta_k \mathbf{\Delta}_2 + \gamma_k \mathbf{\Delta}_3 \,, \quad (k = 1, 2) \,. \tag{2.39}$$

In return, we would obtain,

$$\sum_i m_i \mathbf{\Delta}_i = \left(\sum_k \alpha_k v_k \right) \mathbf{\Delta}_1 + \left(\sum_k \beta_k v_k \right) \mathbf{\Delta}_2 + \left(\sum_k \gamma_k v_k \right) \mathbf{\Delta}_3 \tag{2.40}$$

giving the relations for the masses

$$m_1 = \sum_k \alpha_k v_k \,, \qquad m_2 = \sum_k \beta_k v_k \,, \quad m_3 = \sum_k \gamma_k v_k \,. \tag{2.41}$$

Realize that, by substituting the ansatz defined in Eq. (2.39) into Eq. (2.36), each Yukawa matrix becomes diagonal in the mass-basis and therefore, it guarantees the absence of tree-level FCNCs. The new diagonal Yukawa matrix can be written as follows

$$\overline{\mathbf{Y}}_k = \mathbf{L}\mathbf{Y}_k\mathbf{R}^\dagger = \alpha_k \mathbf{P}_1 + \beta_k \mathbf{P}_2 + \gamma_k \mathbf{P}_3 \,. \tag{2.42}$$

Moreover, we recover the Yukawa alignment in the limit where $\alpha_k \propto \beta_k \propto \gamma_k$ [44]. It is clear from here how the singular alignment can be seen as the generalized version of the Yukawa alignment [44] and thus equivalent to [45].

2.8 Model Setups

We have gathered all the requirements to build a successful model where the hierarchy between the two vevs can be directly transferred as two dominant mass scales in the fermion spectrum. We use this to explain two independent aspects of the problem of mass. Each aspect gives place to a different model setup as follows:

- **Type A** (or top-quark dominance): It offers a clear distinction between the top quark and all the other fermion masses as motivated by the large mass splitting,

$$m_t \sim v \gg m_f \,. \tag{2.43}$$

- **Type-B** (or third-fermion-family dominance): It creates a distinction between the whole third fermion family and the two lighter ones

$$m_3 \gg m_{1,2} \,, \tag{2.44}$$

where this relation holds for each kind of fermion.

From the point of view of naturalness, 't Hooft's criterion is fulfilled in both models, as in the limit where the small vev, connected to all light fermion masses is taken to be zero, $v_1 \to 0$, then the Z_2 symmetry is recovered. On the other hand, Dirac's criterion gets realized slightly different in each model. Type-A has four natural Yukawa couplings, $\{y_t, y_b, y_c, y_\tau\} \sim \mathcal{O}(1)$, while Type-B has only two, $\{y_t, y_c\} \sim \mathcal{O}(1)$. Thus, even though both types have a certain degree of naturalness in action, overall, Type-A offers a more *natural* scenario than Type-B.

The field content of both models is that of a general 2HDM with a softly-broken Z_2 symmetry as discussed in Sec. 2.2. Also, in both of them we employ the singular alignment ansatz to guarantee the absence of FCNCs at tree level.

The Z_2 assignments for Type-A are:

$$u_{3,R} \to +u_{3,R}$$
$$\{u_{j,R}, d_{j,R}, e_{j,R}\} \to -\{u_{j,R}, d_{j,R}, e_{j,R}\} \tag{2.45}$$

whereas Type B:

$$\{u_{3,R}, d_{3,R}, e_{3,R}\} \to +\{u_{3,R}, d_{3,R}, e_{3,R}\}$$
$$\{u_{j,R}, d_{j,R}, e_{j,R}\} \to -\{u_{j,R}, d_{j,R}, e_{j,R}\} \,. \tag{2.46}$$

Here, j denotes the remaining RH fermions. All left-handed ones are chosen even under the Z_2 symmetry. We summarize the charge distribution of the two models in Table 2.2.

Then, the Yukawa Lagrangian for Type-A reads

$$-\mathcal{L}_{A,Y}^Q = \sum_{i=1}^3 \bar{Q}_{i,L} \left[y_i^t \widetilde{\Phi}_2 u_{3,R} + \widetilde{\Phi}_1 (y_i^c u_{2,R} + y_i^u u_{1,R}) \right]$$

$$+ \sum_{i=1}^3 \bar{Q}_{i,L} \Phi_1 (y_i^b d_{3,R} + y_i^s d_{2,R} + y_i^d d_{1,R}) + \text{h.c.}$$

$$-\mathcal{L}_{A,Y}^\ell = \sum_{i=1}^3 \bar{\ell}_{i,L} \Phi_1 (y_i^\tau e_{3,R} + y_i^\mu e_{2,R} + y_i^e e_{1,R}) + \text{h.c.} \,, \tag{2.47}$$

while for Type-B reads

$$-\mathcal{L}_{B,Y}^Q = \sum_{i=1}^3 \bar{Q}_{i,L} \left[y_i^t \widetilde{\Phi}_2 u_{3,R} + \widetilde{\Phi}_1 (y_i^c u_{2,R} + y_i^u u_{1,R}) \right]$$

$$+ \sum_{i=1}^3 \overline{Q}_{i,L} \left[y_i^b \Phi_2 d_{3,R} + \Phi_1 (y_i^s d_{2,R} + y_i^d d_{1,R}) \right] + \text{h.c.}$$

$$-\mathcal{L}_{B,Y}^\ell = \sum_{i=1}^3 \bar{\ell}_{i,L} \left[y_i^\tau \Phi_2 e_{3,R} + \Phi_1 (y_i^\mu e_{2,R} + y_i^e e_{1,R}) \right] + \text{h.c.} \,. \tag{2.48}$$

In general, the two models presented here, feature FCNCs at tree level. However, as

Type-	A	B
$u_{3,R}$	Φ_2	Φ_2
$d_{3,R}$, $e_{3,R}$	Φ_1	Φ_2
Other RH fermions	Φ_1	Φ_1

TABLE 2.2: Each column shows the fermions with the same $\mathbb{Z}_2$ charge assignment as a certain Higgs doublet, $\Phi_{1(2)}$. This defines the new types A and B. Note that a flavour conserving ansatz is required in order to avoid tree-level FCNCs.

discussed before, through the introduction of the singular alignment ansatz we choose the right parameter region of family space such that the Yukawa matrices become diagonal in the mass basis. Thus, FCNCs are absent at tree level. For further details on the application of the singular alignment in a multi-Higgs scenario, we refer to Ref. [8].

Note that, as the fermion mass matrices are given in terms of two hierarchical vevs, $v_1 \ll v_2$, we can explore the scenario where the smaller vev is set to zero and study the possible consequences. In Type-A all mass matrices are equal to zero except the one for the up-type quarks which takes the form

$$\mathbf{M}_u = v_2 \begin{pmatrix} 0 & 0 & y_1^t \\ 0 & 0 & y_2^t \\ 0 & 0 & y_3^t \end{pmatrix} . \tag{2.49}$$

As the down-type quarks have a null mass matrix, a simultaneous unitary transformation in the quark weak doublet leaves the kinetic terms invariant and simultaneously brings us to the mass basis. Therefore, at this level the quark mixing matrix is given by the identity which is a good first approximation to the observed CKM mixing matrix.

In order to discuss lepton mixing in our models, we must introduce massive neutrinos to the setup. For the moment, we let open the possibility of Dirac or Majorana nature. Under this circumstance, as the mass matrices for both the charged leptons and neutrinos depend on the same vev (even in the Majorana scenario), the mixing among them is expected to strongly deviate from the identity and behave more anarchically which is aligned with the observations of the PMNS matrix [60].

On the other hand, the Type-B mass matrices in the limit where $v_1 \to 0$ take the form

$$\mathbf{M}_u = v_2 \begin{pmatrix} 0 & 0 & y_1^t \\ 0 & 0 & y_2^t \\ 0 & 0 & y_3^t \end{pmatrix} , \quad \mathbf{M}_d = v_2 \begin{pmatrix} 0 & 0 & y_1^d \\ 0 & 0 & y_2^d \\ 0 & 0 & y_3^d \end{pmatrix} , \quad \mathbf{M}_e = v_2 \begin{pmatrix} 0 & 0 & y_1^e \\ 0 & 0 & y_2^e \\ 0 & 0 & y_3^e \end{pmatrix} . \tag{2.50}$$

This implies that all fermion should mix anarchically, and therefore in disagreement with the experimental observations. Nevertheless, this undesired issue can be solved by reassigning all Z_2 odd charges to the left-handed fermions instead of the right-handed ones. Thereafter, a weak-basis transformation in the RH fields would be enough to diagonalize the Yukawa matrices and recover the trivial quark mixing. However, in

the lepton sector one would have anarchic mixing, but only under the assumption of a Majorana neutrino nature.

To summarize the discussion on fermion mixing, both models are able to predict trivial mixing for the quark sector under the right Z_2 charge assignment. Additionally, we predict anarchic mixing for the lepton sector if neutrinos are considered to have Majorana nature. Additionally, fermion mixing can be explicitly related to t_β in the recent study in Ref. [61]. We achieve similar conclusions for the Type-B scenario as in [62] where a similar model is investigated.

2.9 Scalar Couplings

The Yukawa Lagrangian in the mass basis is expressed by:

$$-\mathcal{L}_Y \supset \sum_f \frac{m_f}{(246\,\text{GeV})} \left(\xi_f^h \bar{f} f h + \xi_f^H \bar{f} f H - i\xi_f^A \bar{f}\gamma_5 f A \right)$$
$$- H^+ \frac{\sqrt{2}\sum_{ij} \mathbf{V}_{ij}^{\text{CKM}}}{(246\,\text{GeV})} \, \bar{u}_i \left(m_{u_i}\xi_{q_u}^{H^+} P_L + m_{d_j}\xi_{q_d}^{H^+} P_R \right) d_j$$
$$- H^+ \frac{\sqrt{2} m_\ell}{(246\,\text{GeV})} \, \xi_\ell^{H^+} \bar{\nu}_{L,i}\ell_{R,j} + \text{h.c.} \tag{2.51}$$

where $\mathbf{V}^{\text{CKM}}$ is the quark mixing matrix (See Appendix A for further details). The SM is recovered for $\xi_f^h = 1$ and $\xi_f^{H,A,H^+} = 0$. In Table 2.3 we show the corresponding couplings for the conventional NFC scenarios, while in Table 2.4 the respective ones for our Types-A and B. The two tables show great similarities, as the main change from the conventional ones is breaking their family universality.

To derive the Yukawa couplings shown in Tables 2.3 and 2.4 we first insert $\Phi_{1,2}$ from Eq. (2.7) into Eqs. (2.47) and (2.48). Then we perform a rotation in the neutral and charge scalar sector to move to the mass basis as in Eq. (2.26). The resulting terms depend on β and α as well as on the two vevs, $v_{1,2}$. In addition, we use the relations between the fermionic Yukawa couplings and masses,

$$y_f = \frac{m_f}{c_\beta v} \qquad \text{or} \qquad y_f = \frac{m_f}{s_\beta v} \,. \tag{2.52}$$

The former relation is then used if the given fermion couples to Φ_1 whereas the latter if it couples to Φ_2. For an example where the couplings acquire a completely different behaviour when enlarging the flavour symmetry to a larger group refer to Ref. [63]. For other related phenomenological applications of the Yukawa alignment see for example [64].

Moving forward, the couplings of the CP-even scalars, h and H, to a pair of vector bosons, $V = W^\pm, Z$, are modified by

$$\xi_{VV}^h = \sin(\beta - \alpha) \quad \text{and} \quad \xi_{VV}^H = \cos(\beta - \alpha) \,. \tag{2.53}$$

Type-	I	II	X	Y
$\xi_{q_u}^h$	c_α/s_β	c_α/s_β	c_α/s_β	c_α/s_β
$\xi_{q_d}^h$	c_α/s_β	$-s_\alpha/c_\beta$	c_α/s_β	$-s_\alpha/c_\beta$
ξ_ℓ^h	c_α/s_β	$-s_\alpha/c_\beta$	$-s_\alpha/c_\beta$	c_α/s_β
$\xi_{q_u}^H$	s_α/s_β	s_α/s_β	s_α/s_β	s_α/s_β
$\xi_{q_d}^H$	s_α/s_β	c_α/c_β	s_α/s_β	c_α/c_β
ξ_ℓ^H	s_α/s_β	c_α/c_β	c_α/c_β	s_α/s_β
$\xi_{q_u}^A$	$1/t_\beta$	$1/t_\beta$	$1/t_\beta$	$1/t_\beta$
$\xi_{q_d}^A$	$-1/t_\beta$	t_β	$-1/t_\beta$	t_β
ξ_ℓ^A	$-1/t_\beta$	t_β	t_β	$-1/t_\beta$
$\xi_{q_u}^{H^+}$	$1/t_\beta$	$1/t_\beta$	$1/t_\beta$	$1/t_\beta$
$\xi_{q_d}^{H^+}$	$1/t_\beta$	$-t_\beta$	$1/t_\beta$	$-t_\beta$
$\xi_\ell^{H^+}$	$1/t_\beta$	$-t_\beta$	$-t_\beta$	$1/t_\beta$

TABLE 2.3: Flavour universal Yukawa couplings of the charged fermions to the Higgs bosons h, H, A, and H^+ in the four conventional 2HDMs.

Nevertheless, SM values are favored by present data, meaning that to a very good degree of approximation,

$$\sin(\beta - \alpha) \simeq 1 . \tag{2.54}$$

This is the so called *alignment limit* (AL) and whenever satisfied, the CP-even neutral scalar, h, will have identical couplings as the SM one. We can approach the alignment limit in terms of angles as: $\beta = \alpha + \pi/2 - \epsilon$ with $\epsilon \to 0$. An implication of the latter is reflected in $\xi_f^h \to 1$ in Tables 2.3 and 2.4. This again reinforces the fact that h behaves as the SM Higgs in the AL. Our two proposed models satisfy the same alignment conditions as the conventional NFC ones. To better understand the behaviour of the Yukawa couplings we rewrite the relevant $\xi_f^{(h,H)}$ in terms of t_β, $c_{\beta-\alpha}$, and $s_{\beta-\alpha}$. Including terms for the AL up to $\mathcal{O}(\epsilon)$ leads to

$$
\begin{aligned}
c_\alpha/s_\beta &= s_{\beta-\alpha} + c_{\beta-\alpha}/t_\beta &\simeq 1 + \epsilon/t_\beta , \\
-s_\alpha/c_\beta &= s_{\beta-\alpha} - c_{\beta-\alpha} t_\beta &\simeq 1 - \epsilon t_\beta , \\
c_\alpha/c_\beta &= c_{\beta-\alpha} + s_{\beta-\alpha} t_\beta &\simeq \epsilon + t_\beta , \\
s_\alpha/s_\beta &= c_{\beta-\alpha} - s_{\beta-\alpha}/t_\beta &\simeq \epsilon - 1/t_\beta .
\end{aligned}
\tag{2.55}
$$

Thus, away from the exact AL, we expect significant deviations in Type-A and B compared to the SM Higgs couplings to the first and second fermion generations.

Before discussing the phenomenology of our two models, note that, regarding the Higgs couplings, Type-A is closely related to Type-II besides the up and charm quark couplings. Due to their small Yukawa values they have limited phenomenological relevance at colliders, although some efforts have been made to constrain their values. In particular, the decay $h \to J/\Psi + \gamma$ is sensitive to potential deviations in the charm-Yukawa coupling which could be tested [65] see also [66]. For Type-B, the situation

Type-	A	B
ζ_t^h	c_α/s_β	c_α/s_β
$\zeta_{b,\tau}^h$	$-s_\alpha/c_\beta$	c_α/s_β
ζ_{light}^h	$-s_\alpha/c_\beta$	$-s_\alpha/c_\beta$
ζ_t^H	s_α/s_β	s_α/s_β
$\zeta_{b,\tau}^H$	c_α/c_β	s_α/s_β
ζ_{light}^H	c_α/c_β	c_α/c_β
ζ_t^A	$1/t_\beta$	$1/t_\beta$
$\zeta_{b,\tau}^A$	t_β	$-1/t_\beta$
$\zeta_{u,c}^A$	$-t_\beta$	$-t_\beta$
$\zeta_{d,s,\ell}^A$	t_β	t_β
$\zeta_t^{H^\pm}$	$1/t_\beta$	$1/t_\beta$
$\zeta_{b,\tau}^{H^\pm}$	$-t_\beta$	$1/t_\beta$
$\zeta_{\text{light}}^{H^\pm}$	$-t_\beta$	$-t_\beta$

TABLE 2.4: Flavour non-universal Yukawa couplings, cf. Eq. (2.51), of the charged fermions to the scalars h, H, A, and H^+ in Type-A and B with light $= \{u,c,d,s,\ell\}$ and $\ell = \{e,\mu\}$.

is slightly different. Compared to Type-I, the couplings to d, s, u, c, e, μ are changed. Thus, in Type-B in case of deviations from the AL those couplings can be enhanced for large values of t_β instead of being suppressed as in Type-I. Therefore, the changes in the muon coupling are of special interest as it is experimentally constrained [67–69]. Lastly, Type-I is mostly constrained for $t_\beta \lesssim 10$ due to the $1/t_\beta$ suppressed b-Yukawa coupling, while for Type-II relevant constraints also arise for large values of t_β [70]. We investigate all the aforementioned channels and compare the results between Type-A, Type-B, Type-I and Type-II in Sec. 2.11.

To visualize the deviations from the SM Higgs couplings, in the four different scenarios: A, B, I and II; we show the branching ratios (BRs) of h as a function of t_β in Figure 2.1 with $\cos_{\beta-\alpha} = 0.1$ for Type-A (II) in the right panel, as well as for Type-B (I) in the left one [71,72] Here Type-A and B are presented in solid lines while Type-I and II as dashed lines. We notice that for Type-A, most decay modes behave very similar to Type-II, except for the BR($h \to c\bar{c}$) which differs significantly. On the other side, in Type-B all BRs differ considerably compared to Type-I for $t_\beta \gtrsim 30$ as BR($h \to c\bar{c}$) becomes sizeable. Similarly, BR($h \to \mu^+\mu^-$) also shows deviations from predictions in the usual 2HDM-types. A more detailed discussion of the $h \to \mu^+\mu^-$ mode and the Higgs decay into charmonium plus a photon is presented in Sec. 2.11. Additionally, the total decay width deviates stronger from the SM value for Type-A than for Type-B as shown in Figure 2.2. In the left panel, regions outside the solid contour lines are excluded at 95% CL by CMS [73].

Similarly, in Figure 2.3 we show the BRs for the heavy scalar, H. The BRs of the pseudoscalar A, behave similarly and therefore, we do not discuss them explicitly. In
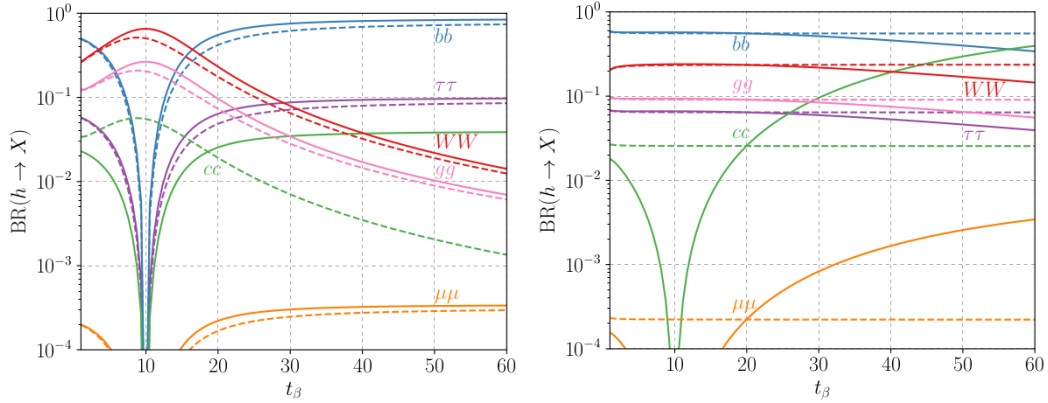
FIGURE 2.1: Branching ratios of the SM-like scalar h in Type-A (left) and B (right) for $c_{\beta-\alpha} = 0.1$ [71,72]. For comparison we show the BRs in Type II (left) and I (right), as dashed lines using the same color for each mode.

general, the left panel shows good agreement between Type-A and II, as expected. Additionally, the BR($H \to t\bar{t}$) dominates for $t_\beta \lesssim 5$ in Type-A and II, respectively for $t_\beta \lesssim 12$ in Type-B, and for all values of t_β in Type-I. For values of $t_\beta \gtrsim 10$ BR($H \to b\bar{b}$) becomes dominant in Type-A and II, while in Type-B the BR($H \to c\bar{c}$) takes over. In Type-A and II, the decay $H \to \tau^+\tau^-$ features the second biggest BR for $t_\beta \gtrsim 10$. While in Type-B the BR($H \to \mu^+\mu^-$) is the second dominant for $t_\beta \gtrsim 43$. Note that the latter BR for Type-I is small and therefore not appearing in the plot. In Type-I, the ratios of the BRs stay constant and the gg channel is next-to-dominant. Considering deviations from the alignment limit decays to weak gauge bosons become relevant. For example, for $c_{\beta-\alpha} = 0.1$ the maxima of BR($H \to WW$) $\simeq 0.33$ and BR($H \to ZZ$) $\simeq 0.16$ are at $t_\beta \approx 5$. For higher values of t_β, both approach values of $\mathcal{O}(1\%)$.

To understand the importance of studying the couplings of the SM Higgs as a way to distinguish among different multi-scalar scenarios please refer to Ref. [74]. In particular, different imprints that the SM and BSM scenarios leave on the Higgs Yukawa couplings were identified. Namely, in the SM those couplings lay on a single line if plotted as a function of the fermion masses. This also occurs for the 2HDM of Type-I but with a different slope. On the other hand, for the Type-II the Higgs Yukawa couplings will lay on two lines, one for down-type quarks and leptons and one for up-type quarks. Now, within Type-A the top quark Yukawa coupling will deviate from the line defined by the remaining fermions. In Type-B, all third generation Yukawa couplings will lay on a different line than the ones of the light fermions.

2.10 Experimental Constraints and Benchmarks

In Sec. 2.6 we briefly discussed the theoretical constraints for 2HDMs. However, we also need to include experimental limits that have been set by different channels. There
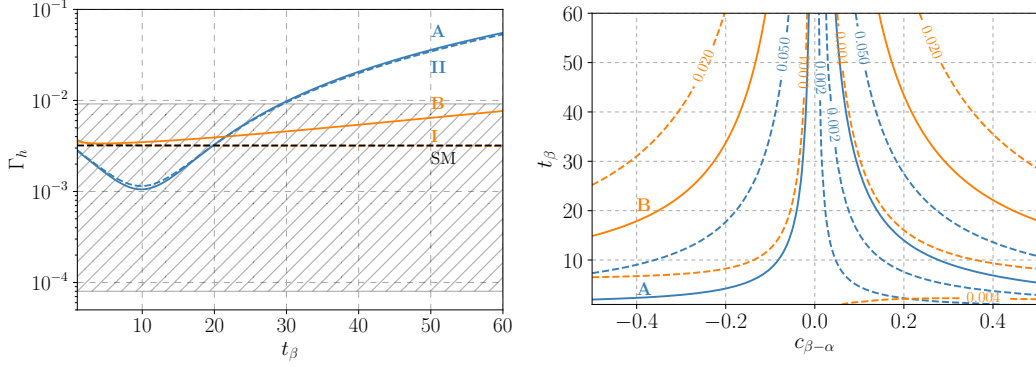
FIGURE 2.2: Left panel: Total decay width of h for Type-A, B, I, and II with $c_{\beta-\alpha} = 0.1$. The SM value is depicted as the black dotted line and the experimentally allowed band [73] at 95% CL as the grey hatched region. Right panel: Contours of $\Gamma_h = $ const. for Type-A (blue) and B (orange). Regions outside the solid lines are excluded at 95% CL [73].

are two ways to study multi-scalar scenarios: i) by possible deviations from the SM predictions, specially on the SM Higgs properties, and ii) by direct searches for the new scalar states. We take both into consideration. Furthermore, we make use of results derived for the well-studied Types-I and II, and discuss the main differences occurring in our Types-A and B. A full investigation of the 2HDM parameter space is beyond the scope of this thesis and therefore will not be discussed in detail. Instead, we refer the reader to Ref. [70] for a comprehensive analysis regarding the present status of the 2HDM neutral scalars from current LHC searches. Additionally, a summary of the most relevant theoretical and experimental constraints is presented. In the following we mention the most important experimental limits for our analysis and define several benchmark scenarios.

2.10.1 Experimental Constraints

We consider the following experimental constraints for 2HDMs as the most relevant ones for our study:

- **Higgs Couplings**: As mentioned before, one important constraint to consider is the deviation of the SM-like Higgs couplings, as they get modified when more scalars are included. To this end, we use the Higgs coupling modifiers, κ_i. They are defined such that for a given production process or decay mode one has [69, 75]

$$\kappa_i^2 = \frac{\sigma_i}{\sigma_i^{\text{SM}}} \qquad \text{or} \qquad \kappa_i^2 = \frac{\Gamma_i}{\Gamma_i^{\text{SM}}} , \qquad (2.56)$$

which correspond to $(\xi_i^h)^2$ in our models. In Table 2.5 we summarize the current limits on the coupling modifiers derived from combined measurements of ATLAS
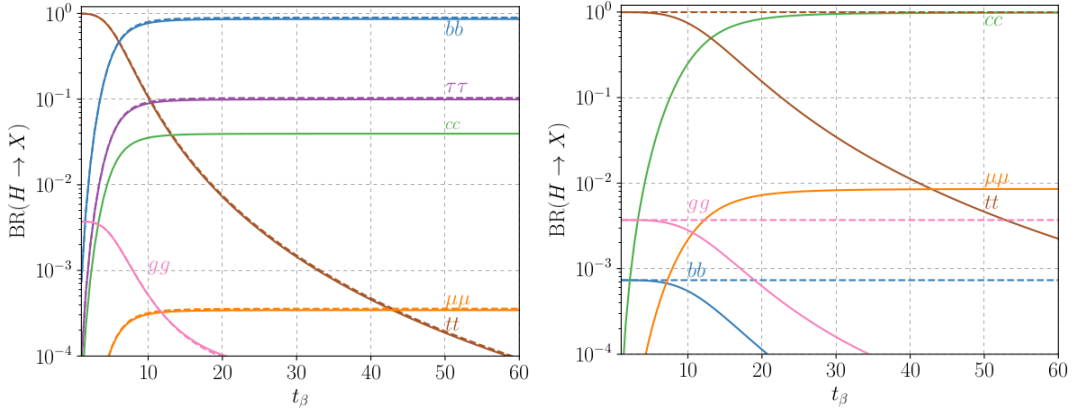
FIGURE 2.3: Dominant BRs of the heavy CP-even scalar, H, in Type-A (left) and B (right) for $c_{\beta-\alpha} = 0$ and $m_H = 500\,\text{GeV}$. For comparison we also show the BRs for Type-II (top) and Type-I (bottom) as dashed lines. The BRs of the pseudoscalar, A, behave similarly.

and CMS [75,76]. Note that the channels $h \to \mu\mu$ and $h \to J/\Psi + \gamma$ are of special interest for the models under consideration, as in those decays, the coupling structure differs from the conventional types (I and II).

Additionally, the recent limit on the total decay width of the SM Higgs by CMS [75] ($0.08\,\text{MeV} < \Gamma_h < 9.16\,\text{MeV}$ at 95 % CL) strongly constrains the enhanced couplings of h to SM fermions and other decay modes. In this regard, Figure 2.2 shows the observed limit together with Γ_h as a function of t_β in Types-I, II, A, and B for $c_{\beta-\alpha} = 0.1$ as well as a contour plot in the $(c_{\beta-\alpha}, t_\beta)$ plane.

- **Direct Collider Searches**: Here, we consider the LHC collider, in particular we take limits for the heavy scalar resonances from ATLAS and CMS [75,77]. In these searches we expect significant deviations for Type-B compared to Type-I. In [75], model-independent exclusion limits on the production cross section times the BR have been determined for scalars in the mass range from (130-1000) GeV. As shown in Ref. [70], values of $t_\beta \gtrsim 10$ are excluded by searches for $A/H \to \tau^-\tau^+$ for the mass degenerated scenario and $c_{\beta-\alpha} = 0.05$. Therefore, we adapt these constraints for Type-A and II.

- **Electroweak Precision Constraints**: The two terms in the scalar potential proportional to λ_4 and λ_5 break the custodial symmetry. This leads to additional contributions to the ρ parameter which can be avoided by taking $m_A = m_{H^\pm}$ or/and $m_H = m_{H^\pm}$ [78–80].

- **Flavour Observables**: Constraints from the Belle II dataset [81, 82] on $b \to s\gamma$ decays are particularly relevant. They require $m_{H^\pm} > 600\,\text{GeV}$. The Type-II is most sensitive to this constraint. After a careful study of the involved couplings it is

	Bayesian fit [83]	CMS [75]	ATLAS [76]
κ_W	1.01 ± 0.06	$1.10^{+0.12}_{-0.17}$	1.05 ± 0.08
κ_Z	1.01 ± 0.06	$0.99^{+0.11}_{-0.12}$	1.10 ± 0.08
κ_t	$1.04^{+0.09}_{-0.10}$	$1.11^{+0.12}_{-0.10}$	$1.02^{+0.11}_{-0.10}$
κ_b	0.94 ± 0.13	$-1.10^{+0.33}_{-0.23}$	$1.06^{+0.19}_{-0.18}$
κ_τ	1.0 ± 0.1	$1.01^{+0.16}_{-0.20}$	1.07 ± 0.15
κ_μ	$0.58^{+0.40}_{-0.38}$	$0.79^{+0.58}_{-0.79}$	< 1.53 at 95% C.L.

TABLE 2.5: Current 68% probability sensitivities and best fit values for the Higgs coupling modifiers, κ_i, as obtained from a Bayesian statistical analysis and from combined data taken by ATLAS and CMS at $\sqrt{s} = 13$ TeV. The ATLAS fit assumes all coupling modifiers to be positive.

possible to show that our two proposed types behave in the same way as the Type-II for this flavour violating transition. Therefore, we constrain the charged scalar mass to be larger than 600 GeV. Note that these flavour constraints are model-dependent and could be relaxed in the presence of more intricate BSM sectors.

2.10.2 Benchmark Scenarios

As mentioned in Sec 2.6, the number of independent (physical) free parameters in the scalar sector is seven. We choose them to be given by

$$\{m_{12}^2, m_h, m_H, m_A, m_{H^\pm}, t_\beta, \alpha\} \, . \tag{2.57}$$

In order to simplify the analysis and reduce the number of physical parameters, we investigate the most relevant phenomenological aspects of our two models by focusing on the following well motivated benchmarks:

- **Alignment Limit**: So far there are two constraints that help us to reduce the parameter space: i) we have $\beta = \alpha + \pi/2$ and ii) we know that $v_2 \gg v_1$ such that we could take $v_1 \in (3, 58)\,\text{GeV}$. In the latter, the lower bound is obtained by demanding the bottom Yukawa coupling to be of order one, $y_b \sim \mathcal{O}(1)$, i.e. $m_b \approx 3$ GeV. The upper bound is then obtained by relaxing the previous condition and just demanding $v_1/v_2 \lesssim \mathcal{O}(10^{-1})$. In return, we obtain a region for $t_\beta \in (3, 58)$ that implies for the scalar mixing angle

$$\alpha \in (-18.43, -0.99)^\circ \, . \tag{2.58}$$

In the AL, the Yukawa couplings flavour universality is restored for h, but not for H and A.

We recall the two employed criteria for naturalness mentioned in Sec. 2.2, as they are crucial to understand why we conceive $t_\beta \in (3, 58)$ as the natural range for our
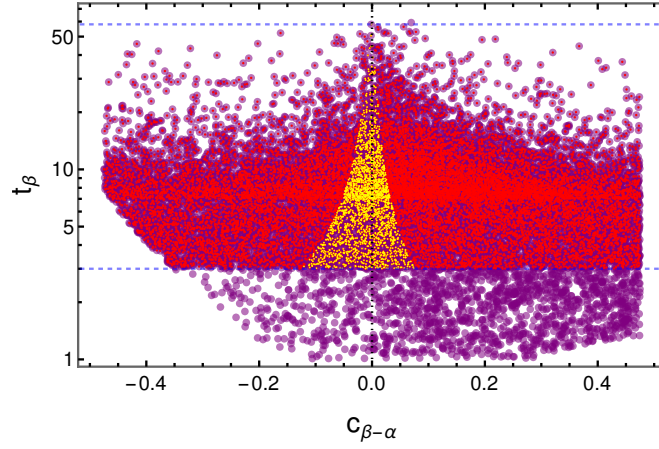
FIGURE 2.4: Current allowed regions from the measured SM-like Higgs couplings to fermions, $\kappa^h_{t,b,\tau}$, and gauge bosons, κ^h_V, at 95% CL for 2HDMs of Type-I (purple), B (red), A and II (both in yellow). The vertical dashed line corresponds to the AL, whereas the two horizontal ones to the previously discussed *natural* range ($3 < t_\beta < 58$).

discussion[6]. First, notice that only for $t_\beta \sim (20, 58)$ hierarchical fermion masses, $(m_b, m_\tau, m_c) \sim \mathcal{O}(1)$ GeV or $m_c \sim \mathcal{O}(1)$ GeV, are natural regarding Dirac's criterion, whereas for $t_\beta \sim (3, 20)$ they stop being so. However, we also employ the latter range as it is connected to a small value of v_1 which is natural according to 't Hooft's criterion. In order to understand the last point, we need to consider that the possibility to neglect v_1 is only subject to its appearance in $v_2^2 + v_1^2 = v^2$. So, even if v_1 is not much smaller than v_2, their squared may still be sufficiently small to allow the approximate relation $v_2 \approx v$.

- **Degenerate Masses**: Contributions to the oblique parameter T (or ρ) are the most restrained ones, as they depend on the relative mass squared differences. We can define three different cases: i) $m_H = m_{H^\pm}$, ii) $m_A = m_{H^\pm}$, and iii) $m_H = m_A = m_{H^\pm}$. The full bounds from electroweak precision measurements can be more easily satisfied in the last case.

- **Unitarity and Vacuum Stability**: It has been shown that in the AL the soft Z_2 symmetry breaking parameter is fixed, by unitarity and vacuum stability bounds for arbitrary values of $\tan \beta$, to [84]

$$m_{12}^2 = \frac{t_\beta}{1 + t_\beta^2}\, m_H^2\,, \tag{2.59}$$

with deviations possible only at $\tan \beta \sim 1$. This can be understood as, after imposing the perturbativity condition $|\lambda_i| \leq 4\pi$, the strongest constraints in the alignment limit come, respectively, from $v^2 \lambda_1 \sim t_\beta^3 (m_{12}^2 - m_H^2 s_\beta c_\beta)$ for $t_\beta \gg$

---

[6]Please note that as 174 is a common multiple for the numbers 3 and 58, the allowed ranges for v_1 and $\tan \beta$ turned out to be the same.
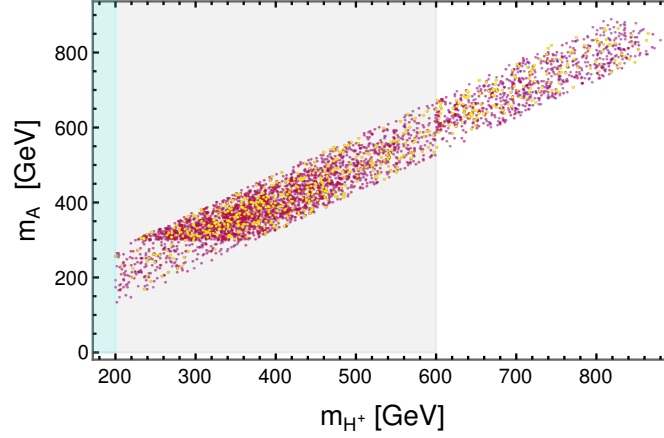
FIGURE 2.5: Allowed masses for the 2HDM Type-I (purple), B (red), A
and II (both in yellow) in the bi-dimensional plane ($m_{H^\pm}$, m_A). The gray
(applicable to Type-II, A, and B) and cyan (applicable to Type-I and $t_\beta <$
2) regions are excluded by flavour constraints (mostly $b \to s$ transitions).
A similar looking plot can be obtained for ($m_{H^\pm}$, m_H).

1 and $v^2\lambda_2 \sim t_\beta^{-3}(m_{12}^2 - m_H^2 s_\beta c_\beta)$ for $t_\beta \ll 1$. Thus, perturbativity demands
$|m_{12}^2 - m_H^2 s_\beta c_\beta| \lesssim v^2$ unless $t_\beta \sim 1$.

If the different viable regions, mentioned above, are simultaneously employed, it
could significantly reduce the number of physical parameters. In its two minimal
forms, the analysis could require three or four free parameters. This is a consequence of
Eq. (2.59), the AL, and the degenerate masses assumption. In the following, we make
use of these regions as a complimentary aspect of our discussion. Additionally, we
present the phenomenology of our two models and its respective comparisons with
Type-I and II.

2.11 Phenomenological Results

We start this section by commenting on the plane spanned by t_β and $c_{\beta-\alpha}$. In Figure 2.4
we show the allowed regions from the measured SM-like Higgs couplings depicted
in Table 2.5. Here, each plotted point satisfies the contributions to the ρ parameter
and the BFB, unitarity, perturbativity, and global minimum conditions. Additionally,
the charged scalar mass is required to be $m_{H^\pm} > 600$ GeV as implied by the $b \to s$
flavour violating transitions. The AL and the *natural* range for t_β are also included as
dashed lines. The range of scalar masses for m_{H^+} and m_A satisfying the aforementioned
conditions are shown in Figure 2.5. We present in both figures the Type-A and B models
as well as the corresponding comparison with the Types I and II.

Moving forward, one of the salient features of our two models, concerns the Higgs
coupling with muons, which could significantly deviate from the SM. The CMS col-
laboration announced results for the Higgs decay into a muon pair [85]. The obtained
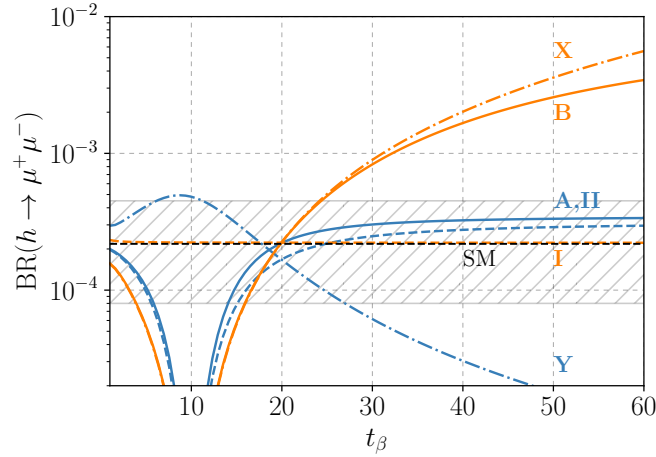
FIGURE 2.6: BR($h \to \mu^+\mu^-$) in all six 2HDM types for $c_{\beta-\alpha} = 0.1$. The SM value is shown as a dashed black line and the experimental allowed region at 95% CL as the hashed band [85].

limits are $0.8 \times 10^{-4} < $ BR($h \to \mu^+\mu^-$) $< 4.5 \times 10^{-4}$ at 95% CL. A comparison of BR($h \to \mu^+\mu^-$) in the four common types (I, II, X, Y) and our types (A, B) is depicted in Figure 2.6 for $c_{\beta-\alpha} = 0.1$. We note that large values of t_β are excluded for Type-B, while for Type-A most of the range of t_β is still consistent with the current data.

Another interesting prediction of our models is the enhancement of the Higgs coupling to charm quarks. Although the detection of the Higgs decay to a charm pair probably has to wait for a linear collider, it might be possible to search for the Higgs decay to $J/\psi + \gamma$ at the High-Luminosity LHC (HL-LHC). In Figure 2.7, we present the BR($h \to J/\psi + \gamma$) for Type-A, B, I, and II. We note that the newly proposed types give the strongest enhancement above the SM value [86].

Finally, the most direct signature of any 2HDM is the discovery of the full Higgs spectrum at the (HL-)LHC. The main production mechanism of the heavy scalar, H, for $t_\beta \lesssim 10$ is gluon-fusion, where the top-loop dominants the cross section. However, for larger values of t_β other contributions become relevant. In this case the bottom-loop in Type-A and II or the charm-loop in Type-B have to be included. In fact, the large enhancement for the bottom-Yukawa coupling arising in Type-A, opens the possibility to consider the b-associated production of H. For Type-B due to the enhancement of the charm-Yukawa coupling also c-associated production could become relevant. Even though those are certainly interesting aspects, a detailed discussion of is beyond the scope of this thesis.

Searches for heavy resonances decaying into muon pairs are of potential interest for our models. The recent ATLAS and CMS searches in [75, 76] distinguish between the gluon-fusion and b-associated production channels. The results are present as upper limits on the production cross section, σ, times the BR($H \to \mu^+\mu^-$). To obtain the production cross sections of H we rescaled the next-to-next-to-leading-order results from Ref. [87] to our parameter space. For small to intermediate values of t_β, the suppression
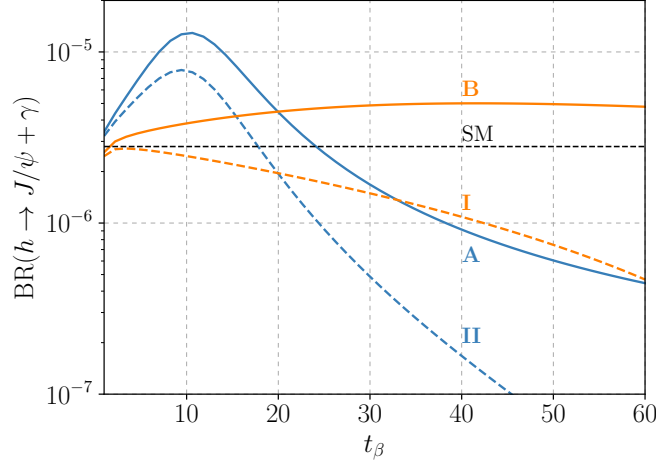
FIGURE 2.7: $\text{BR}(h \to J/\psi + \gamma)$ in the four 2HDMs types (Type-X and Y are identical to Type-I and II, respectively) for $c_{\beta-\alpha} = 0.1$. The SM value is depicted as the dashed black line.

of ξ_t^H is already effective but $\xi_{b(c)}^H$ is not strongly enhanced yet. For $m_H = 500\,\text{GeV}$ and $t_\beta > 10\,(50)$ the bottom (charm) contributions to gluon-fusion start to compensate the top coupling suppression in Type-A (B). For Type-A, the enhancement of ξ_b^H is strong enough to exclude high values of t_β in b-associated production. These effects are shown in Figure 2.8. There we adopted the slightly stronger upper bounds from CMS [75] considering both production modes. To summarize the constraints of special interest for Type-A and B, we show them together in Fig. 2.9 in the $(c_{\beta-\alpha}, t_\beta)$ plane. We find that even with this selection of channels large parts of the parameter space can be excluded.

So far we have extended the SM scalar sector in a minimal renormalizable way, and even in this simple scenario we have addressed a fundamental question regarding the mass pattern shown in the SM fermions. The architecture of the Type-A and B models offers new exciting possibilities to construct multi-Higgs models. In both scenarios the observed hierarchies in the fermion mass spectrum were taken into account while, at the same time, avoiding dangerous FCNCs through the implementation of the singular alignment ansatz [8]. There are still many details that need to be addressed to fully understand the pros and cons compared to the well studied conventional types. However, this is let for future work. In the next chapters, we go a step further and include non-renormalizable operators to the SM Lagrangian and study the richness of the augmented parameter space.
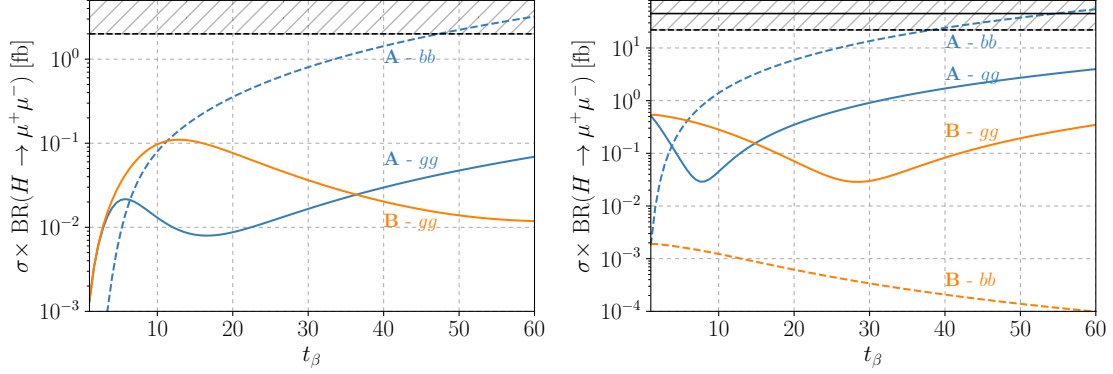
FIGURE 2.8: Values of $\sigma \times \mathrm{BR}(H \to \mu^+ \mu^-)$ with $c_{\beta-\alpha} = 0$ for $M_H = 500\,\mathrm{GeV}$ (left) and $M_H = 250\,\mathrm{GeV}$ (right) in Type-A (blue) and B (orange) together with the corresponding limits from CMS (black) [75]. The dashed (solid) lines indicate b-associated (gluon fusion) production. Contributions from b- and c-loops to the gluon fusion production are included. We note that Type-A is identical to Type-II in these channels.
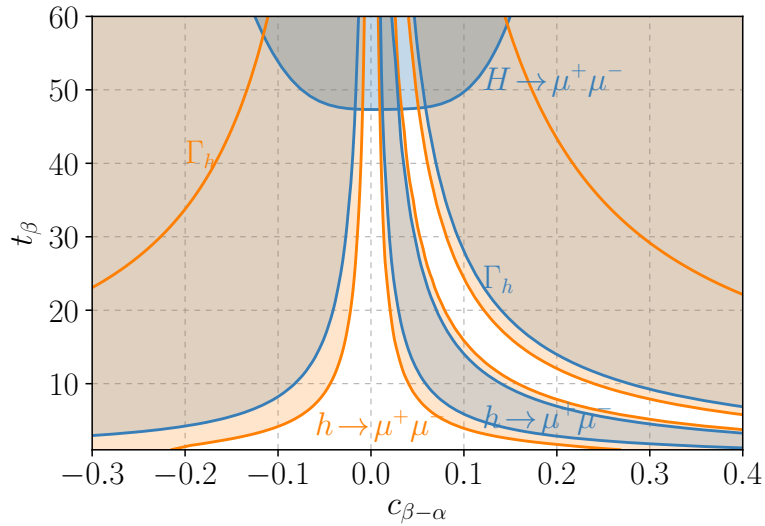
FIGURE 2.9: Summary of the discussed constraints on Type-A (blue) and B (orange) for $M_H = 500\,\mathrm{GeV}$. For Type-A we observe an interesting interplay of various measurements. For Type-B the dominant constraint arises from deviations of $\mathrm{BR}(h \to \mu^+ \mu^-)$.

Part II

Non-Renormalizable Extensions of the Scalar Sector

Chapter 3

extended Dark Matter EFT: Phenomenology and Matching

So far, we have been concerned with models where the SM Lagrangian was extended with renormalizable (dim ≤ 4) operators. However, the SM can be seen as an effective field theory at the electroweak scale (see B.1). New physics (NP) effects, coming from higher energy (or heavy) physics, then manifest by introducing higher-dimensional operators which are non-renormalizable and get suppressed by corresponding powers of the high-energy scale, Λ_{NP}. In the following, we focus only on non-renormalizable extensions to the SM. Additionally, from now on we address the existence of dark matter by including a new fermion field to the SM particle content.

The outline of this chapter is as follows. In Sec. 3.1 we introduce all the formalism of effective field theories (EFTs), in a top-down (Sec. 3.1.1) and bottom-up (Sec. 3.1.2) approach. We then study the dark matter evidence and its current status in Sec. 3.2 including a brief discussion on simplified models in Sec. 3.2.1. With this we cover all the three main components of the eDMEFT framework, which is extensively studied in Sec. 3.3. We follow by presenting a case study in Sec. 3.4. Here, the new mediator is charged under a Z_2 symmetry as well as the first fermion generation, giving (as in the previous chapter) a possible explanation of the smallness of the first fermion family. Within the same section, we also present exclusion limits on the coupling of the new scalar with the electron, up-quark and DM ($Y_{\mathcal{S}e,u}$, $Y_{\mathcal{S}\chi}$) correspondingly, for the (HL-)LHC and CLIC colliders. This scenario will be crucial for the next chapter, as we will use a similar framework to explain the XENON1T excess while being able to explain the lightness of electrons and neutrinos. Lastly, in Sec. 3.5 we perform the matching of the eDMEFT, with UV complete theories such as 2HDM + $\widetilde{S}$ (S) and vector-like fermions.

3.1 Effective Field Theories

Quantum physics phenomena manifest at multiple energy scales varying over many orders of magnitude, for example, from the neutrino mass scale $\sim 10^{-9}$ GeV to the Planck mass $\sim 10^{19}$ GeV. This makes it impossible to a theory to explain, in a single, yet practical, framework all the physics involved in such a large energy range. A theoretical approach that systematically separates the effects related to different energy scales,

keeping only the relevant physics at any given scale, is called an effective field theory. This is done under the consideration that physics effects, at small length scales (high-energy), start becoming negligible and do not affect any physics observable when moving to sufficiently larger scales (low-energy). In general, if a theory is assumed to be the low-energy limit of a more fundamental UV description then it should be approached as an EFT. Its Lagrangian would then get extended by a set of higher-dimensional operators. Note how the low-energy effective theory is only valid where the new, UV ingredients cannot be excited directly, and would break outside this range. The beauty of EFTs relay on the fact that they provide a multi-scale and model independent approach.

There are two different ways to construct an effective theory: top-down and bottom-up. The first one starts with a high-energy theory which spans several energy scales. Then, by conveniently choosing a cutoff scale the modes with energy above the cutoff, or also called *heavy* fields, are systematically integrated out such that the low energy theory is parameterized by only the *light* fields and the cutoff scale, Λ_{cutoff}. The top-down approach will be crucial when constructing the model in Sec. 3.4 and the next Chapter 4. On the other hand, the bottom-up approach is more focused on the possible degrees of freedom (DOF) at low energy, thus, the aim is to find the full UV theory starting from the operators constructed from low-energy DOF and use the experimental measurements to compute the coefficients. This approach is of special relevance when either the high-energy theory is unknown, or it is known but it is impossible to find its low-energy description in a top-down approach. Furthermore, in the case where the UV theory is not known, the model can be constructed with only a few assumptions and therefore, in a more model independent way [88]. In the following, we study the EFT formalism starting from a top-down and continuing with a bottom-up approach. For an exhaustive review on EFTs, please see Ref. [89–96].

3.1.1 Top-Down Approach

To exemplify this approach, let us consider a quantum field theory with a large energy scale M, normally associated with a large (Euclidean) momentum transfer or, most commonly, to the mass of a heavy particle. As the experimental energies typically run at $E \ll M$, we can build an EFT, starting from the full theory, to compute the observables at experimental level. To construct such a theory, we follow the steps below, allowing to expand the decay amplitudes of our theory in powers of E/M.

1. Fixing a cutoff in the energy scale $\Lambda < M$ and divide the QFT fields into high-frequency or heavy ($\phi_H \rightarrow w > \Lambda$) and low-frequency or light ($\phi_L \rightarrow w < \Lambda$) Fourier modes, such that $\phi = \phi_L + \phi_H$.

   The cutoff Λ represents the upper limit in which we have information on the theory, therefore, everything beyond the cutoff is out of reach. Is in that sense that our theory, at low energies is only governed by the light fields ϕ_L. Then

vacuum correlation function and the generating functional of the theory are:

$$\langle 0|T\{\phi_L(x_1)...\phi(x_n)\}|0\rangle = \frac{1}{Z[0]}\left(\frac{-i\delta}{\delta J_L(x_1)}\right)...\left(\frac{-i\delta}{\delta J_L(x_n)}\right)Z[J_L]|_{J_L=0} \quad (3.1)$$

and

$$Z[J_L] = \int \mathcal{D}\phi_L\mathcal{D}\phi_H e^{iS(\phi_L,\phi_H)+i\int d^dx J_L(x)\phi_L(x)} , \quad (3.2)$$

respectively. Here $S(\phi_L, \phi_H) = \int d^dx\mathcal{L}(x)$ corresponds to the action of the QFT in d space-time dimensions.

2. Integrating out the heavy fields by solving the corresponding path integral over ϕ_H, where the high energy modes have been removed,

$$Z[J_L] = \int \mathcal{D}\phi_L e^{iS_\Lambda(\phi_L)+i\int d^dx J_L(x)\phi_L(x)} \quad (3.3)$$

where

$$e^{iS_\Lambda(\phi_L)} = \int \mathcal{D}\phi_H e^{iS(\phi_L,\phi_H)}. \quad (3.4)$$

where $S_{eff}^\Lambda(\phi_L)$ is called the *"Wilsonian effective action"* and has a Λ dependence. As the high-frequency fluctuations have been removed from the theory, the latter is non-local at distances $\Delta x^\mu \sim 1/\Lambda$. Note that it is not always possible to solve the path integrals and therefore further mechanisms like the amplitude matching or the covariant derivative expansion should be used. In particular, the latter will be employ below.

3. Expanding Eq. (3.4) in terms of the light fields, is performing an operator product expansion (OPE)[1]. This is possible due to $E \ll \Lambda$, thus the effective action reads,

$$S_\Lambda(\phi_L) = \int d^dx\mathcal{L}_\Lambda^{eff}(x) \quad (3.5)$$

where

$$\mathcal{L}_\Lambda^{eff}(x) = \sum_i g_iQ_i(\phi_L(x)) . \quad (3.6)$$

This is known as the *Effective Lagrangian*. Here g_i are called the *Wilson Coefficients* while Q_i are all possible operators that can appear given the symmetries and quantum numbers. In principle, $\mathcal{L}_\Lambda^{eff}(x)$ can be composed of an unlimited number of operators Q_i, resulting in an very large series. This severely affects the predictivity, as we would then have an infinite amount of coefficients to fix, making predictions impossible. Nevertheless, the high-dimensional operators, have rather small contributions to the low energy observables. Consequently, only a few operators are in fact relevant and we can truncate the infinite sum by performing a *dimensional analysis* and fully recover the predictivity.

---

[1]The OPE expresses the product of two (or more) fields as a sum of local fields. As an axiom, it offers a non-perturbative approach to quantum field theory.

To perform such an analysis we do the following. As M is supposed to be the only relevant scale in the theory, we can write the Wilson coefficients in terms of it as[2]

$$g_i = C_i M^{-(D-d)} \tag{3.7}$$

where d is the number of dimensions, D is the full high-dimension of the operators Q_i and, as the action is dimensionless by definition, g_i must have a mass dimension $(d - D)$. The C_i are natural constants of order $\mathcal{O}(1)$. In the validity range ($E \ll \Lambda < M$), the operators Q_i scale as E^{D-d}, and the effective Lagrangian can be expanded in terms of $E/M \ll 1$. The contribution of $C_i(E/M)^{D-d}$ to the observables can be classified into three different scenarios:

- $D = d$ thus $C_i(E/M)^{D-d} \sim \mathcal{O}(1)$. The operators with this contribution are called *"marginal"* or renormalizable. In this case the operator is equally important at all energy scales. This operators are normally consider in QFTs and renormalizable theories as the SM.

- $D < d$ thus $C_i(E/M)^{D-d} \gg 1$. The operators with this contribution are called *"relevant"* or super-renormalizable. Unlike non-renormalizable terms, the relevant operators grow in the limit $E \to 0$. This operators are usually forbidden by symmetries, otherwise could have lead to problematic effects, for example, the scalar mass-term in a ϕ^4 theory would generate a mass $\sim \Lambda^2$ which push the particle outside the EFT.

- $D > d$ thus $C_i(E/M)^{D-d} \ll 1$. These contributions are called *"irrelevant"* or non-renormalizable. These terms typically vanish at low-energies and are numerically suppressed, however, are not forbidden. In fact, irrelevant operators tend to be the most important ones, as they can describe new physics. In addition they are essential for precision measurements and are the only ones who can say something at scales $\Lambda \sim M$. The latter will be studied in detail in Section 3.5.

After evaluating the contribution of each operator in the expansion, for a demanded accuracy on E/M, we indeed realize that only a few terms are kept and the infinite series become feasible, successfully recovering the predictivity. For an exhaustive review on the validity and the dimensional analysis for EFTs, see Ref. [94,97,98] and Ref. [99–107]

3.1.2 Bottom-Up Approach

As mentioned before, in this approach the aim is not to start from the full theory and then integrate out the heavy fields, but rather to start from what we know and construct all possible non-redundant terms to describe our theory. The bottom-up approach is very useful when the UV theory is not known. To build such a list of operators in a model-independent way, we need to consider three ingredients: the particle content

---

[2]We use the natural units where $[E] = [M] = [p] = [t]^{-1} = [x]^{-1} = \text{GeV}$.

(degrees of freedom), the symmetries, and a counting scheme that decides which operators are relevant in the validity regime.

1. The first one defines the minimum fields as dynamical degrees of freedom relevant for the theory. This can be for example, all possible fields that can take part in Feynman diagrams as either internal propagators or external legs. In principle, all particles with masses $m_p \ll \Lambda$ should be included.

2. To reduce the complexity and the amount of operators, it is imperative to make sure that the constructed terms do not violate the symmetries of the theory. This can be gauge symmetries, space-time symmetries (such as Lorentz symmetry), or global symmetries (such as flavour symmetries).

3. Lastly, even though we have only a few fields constrained by symmetries in our EFT, we could still write down an infinite expansion of the operators, therefore it is important to evaluate the importance of each operator by its dimensionality and truncate the series at a given order of accuracy.

To exemplify the points mentioned above, let us construct a bottom-up EFT from scratch [98]. A generic EFT Lagrangian can be written as

$$\mathcal{L}_{eff} = \mathcal{L}_{SM} + \sum_i \frac{C_i^{(5)}}{\Lambda} O_i^{(5)} + \sum_i \frac{C_i^{(6)}}{\Lambda^2} O_i^{(6)} + \sum_i \frac{C_i^{(7)}}{\Lambda^3} O_i^{(7)} + \sum_i \frac{C_i^{(8)}}{\Lambda^4} O_i^{(8)} + ... , \quad (3.8)$$

If, for example, we focus only in the SM effective field theory (SMEFT), we could remove all $D = 5$ operators as they violate the lepton number symmetry. In addition the $D = 7$ operators violate $B - L$ number Furthermore, operators of $D \geq 8$ are strongly suppressed as the couplings have a suppression term $\geq 1/\Lambda^4$, and therefore only operators of $D = 6$ survive. Then, the effective Lagrangian takes the form

$$\mathcal{L}_{eff} = \mathcal{L}_{SM} + \sum_i \frac{C_i^{(6)}}{\Lambda^2} O_i^{(6)}. \quad (3.9)$$

In general the list of operators kept in the theory must form a basis. The selection of such a basis can allow us to concentrate in specific BSM models. The most popular ones are SILH, Warsaw and Higgs [108–112]. An example of a dimension 6 operator in the SILH basis is $(2v^2)^{-1}(\partial_\mu(H^\dagger H))^2$.

Even though the effective Lagrangian in Eq. 3.9 contains, in principle, a very large sum of dimension 6 operators, we still need to make assumptions on the symmetries. For example, the number of independent operators for D=6 after imposing lepton and baryon number conservation reduces to 2499. Furthermore, if we consider flavour universality, we can cut down the operators to 76. For a particular model, with additional symmetries can dramatically reduce the number of independent operators to just a few [3].

---

[3]Another common assumption is that UV physics is minimally coupled, i.e. some operators are generated only at the loop level.

After constructing the EFT, we must measure the Wilson coefficients in the experiment, and depending on the outcome we could consider adding higher-dimensional operators to the effective Lagrangian. If the experimental value of the Wilson coefficient is small then the suppression scale Λ is estimated to be large and we can safely neglect higher dimensional operators. On the contrary, if the experimental value is large, it means that the coefficient is less suppressed, then, the value of Λ would not be big and the presence of high-dimensional operators could be important. For more examples of EFTs in the top-down and bottom-up approaches, go to Appendix B.

3.2   Dark Matter

Since it was first mentioned [113–115], DM has being of great interest for the physics and astrophysics community. High precision measurements of the cosmic microwave background (CMB) from the WMAP [116, 117] to the Planck mission [118, 119] confirmed that DM comprises around 23% of the total energy density of the universe, giving place to 73% of dark energy and only 4% of luminous (known) matter, like stars, planets, etc. We have evidence of its existence due to its gravitational interactions. Fritz Zwicky was one of the first ones to spot the existence of dark matter. This by realizing that the measured mass of the *Coma cluster* was around ten times larger than the one expected from luminous stars [120]. More evidence of the existence of DM originates from the flattening of galactic rotation curves [121, 122]. Explaining the observed rotation curves then requires more matter abundance than the visible one, and differently distributed, which can only be accomplished by adding another kind of matter.

Another DM imprint comes through the famous *Bullet cluster* observation [123], where the merging of two galaxy clusters show a clear separation of the gravitational potential and ordinary matter [124]. Finally, we know that in order to agree with the observations of large scale structure formation [125, 126], DM should play a major role in the theoretical simulations [123, 127].

After almost a century of research, it has been possible to identify several of its properties: it is not electrically charged, and therefore it does not interact electromagnetically; it is massive, and as consequence, can interact gravitational; it must be stable at cosmological scales, otherwise it would not be abundant today, in contrast with astrophysical and cosmological observations; it cannot be made of protons or neutrons, however, its composition is still unknown; finally, it is cold, i.e non-relativistic, or at least cold enough to allow for structure formation in the early universe. The latter is essential for the formulation of the cosmology ΛCDM model, where Λ stands for the cosmological constant describing dark energy and CDM for cold dark matter. For an extensive review of DM and its properties, refer to Refs. [128–131].

Although this knowledge is already of great value, we still need to detect the associated DM particle and its interactions with the SM fermions (if any). There are several candidates that have been proposed along the years, and their masses reach from 10^{-20} eV for the case of axion-like particles, to masses (solar masses) $\gtrsim M_\odot \sim 10^{66}$ eV for primordial black holes [132]. Among all the candidates, one that has been of special interest and is rather easy to include it in several beyond the SM scenarios, is a new

massive (~ 100 GeV) elementary particle, that interacts weakly with the SM fermions. This weakly interacting massive particle (WIMP) has the property to reproduce the observed relic density. The production mechanism associated to this kind of particle is the thermal freeze-out mechanism. To explain the concept of such mechanism we consider a WIMP particle χ, and a SM fermion f, both in thermal equilibrium in the hot plasma, that is, $ff \longleftrightarrow \chi\chi$. However, as the universe expands, the rate for the aforementioned processes becomes slower than the expansion rate of the universe. At the point where the annihilation rate $\Gamma \lesssim H$, with H the Hubble constant, such reactions go out of equilibrium. Then, on one hand the production reaction ($ff \to \chi\chi$) is kinematically suppressed and, on the other hand, DM particles become increasingly separated in space which makes it harder for them to find each other and annihilate. From this point on, the DM decouples from the plasma remaining with a constant density which is known as the *relic density*. Surprisingly, it happens that a particle with the WIMPs characteristics, i.e weak-scale mass and couplings, gives rise to a relic abundance in the right ballpark of the observed DM abundance. In the literature, this is called the *WIMP miracle* [133]. WIMP particles are a guideline for several new DM experiments.

There are three different search strategies to detect DM particles: Direct, Indirect and Collider detection. The former one (DD), make use of low momentum transfer. The detection is done trough the observation of the atomic nuclei recoil scattering processes, in ultra-sensitive low-background experiments. As WIMPs are not electrically charged, is unlikely that they interact with atomic electrons, but instead elastically scatter off the atomic nucleus, where the momentum transfer gives place to a nuclear recoil that can be detectable. For a detail introduction to DD please refer to Ref. [134,135]. The leading exclusion limits are obtained with liquid xenon detectors, such as XENON1T [136], PandaX [137], or LUX [138]. On the other hand, indirect detection (ID) explores the annihilation and decay of two DM particles into SM ones, so its aim is either to detect SM particles arising from the collision, or their side effects. For a review of ID searches with Neutrinos, X-Rays, Gamma Rays, Micro and Radio waves and Charged Cosmic Rays please refer to Ref. [139]. For a broader review, see e.g. Ref. [140,141]. Ultimately, collider searches study the annihilation of two SM fermions into a pair of DM particles. This is done through high-energy particle collisions, for example, at the Large Hadron Collider (LHC). As mentioned before, DM particles are electrically neutral, and in consequence, evade the detectors at colliders and only manifest as missing transverse energy ($\not{E}_T$). Fortunately, we can look for the visible, highly energetic counterparts of the event, leading to the so called *mono-X events*. The experiments ATLAS [142] and CMS [143] at the LHC are currently looking for such *mono-X* signatures, where X represents either a jet, photon, $Z/W^\pm$ bosons or the SM Higgs boson and are mainly produced as initial state radiation. For a summary of the searches, please see Fig. 3.1. The main difference between collider searches and direct/indirect detection is that, in the former, all the particles with a lifetime longer that $O(10^{-8})$s escape the detectors, and therefore are counted as $\not{E}_T$. As a consequence, we could not be certain about our signal to be DM or any other new or long-lived particle. Therefore, it is of convenience to combine results from several searches to accurate determine the DM properties.
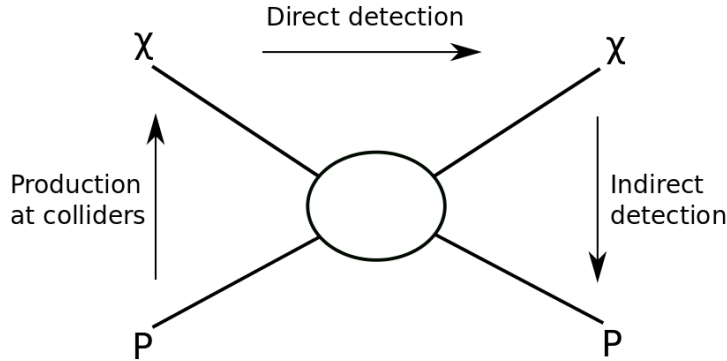
FIGURE 3.1: Scheme for the three different dark matter searches for
fermionic DM (χ) and SM particles (P).

3.2.1 Simplified Models

As mentioned before, new physics models can be described by an effective Lagrangian and a high-energy scale $\Lambda \gtrsim 1$ TeV. However, full BSM models tend to be rather complex, and even though EFTs can describe new physics with a few high-dimensional operators, the validity gets questionable at high energies. The latter is specially dangerous at the LHC, where the particles (protons) are accelerated along the 27 Km ring, acquiring an energy of approximate 6.5 TeV and producing a collision at a center of mass energy of $\sqrt{s} = 13$ TeV, while limits on cross sections are, on the other hand, rather weak. To overcome these issues, systematic simplifications, valid in a wider range of energy have been developed in the last years, facilitating searches of new physics, and are called *simplified models* [4]. This kind of model extents the SM content by only a couple of new particles along with their interactions and decay channels (to either BSM or SM particles). Simplified models have many benefits, for example, as aforementioned, they include operators with all new particles, regardless of their mass, thus increasing the validity to a wider energy range. Additionally, simplified models allow the explicit search for the mediator, unlike EFTs, where it is not present as an active degree of freedom and producing it puts into question the validity of the theory, as the mediator's mass is also the cutoff of the theory. However, this also implies that simplified models are model-dependent, and thus suffer from a loss of generality. Moreover, a potential problem with these models is that certain type of relevant operators violate gauge invariance, for example, the one connecting the SM fermions with the new mediator, $g_{fS}\overline{F}_L S f_R$, as the term still transforms as a weak doublet instead of a weak singlet due to the transformation properties of the fermion current, $\overline{F}_L f_R \sim \mathbf{2}$, and mediator, $S \sim \mathbf{1}$, under $SU(2)_L$.

Some of the primary applications for simplified model results are:

---

[4]In fact, the LHC-Run I used EFT to derive exclusion limits via mono-X searches whereas LHC-Run II employed simplified models.
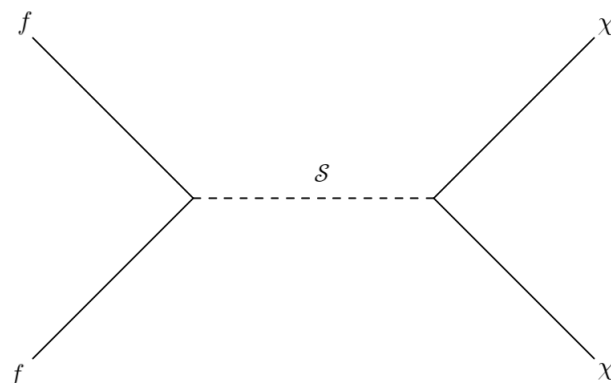
FIGURE 3.2: Feynman diagram of the DM simplified model. Here f represents a SM fermion whereas χ a fermionic DM particle and $\mathcal{S}$ a scalar mediator.

- **Identifying sensitivity boundaries**: The evaluation of any LHC searches must include sensitivity boundaries, with this information both theorists and experimentalists can identify kinematic regions where the search strategies need to be improved or generalized. Simplified models are also useful for estimating a search's sensitivity to alternative BSM models in simulated Monte Carlo events.

- **Characterizing new physics signals**: It is important to fully characterize the physics of a NP signal once it is observed. Simplified models can help to identify important mass ranges, decay widths, cross sections and, in particular, the particle quantum numbers [144, 145].

- **Deriving limits on more general models**: By using limits from simplified models, one can derive constraints on a variety of models. This can be done by adding the effective cross-section for each model's topology, weighted by their experimental efficiencies, and then comparing the result to the upper bound imposed by the simplified model.

For more information on simplified models and its applications see Ref. [88, 146–150]. Let us now explore an explicit example of a simplified model in which both the dark matter particle as well as a new scalar mediator are added to the SM content.

Simplified Dark Matter Models

There are several simplified DM models [150–154] that are well summarized in Figure 1 of Ref [154]. In general, these models are characterized by a DM particle and a mediator. The latter typically serves as a bridge between the SM fields and the dark sectors [5], see, for example, Fig. 3.2.

The most conventional choice for simplified models is the following one. The particles and interactions for the model with fermionic DM (χ) and a scalar mediator ($\mathcal{S}$) is

---

[5]In principal, the mediator could also couple to gluons or other SM bosons.

described by the following Lagrangian:

$$\mathcal{L}_{simp} = \mathcal{L}_{SM} + \frac{1}{2}(\partial_\mu \mathcal{S})^2 - \frac{1}{2}m_{\mathcal{S}}^2 \mathcal{S}^2 + i\overline{\chi}\slashed{\partial}\chi - m_\chi\overline{\chi}\chi - g_\chi \mathcal{S}\overline{\chi}\chi - \sum_{fermions} g_{sf}\frac{y_f}{\sqrt{2}}\mathcal{S}\overline{f}_R f_L \ , \quad (3.10)$$

notice how all operators in the simplified Lagrangian are renormalizable. The SM then acquires five new free parameters: The DM particle and the mediator mass m_χ and $m_{\mathcal{S}}$, the DM-S coupling g_χ, the SM-S coupling g_{sf} and the mediator decay width $\Gamma_{\mathcal{S}}$. The latter can be either fix or let open, allowing the possibility of decaying to additional (new) particles. For a pseudo scalar mediator approach see Ref. [151, 155].

In DM models, it is common to implement a Z_2 symmetry and assign an odd parity to the DM particle, so it becomes stable. We can also consider the mediator or a set of SM fermions to be charged under such a symmetry, as we will see in Sec. 3.3. It is important to be careful with the SM accidental global symmetries, in fact, processes that violate such symmetries are highly constrained.

3.3 extended Dark Matter Effective Field Theory

Now that we have discussed EFTs, dark matter and simplified models, we have all the requirements needed to explain the extended dark matter EFT (eDMEFT). As depicted in Fig. 3.3, EFTs are model independent, as the heavy new particles do not appear explicitly in the Lagrangian, but are rather manifested as a suppression factor, Λ^{-1}. Therefore, Λ can represent any new particle at energies higher than the effective theory. On the other hand, DM experiments run in a wide energy range. From DD experiments, probing recoil energies at keV, to the large momentum transfer in LHC collisions at TeV range. EFTs are particularly useful for the former, as the SM content is extended uniquely by a DM candidate, then we can set limits on the Wilson coefficients, (see e.g. Ref. [116, 156–158]) while the mediator, with mass typically assumed in the GeV range, can be safely integrated out. On the other hand, EFTs suffer a breakdown in searches at colliders, which are normally sensitive to mediator masses at/or below the scale of reached momentum transfers, in the case of LHC the energy of the collisions is high enough to detect particles of mass~TeV, and therefore would require the explicit presence of the heavy particle in the Lagrangian. Moving forward, simplified models include all new (heavy) particles, in a renormalizable theory, allowing a direct search for the mediators. This also improves the LHC kinematics, as we have much more information to characterize and reconstruct the events. However, the presence of the mediator in the simplified models has a price to pay, as we lose the model-independence that was present in the EFTs, furthermore, some important terms might not be gauge invariant, and therefore problematic, as mentioned above. Finally, simplified models still make very specific assumptions on the new particles, and do not allow to model a richer NP sector.

We then would like a single, consistent, and general framework with as few free parameters as possible. As an attempt to reach this theory in Ref. [9] is proposed a hybrid approach that combines the best of EFTs and simplified models in a DM framework. This model is a proper field theory, where gauge invariance stays intact. It offers the
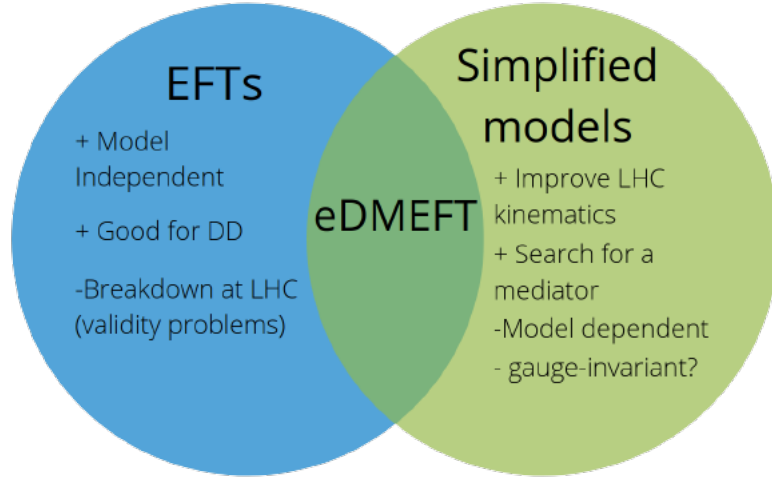
FIGURE 3.3: Pros (+) and cons (-) of EFTs and simplified models. Here the intersection of the positive aspects of the two approaches represents the extended dark matter EFT framework.

possibility to interpret various DD, ID and collider DM searches. The eDMEFT content consists of the SM enlarged by a (Dirac) DM fermion χ, that behaves as a singlet under the SM gauge group[6] and a (pseudo-)scalar mediator $(\widetilde{S})S$. The interactions of the mediator with SM fields are realized, in a gauge invariant way, via dimension five operators, this allows the search of the mediator at colliders. Additionally, we can achieve the correct DM relic abundance in several regions as will be discussed later. The inclusion of the most general set of (non-redundant) dimension five operators, allows us to consider richer new physics sectors, than the ones extended by only a single dark state and a mediator.

We will introduce the corresponding effective Lagrangians for a (pseudo-)scalar in Sec. 3.3.1 and discuss their basic features [9, 160]. We also present a case study in Sect. 3.4 and explore the phenomenology in current (LHC) and future (HL-LHC and CLIC) colliders [10].

---

[6]Even though it is possible to consider vectorial and scalar DM, they are not included in the following, and therefore will not be mentioned. For more information refer to Ref. [159].

3.3.1 (Pseudo-)Scalar Mediator

The effective Lagrangian, for a scalar mediator $\mathcal{S}$ and fermionic DM χ, including operators up to dimension five reads [9]

$$
\begin{aligned}
\mathcal{L}_{\text{eff}}^{\mathcal{S}\chi} =\ & \mathcal{L}_{\text{SM}} + \frac{1}{2}\partial_\mu \mathcal{S}\partial^\mu \mathcal{S} - \frac{1}{2}\mu_{\mathcal{S}}^2 \mathcal{S}^2 + \bar{\chi}i\slashed{\partial}\chi - m_\chi \bar{\chi}\chi - \lambda_{S1}' v^3 \mathcal{S} - \frac{\lambda_S'}{2\sqrt{2}}v\mathcal{S}^3 - \frac{\lambda_S}{4}\mathcal{S}^4 \\
& - \lambda_{HS}' v|H|^2 \mathcal{S} - \lambda_{HS}|H|^2 \mathcal{S}^2 - (y_S \mathcal{S}\bar{\chi}_L \chi_R + \text{h.c.}) \\
& - \frac{\mathcal{S}}{\Lambda}\left[c_{\lambda S}\mathcal{S}^4 + c_{HS}|H|^2 \mathcal{S}^2 + c_{\lambda H}|H|^4 \right] \\
& - \frac{\mathcal{S}}{\Lambda}\left[(y_d^S)^{ij}\overline{Q}_L^i H d_R^j + (y_u^S)^{ij}\overline{Q}_L^i \tilde{H}u_R^j + (y_\ell^S)^{ij}\overline{L}_L^i H\ell_R^j + \text{h.c.} \right] \\
& - \frac{y_S^{(2)}\mathcal{S}^2 + y_H^{(2)}|H|^2}{\Lambda}\overline{\chi}_L \chi_R + \text{h.c.} \\
& - \frac{\mathcal{S}}{\Lambda}\frac{1}{16\pi^2}\left[g'^2 c_B^S B_{\mu\nu}B^{\mu\nu} + g^2 c_W^S W^{I\mu\nu}W_{\mu\nu}^I + g_s^2 c_G^S G^{a\mu\nu}G_{\mu\nu}^a \right].
\end{aligned}
\tag{3.11}
$$

Here Q_L^i and L_L^i are the i-th generation left-handed $SU(2)_L$ quark and lepton doublets, respectively, while d_R^j, u_R^j, and ℓ_R^j are the right-handed singlets for generation j. $H = (2)^{-1/2}(0, v+\phi)^T$ is the SM Higgs scalar doublet in the unitary gauge with a vev, $v = 246$ GeV. In this case the extra scalar singlet does not get a vev and thus, develop a mass $m_S = (\mu_S^2 + \lambda_{HS}v^2)^{1/2}$ after the EWSB. In order to couple the mediator to the SM fermions, it is necessary the presence of a Higgs doublet, allowing for dimension five Yukawa-like couplings, $\sim (y_d^S)^{ij}, (y_u^S)^{ij}$. All high-dimensional terms are suppressed by the energy scale Λ. The interactions between DM and the SM fields involve one or two scalar singlets or two doublets due to gauge invariance, parametrized by y_S, $y_S^{(2)}$ and $y_H^{(2)}$, respectively. $c_B^{\mathcal{S}}$, $c_G^{\mathcal{S}}$ and $c_W^{\mathcal{S}}$ correspond to the effective couplings between $\mathcal{S}$ and the $U(1)_Y$, $SU(3)_c$ and $SU(2)_L$ field strength squared.

The complete set of coefficients in the Lagrangian are assumed to be real as the scalar interactions are invariant under CP. A symmetry for stabilizing the DM particle forbids the $L\tilde{H}\chi_R$ term preventing it from acting like a right handed neutrino. Lastly, if the suppressed dimension five sector is governed by a coupling g_*, then, the effective couplings can obtain a scaling, in this case is $c_{\lambda S} \sim c_{HS} \sim c_{\lambda H} \sim g_*^3$, $y_f^S \sim y_f g_*$, $y_{S,H}^{(2)} \sim g_*^2$ and $c_V^S \sim g_*$. This order the operators by their expected importance in a certain couple regime, and can allow to reduce the number of higher-dimension operators at leading order approximation, for example, in the case of $D = 6$ operators for a vector mediator [9].

The eDMEFT Lagrangian allows all possible DM searches. For example, if the coupling $(y_q^S)^{ij}/\Lambda$ is non-negligible, the interaction between DM and a nucleus can be mediated by the $\mathcal{S}\overline{Q}_L^i Hq_R^j$ operator, coupling the scalar mediator to the DM via the linear term $\mathcal{S} \to \chi\chi$, which is allowed. Additionally, DM can be searched at the LHC via mono-jet or mono-Higgs + missing transverse energy ($\not{E}_T$). Finally, direct detection

bounds can be set, for example, if we turn on the coupling $(y_u^s)^{11}$, while y_S is fixed such as to produce the correct relic abundance, via $\chi\overline{\chi} \to \mathcal{S}\mathcal{S}$ decay (here $m_{DM} > m_{\mathcal{S}}$).

The Yukawa couplings $(y_q^{\mathcal{S}})^{ij}$ can produce FCNCs. Some mechanisms like minimal flavour violations could be implemented, however, this could lead to a suppression in the coupling to the light valence quarks and these small effects at colliders. In Chapter 2 and Sec. 3.4, we explored other options to avoid FCNCs. For more information, please refer to [9, 160].

In the case of a CP-odd scalar mediator $\widetilde{\mathcal{S}}$, DD searches are much weaker, due to momentum suppression of the cross section. The effective Lagrangian in the pseudo-scalar case reads

$$
\begin{aligned}
\mathcal{L}_{\text{eff}}^{\widetilde{\mathcal{S}}\chi} = {} & \mathcal{L}_{\text{SM}} + \frac{1}{2}\partial_\mu\widetilde{\mathcal{S}}\partial^\mu\widetilde{\mathcal{S}} - \frac{1}{2}\mu_{\widetilde{\mathcal{S}}}^2\widetilde{\mathcal{S}}^2 + \overline{\chi}i\partial\!\!\!/\chi - m_\chi\overline{\chi}\chi - \frac{\lambda_{\widetilde{\mathcal{S}}}}{4}\widetilde{\mathcal{S}}^4 \\
& - \lambda_{H\widetilde{\mathcal{S}}}|H|^2\widetilde{\mathcal{S}}^2 - (y_{\widetilde{\mathcal{S}}}\widetilde{\mathcal{S}}i\overline{\chi}_L\chi_R + \text{h.c.}) \\
& - \frac{\widetilde{\mathcal{S}}}{\Lambda}\left[i(y_d^{\widetilde{\mathcal{S}}})^{ij}\overline{Q}_L^i H d_R^j + i(y_u^{\widetilde{\mathcal{S}}})^{ij}\overline{Q}_L^i \tilde{H} u_R^j + i(y_\ell^{\widetilde{\mathcal{S}}})^{ij}\overline{L}_L^i H \ell_R^j + \text{h.c.} \right] \\
& - \left[\frac{y_{\widetilde{\mathcal{S}}}^{(2)}\widetilde{\mathcal{S}}^2 + y_H^{(2)}|H|^2}{\Lambda}\overline{\chi}_L\chi_R + \text{h.c.} \right] \\
& - \frac{\widetilde{\mathcal{S}}}{\Lambda}\frac{1}{16\pi^2}\left[g'^2 c_B^{\widetilde{\mathcal{S}}}\tilde{B}_{\mu\nu}B^{\mu\nu} + g^2 c_W^{\widetilde{\mathcal{S}}}W^{I\mu\nu}\tilde{W}_{\mu\nu}^I + g_s^2 c_G^{\widetilde{\mathcal{S}}}G^{a\mu\nu}\tilde{G}_{\mu\nu}^a \right] \, .
\end{aligned}
\tag{3.12}
$$

Note that, due to CP-conservation, the portal with a single mediator vanishes. We assume that $\widetilde{\mathcal{S}}$ does not develop a vacuum expectation value. Therefore, there is no mixing between the SM Higgs and the pseudoscalar mediator, and Higgs precision observations are less sensitive to this model. For further details on the DM phenomenology in both the scalar and pseudoscalar cases, see Ref. [160]. Additionally, in the next section, we investigate an end-to-end case study to explore the power of eDMEFT.

3.4   Case Scenario: $Di - jet/e^+e^-$

Let us now exemplify the eDMEFT through a case study based on Ref. [10]. We start from the Lagrangian in Eq. (3.11) where the SM gets enlarged by a Dirac fermion, χ, which represents DM, and a real scalar mediator, $\mathcal{S}$. DM stability comes from implementing a parity symmetry, Z_2, where the new fermion, χ, is assigned an odd parity, $\chi \xrightarrow{Z_2} -\chi$. Furthermore, the new scalar mediator together with the first fermion generation, gets an odd parity, thus an explanation to the smallness of the first-generation fermion masses via suppressed Z_2-breaking effects, see below. We then focus in the phenomenology of the $D = 5$ operator $\mathcal{S}^2\overline{\chi}_L\chi_R$, which can give rise to interesting di-jet/lepton + $\not{E}$ phenomenology at colliders. If the dimension four operator $\mathcal{S}\overline{\chi}_L\chi_R$ is forbidden by imposing the Z_2 symmetry, its coupling, which is the main portal to the dark sector, could be missed in DD experiments, while mono-jet searches should be adjusted to take advantage of the di-fermion final state. In the following, we perform

	$\chi_{L(R)}$	$\mathcal{S}$	q_{uR}	q_{cR}	q_{tR}	q_{dR}	q_{sR}	q_{bR}	e_R	μ_R	τ_R
Z_2	-	-	-	+	+	-	+	+	-	+	+

TABLE 3.1: Transformation sign under the Z_2 symmetry for the scalar mediator $\mathcal{S}$, the DM fermion, and the SM right-handed fermions.

di-jet searches in the (HL-)LHC and the e^+e^- future collider CLIC. We find that the latter delivers better constraints and therefore motivates a leptophilic mediator. We also highlight the parameter space that allows us to produce the observed DM density and include constraints from DD.

General Setup

As mentioned before, we start from Eq. (3.11) with the additional assumption of a symmetry forbidding the $D = 4$ interaction of $\mathcal{S}$ with DM. To this end, we assigned an odd parity to the scalar mediator, $\mathcal{S} \xrightarrow{Z_2} -\mathcal{S}$. The smallness of the first-fermion generation, $m_{2,3} \gg m_1$, can be tackled by assuming that all the SM fields are even under the parity symmetry, with the exception of the right-handed first fermion generation, which is considered odd. A summary of the charges is shown in Table 3.1. As a consequence the new CP-even mediator will uniquely couple to the first fermion generation and will be blind to the others. On the other hand, the Z_2-odd fermions are blind to the SM Higgs boson. However, as now $\mathcal{S}$ has a vev, their mass will only come through $\mathcal{S}$, as discussed later. In the following, we assume the absence of right handed neutrinos, hence no mass term is included in the Lagrangian.

After implementing the Z_2 symmetry, many terms of the original eDMEFT Lagrangian in Eq. (3.11) vanish: those with an odd power of the mediator, unless they feature a right-handed fermion from the first generation (e_R, u_R, d_R). The corresponding Lagrangian for this specific setup then reads

$$
\begin{aligned}
\mathcal{L}_{\text{eff}}^{\mathcal{S}\chi} = {} & \mathcal{L}_{\text{SM}} + \frac{1}{2}\partial_\mu\mathcal{S}\partial^\mu\mathcal{S} - \frac{1}{2}\mu_{\mathcal{S}}^2\mathcal{S}^2 + \overline{\chi}i\slashed{\partial}\chi - m_\chi\overline{\chi}\chi \\
& - \frac{\lambda_{\mathcal{S}}}{4}\mathcal{S}^4 - \lambda_{H\mathcal{S}}|H|^2\mathcal{S}^2 \\
& - \frac{\mathcal{S}}{\Lambda}\left[(y_d^{\mathcal{S}})_i\overline{Q}_L^i H d_R + (y_u^{\mathcal{S}})_i\overline{Q}_L^i \tilde{H} u_R + (y_\ell^{\mathcal{S}})_i\overline{L}_L^i H e_R + \text{h.c.}\right] \\
& - \left[\frac{y_\chi^H|H|^2}{\Lambda}\overline{\chi}_L\chi_R + \frac{y_\chi^{\mathcal{S}}\mathcal{S}^2}{\Lambda}\overline{\chi}_L\chi_R + \text{h.c.}\right],
\end{aligned}
\tag{3.13}
$$

where we follow the notation presented in Sec. 3.3.1. The red-colored operators are the main focus for the phenomenology study below.

Unlike the original eDMEFT setup, the SM Yukawa couplings of the first generation are now forbidden at the renormalizable level, therefore, their masses will only be generated via small Z_2-breaking effects equipped with an additional cutoff suppression. In return, we assume the mediator develops a small vev $|\langle\mathcal{S}\rangle| \equiv v_{\mathcal{S}} \sim \mathcal{O}(10)$ MeV, which

is enough to generate the masses for the first fermion generation. The fact that there are now two scalars ($\mathcal{S}$ and H) with two different vev scales (MeV and GeV) offers the possibility to address the lightness of the light fermions. Although it would be interesting to tackle all flavour hierarchies with a more extended scalar sector, this is beyond the scope of this discussion. The resulting mixing with the Higgs via the $|H|^2 \mathcal{S}^2$ operator is suppressed, and thus it is not considered in the following. Furthermore, the *usual* dark matter coupling $\mathcal{S}\bar{\chi}\chi$ is generated by the spontaneous breaking of the Z_2 symmetry, with coefficient $\sim 2y_\chi^\mathcal{S} v_\mathcal{S}/\Lambda$. The latter is highly suppressed and only plays a role in DD experiments. In order to avoid DD constraints and limits from invisible Higgs decays (for light dark matter) [161], the coefficient of the second $D = 5$ portal to the dark sector allowed by the symmetry, $|H|^2 \bar{\chi}_L \chi_R$, is taken to be small from the start (recall that $v_\mathcal{S}/v \sim \mathcal{O}(10^{-4})$) and therefore is not included in the discussion below.

Fermion Masses

For simplicity, we only present the mass mechanism for quarks. However, the lepton case is analogous. The resulting mass terms after spontaneous symmetry breaking read

$$\mathcal{L} \supset - \sum_{q=u,d} \bar{q}_L \frac{v}{\sqrt{2}} \left(\mathbf{Y}_q^H + \frac{v_\mathcal{S}}{\Lambda} \mathbf{Y}_q^\mathcal{S} \right) q_R \equiv - \sum_{q=u,d} \bar{q}_L \mathbf{M}^q q_R \,, \tag{3.14}$$

where $q = u, d$ are three-vectors in flavour space and the Yukawa matrices

$$\mathbf{Y}_q^H = \begin{pmatrix} 0 & y_{12}^q & y_{13}^q \\ 0 & y_{22}^q & y_{23}^q \\ 0 & y_{32}^q & y_{33}^q \end{pmatrix} \,, \qquad \mathbf{Y}_q^\mathcal{S} = \begin{pmatrix} (y_q^\mathcal{S})_1 & 0 & 0 \\ (y_q^\mathcal{S})_2 & 0 & 0 \\ (y_q^\mathcal{S})_3 & 0 & 0 \end{pmatrix} \tag{3.15}$$

reflect the Z_2 assignments. Here we can explicitly see that without the breaking of the latter symmetry via $v_\mathcal{S} > 0$, the first quark family would remain massless, corresponding to the vanishing eigenvalue of $\mathbf{Y}_q^H$. On the other hand, a small breaking of $v_\mathcal{S} \sim \mathcal{O}(10)$ MeV is enough to generate $m_u \sim m_d \sim 5$ MeV with $\mathcal{O}(1)$ Yukawa couplings and $\Lambda \gtrsim 1$ TeV. Note that, even though the main contribution for the masses of the first quark generation comes through the scalar mediator $\mathcal{S}$, when moving to the mass basis, the diagonal terms will have the form $\sim v\hat{\mathbf{Y}}_{kk}^H + v_\mathcal{S}\hat{\mathbf{Y}}_{kk}^\mathcal{S}$ and therefore the SM Higgs will have a non-neglecting contribution too. However, these could be cancelled by an appropriate choice of alignment for the Yukawa matrices, i.e. if one forces the columns to be orthonormal among each other. We will come back to this point later.

After performing a rotation to the mass basis

$$\begin{aligned} \mathbf{M}_{diag}^u &= \mathrm{diag}(m_u, m_c, m_t) = \mathbf{U}_L^u \, \mathbf{M}^u \mathbf{U}_R^{u\,\dagger} \,, \\ \mathbf{M}_{diag}^d &= \mathrm{diag}(m_d, m_s, m_b) = \mathbf{U}_L^d \, \mathbf{M}^d \mathbf{U}_R^{d\,\dagger} \end{aligned} \tag{3.16}$$

with $\mathbf{U}_L^d = \mathbf{U}_L^u \, \mathbf{V}_{\mathrm{CKM}}$, we obtain the couplings of the physical quarks to the Higgs boson and the scalar mediator $\hat{\mathbf{Y}}_q^s = \mathbf{U}_L^{q\,\dagger} \mathbf{Y}_q^s \mathbf{U}_R^q$, $s = H, \mathcal{S}$; with $q = u, d$. In the new basis, the

interaction Lagrangian then reads

$$\mathcal{L} \supset - \sum_{q=u,d} \bar{q}_L \left(\frac{\hat{\mathbf{Y}}_q^H}{\sqrt{2}} h + \frac{v_\mathcal{S} \hat{\mathbf{Y}}_q^S}{\sqrt{2}\Lambda} h + \frac{v \, \hat{\mathbf{Y}}_q^S}{\sqrt{2}\Lambda} \, \mathcal{S} \right) q_R \,, \tag{3.17}$$

where the second term is small and then ignored. In particular the last term in Eq.(3.17) is crucial to test the $\mathcal{S}^2\chi^2$ operator at colliders, as it bridges the SM with the dark sector. As the mass matrices $\mathbf{M}^{u,d}$ receive contributions from different sources (see Eq. (3.14)) and are, in general, not aligned with the individual scalar-fermion couplings $\sim y_q^{H,S}$, the new Yukawa matrices $\hat{\mathbf{Y}}_q^{H,S}$ are not diagonal thus inducing FCNCs. In the following, we present a way to overcome such undesirable effects.

Flavour Structure

As seen before, FCNCs are present in the model. Although this might provide interesting phenomenology, here we opt for a simpler scenario where they are absent at tree level. To this end, we first note that, in the interaction basis, the Yukawa matrices can be expressed in terms of the mass matrices as

$$\mathbf{Y}_q^S = \frac{\sqrt{2}\Lambda}{vv_\mathcal{S}} \mathbf{M}^q \operatorname{diag}(1,0,0) = \frac{\sqrt{2}\Lambda}{vv_\mathcal{S}} \mathbf{U}_L^q \mathbf{M}_{\operatorname{diag}}^q \mathbf{U}_R^{q\dagger} \operatorname{diag}(1,0,0) \,,$$

$$\mathbf{Y}_q^H = \frac{\sqrt{2}}{v} \mathbf{M}^q \operatorname{diag}(0,1,1) = \frac{\sqrt{2}}{v} \mathbf{U}_L^q \mathbf{M}_{\operatorname{diag}}^q \mathbf{U}_R^{q\dagger} \operatorname{diag}(0,1,1) \,. \tag{3.18}$$

In the mass basis, they become

$$\hat{\mathbf{Y}}_q^S = \frac{\sqrt{2}\Lambda}{vv_\mathcal{S}} \mathbf{M}_{\operatorname{diag}}^q \mathbf{U}_R^{q\dagger} \operatorname{diag}(1,0,0) \mathbf{U}_R^q \,,$$

$$\hat{\mathbf{Y}}_q^H = \frac{\sqrt{2}}{v} \mathbf{M}_{\operatorname{diag}}^q \mathbf{U}_R^{q\dagger} \operatorname{diag}(0,1,1) \mathbf{U}_R^q \,, \tag{3.19}$$

where the unitary rotations of the left-handed fermion fields drop out since they share the same Z_2 charges and their couplings with a fixed right-handed fermion are thus aligned with the corresponding mass terms. This is not true for the right handed fermions, where the corresponding rotation matrices induce a misalignment

$$\mathbf{U}_R^{q\dagger} \operatorname{diag}(0,1,1) \mathbf{U}_R^q \neq \operatorname{diag} \tag{3.20}$$

and thus, FCNCs could be produced at tree level.

However, the latter could be avoided by introducing the ansatz $\mathbf{U}_R^u = \mathbf{1} = \mathbf{U}_R^d$ [7]. The left-handed rotations can be arbitrary with the only constraint $\mathbf{U}_L^{u\dagger}\mathbf{U}_L^d = \mathbf{V}_{\text{CKM}}$ [8]. The ansatz is equivalent to having assumed the Yukawa matrices to be singularly aligned in

---

[7] A more extensive analysis of FCNCs could be interesting but it is out of the scope of this thesis.

[8] It would not be possible to ask for $\mathbf{U}_L^u = \mathbf{1} = \mathbf{U}_L^d$, since then, $\mathbf{V}_{CKM} = \mathbf{1}$ is in conflict with observations
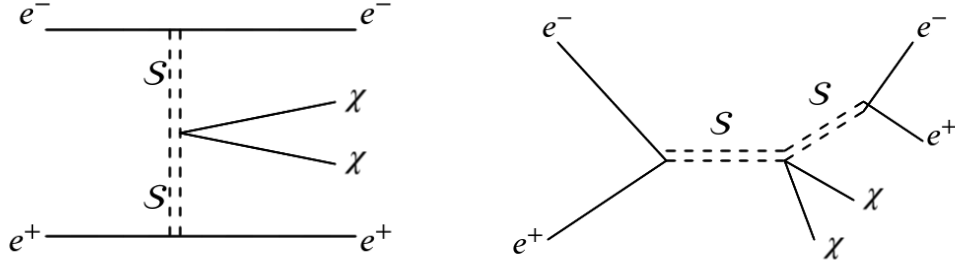
FIGURE 3.4: Feynman diagrams for dark matter + di-electron production at CLIC – for the (HL-)LHC case, the electrons are replaced by up and down quarks.

flavour space [8] as discussed in Sec. 2.7. We thus end up with only diagonal couplings

$$\hat{\mathbf{Y}}_u^S = \frac{\sqrt{2}\Lambda}{v v_S} \operatorname{diag}(m_u, 0, 0) \qquad \hat{\mathbf{Y}}_d^S = \frac{\sqrt{2}\Lambda}{v v_S} \operatorname{diag}(m_d, 0, 0)$$
$$\hat{\mathbf{Y}}_u^H = \frac{\sqrt{2}}{v} \operatorname{diag}(0, m_c, m_t) \qquad \hat{\mathbf{Y}}_d^H = \frac{\sqrt{2}}{v} \operatorname{diag}(0, m_s, m_b). \tag{3.21}$$

As mentioned in the beginning of this section, the lepton sector has a similar setup leading directly to

$$\hat{\mathbf{Y}}_e^S = \frac{\sqrt{2}\Lambda}{v v_S} \operatorname{diag}(m_e, 0, 0), \quad \hat{\mathbf{Y}}_e^H = \frac{\sqrt{2}}{v} \operatorname{diag}(0, m_\mu, m_\tau). \tag{3.22}$$

The Higgs boson is then responsible for the mass of the second and third generation only, while the first generation couples instead to the DM mediator, with strength determined by the free parameter v_S, which we will trade for $y_u^S/\Lambda \equiv (\hat{Y}_u^S)_{11}/\Lambda$ in the following. This requires the previous ratio to not be too tiny, since then a very large Z_2-breaking v_S would be required to reproduce the quark masses, as discussed, $\mathcal{O}(1)$ values of $y_u^S v/\Lambda$ are in perfect agreement with a modest vev of 10 MeV and a reasonable cutoff of 1 TeV. Thus, we can express all S-Yukawas in terms of y_u^S. We obtain the approximate relations

$$y_e^S = 0.1 \, y_d^S = 0.2 \, y_u^S \tag{3.23}$$

for the couplings of the mediator to SM fermions, and the values $m_u = 2.5\,\text{MeV}, m_d = 5\,\text{MeV}, m_e = 0.5\,\text{MeV}$. As mentioned, y_u^S/Λ can be chosen basically free as long as it does not violate perturbativity of the EFT (and of the potentially UV completion), which constrains $y_f^S v/(\sqrt{2}\Lambda) < 4\pi$ $(y_f^S < (4\pi)^2)$, for $f = u, d, e$, where we made use of the fact that the S−Yukawa scales like $y_f^S \sim g_{\text{UV}}^2$. This relation is particularly important because it allows a connection between the quark and lepton sectors, that later will allow to convert, for example, direct detection limits, made for quarks only, to lepton colliders.

Relevant Parameters

In the coming sections, we derive the prospects to constrain the $\mathcal{S}^2\overline{\chi}_{\mathrm{L}}\chi_{\mathrm{R}}$ portal and the $\mathcal{S}$-Yukawa coupling from (HL)-LHC and future e^+e^- collider data, meeting constraints from DD and the observed relic density. For that purpose, note that the relevant physical parameters in the model are:

- the DM mass m_χ,

- the mediator mass $m_\mathcal{S} = \sqrt{\mu_\mathcal{S}^2 + 3\lambda_\mathcal{S} v_\mathcal{S}^2}$,

- the bi-quadratic portal coupling $y_\chi^\mathcal{S}/\Lambda$,

- and the $\mathcal{S}-$Yukawa coupling $y_u^\mathcal{S}/\Lambda$,

where we neglected the potential scalar mixing from $\lambda_{H\mathcal{S}}$. While this defines the main full model, where the mediator couples to both quarks and leptons, there are also two interesting variants obtained by either assigning positive Z_2 parity to all leptons or to all quarks, then the mediator would just couple to one sector in each case. In return, this would lead to a *leptophobic* or *hadrophobic* mediator, respectively, with $y_e^\mathcal{S} = 0$ and finite $y_d^\mathcal{S} = 2y_u^\mathcal{S}$ or vice versa.

In the following, we study a unique process where the new portal manifests through the fermion-pair-associated DM production, in both the t and s channel, as depicted in Fig. 3.4, where the DM is presented as a signature of missing energy. We consider the mediator to be much heavier than its vev ($m_\mathcal{S} = 200$ GeV), which requires a decoupling by an additional contribution to the Lagrangian in Eq. (3.13). This however has several solutions. One is to add a cubic term of the form $g_{\mathcal{S}3}v_\mathcal{S}\mathcal{S}^3$. Nonetheless it needs a very large (non-perturbative) coefficient of around 100 TeV. Another possibility is to add a second singlet $\mathcal{S}_2$, already envisaged before, with a vev v_2 around 10^2 GeV and a mixing between $S S_2$ of around $\mu_{12} \sim 1$ GeV. Finally, another possibility is to look for a $\mathcal{S}\mathcal{S}_2^3$ portal with coefficient $\mathcal{O}(10^{-6})$. We have checked other effects of the new scalar including mixing with the Higgs, and in all cases the vev and the mass can be effectively decoupled.

(HL-)LHC Searches

For simplicity, in this section we assume that the mediator only couples to the quarks, i.e. $y_e^\mathcal{S} = 0$. Then, we say that the scalar singlet has a *leptophobic* (or *hadrophilic*) nature. To constrain $y_\chi^\mathcal{S}$ we use a unique signature, di-jet + $\not{E}$ as shown in Fig. 3.4 by replacing the electrons with up or down quarks. To derive bounds from (projected) current (HL-)LHC runs on the new DM portal, we employ the eDMEFT UFO [162] file generated with FeynRules [163, 164] then, we simulate events with Mad-Graph5_aMC@NLO (v 2.6.5) [165,166] and perform the detector simulation and parton-showering with `Delphes` [167] and `Pythia` [168,169], accordingly. Lastly, we employ CheckMate [170,171] implementations of ATLAS analyses, in particular we considered the mono-jet search in Ref. [172] using 36.1 fb^1 of data and a search for multiple jets
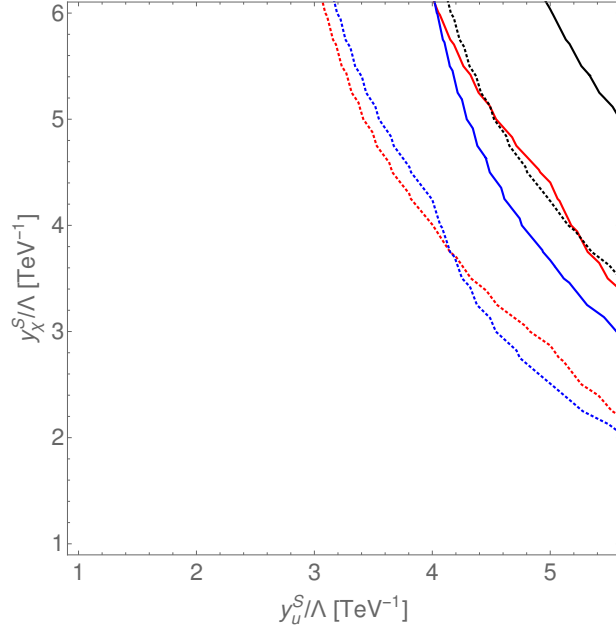
FIGURE 3.5: Exclusion reach of the current (solid) and future HL-LHC run (dotted) for $m_\mathcal{S} = 200$ GeV and DM masses of 5 GeV (red), 100 GeV (blue), 300 GeV (black).

+ $\not{E}_T$ in Ref. [173]. A dedicated analysis of the particular di-jet signature is expected to improve the sensitivity. However, we leave a detailed and personalized study for future work and only focus on future leptonic colliders. The latter having an advantageous reduction of the large QCD background faced at the LHC searches, thus we expect tighter limits [9].

One disadvantage of the aforementioned ATLAS analyses is the high energy used for the events, as it is above the suggested cutoff $\Lambda = \mathcal{O}(1)$ TeV and then the validity become questionable [98, 174, 175]. The scalar sum of the transverse momenta of the leading N jets and E_T^{miss} is required to be at least 1.6 TeV. Therefore, a reasonable value for the cutoff is at least $\Lambda \gtrsim 3$ TeV . In addition, all signal regions are inclusive ones, which means that they include events with even higher energies, such that the resulting constraints would only be valid for borderline large couplings $y_u^\mathcal{S}$. In contrast, exclusive signal regions (EM) for the the mono-jet analysis provided in [172] allow for a better estimate of the momentum flow of an event. To obtain robust limits we constrain our analysis to signal regions up to EM6 of Ref. [172], containing events with missing energy $(\not{E}_T) = (600 - 700)$ GeV.

In Fig. 3.5, we show the actual bounds on the $y_u^\mathcal{S} - y_\chi^\mathcal{S}$ plane for the LHC (solid lines) and the projections for the HL-LHC with a luminosity of 3 ab^{-1} (dotted lines).

---

[9]The final state of Higgs-to-invisible in VBF production searches, is indeed similar to the final state in the current analysis. Nevertheless, we find that the signal and background distributions in the important kinematic variables are very similar and no efficient separation is possible.

Stage	$\sqrt{s}$ [TeV]	$\mathcal{L}$[ab^{-1}]
I	0.380	1.0
II	1.5	2.5
III	3	5.0

TABLE 3.2: Center of mass energy and luminosity for each realization of CLIC.

The masses considered for the analysis are m_S = 200 GeV for the mediator [10] and $m_\chi = \{5, 100, 300\}$ for the DM particle depicted in red, blue and black, correspondingly.

To obtain the projections, we use the r-value defined in CheckMate [171] with hand-scaling event numbers, thus assuming that ATLAS measures the same distributions. Following Ref. [177], we further assume that the systematic uncertainty on the SM background can be lowered by a factor of four. Note that, due to the nature of the process, the radiation of two DM particles coming from an internal mediator, the limits do not die off quickly when $m_\chi > m_S/2$, allowing this mass hierarchy to be tested, typically inaccessibly for colliders. As mentioned, further improvement could be reached by adjusting the analysis to the specific signature, e.g. by demanding two correlated jets in the final state.

Finally, we also estimate the effects of gauge boson couplings induced by light quark loops. These are suppressed by a quark mass insertion needed by the chirality flip. Therefore, the partial width of S to photons and gluons is smaller than the corresponding Higgs width by a factor of $\sim 10^5$ for photons and $\sim 10^3$ for gluons. We then conclude that the contribution of gluon-fusion to the production cross section can be neglected. The width to photons is more strongly suppressed, since the W-loop dominating the partial width of the SM Higgs [178], is absent. In addition, the $BR(S \to \gamma\gamma)$ is suppressed by the large decay width of the scalar mediator to quarks leading to no relevant constraints from present di-photon searches, see e.g. [179].

The Compact Linear Collider

An interesting proposal for a next high-energy e^+e^- collider is the Compact Linear Collider (CLIC) [11] to be build at CERN. It would be the first mature realization of a collider of such nature and, if realized, its first run would be in the year 2035. The plan includes three stages of 11, 29 and 50 Km long correspondingly. The luminosity per stage is depicted in Table 3.2.

In the following, we propose a search in the $e^+e^- + \not{E}_T$ final state as depicted in Fig. 3.4 where the right process dominates the cross section for large parts of the parameter space. From now on, we assume the mediator to be *hadrophobic*, i.e. S only couples to leptons, specifically to electrons and $y_u^S = y_d^S = 0$. The main irreducible background is

---

[10]While with this choice the flavour model considered is fine, note that for $m_S \gtrsim 225$ GeV strong bounds on the S-Yukawa couplings arise from the recent ATLAS search for resonant di-lepton production [176], which would exceed the projected limits of Fig. 3.5. Clearly, this can be avoided by moving either to the leptophobic or the hadrophobic scenario.
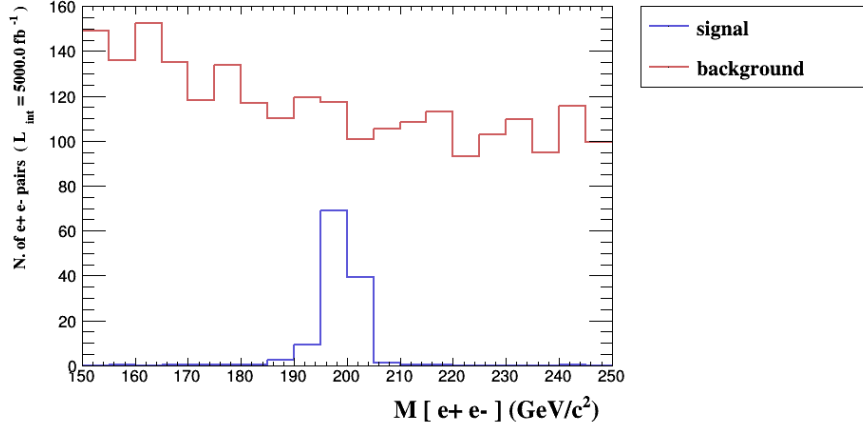
FIGURE 3.6: Comparison of the signal and background shape for CLIC Stage III. The signal events correspond to $y_e^S/\Lambda = 1.5/\text{TeV}$ and $y_\chi^S/\Lambda = 0.25/\text{TeV}$, close to the exclusion limit.

$e^+e^- \to e^+e^-\bar{\nu}\nu$ with the most important contribution coming from a ZZ intermediate state, and further backgrounds turn out to be negligible[11] as shown in Ref. [179]. To simulate the events, we use again MadGraph5_aMC@NLO for the event generation [165,166], `Pythia` 8.1 for the hadronization [168,169] and `Delphes` 3 for a fast detector simulation, fortunately, the latter has already a existing parameter card for the three CLIC stages [167]. The final analysis is performed with MadAnalysis 5 [180,181].

Even though the cut-and-count method is considerably better than in the previous LHC analysis, we still have to face a rather small signal with a sizable background. In particular, when the uncertainty in the background cross-section normalization is taken into account, leading to weak constraints. Nonetheless, the signal has a peak-like structure in the m_{ee}-variable compared to a smoothly falling background as shown in Fig. 3.6. This is observed due to an on-shell S decaying to electrons, as the resonant diagram in the right panel of Fig. 3.4 dominates the cross section. Therefore, we improve the analysis by performing a statistical shape analysis with a binned likelihood approach. This also reduces the impact of the uncertainty of the background normalization. Details to this procedure are laid out in Appendix C.

To achieve a preliminary separation between signal and background, we apply in all the stages the following cuts:

MET [GeV]	$m_{e^+e^-}$ [GeV]	$p_T(e)$ [GeV]	$\Delta R(e^+e^-)$	$\theta(e^+)$	$\theta(e^-)$
> 80	> 150	> 25	< 3.25	> 0.6	< 2.4

where the $m_{e^+e^-}$ cut is applied to lower the impact of Z decays. An example, for stage III, of the shape of the signal and background, after cuts and before fitting, are shown in Fig. 3.6. Here, the couplings $y_e^S/\Lambda = 1.5$ TeV and $y_\chi^S/\Lambda = 0.25$ TeV are chosen to be close to the exclusion limit.

---

[11]In general, neutrinos are the main background as they manifest also as missing energy at the detectors and then any process with neutrinos as a final state could affect the DM signal.
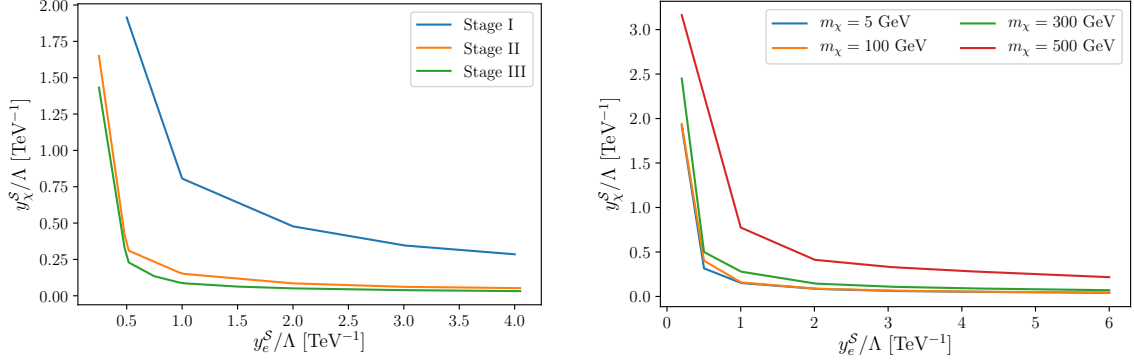
(A) Comparison of the expected limits on the couplings obtained at the three different stages of CLIC, assuming $m_\mathcal{S} = 200\,\mathrm{GeV}$ and $m_\chi = 5\,\mathrm{GeV}$.

(B) Expected limits on the couplings obtained at the second stage of CLIC, with $\sqrt{s} = 1.5\,\mathrm{TeV}$, for $m_\mathcal{S} = 200\,\mathrm{GeV}$ and several dark matter masses.

FIGURE 3.7: Exclusion Limits for CLIC in the $y_e^\mathcal{S} - y_\chi^\mathcal{S}$ plane.

Fitting Signal and Background

In order to use the m_{ee} spectrum to discriminate signal and background, we generate 50.000 signal and 10^6 background events. Since the signal shape depends on the width of $\mathcal{S}$, it is simulated for several values of the latter, depending non-trivially on the input parameters $m_\mathcal{S}$ and $y_e^\mathcal{S}/\Lambda$, given at the end of Sec. 3.4 where $m_\mathcal{S}$ and $y_e^\mathcal{S}$ have the greatest impact. To perform the analysis, we implement the corresponding cuts in MadAnalysis and generate histograms that are fitted to a fourth order polynomial for the background, and a simple Breit-Wigner distribution for the signal. Finally, the signal is characterized by the total number of events and the width of the Breit-Wigner distribution, allowing to easily test several couplings.

Resulting Constraints for CLIC

To establish constraints on the model parameters, it is necessary to translate the limits on the signal strength modifier, μ, into limits on the Yukawa couplings. Details on the statistics analysis and the Likelihood function are given in Appendix C. Note that, for fixed $y_\mathcal{S}^e$ and thereby for a fixed width and fixed shape of the m_{ee} distribution, we have $\mu = (y_\chi^\mathcal{S}/\Lambda)^2$. We also take into account for all limits a 5% uncertainty on the background normalization i.e., $\sigma_B = 0.05$, while σ_S is negligible.

The resulting limits in the $y_e^\mathcal{S} - y_\chi^\mathcal{S}$ plane are summarized in Fig. 3.7. In the left panel, Fig. 3.7a, we compare the reach of the three CLIC stages, assuming $m_\mathcal{S} = 200\,\mathrm{GeV}$ and $m_\chi = 5\,\mathrm{GeV}$. Note that the choice of the mass of the mediator is set in such a way that we evade LEP limits. We observe that already at the first stage we would be sensitive to $\mathcal{O}(1/\mathrm{TeV})$ couplings, while at the later stages the reach extends well beyond a TeV. On the other hand, in Fig. 3.7b, we explore the constraints for several DM masses, with a fixed $m_\mathcal{S} = 200\,\mathrm{GeV}$. The obtained limits are shown for the stage II, which demonstrates that the sensitivity does not vanish for $m_\chi/2 > m_\mathcal{S}$. We further note that our search is just sensitive to the product of the couplings, while e^+e^- resonance would be sensitive
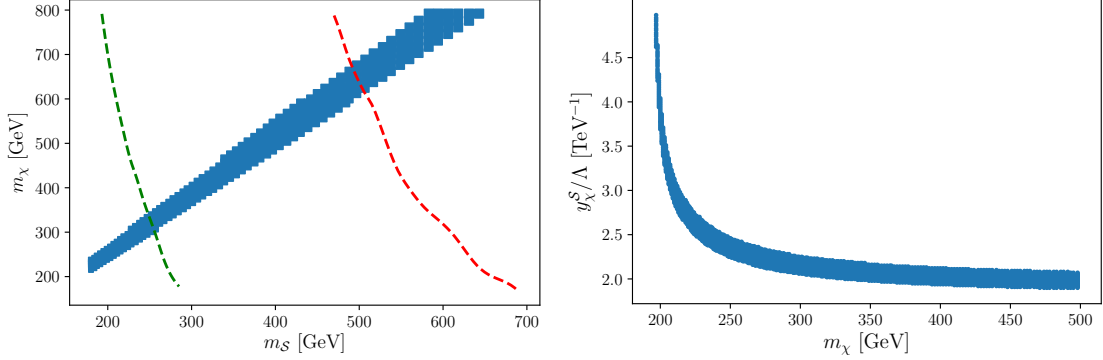
FIGURE 3.8: Left panel: Band of relic density $0.11 < h^2\Omega_{DM} < 0.13$ (dark blue) for $y_\chi^{\mathcal{S}} = 2.25$, independent of $y_{u,d,e}^{\mathcal{S}}$. Exclusions from XENON1T (to the left of the green line) and the LZ projection (to the left of the red curve) are superimposed (which however are not present for the hadrophobic model). The leftover space can be tested with DAR-WIN. Right Panel: Band of relic density $0.11 < h^2\Omega_{DM} < 0.13$ for $m_{\mathcal{S}} = 200\,\text{GeV}$.

only to the $y_e^{\mathcal{S}}$, breaking this degeneracy. This offers another way to test either full or part of the model, while still the dark matter search above would be crucial to probe the new $\mathcal{S}\mathcal{S}\chi\chi$ portal.

DM Phenomenology

Let us now address the fulfilment of the relic density. In this case, as we have allowed regions where the DM mass is larger than the mediator mass ($m_\chi \gtrsim m_{\mathcal{S}}$), the DM relic density is set via the process $\overline{\chi}\chi \to \mathcal{S}\mathcal{S}$, while for smaller dark matter masses it is always far above the measured value since no decay channel is kinematically allowed. We have verified that the s-channel decay (where one of the scalar singlets gets a $v_{\mathcal{S}} > 0$) is negligible even in the resonance region. We use microOmegas 5.0.8 [182] for the numerical values. The viable parameter region, for a relic density between $0.11 < h^2\Omega_{DM} < 0.13$, is shown as a blue band in the left panel of Fig. 3.8 in the $m_{\mathcal{S}} - m_\chi$ plane, where we set $y_\chi^{\mathcal{S}} = 2.25$. Light mediators $m_{\mathcal{S}} < 200\,\text{GeV}$, below the green line, are already excluded by XENON1T [183] and heavier once will be tested in future experiments like LZ [184] (red line) and DARWIN [185] (remaining region). The dominant contribution to direct detection rates arises from tree-level s-channel exchange of $\mathcal{S}$ with the up and down quarks and therefore vanishes in the hadrophobic case. Since $v_{\mathcal{S}} \propto 1/y_f^{\mathcal{S}}$, the cross section is independent of the Yukawa couplings. Finally, in the right panel of Fig. 3.8 we show the $y_\chi^{\mathcal{S}}$ vs m_χ, for $m_{\mathcal{S}} = 200$ GeV. Note that also the relic density is independent of the values of $y_u^{\mathcal{S}}$ (or $y_e^{\mathcal{S}}$), which do not enter the dominant annihilation amplitude. We find that, unless the electron $\mathcal{S}-$Yukawa coupling is very small, most of the viable parameter space will be tested at CLIC.

3.5 Matching the eDMEFT with More-UV-Complete Theories

The concept of matching in EFTs can be broken down into a single question: How does the physics at high energies show up in the low energy effective theory? Every time we remove a heavy field from the high energy theory, it is crucial to verify whether the physics in the low energy theory has changed or not. Thus, the need to keep track of physical effects in order to have consistency between both the high and low energy theories. Matching is nothing else but the right establishment of that connection.

When performing the matching, it is necessary to be at energies close to the range in which the heavy particles were integrated out, as shown in Fig. 3.9. This, because is precisely in that limit when the physics behaviour starts to be unclear. Furthermore, if the matching is done at scales far from $\mu = M$ (where the latter is the mass of the heavy integrated-out field), we would have a two-scale problem, and therefore large logarithms. When performing the matching, the physics of the heavy fields is then captured in the so called Wilson coefficients.

In a nutshell, the matching consist of the following steps:

1. Computing the amplitudes in both the full and EFT theory, taking diagrams up to a certain loop level into account.

2. Then equate the resulting amplitudes, order by order in perturbation theory, from the high energy theory with the ones in the low-effective one.

3. Finally, solve for the Wilson coefficients C_i.

As we see in the following, matching is specially useful when calculating one loop processes. When loop corrections are taken into account, EFTs become a strong tool to calculate and deal with large separated energy scales. Acting accordingly with the regular procedure of an EFT, logarithms of the large ratio of such energy scales, appearing in the perturbative expansion, are handled by effectively splitting them into a heavy and light fields. While the fraction above the matching scale is associated to the Wilson coefficients, the light (or low-energetic) one is captured in the matrix elements of the effective operators. Then, the Wilson coefficients are derived at the high scale by the matching procedure. There, the corresponding large logarithms disappear in the calculations, since the matching is independent of the IR regime, where both theories are identical. Then, as depicted in the right panel of Fig. 3.9, we can run down the Wilson coefficients by using the renormalization group equations (RGE). In this way, one is left with an EFT for the IR featuring only one scale. The repeated combination and running of the Wilson coefficients allows to sum up the logarithms in all orders of perturbation theory [106]. For a full study, please refer to Refs. [96, 101, 103, 106].

The approach used below, consists of using the equations of motion for the heavy fields that are integrated out. The effective Lagrangian is thus derived by solving them, and inserting the results in the corresponding UV theory Lagrangian. This approach is particularly straightforward for tree-level matching and has been extended to one-loop level under the name of *covariant-derivative-expansion* [186–188]; applications to SMEFT can be read at Refs. [189–192]. In the upcoming sections, we present the matching of
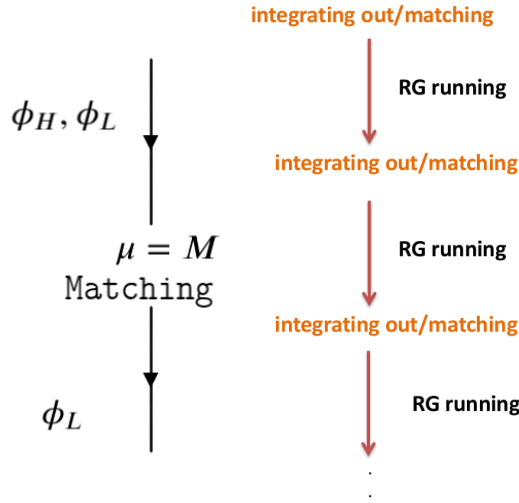
FIGURE 3.9: A regular matching scheme is presented in the left panel. Here ϕ_H represent the heavy fields while ϕ_L the lights fields, μ is the renormalization energy scale and M is the fundamental energy scale for the new effective theory. The running of the couplings is then presented in the right panel. Here RG running represents the corresponding renormalization group equations necessary for the running.

the eDMEFT with two more-UV-complete theories: 2HDM + Pseudoscalar and SM + vector-like-quarks.

3.5.1 2HDM + Pseudoscalar

In Chapter 2, we introduced the 2HDM as a renormalizable extension of the SM. Let us now explore the scenario where we augment the SM by a second doublet and a pseudoscalar field ($\widetilde{S}$) as reviewed in [193]. We start by briefly exploring the theoretical properties of the 2HDM+$\widetilde{S}$ [12], afterwards, we examine the limit where the mass scale of the second doublet is far above the EW scale. In this case, the doublet can be integrated out, generating a combination of Wilson coefficients of the eDMEFT.

The general potential of the 2HDM+$\widetilde{S}$ is expressed as [193–195]

$$V(\Phi_1, \Phi_2, \widetilde{S}) = V_{2\mathrm{HD}}(\Phi_1, \Phi_2) + V_{\widetilde{S}}(\widetilde{S}) + V_{\widetilde{S}2\mathrm{HD}}(\Phi_1, \Phi_2, \widetilde{S}), \qquad (3.24)$$

---

[12]In the literature, the 2HDM plus a pseudoscalar is commonly referred as 2HDM+a where a is a pseudoscalar field. However, for consistency we use the notation where $\widetilde{S}$ is the pseudoscalar singlet mediator.

where the different parts of the potential are given by

$$
\begin{aligned}
V_{2\text{HD}}(\Phi_1, \Phi_2) =\ & M_{11}^2 \Phi_1^\dagger \Phi_1 + M_{22}^2 \Phi_2^\dagger \Phi_2 + \left[M_{12}^2 \Phi_2^\dagger \Phi_1 + \text{h.c.} \right] + \tfrac{1}{2}\lambda_1 (\Phi_1^\dagger \Phi_1)^2 \\
& + \tfrac{1}{2}\lambda_2 (\Phi_2^\dagger \Phi_2)^2 + \lambda_3 (\Phi_1^\dagger \Phi_1)(\Phi_2^\dagger \Phi_2) + \lambda_4 (\Phi_2^\dagger \Phi_1)(\Phi_1^\dagger \Phi_2) \\
& + \left[\tfrac{1}{2}\lambda_5 (\Phi_2^\dagger \Phi_1)^2 + \left\{ \lambda_6 (\Phi_1^\dagger \Phi_1) + \lambda_7 (\Phi_2^\dagger \Phi_2) \right\} (\Phi_1^\dagger \Phi_2) + \text{h.c.} \right] ,
\end{aligned}
\tag{3.25}
$$

$$
V_{\widetilde{S}}(\widetilde{S}) = \tfrac{1}{2} M_{\widetilde{S}\widetilde{S}}^2 \widetilde{S}^2 + \tfrac{1}{4} \lambda_{\widetilde{S}} \widetilde{S}^4 ,
\tag{3.26}
$$

$$
V_{\widetilde{S}2\text{HD}}(\Phi_1, \Phi_2, \widetilde{S}) = \lambda_{\widetilde{S}1} (\Phi_1^\dagger \Phi_1)\widetilde{S}^2 + \lambda_{\widetilde{S}2} (\Phi_2^\dagger \Phi_2)\widetilde{S}^2 + \mu_{\widetilde{S}12} \widetilde{S}(i\Phi_1^\dagger \Phi_2 + \text{h.c.}) .
\tag{3.27}
$$

Here, $\lambda_{5,6,7}$ and M_{12}^2 are potentially complex parameters. To ensure a CP-conserving potential and vacuum stability all coefficients and both vevs are taken to be real [196]. For more a more detail explanation on the 2HD potential please refer to Sec. 2.6 and Sec. 2.3. To identify the doublet containing the new states and to consistently integrate them out, it is convenient to rotate $\{\Phi_1, \Phi_2\}$ to the Higgs basis, $\{\Phi_h, \Phi_H\}$. There the two doublets are defined as [13]

$$
\Phi_h = c_\beta\, \Phi_1 + s_\beta\, \Phi_2 = \begin{pmatrix} G^+ \\ \frac{v + \hat{\rho}_1 + iG^0}{\sqrt{2}} \end{pmatrix} , \qquad \Phi_H = -s_\beta\, \Phi_1 + c_\beta\, \Phi_2 = \begin{pmatrix} H^+ \\ \frac{\hat{\rho}_2 + i\hat{\rho}_3}{\sqrt{2}} \end{pmatrix} , \tag{3.28}
$$

such that the vev of the heavy and light higgs are $\langle\Phi_H\rangle = 0$ and $\langle\Phi_h\rangle = v \approx 246\,\text{GeV}$. The SM Goldstone bosons, $G^\pm$, G^0, and the charged scalar pair, $H^\pm$, are already mass eigenstates. On the other hand, the CP-even scalars $\hat{\rho}_{1,2}$ are linear combinations of the SM Higgs, h, and an additional heavy scalar, H. In addition, $\hat{\rho}_3$ and $\widetilde{S}$ are CP-odd with mass eigenstates a and A.

The potential in the Higgs basis reads

$$
\hat{V}(\Phi_h, \Phi_H, \widetilde{S}) = \hat{V}_{2\text{HD}}(\Phi_h, \Phi_H) + \hat{V}_{\widetilde{S}}(\widetilde{S}) + \hat{V}_{\widetilde{S}2\text{HD}}(\Phi_h, \Phi_H, \widetilde{S}) ,
\tag{3.29}
$$

where each part is given by

$$
\begin{aligned}
\hat{V}_{2\text{HD}}(\Phi_h, \Phi_H) =\ & \hat{M}_{hh}^2 \Phi_h^\dagger \Phi_h + \hat{M}_{HH}^2 \Phi_H^\dagger \Phi_H + \left[\hat{M}_{hH}^2 \Phi_H^\dagger \Phi_h + \text{h.c.} \right] + \tfrac{1}{2}\hat{\lambda}_h (\Phi_h^\dagger \Phi_h)^2 \\
& + \tfrac{1}{2}\hat{\lambda}_H (\Phi_H^\dagger \Phi_H)^2 + \hat{\lambda}_3 (\Phi_h^\dagger \Phi_h)(\Phi_H^\dagger \Phi_H) + \hat{\lambda}_4 (\Phi_H^\dagger \Phi_h)(\Phi_h^\dagger \Phi_H) \\
& + \left[\tfrac{1}{2}\hat{\lambda}_5 (\Phi_H^\dagger \Phi_h)^2 + \left\{ \hat{\lambda}_6 (\Phi_h^\dagger \Phi_h) + \hat{\lambda}_7 (\Phi_H^\dagger \Phi_H) \right\} (\Phi_H^\dagger \Phi_h) + \text{h.c.} \right] ,
\end{aligned}
\tag{3.30}
$$

$$
\hat{V}_{\widetilde{S}(\widetilde{S})} = \tfrac{1}{2} M_{\widetilde{S}\widetilde{S}}^2 \widetilde{S}^2 + \tfrac{1}{4} \lambda_{\widetilde{S}} \widetilde{S}^4 ,
\tag{3.31}
$$

---

[13]From now on we make use of the shorthand notation $s_\beta \equiv \sin\beta$ and $c_\beta \equiv \cos\beta$.

$$\hat{V}_{\widetilde{S}2\mathrm{HD}}(\Phi_h, \Phi_H, \widetilde{S}) = \hat{\lambda}_{HH\widetilde{S}}\, \Phi_H^\dagger \Phi_H \widetilde{S}^2 + \hat{\lambda}_{hh\widetilde{S}}\, \Phi_h^\dagger \Phi_h \widetilde{S}^2 + \hat{\lambda}_{hH\widetilde{S}}\, \widetilde{S}^2 (\Phi_H^\dagger \Phi_h \tag{3.32}$$
$$+ \,\mathrm{h.c.}) + \mu_{\widetilde{S}hH}\, \widetilde{S}\left(i\Phi_h^\dagger \Phi_H + \mathrm{h.c.}\right),$$

where the couplings mediating the mixing between the Higgs fields (H,h) and the pseudoscalar mediator ($\widetilde{S}$) in Eq. (3.32) are

$$\hat{\lambda}_{HH\widetilde{S}} = s_\beta^2\, \lambda_{\widetilde{S}1} + c_\beta^2\, \lambda_{\widetilde{S}2}, \tag{3.33}$$
$$\hat{\lambda}_{hh\widetilde{S}} = c_\beta^2\, \lambda_{\widetilde{S}1} + s_\beta^2\, \lambda_{\widetilde{S}2}, \tag{3.34}$$
$$\hat{\lambda}_{hH\widetilde{S}} = s_\beta c_\beta\, (\lambda_{\widetilde{S}2} - \lambda_{\widetilde{S}1}). \tag{3.35}$$

In general, the terms $\hat{\lambda}_6$, $\hat{\lambda}_7$, and $\hat{\lambda}_{hH\widetilde{S}}$ get defined during the basis transformation. We comment on them in the following. Moreover, the coefficient of $\widetilde{S}(i\Phi_h^\dagger \Phi_H + \mathrm{h.c.})$ does not change under this rotation. The minimization conditions of Eq. (3.30) are given by

$$M_{hh}^2 = -\hat{\lambda}_h v^2/2, \tag{3.36}$$
$$M_{hH}^2 = -\hat{\lambda}_6 v^2/2 = -\tfrac{1}{2}(m_h^2 - m_H^2)c_{\beta-\alpha}s_{\beta-\alpha}. \tag{3.37}$$

As seen before, a Z_2-symmetry is typically imposed to ensure the absence of FCNCs in 2HDMs. Here the doublets carry different charges, eg. $\Phi_1 \to +\Phi_1$ and $\Phi_2 \to -\Phi_2$. Applying this symmetry to the scalar potential in Eq. (3.25) and only allowing for it to be softly broken by the M_{12}^2 term sets

$$\lambda_6 = \lambda_7 = 0. \tag{3.38}$$

In agreement with the original papers and experimental searches, we focus on the phenomenologically well motivated alignment limit, which can be guaranteed by a specific choice of the potential coefficients [197]

$$\lambda_1 = \lambda_2 = \lambda_3 + \lambda_4 + \lambda_5. \tag{3.39}$$

In this limit, the potential parameters from the Z_2 transfer directly to the Higgs basis as $\lambda_i = \hat{\lambda}_i$ for $i = \{1, h\}, \{2, H\}, 3, 4, 5$ and $\hat{\lambda}_6 = \hat{\lambda}_7 = 0$. This implies $c_{\beta-\alpha} \propto \hat{\lambda}_6 = 0$. The minimization conditions simplify to

$$\hat{M}_{hh}^2 = -\lambda_1 v^2/2 \qquad \text{and} \qquad \hat{M}_{hH}^2 = 0. \tag{3.40}$$

Therefore, the potential in Eq. (3.30) reads

$$\hat{V}_{2\mathrm{HD}}(\Phi_h, \Phi_H) = \hat{M}_{hh}^2 \Phi_h^\dagger \Phi_h + \hat{M}_{HH}^2 \Phi_H^\dagger \Phi_H \tag{3.41}$$
$$+ \tfrac{1}{2}\lambda_1 \left[(\Phi_h^\dagger \Phi_h)^2 + (\Phi_H^\dagger \Phi_H)^2 \right] + \lambda_3 (\Phi_h^\dagger \Phi_h)(\Phi_H^\dagger \Phi_H)$$
$$+ \lambda_4 (\Phi_H^\dagger \Phi_h)(\Phi_h^\dagger \Phi_H) + \tfrac{1}{2}(\lambda_1 - \lambda_3 - \lambda_4)\left[(\Phi_H^\dagger \Phi_h)^2 + \mathrm{h.c.}\right],$$

where the CP-even scalars are now mass eigenstates and Eq. (3.28) simplifies to

$$\Phi_h = \begin{pmatrix} G^+ \\ \frac{v+h+iG^0}{\sqrt{2}} \end{pmatrix} \qquad \text{and} \qquad \Phi_H = \begin{pmatrix} H^+ \\ \frac{H+i\hat{\rho}_3}{\sqrt{2}} \end{pmatrix}. \tag{3.42}$$

Therefore, Φ_h corresponds to the SM Higgs doublet, c.f. [196,198–200], and Φ_H contains the new physics contributions. The CP-odd state $\hat{\rho}_3$ mixes with $\widetilde{S}$ to form the mass eigenstates a and A with masses $M_A > M_a$ and the mixing angle

$$\sin 2\theta = \frac{2\,v\,\mu_{12\widetilde{S}}}{M_A^2 - M_a^2}. \tag{3.43}$$

We note that in the limit $\hat{M}_{HH}^2 \gg v^2$ the new states, H, A, and $H^\pm$ are nearly mass degenerated with the common mass scale $\hat{M}_{HH}$.

For completeness, the DM and Yukawa Lagrangians in the Higgs basis are given by

$$\mathcal{L}_{\text{Yukawa}} = -\sum_{n=h,H} \left(\hat{\mathbf{Y}}_{n,ij}^u\, \overline{Q}_L^i u_R^j \widetilde{\Phi}_n + \hat{\mathbf{Y}}_{n,ij}^d\, \overline{Q}_L^i d_R^j \Phi_n + \hat{\mathbf{Y}}_{n,ij}^l\, \overline{L}_L^i l_R^j \Phi_n + \text{h.c.} \right), \tag{3.44}$$

$$\mathcal{L}_{\text{DM}} = -y_\chi^{\widetilde{S}}\, \widetilde{S}\, \overline{\chi}\gamma^5\chi. \tag{3.45}$$

Since Φ_h corresponds to the SM Higgs doublet the Yukawa matrices $\mathbf{Y}_h^{u,d,l}$ have to be the SM ones. The matrices of the second doublet are assumed to be proportional to them, namely

$$\hat{\mathbf{Y}}_h^i \equiv \mathbf{Y}_{\text{SM}}^i \qquad \text{and} \qquad \hat{\mathbf{Y}}_H^i = \epsilon_i \mathbf{Y}_{\text{SM}}^i, \tag{3.46}$$

with the scaling factors ϵ_i and $i = u$, d, ℓ. Due to the mass mixing between the SU(2) singlet and doublet scalars, DM couples to both CP-odd physical states.

Matching

After introducing the full theory, we are now able to integrate out the second Higgs doublet, Φ_H. To do so, we employ its equation of motion at zero momentum, which is given by

$$\begin{aligned} &\hat{M}_{HH}^2\Phi_H + \lambda_1(\Phi_H^\dagger\Phi_H)\Phi_H + \lambda_3(\Phi_h^\dagger\Phi_h)\Phi_H \\ &+ \lambda_4\Phi_h(\Phi_h^\dagger\Phi_H) + (\lambda_1 - \lambda_3 - \lambda_4)(\Phi_H^\dagger\Phi_h)\Phi_h \\ &+ \hat{\lambda}_{HH\widetilde{S}}\,\widetilde{S}^2\Phi_H + \hat{\lambda}_{hH\widetilde{S}}\,\widetilde{S}^2\Phi_h - i\mu_{\widetilde{S}hH}\,\widetilde{S}\Phi_h \\ &+ \mathbf{Y}_{H,ij}^{u*}\overline{u}_R^i\epsilon Q_L^j + \mathbf{Y}_{H,ij}^{d*}\overline{d}_R^i Q_L^j + \mathbf{Y}_{H,ij}^{l*}\overline{l}_R^i L_L^j = 0. \end{aligned} \tag{3.47}$$

Linearizing in Φ_H and expanding in large $\hat{M}_{HH}$ leads to

$$\begin{aligned} &\hat{M}_{HH}^2\Phi_H + \hat{\lambda}_{hH\widetilde{S}}\,\widetilde{S}^2\Phi_h - \mu_{\widetilde{S}hH}\,i\,\widetilde{S}\Phi_h \\ &+ \left(\mathbf{Y}_{H,ij}^{u*}\overline{u}_R^i\epsilon Q_L^j + \mathbf{Y}_{H,ij}^{d*}\overline{d}_R^i Q_L^j + \mathbf{Y}_{H,ij}^{l*}\overline{l}_R^i L_L^j \right) = 0. \end{aligned} \tag{3.48}$$

We note that this approach is appropriate only if the mixing satisfies $\sin \theta \sim \mu_{\widetilde{S}hH}$ between the heavy CP-odd Higgs and $\widetilde{S}$ in the UV theory after EWSB (the latter identified with $\widetilde{S}$ in the EFT), is not too large, corresponding to a valid mass-insertion approximation. We thus write $\mu_{\widetilde{S}hH} = \lambda_{\widetilde{S}12}M$, requiring $M/\Lambda \equiv \epsilon_M < 1$, as also suggested by perturbative unitarity. Moreover, identifying the mass scale of the heavy doublet with the cutoff, $\hat{M}_{HH} = \Lambda \gg v$ [191, 198], and setting the off-diagonal operator $\hat{M}^2_{hH} = 0$ due to the alignment limit, leads to

$$\Phi_H = -\frac{\hat{\lambda}_{hH\widetilde{S}}}{\Lambda^2} \widetilde{S}^2 \Phi_h + \frac{\lambda_{\widetilde{S}12}}{\Lambda} \epsilon_M \, i \, \widetilde{S} \Phi_h$$
$$- \frac{1}{\Lambda^2} \left(\mathbf{Y}^{u*}_{H,ij} \overline{u}^i_R \epsilon Q^j_L + \mathbf{Y}^{d*}_{H,ij} \overline{d}^i_R Q^j_L + \mathbf{Y}^{l*}_{H,ij} \overline{l}^i_R L^j_L \right) \,. \tag{3.49}$$

This result will be inserted into the Lagrangian (3.41).

For a CP-conserving potential, terms with odd powers of $\widetilde{S}$ besides $\widetilde{S} \Phi_H \Phi_h$ vanish. Therefore, at $D \leq 4$ only the Higgs-portal gets higher order corrections. At $D = 5$ an effective Yukawa-like coupling is generated:

$$\mathcal{L}^{D=4}_{\widetilde{S}} = \left(-\hat{\lambda}_{hh\widetilde{S}} + \lambda^2_{\widetilde{S}12}\epsilon^2_M \right) \widetilde{S}^2 \, \Phi^\dagger_h \Phi_h \tag{3.50}$$

$$\mathcal{L}^{D=5}_{\widetilde{S}2\text{HD}} = \frac{i\lambda_{\widetilde{S}12}\epsilon_M}{\Lambda} \widetilde{S} \left(\mathbf{Y}^u_{H,ij} \bar{Q}^i_L u^j_R \widetilde{\Phi}_h + \mathbf{Y}^d_{H,ij} \bar{Q}^i_L d^j_R \Phi_h + \mathbf{Y}^l_{H,ij} \bar{L}^i_L l^j_R \Phi_h + \text{h.c.} \right) \,. \tag{3.51}$$

To translate the coefficients from the Higgs basis to the interaction basis, we employ Eq. (3.33) to (3.35). We obtain

$$\lambda_{H\widetilde{S}} = s^2_\beta \lambda_{\widetilde{S}2} + c^2_\beta \lambda_{\widetilde{S}1} - \frac{\lambda^2_{\widetilde{S}12} v^2}{\Lambda^2} \tag{3.52}$$

with

$$\lambda_{\widetilde{S}12} = \sin(2\theta) \frac{M^2_A - M^2_a}{2vM} \,. \tag{3.53}$$

For the Yukawa couplings with the Z_2 charges similar to the 2HDM Type-II we get the final relation

$$y^{\widetilde{S}}_t = \frac{\mu_{\widetilde{S}hH}}{\Lambda} Y^u_{H,33} = \lambda_{\widetilde{S}12}\epsilon_M Y^u_{H,33} \,. \tag{3.54}$$

3.5.2 2HDM + Scalar

A similar procedure can be done for 2HDM + scalar. However, unlike the 2HDM + pseudoscalar, where the DD limits are only relevant for light mediators as the cross section is strongly suppressed by the momentum transfer, the scalar case generates spin independent interactions via t-channel scalar exchange. Therefore, DD experiments get sensitive to mediators masses around TeV scale and as a consequence, the exclusion limits should be taken into account in the phenomenological studies [193]. This model

has been already considered in the literature [193, 199–202]. A study on the constraints and implications in the search for heavy bosons for 2HDM + S at the LHC can be found in Ref. [201] while an extensive comparison between 2HDM + scalar/pseudoscalar can be found in Ref. [193].

The 2HDM + S general potential can be expressed as [193, 201]

$$V(\Phi_1, \Phi_2, S) = V_{2\mathrm{HD}}(\Phi_1, \Phi_2) + V_S(S) + V_{S2\mathrm{HD}}(\Phi_1, \Phi_2, S). \tag{3.55}$$

After consideration of the Z_2 charge assignments and assuming S to be even under it, the different parts of the scalar-related potential are now given by

$$V_{S2\mathrm{HD}}(\Phi_1, \Phi_2, S) = \mu_{11S}(\Phi_1^\dagger \Phi_1)S + \mu_{22S}(\Phi_2^\dagger \Phi_2)S + \mu_{12S}S(\Phi_2^\dagger \Phi_1 + \mathrm{h.c.}) \tag{3.56}$$
$$+ \tfrac{\lambda_{11S}}{2}(\Phi_1^\dagger \Phi_1)S^2 + \tfrac{\lambda_{22S}}{2}(\Phi_2^\dagger \Phi_2)S^2 + \tfrac{\lambda_{12S}}{2}(\Phi_1^\dagger \Phi_2 + \mathrm{h.c.})S^2 \,,$$
$$V_S(S) = \tfrac{1}{2}M_{SS}^2 S^2 + \tfrac{1}{3}\mu_S S^3 + \tfrac{1}{4}\lambda_S S^4 \,. \tag{3.57}$$

Rewriting the potential in the Higgs basis leads to

$$\hat{V}(\Phi_h, \Phi_H, S) = \hat{V}_{2\mathrm{HD}}(\Phi_h, \Phi_H) + V_S(S) + \hat{V}_{S2\mathrm{HD}}(\Phi_h, \Phi_H, S), \tag{3.58}$$

with $\hat{V}_{2\mathrm{HD}}$ as given in Eq. (3.41). The corresponding part mixing the singlet with the two doublets then reads

$$\hat{V}_{S2\mathrm{HD}}(\Phi_h, \Phi_H, S) = \tfrac{1}{2}\hat{\mu}_{HHS}(\Phi_H^\dagger \Phi_H)S + \tfrac{1}{2}\hat{\mu}_{hhS}(\Phi_h^\dagger \Phi_h)S + \tfrac{1}{2}\hat{\mu}_{hHS}S\left(\Phi_H^\dagger \Phi_h + \mathrm{h.c.}\right)$$
$$+ \tfrac{1}{2}\hat{\lambda}_{HHS}(\Phi_H^\dagger \Phi_H)S^2 + \tfrac{1}{2}\hat{\lambda}_{hhS}(\Phi_h^\dagger \Phi_h)S^2 + \tfrac{1}{2}\hat{\lambda}_{hHS}S^2\left(\Phi_H^\dagger \Phi_h + \mathrm{h.c.}\right),$$
$$\tag{3.59}$$

where the $\hat{\lambda}_{ijS}$ are analogue to Eq. (3.33) to (3.35) and

$$\hat{\mu}_{HHS} = s_\beta^2 \lambda_{S1} + c_\beta^2 \mu_{S2}, \tag{3.60}$$

$$\hat{\mu}_{hhS} = c_\beta^2 \lambda_{S1} + s_\beta^2 \mu_{S2}, \tag{3.61}$$

$$\hat{\mu}_{hHS} = s_\beta c_\beta (\mu_{S2} - \mu_{S1}). \tag{3.62}$$

In the following, we set $\mu_{hhS} = 0$ to reach the aligment limit and to avoid mixing between the scalar and the SM Higgs. Also, for simplicity, $\mu_{HHS} = 0$. The resulting potential is then identical to the one for the 2HDM + pseudoscalar in Eq. (3.32). As a consequence, the matching is the same, and the corresponding relation for the Type-II 2HDM for the bottom quark is

$$y_b^S = \frac{\mu_{hHS}}{\Lambda} Y_{H,33}^d = \lambda_{S12}\epsilon_M Y_{H,33}^d. \tag{3.63}$$

3.5.3 SM + Vector-Like Quarks

In the SM, the left-handed fermions transforms as doublets under the $SU(2)_L$ symmetry while the right-handed ones transform as singlets. Therefore, to construct the mass term it is required the product of both the left- and right-handed parts and the presence of the SM Higgs field to be gauge invariant. However, the possibility of introducing *exotic* fermions transforming as weak singlets also exists. This kind of fermion is called vector-like [203–207], their left- and right-handed components now transform equally, making the mass term automatically gauge invariant, independently of the Higgs boson. As a consequence, this kind of fermions have the freedom to be much heavier than the SM ones. In this Section, we focus on them and include vector-like quarks (VLQ) [208]. The latter transform as triplets under the $SU(3)_c$ gauge group. Recent experimental limits on such exotic fermions can be found in Refs. [209–213].

We then consider a more-UV-complete model by extending the SM with a scalar singlet, $\mathcal{S}$, a DM fermion, χ, and two new coloured VLQs. All singlets under the $SU(2)_L$ symmetry. We consider two types of VLQs, T with $Q = 2/3$ and B with $Q = -1/3$ [214]. The corresponding Lagrangian then reads

$$
\begin{aligned}
\mathcal{L} = & - M_T \, \overline{T}_L T_R - M_B \, \overline{B}_L B_R - \frac{1}{2} \mu_{\mathcal{S}}^2 \mathcal{S}^2 - m_\chi \overline{\chi} \chi - y_\chi \mathcal{S} \overline{\chi} \chi \\
& - \left(y_T \, \mathcal{S} \overline{T}_L T_R + y_{St} \, \mathcal{S} \overline{T}_L t_R + \mu_{Tt} \, \overline{T}_L t_R + y_{HT} \, \overline{Q}_L \widetilde{H} T_R + y_t \, \overline{Q}_L \widetilde{H} t_R \right. \\
& \left. + y_B \, \mathcal{S} \overline{B}_L B_R + y_{Sb} \, \mathcal{S} \overline{B}_L b_R + \mu_{Bb} \, \overline{B}_L b_R + y_{HB} \, \overline{Q}_L H B_R + y_b \, \overline{Q}_L H b_R + \text{h.c.} \right)
\end{aligned}
\tag{3.64}
$$

By performing a rotation in the (T_R, t_R) and (B_R, b_R) fields, the terms proportional to $\mu_{Tt(Bb)}$ can be removed. Additionally, $y_{t,b}$ are fixed while $y_{T(B)}, y_{St(Sb)}$ and $y_{HT(HB)}$ are free parameters. In the following, we present the derivation for the top-quark only, but it applies similar to every quark generation. The Yukawa Lagrangian can be written in matrix form.

$$
\mathcal{L}_{\text{yuk}}^t = -(\overline{Q}_L, \overline{T}_L) \begin{pmatrix} y_t \widetilde{H} & y_{HT} \widetilde{H} \\ y_{St} \mathcal{S} & y_T \mathcal{S} + M_T \end{pmatrix} \begin{pmatrix} t_R \\ T_R \end{pmatrix} + \text{h.c.}
\tag{3.65}
$$

To focus only on the VLQ related effects, we consider the case where $\mathcal{S}$ neither develops a vev i.e $\langle \mathcal{S} \rangle = 0$, nor mixes with the SM Higgs. Therefore, after EWSB Eq. (3.65) can be written as

$$
\mathcal{L}_{\text{yuk}}^t = - (\bar{t}_L, \overline{T}_L) \, \mathbf{M} \begin{pmatrix} t_R \\ T_R \end{pmatrix} - (\bar{t}_L, \overline{T}_L) \, \mathbf{\Delta}(h, S) \begin{pmatrix} t_R \\ T_R \end{pmatrix},
\tag{3.66}
$$

where

$$
\mathbf{M} = \begin{pmatrix} \frac{y_t}{\sqrt{2}} v & \frac{y_{HT}}{\sqrt{2}} v \\ 0 & M_T \end{pmatrix}
\quad \text{and} \quad
\mathbf{\Delta}(h, S) = \begin{pmatrix} \frac{y_t}{\sqrt{2}} h & \frac{y_{HT}}{\sqrt{2}} h \\ y_{St} \, S & y_T \, S \end{pmatrix}.
\tag{3.67}
$$

and v is the vev of the SM Higgs $v = 246$ GeV. As in the previous models, in order to

diagonalize the mass matrix, **M**, we introduce the unitary rotation matrices, **L** and **R**, chosen such that $\mathbf{L\,M\,R^{\dagger}} = \mathrm{diag}(m_t, m_T)$. The resulting fermion mass eigenstates read

$$t'_i = \cos\theta_i\, t_i + \sin\theta_i\, T_i, \tag{3.68}$$

$$T'_i = -\sin\theta_i\, t_i + \cos\theta_i\, T_i, \tag{3.69}$$

with $i = L, R$ and the mixing angles [215, 216]

$$\sin(\theta_L) = \frac{y_{HT}\, v\, M_T}{\sqrt{2}\sqrt{(M_T^2 - m_t^2)^2 + (y_{HT}v\, M_T)^2}}, \tag{3.70}$$

$$\sin(\theta_R) = \frac{m_t}{M_T}\,\sin(\theta_L). \tag{3.71}$$

Therefore, the corresponding mass eigenvalues for the SM top-quark and the new VLQ T can be written as

$$\{M_T^2, m_t^2\} = \frac{1}{2}\left(\mathrm{tr}(\mathbf{MM^{\dagger}}) \pm \sqrt{\mathrm{tr}(\mathbf{MM^{\dagger}})^2 - 4\det(\mathbf{MM^{\dagger}})}\right), \tag{3.72}$$

where the trace and determinant are given by

$$\mathrm{tr}(\mathbf{MM^{\dagger}}) = M_T^2 + \frac{1}{2}v^2\left(y_{HT}^2 + y_t^2\right), \tag{3.73}$$

$$\det(\mathbf{MM^{\dagger}}) = \frac{1}{2}\left(y_t\, v\, M_T\right)^2. \tag{3.74}$$

Here m_t is the measured top quark mass, thereby y_t is fixed and as consequence the mass of the VLQ reads

$$m_T^2 = M_T^2\left(1 + \frac{(y_{HT}\, v)^2}{2(m_t^2 - (y_{HT}\, v)^2)}\right). \tag{3.75}$$

After diagonalizing the mass matrix, Eq. (3.66) takes the form

$$\mathcal{L}_{\mathrm{yuk}} = -\left(\bar{t}'_L, \bar{T}'_L\right)\begin{pmatrix} m_t & 0 \\ 0 & m_T \end{pmatrix}\begin{pmatrix} t'_R \\ T'_R \end{pmatrix} - \left(\bar{t}'_L, \bar{T}'_L\right)\begin{pmatrix} \Delta_{11} & \Delta_{12} \\ \Delta_{21} & \Delta_{22} \end{pmatrix}\begin{pmatrix} t'_R \\ T'_R \end{pmatrix}, \tag{3.76}$$

where the interaction part is now described by

$$\Delta_{11} = S(\beta_2 y_{St} + \beta_4 y_T) + \frac{h}{\sqrt{2}}\left(\beta_1 y_t + \beta_3 y_{HT}\right) \tag{3.77}$$

$$\Delta_{12} = S(\beta_2 y_T - \beta_4 y_{St}) + \frac{h}{\sqrt{2}}\left(\beta_1 y_{HT} - \beta_3 y_t\right) \tag{3.78}$$

$$\Delta_{21} = S(\beta_1 y_{St} + \beta_3 y_T) - \frac{h}{\sqrt{2}}\left(\beta_2 y_t + \beta_4 y_{HT}\right) \tag{3.79}$$

$$\Delta_{22} = S(\beta_1 y_T - \beta_3 y_{St}) + \frac{h}{\sqrt{2}}\left(-\beta_2 y_{HT} + \beta_4 y_t\right), \tag{3.80}$$
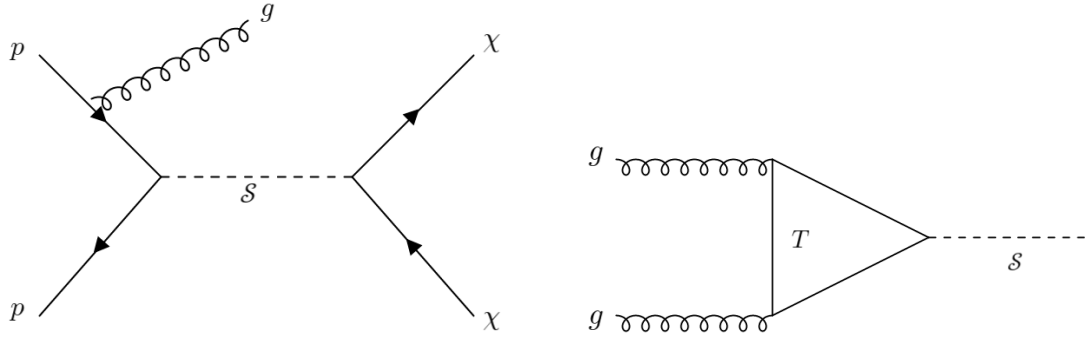
FIGURE 3.10: Feynman diagrams for a mono-jet signal in the left panel
and gluon fusion scalar production in the right panel.

with $\beta_1 = \cos(\theta_L)\cos(\theta_R)$, $\beta_2 = \cos(\theta_R)\sin(\theta_L)$, $\beta_3 = \cos(\theta_L)\sin(\theta_R)$, and $\beta_4 = \sin(\theta_L)\sin(\theta_R)$. We note that β_3 and β_4 are strongly suppressed for $M_T \gtrsim$ TeV.

Matching

We now match the UV-complete VLQ model explored above to the eDMEFT. This is done by following the three steps mentioned at the beginning of the section. Thus we start by deriving the equations of motion, that are linear in $T_{L(R)}$ at zero momentum, from the Lagrangian (3.64). We obtain

$$T_R = -\frac{y_{St}}{M_T} S\, t_R \qquad \text{and} \qquad T_L = -\frac{y_{HT}}{M_T} \widetilde{H}^\dagger Q_L \,. \tag{3.81}$$

Inserting it back into the original Lagrangian leads to the dimension five operator

$$\mathcal{L}_{\text{VLQ}}^{\text{eff}} = \frac{y_{HT}\, y_{St}}{M_T} S\, \overline{Q}_L \widetilde{H} t_R \,. \tag{3.82}$$

By identifying $\Lambda = M_T$ in the eDMEFT Lagrangian shown in Eq. (3.11), the corresponding Wilson coefficients read

$$(\mathbf{Y}_u^S)_{33} = -y_{HT}\, y_{St} \,. \tag{3.83}$$

Note that by exchanging, for example, the top quark in Eq. (3.64) for the up quark, we could generate $(\mathbf{Y}_u^S)_{11}$ in a similar way. Moreover, at one-loop the $\mathcal{S}G^{a\mu\nu}G^a_{\mu\nu}$ vertex is generated. By comparison with the SM top quark loop, we derive for the effective coupling appearing in Eq. (3.11)

$$\frac{c_G^{\mathcal{S}}}{\Lambda} = \frac{y_T}{3\,M_T} \,. \tag{3.84}$$

Further details on the phenomenology of this coupling will be discussed in the section below. For more detail on the general eDMEFT's phenomenology please refer to Ref. [12].
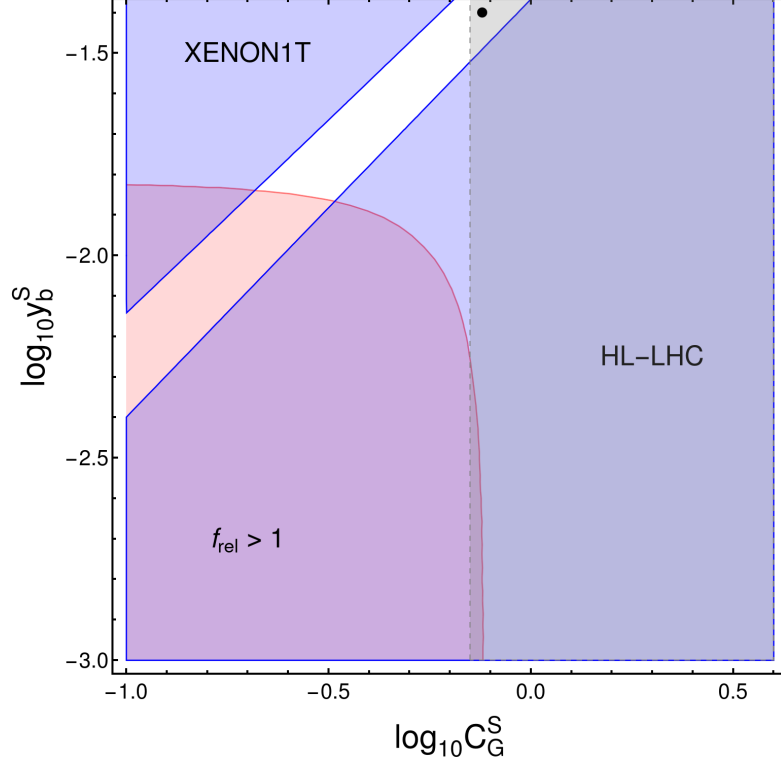
FIGURE 3.11: Blind spot region for the annihilation cross section in the $y_b^S - c_G^S$ plane. The solid red line shows a relic abundance of $f_{rel} = 1$, while the light red shaded region gets excluded by overabundance. The two different blue shaded regions describe the DD XENON1T exclusion limits. The gray region depicts the mono-jet exclusion at the projected 2σ sensitivity at HL-LHC. Here we have fixed the masses to $m_\chi = 65$ GeV and $m_S = 140$ GeV, while the cutoff is set to $\Lambda = 1$ TeV. The black dot is a benchmark point.

3.6   Collider Signatures

There are various kinds of collider signatures that can be studied in the specific models we are exploring, and the relative relevance of such signals depends upon the values of the different effective couplings. Most of these, are associated to the single production of the scalar mediator, S, that further decays into DM particles. The main signal investigated in this section and its leading process are summarized in Fig. 3.10. In the left panel, we show the mono-jet signature that gets characterized in the detector, by a jet coming from a radiated gluon which was generated in the initial state and the missing energy coming from the DM pair after the mediator decays. On the other hand, the right panel depicts a gluon fusion scalar production process. In the SM, the top-quark would be running inside the loop and the Higgs boson would be produced. In our model, however, we consider a heavy VLQ, denoted by T, running inside the loop and coupling to the new scalar mediator, S.
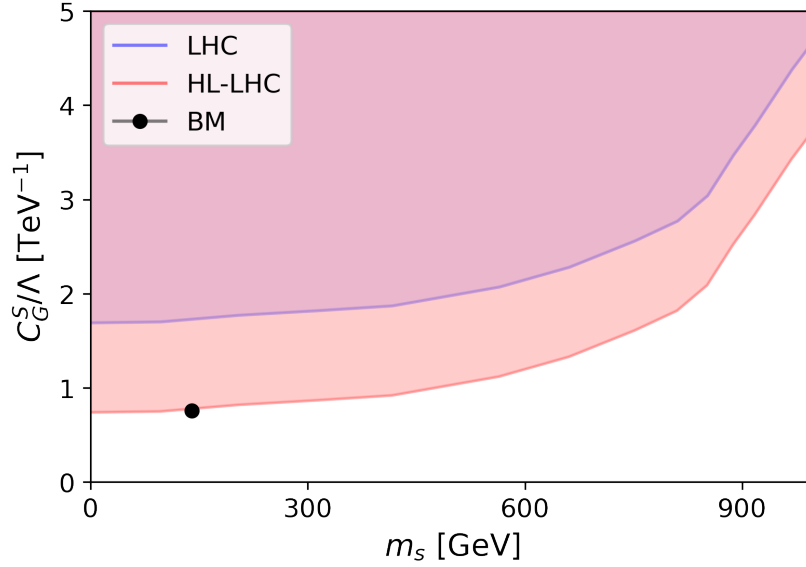
FIGURE 3.12: Exclusion limits from the ATLAS mono-jet search [221] and the 2σ HL-LHC projections in the $m_S - c_G^S$ plane normalized to Λ for $m_\chi = 10\,\mathrm{GeV}$, $y^S = 1$, and all other couplings are equal to zero.

We can integrate out the heavy VLQ and identify its mass with the scale Λ ending up with the coupling shown in Eq. (3.84). Additionally, if the VLQ coupling y_{HT} is set to zero, the qq initial state of the diagram could originate from the 2HDM+S and the VLQ model would induce the c_G^S operator. Then we have a non-trivial interplay between both more-UV theories that could come from a richer NP sector. Here we are interested in exploring such interplay. The dimension five gluon-mediator coupling then contributes with a different sign than the dimension five quark-mediator to the DD cross section. As a consequence, the operators cancel each other and blind regions appear. For general examples of blind regions in different contexts, see Refs. [9, 217–220]. In our case, we find more subtle blind spot regions in the EFT context, where it can appear between different operators featuring only one type of mediator [9]. The effect is phenomenologically more relevant near the resonant region. In Figure 3.11, we show the blind region in a $y_b^S - c_G^S$ plane for a $m_\chi = 10\,\mathrm{GeV}$, $m_S = 140\,\mathrm{GeV}$, $y_f^S = 1$ and $\Lambda = 1\,\mathrm{TeV}$. We then confront the annihilation cross sections with the XENON1T limits (blue shaded regions) and the correct relic abundance curve (light red solid line). The light red shaded region is excluded by an overabundance in the relic density ($f_{rel} > 1$). The grey shaded region is the 2σ projected HL-LHC exclusion region. The projection was done by employing the 2017 ATLAS analysis [221] in CheckMate [171] and scaling the results for the corresponding high luminosity [9]. We can see that the HL-LHC can already explore the blind spot region for couplings of $y_b^S = 0.4$ and $c_G^S = 0.7$ (see the black dot in Figs. 3.11-3.13). For more details of the blind regions coming from the eDMEFT, please see Ref. [9].
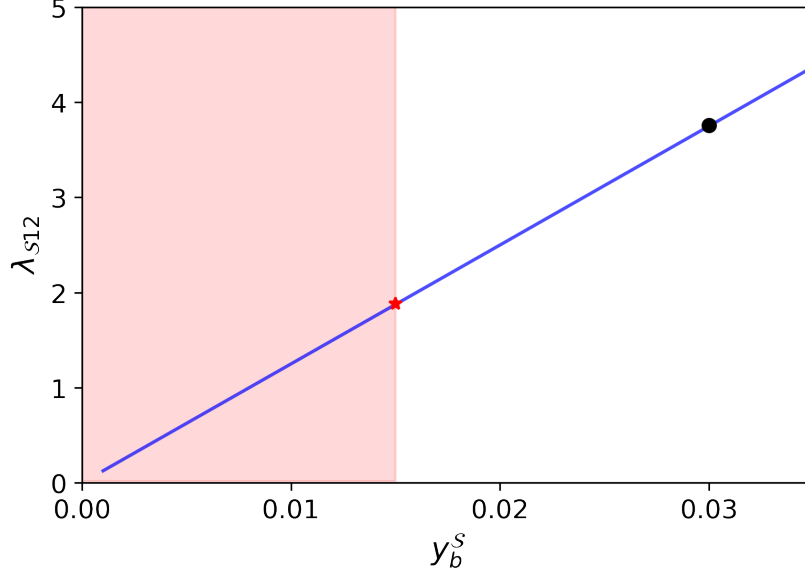
FIGURE 3.13: Translation of the eDMEFT y_b^S coupling into the 2HDM+S coefficient λ_{S12} using Eq. (3.63). Here $\epsilon_M = 0.5$, and the bottom Yukawa $Y_{H,33}^d = 0.16$. The shaded red region is excluded by the overabundance of the relic density, the red star is the point that reproduces the correct relic density. The black dot point is the benchmark point depicted in the plots above which can be tested at HL-LHC with perturbative couplings for the VLQ and lies in the blind region.

On the other hand, in Figure 3.12, we study the exclusion limits for the LHC and the HL-LHC projections from mono-jet searches as a function of the mediator mass. Here we fixed the value of $m_\chi = 10$ GeV. Nonetheless, the choice of the DM mass can be freely selected as long as it is not close to the $m_S \approx 2m_\chi$ threshold. In fact, in Ref. [12], it was verified that the experimental sensitivity is independent of the DM mass in that region. Here the parameter space which can be probed through current ATLAS mono-jet searches is limited, allowing only to $\mathcal{O}(1)$ couplings to be tested [12]. Nevertheless, future HL-LHC limits can cover regions where $c_G^S < 1$. In particular, the limits are tighter for light mediators.

Coming back to Eq. (3.84), and identifying $\Lambda = M_T \sim 1$ TeV, we can translate the limits in Fig. 3.12 as a coupling for the VLQ. As an example, for the benchmark $m_S = 140$ GeV and $c_G^S = 0.7$ (black dot in Figure 3.12), the corresponding VLQ coupling is $y_T \approx 2$, being well in the perturbative regime. Note that the current LHC limits can be improved by using the newest results from ATLAS [222] that were recently implemented in CheckMate2 [171].

Regarding the 2HDM+S model only, we were not able to find a concrete parameter space that lead to an observable LHC signal, and therefore neglect its contribution in the regime where the VLQ becomes relevant. However, when looking at the combination of 2HDM+S and VLQ, the values on the bottom-Yukawa coupling can be translated into

the 2HDM+S coupling λ_{S12}. This is done by using the relation obtained after performing the matching in Eq. (3.63). Specifically for the benchmark point in the blind region where $y_b^S = 0.03$, the corresponding value for the 2HDM+S parameter is $\lambda_{S12} = 3.8$. We assume the heavy Higgs, H, dominantly coupling to bottom quarks and therefore, $\epsilon_{u,l} = 0$ and $\epsilon_d = 1$ (see Eq. (3.46)). Additionally, by judiciously modifying the flavour structure of the theory, we may safely assume the DD effects of the down and charm quarks to be small enough so they do not play a role in the analysis. We then consider $\epsilon_b = 1$, $\epsilon_M = M/\Lambda = 0.5$, $m_b = 2.86$ GeV (in the Z mass scale) and $Y_{H,33}^d = 0.016$. In Fig. 3.13, we depict the coupling translation as a solid blue line, the red shaded region is excluded by relic density overabundance whereas the red star represent the point were the correct relic density can be achieved. For last, the black dot is the benchmark point depicted in all the aforementioned Figures which can be tested at HL-LHC with perturbative couplings for the VLQ and lies in the blind region.

In general, the findings from the interplay between the VLQ and 2HDM + S models are of special interest as with small coefficients coming from the eDMEFT theory ($c_G^S = 0.7$ and $y_b^S = 0.03$), sitting at a DD blind spot, we can find $\mathcal{O}(1)$ couplings in the more-UV-complete theories. Moreover, the sign difference between operators create blind regions in which DD effects can be suppressed. It is in a corner of that blind region that we find a suitable value for the eDMEFT couplings that could be tested in the future HL-LHC collider. Such limits could then be translated into limits on the parameters of the more-UV-complete theories through the performed matching. We thus showed that a blind spot region, identified in the EFT, can in fact be achieved in a UV complete model, being a combination of VLQ and 2HDM+S, with a reasonable $\mathcal{O}(1)$ values for the fundamental couplings and can be potentially detectable at HL-LHC.

Chapter 4

Addressing the XENON1T Excess within the eDMEFT Framework

As mentioned in Sec. 3.2, DM is one of the strongest evidences which require the presence of new physics. Finding the corresponding particle(s) is one of the biggest tasks for the present century. To this end, several detectors are already trying to detect it and unveil major aspects of its nature. They are designed with different target materials, some of which are [223, 224]:

- **Scintillator crystals detectors:** They use NaI(Tl) or CsI(Tl). The high mass-number of I (A = 127) or Cs (A = 133) lead to high sensitivities for spin-independent interactions [225, 226]. Some experiments that use this kind of detector are DAMA/NaI [227, 228], DAMA/LIBRA [227, 229], UKDMC(NAIAD) [230] and ANAIS [231]. Among all the aforementioned experiments, DAMA/LIBRA has achieved the lowest level of background and accumulated sufficient data to study the annual modulation signature of WIMP interactions.

- **Semi-conductor ionisation detectors:** These ones employ germanium and silicon and are mainly used to search for DM-induced charge signals. One example is the CoGeNT experiment [232] that searches for DM candidates of around ~ 10 GeV with pure germanium detectors. For searches of sub-GeV DM in semi-conductor detectors, please refer to Ref. [233].

- **Crystalline cryogenic detectors (bolometers):** They measure the increase of the small particle interaction-induced temperature ΔT to measure either heat or athermal phonon signals. Cryogenic detectors are specially remarkable to reject backgrounds from interactions of normal matter. Some experiments of this kind are CRESST [234–237] , EURECA [234, 235] and COSINUS [238], where the first two make use of $CaWO_4$ crystals while the last one uses NaI.

- **Noble gases detectors:** These ones use liquid argon (Ar) and xenon (Xe) as scintillators as they are easily ionized. These noble gases have the advantage of being easily liquified to build dense and compact dark matter targets. The detection is done through the heat produced by the interactions. The undetected heat excite and ionise the atoms and as consequence the latter decay under the emission of ultraviolet light at wavelengths of 128 nm for Ar and 178 nm for Xe. Noble gas

detectors have already established important limits on the DM mass and interaction couplings. Some experiments of this kind are XENON1T [183], LUX [239], ZEPLIN-III [240,241], XMASS [242], DARWIN [243], among others [244].

For an extensive review on the experimental status of WIMP-like DM, please refer to Ref. [224].

In the following, we only focus our attention on the noble gas detectors, specially on the XENON1T experiment [183]. The latter employs one ton of liquid-xenon as target material and a time projection chamber (LXe TPC), that perform a three-dimensional reconstruction of particles trajectories or interactions as depicted in Fig. 4.1. XENON1T was primarily designed to detect WIMPs, however, it is also sensitive to interactions from alternative dark matter candidates and to other physics beyond the standard model. In 2020, the XENON1T collaboration announced an excess in the electron recoil events [14], leading to a cascade of theoretical explanations of such phenomena ranging from new neutrino interactions [245–250], the absorption of keV-scale dark matter [251–255], scattering induced by a new $U(1)$ symmetry [256,257], semi-relativistic or boosted DM [258–262], axions [250,263], inelastic DM scattering [264–268], large neutrino magnetic moment [269–271] or more exotic explanations [272–276], a few more examples are [265,277–283]. It is important to mention that most of the theories fitting the excess face astrophysical problems. Here, we explore a scenario where such constraints can be avoided with late-phase transitions [277]. As the XENON1T experiment is able to detect not only DM but also other BSM particles, this motivates the possibility of probing the framework mentioned in Sec. 3.3, where the SM was augmented with fermionic DM and a (pseudo)scalar mediator. Through a slightly extended version of the eDMEFT we explore and address the excess in the low-energy electron recoil spectrum [277].

The chapter is organized as follows. In Sec. 4.1, we introduce the reported XENON1T excess. Then, in Sec. 4.2, we introduce the general setup and the Lagrangian of our model, discussing the masses, scalar mixing and the free parameters of our theory. In Sec. 4.3, we fit the excess via modified neutrinos interactions and DM scattering. In the latter, we also explore the fulfillment of the DM relic abundance. Afterwards, in Sec. 4.4, we discuss the terrestrial and astrophysical constraints, including bounds on electron-neutrino scalar interactions, the electron couplings and the neutrino couplings. Here we also introduce two benchmarks that are used when confronting our model with the astrophysical and laboratory constraints and discuss a more general free-EFT description of our model. In Sec. 4.5, we present scenarios in which we can avoid some astrophysical bounds, specially the ones coming from BBN, where a late phase transition could evade the imposed constraint. Finally, in Sec. 4.6, we discuss the current status of the XENON1T excess.
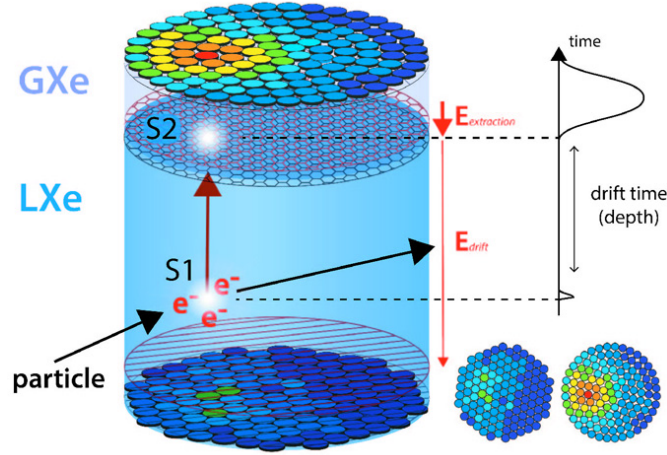
FIGURE 4.1: Illustration of the xenon experiment. The particle (WIMPs) hit the xenon atom when passing through the detector. The energy from the collision excite the electrons orbiting the nucleus and their energy is measured by time projection chambers (TPC) which surround the xenon tank. Image taken from [284].

4.1 The XENON1T Excess

In 2020, the XENON1T collaboration reported an excess of 53 events, as 285 were detected but only 232 events were expected. The excess was observed in the energy range between $1 \rightarrow 7$ keV [14]. Inside this particular range, the collected data enables sensitive searches for solar axions, bosonic dark matter and an enhanced neutrino magnetic moment by solar neutrinos. The interpretation of the data in terms of the first and last possibilities, finds substantial statistical improvements over the background-only hypothesis with a significance around 3.4σ for solar axions and 3.2σ for the neutrino magnetic moment. For further details of the aforementioned models, please refer to Ref. [14].

Even though the excess might be an important hint to new physics, the possibility of a more mundane explanation is considerable. With the current understanding of the experiment, a contamination with tritium, could have contributed to the excess via its beta decays. In addition, the PandaX-II experiment [285], carried on in China, later reported a search for new physics signals using the low energy electron recoil events previously recorded in their complete data sets. They concluded that the expected excess, assuming the best fit signal strength from XENON1T, is compatible with the data within uncertainties. However, the data is also consistent with the background only hypothesis. This cannot confirm or dismiss the presence of NP in the excess, but it is expected that the next generation detectors as PandaX-4T [286], XENONnT [287] and LZ [288] could confirm the nature of such anomaly.

As the XENON1T excess is observed in a few bins above the threshold, only theories that predict a highly localized energy deposit or an IR-dominated recoil spectrum can account for the observation. In this thesis, we attempt to characterize the excess

in a moderately expanded version of eDMEFT presented in Sec. 3.3. Here, instead of having only one extra mediator, we have two: One that only couples with electrons and the other only coupling with neutrinos. This is a result of a broken $Z_2^e \times Z_2^\nu$ symmetry under which neutrinos and electrons are charged. In this approach, modified neutrino interactions with electrons, via a potentially light new scalar sector, are naturally included in the eDMEFT. Therefore, the new extended framework, possesses all the ingredients needed for explaining the excess. The induced non-trivial couplings of the new scalars allow the excess to be related to the observed electron and neutrino masses.

The complete setup is introduced in Sec. 4.2. In Sec. 4.3, we present fits to the XENONT1T electron recoil excess, first assuming neutrino-electron scattering, and second DM-electron scattering as its origin. There, we also examine whether the correct DM relic abundance can be achieved consistently with our fits. Subsequently, in Sec. 4.4, we confront the neutrino explanation with stringent limits on new electron and neutrino interactions, from terrestrial and astrophysical observations. We also identify benchmark points and non-trivial mechanisms to avoid the severe constraints. Furthermore, the case of free couplings is considered corresponding to a subset of eDMEFT operators, to characterize viable parameter regions. Lastly, we show how to avoid astrophysical and BBN constraints via late phase transitions in Sec. 4.5 and summarize in Sec.4.6. The complete chapter is based on the results presented in reference Ref. [277].

4.2   Model Setup

We consider the leptophilic variant of the eDMEFT. Here, the SM scalar sector is extended by assuming two different parity symmetries, $Z_2^e \times Z_2^\nu$, one shared by the neutrinos and the other by the electron. Just as in Sec. 3.4, the mentioned symmetries are broken by vevs of two distinct scalars $\mathcal{S}_{\nu(e)}$ generating the electron and neutrino masses. This allows us to address the smallness of neutrino masses and the charged-lepton masses with two different energy scales coming from the mediator's vev. Following the convention from Eq. (3.11), the corresponding Lagrangian then reads

$$
\begin{aligned}
\mathcal{L}_{\text{eff}}^{\mathcal{S}\chi} = \mathcal{L}_{\text{SM}'} &+ \frac{1}{2}\left(\partial_\mu \mathcal{S}_\ell \partial^\mu \mathcal{S}_\ell - \mu_\ell^2 \mathcal{S}_\ell^2\right) + \overline{\chi}i\partial\!\!\!/\chi - m_\chi \overline{\chi}\chi \\
&- \frac{\lambda_\ell}{4}\mathcal{S}_\ell^4 - \lambda_{\nu e}\,\mathcal{S}_\nu^2 \mathcal{S}_e^2 - \lambda_{H\mathcal{S}_\ell}|H|^2 \mathcal{S}_\ell^2 \\
&- \frac{1}{\Lambda}\left[(y_\nu^{\mathcal{S}})_{ij}\,\overline{L}_L^i \widetilde{H} \nu_R^j\, \mathcal{S}_\nu + (y_e^{\mathcal{S}})_i\,\overline{L}_L^i H e_R\, \mathcal{S}_e + \text{h.c.}\right] \\
&- \left[\frac{y_\chi^\ell \mathcal{S}_\ell^2 + y_\chi^H |H|^2}{\Lambda}\,\overline{\chi}_L \chi_R + \text{h.c.}\right],
\end{aligned}
\tag{4.1}
$$

where a summation over $\ell = \nu, e$ is understood and L_L are the left-handed $SU(2)_L$ lepton doublets, e_R, ν_R^e are the right-handed electron and right-handed neutrinos, while

H is the Higgs doublet, furthermore, $\mathcal{L}_{\text{SM}'}$ denotes the SM Lagrangian without the Yukawa couplings of the electron (and the neutrinos).

Note that, the mediators develop small vevs $|\langle \mathcal{S}_\ell \rangle| \equiv v_\ell \ll v$, which break the $Z_2^{e,\nu}$ symmetries, carried by all the right-handed neutrinos and the right-handed electron, respectively, generating the masses for such light leptons. The mixing with the Higgs via the $|H|^2 \mathcal{S}_\ell^2$ operators has to be small and will not be considered in this section. Additionally, the conventional DM interaction $\mathcal{S}_\ell \bar{\chi} \chi$ is still generated with coefficient $\sim 2 y_\chi^\ell v_\ell / \Lambda$ which will remain relevant for the following analysis. Lastly, we assume the coefficient of the operator $|H|^2 \bar{\chi} \chi$ to be negligibly small, such as to evade DD constraints and limits from invisible Higgs decays [161, 289, 290].

Masses, Scalar Mixing and Free Parameters

We start by studying the fermion and scalar mass spectrum, and summarize the relevant free parameters. The fermion mass terms after electroweak and $Z_2^e \times Z_2^\nu$ symmetry breaking read

$$\mathcal{L} \supset - \sum_{\ell=e,\nu} \bar{\ell}_L \frac{v}{\sqrt{2}} \left(\mathbf{Y}_\ell^H + \frac{v_\ell}{\Lambda} \mathbf{Y}_\ell^{\mathcal{S}} \right) \ell_R \equiv - \sum_{\ell=e,\nu} \bar{\ell}_L M^\ell \ell_R \,, \tag{4.2}$$

where $\ell_{L,R} = e_{L,R}, \nu_{L,R}$ are three-vectors in flavour space and the Yukawa matrices

$$\mathbf{Y}_e^H = \begin{pmatrix} 0 & y_{12}^e & y_{13}^e \\ 0 & y_{22}^e & y_{23}^e \\ 0 & y_{32}^e & y_{33}^e \end{pmatrix}, \quad \mathbf{Y}_\nu^{\mathcal{S}} = \begin{pmatrix} (y_\nu^{\mathcal{S}})_{11} & (y_\nu^{\mathcal{S}})_{12} & (y_\nu^{\mathcal{S}})_{31} \\ (y_\nu^{\mathcal{S}})_{21} & (y_\nu^{\mathcal{S}})_{22} & (y_\nu^{\mathcal{S}})_{32} \\ (y_\nu^{\mathcal{S}})_{31} & (y_\nu^{\mathcal{S}})_{32} & (y_\nu^{\mathcal{S}})_{33} \end{pmatrix}, \quad \mathbf{Y}_e^{\mathcal{S}} = \begin{pmatrix} (y_e^{\mathcal{S}})_1 & 0 & 0 \\ (y_e^{\mathcal{S}})_2 & 0 & 0 \\ (y_e^{\mathcal{S}})_3 & 0 & 0 \end{pmatrix}, \tag{4.3}$$

and $\mathbf{Y}_\nu^H = \mathbf{0}$, reflect the $Z_2^e \times Z_2^\nu$ assignments. Due to vanishing eigenvalues of Y_ℓ^H, the electron and neutrinos would actually remain massless if the latter symmetries were not broken via $v_{e(\nu)} > 0$. On the other hand, and following the idea of Sec. 3.4, a small breaking of $v_\nu \sim \mathcal{O}(\text{eV})$ and $v_e \sim \mathcal{O}(\text{MeV})$ would be enough to generate $m_\nu \sim 0.1 \, \text{eV}$ and $m_e \sim 0.5 \, \text{MeV}$ with natural $(y_\ell^{\mathcal{S}}) \lesssim \mathcal{O}(1)$ and $\Lambda \gtrsim 1 \, \text{TeV}$. We note that, in order to explain the XENON1T excess in light of various constraints, it is necessary to deviate from these natural scales, ending up with a partly explanation of light-fermion masses.

The following steps are very similar to those discussed in Sec. 3.4 with the Z_2 odd mediator. Now, we perform a rotation to the mass basis,

$$\begin{aligned} \mathbf{M}^\nu &= \mathbf{U}_L^\nu \, \mathbf{M}_{\text{diag}}^\nu \mathbf{U}_R^{\nu \, \dagger}, \quad \text{with} \quad \mathbf{M}_{\text{diag}}^\nu = \text{diag}(m_{\nu_1}, m_{\nu_2}, m_{\nu_3}) \,, \\ \mathbf{M}^e &= \mathbf{U}_L^e \, \mathbf{M}_{\text{diag}}^e \mathbf{U}_R^{e \, \dagger}, \quad \text{with} \quad \mathbf{M}_{\text{diag}}^e = \text{diag}(m_e, m_\mu, m_\tau) \,, \end{aligned} \tag{4.4}$$

with $\mathbf{U}_L^e = \mathbf{U}_L^\nu\,\mathbf{V}_{\mathrm{PMNS}}$, the couplings of the physical leptons to the SM Higgs boson and the scalar mediators are given by

$$\mathcal{L} \supset -\sum_{\ell=e,\nu} \bar{\ell}_L \left(\frac{\hat{\mathbf{Y}}_\ell^H + v_\ell/\Lambda\, \hat{\mathbf{Y}}_\ell^{\mathcal{S}}}{\sqrt{2}}\, h + \frac{v\,\hat{\mathbf{Y}}_\ell^{\mathcal{S}}}{\sqrt{2}\Lambda}\,\mathcal{S}_\ell \right) \ell_R\,, \tag{4.5}$$

where $\hat{\mathbf{Y}}_\ell^s = \mathbf{U}_L^{\ell\,\dagger}\mathbf{Y}_\ell^s\mathbf{U}_R^\ell$, $s = H, \mathcal{S}$; $\ell = \nu, e$, and (with some abuse of notation) we denote the mass eigenstates by the same spinors $\ell = e, \nu$. The Yukawa matrices in the mass basis can be expressed as

$$\hat{\mathbf{Y}}_\ell^{\mathcal{S}} = \frac{\sqrt{2}\Lambda}{vv_\ell}\,\mathbf{M}_{\mathrm{diag}}^\ell\,\mathbf{U}_R^{\ell\,\dagger}\mathbf{C}_\ell^S\,\mathbf{U}_R^\ell\,,$$
$$\hat{\mathbf{Y}}_\ell^H = \frac{\sqrt{2}}{v}\,\mathbf{M}_{\mathrm{diag}}^\ell\,\mathbf{U}_R^{\ell\,\dagger}\mathbf{C}_\ell^H\,\mathbf{U}_R^\ell\,, \tag{4.6}$$

where $\mathbf{C}_e^S = \mathrm{diag}(1,0,0)$, $\mathbf{C}_\nu^S = \mathrm{diag}(1,1,1)$, $\mathbf{C}_e^H = \mathrm{diag}(0,1,1)$ and $\mathbf{C}_\nu^H = \mathbf{0}$, and the unitary rotations of the left-handed lepton fields drop out since they share the same Z_2^ℓ charges. Thus, the couplings with a fixed right-handed lepton are aligned with the corresponding mass terms. While this is not true for the right handed leptons, which could introduce FCNCs. Here, we chose the Yukawa matrices $\mathbf{M}_{\mathrm{diag}}^\ell$, such that $\mathbf{U}_R^e = \mathbf{1}$, avoiding FCNCs. The Yukawa matrices then read

$$\hat{\mathbf{Y}}_e^{\mathcal{S}} = \frac{\sqrt{2}\Lambda}{vv_e}\,\mathrm{diag}(m_e, 0, 0)\,,$$
$$\hat{\mathbf{Y}}_\nu^{\mathcal{S}} = \frac{\sqrt{2}\Lambda}{vv_\nu}\,\mathrm{diag}(m_{\nu_1}, m_{\nu_2}, m_{\nu_3})\,,$$
$$\hat{\mathbf{Y}}_e^H = \frac{\sqrt{2}}{v}\,\mathrm{diag}(0, m_\mu, m_\tau)\,, \tag{4.7}$$
$$\hat{\mathbf{Y}}_\nu^H = \mathbf{0}\,.$$

As a consequence, muons and taus interact with the Higgs boson as in the SM, while the electrons and neutrinos couples instead only to $\mathcal{S}_{e,\nu}$, accordingly. The interaction strength is determined by the free parameter $v_{e,\nu}$, which can be traded for $y_e^{\mathcal{S}}/\Lambda \equiv (\hat{\mathbf{Y}}_e^{\mathcal{S}})_{11}/\Lambda$ in the electron case and $y_1^{\mathcal{S}}/\Lambda$, where $y_i^{\mathcal{S}}/\Lambda \equiv (\hat{\mathbf{Y}}_\nu^{\mathcal{S}})_{ii}/\Lambda$, for the neutrino case.

Besides the fermion mixing, the scalar potential term parametrized by $\lambda_{\nu e}$ also leads to a scalar mixing after they obtain their corresponding vevs $|\langle \mathcal{S}_{\nu e}\rangle| = v_{\nu e}$. Such mixing is described by an angle θ as

$$\begin{pmatrix} s \\ S \end{pmatrix} = \begin{pmatrix} \cos\theta & \sin\theta \\ -\sin\theta & \cos\theta \end{pmatrix} \begin{pmatrix} \mathcal{S}_\nu \\ \mathcal{S}_e \end{pmatrix}\,, \tag{4.8}$$

with

$$\tan 2\theta = \frac{4\,\lambda_{ve}v_v v_e}{M_v^2 - M_e^2}\,, \tag{4.9}$$

where $M_\ell^2 = \mu_\ell^2 + 3\lambda_\ell v_\ell^2 + 2\lambda_{ve}\,v_v^2 v_e^2/v_\ell^2$. The resulting physical masses read

$$m_{s/S}^2 = \frac{1}{2}(M_v^2 + M_e^2) \pm \frac{M_v^2 - M_e^2}{2\cos 2\theta}\,. \tag{4.10}$$

Taking the difference in the energy scale between neutrinos and electrons, where in general $m_v \ll m_e$, we assume $v_v \ll v_e$ and accordingly $M_v \ll M_e$. This leads to $m_s \approx M_v$, $m_S \approx M_e$, as well as $\cos\theta \approx 1$, $\sin\theta \ll 1$. The scalar mixing then induces suppressed couplings between the electron and the light mediator s (as well as between the neutrinos and the heavy scalar S), given by

$$\mathcal{L}_s = -s\frac{v}{\sqrt{2}\Lambda}\left(c_\theta y_i^{\mathcal{S}}\,\bar{v}_L^i v_R^i + s_\theta y_e^{\mathcal{S}}\,\bar{e}_L e_R\right),$$

$$\mathcal{L}_S = -S\frac{v}{\sqrt{2}\Lambda}\left(c_\theta y_e^{\mathcal{S}}\,\bar{e}_L e_R - s_\theta y_i^{\mathcal{S}}\,\bar{v}_L^i v_R^i\right), \tag{4.11}$$

where $c_\theta \equiv \cos\theta$, $s_\theta \equiv \sin\theta$.

The couplings of the electrons and the first neutrino to the light (and heavy) mediators s (and S) can then be written as

$$y_e^s \equiv s_\theta \frac{v}{\sqrt{2}\Lambda}y_e^{\mathcal{S}}, \qquad y_v^s \equiv c_\theta \frac{v}{\sqrt{2}\Lambda}y_1^{\mathcal{S}},$$

$$y_e^S \equiv c_\theta \frac{v}{\sqrt{2}\Lambda}y_e^{\mathcal{S}}, \qquad y_v^S \equiv -s_\theta \frac{v}{\sqrt{2}\Lambda}y_1^{\mathcal{S}}. \tag{4.12}$$

At this point, we are in a position to summarize the free parameters of our setup, relevant for our study, which are

- the mediator masses $m_{s,S} \approx M_{v,e}$

- the $\mathcal{S}_e-$Yukawa coupling $y_e^{\mathcal{S}}/\Lambda$

- the $\mathcal{S}_v-$Yukawa coupling $y_1^{\mathcal{S}}/\Lambda$

- the mixing portal λ_{ve},

- the DM mass m_χ

- the bi-quadratic DM portal coupling y_χ^ℓ/Λ,

where the remaining Yukawa couplings are given by Eq. (4.7).

4.3   Fitting the Excess

In this section, we propose two possible scenarios that could fit the XENON1T excess. In the first one, we make use of a modified neutrino interaction and study the corresponding neutrino-electron scattering, whereas in the second one we study the DM-electron scattering. Additionally, we also examine the fulfillment of the DM relic abundance in the aforementioned scenarios. The corresponding Feynman diagrams for the scattering of both models are shown in Fig. 4.2.
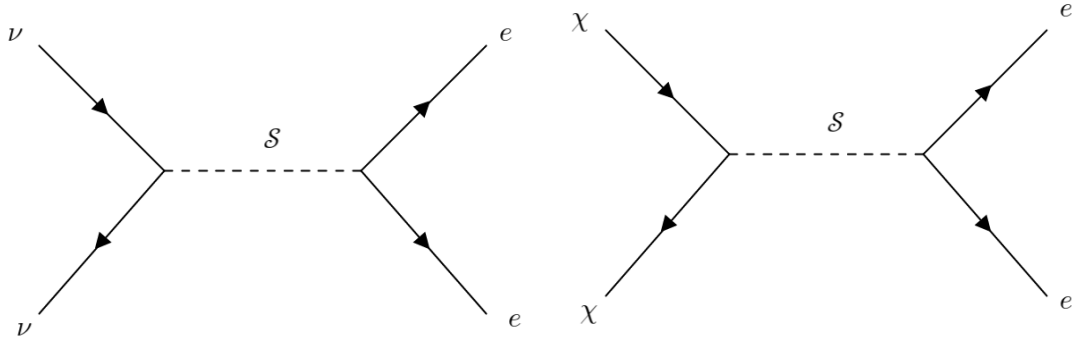
FIGURE 4.2: Corresponding Feynman diagrams for neutrino and DM electron scattering, respectively.

Modified Neutrino Interactions

In this first scenario, we assume the DM-electron scattering inducing an electron recoil to be negligible, and therefore will not be taken into account. Instead, we propose the origin of the excess explained by modified neutrino scattering with electrons, in our model mediated by s and $\mathcal{S}$. As we will see, observational constraints prefer $m_s \ll m_{\mathcal{S}}$ such that neutrino-electron scattering can, to good approximation, be described by s-exchange alone. The differential cross section for the new-physics signal reads [291]

$$\frac{d\sigma_{\nu e}}{dE_r} = \frac{(y_e^s y_\nu^s)^2}{4\pi(2m_e E_r + m_s^2)^2} \frac{m_e^2 E_r}{E_{\nu 2}} \, , \tag{4.13}$$

where m_e is the electron mass, E_ν the energy of the incoming neutrino, E_r the electron recoil energy. The couplings of the electrons and the first neutrino to the light (and heavy) mediators are shown in Eq. (4.12). The true differential event rate is thus given by convoluting the differential cross section and the incident neutrino flux ϕ_ν, weighting by the number of electrons per unit mass N_e

$$\frac{dR}{dE_r} = N_e \int dE_\nu \, \frac{d\sigma_{\nu e}}{dE_r} \frac{d\phi_\nu}{dE_\nu} \, . \tag{4.14}$$

At the energies relevant for the XENON1T excess, the neutrino flux is dominated by *pp* neutrinos from the sun. For the observed value of the *pp*-flux, we use Ref. [292] whereas for the parameterization of the spectrum we employ [293].

In the following, we assume a universal interaction between the light mediator (*s*) and the different neutrino flavours, such that oscillation effects do not affect the scattering rate. To make the connection between our theoretical spectrum and the observed rate, experimental effects have to be included, in particular the efficiency reported in [294] is applied. The limited detector resolution is taken into account via a gaussian smearing function with an energy dependent resolution. As suggested in [295] we take the ansatz

$$\sigma(E)/E = \frac{a}{\sqrt{E}} + b \qquad (4.15)$$

and assume that the resolution varies between $\approx$ 30% at $E_r = 1$ keV and $\approx$ 6% at 30 keV. We adopt the best fit background model from the experimental publication [294] and allow the normalization to vary within the 1σ.

In order to assess the impact of a light scalar on the electron-neutrino scattering, a χ^2 analysis of the signal and background model is performed. We find that a coupling of

$$\sqrt{y_e^s y_\nu^s} \approx 7.9 \times 10^{-7} \qquad (4.16)$$

is preferred with barely no dependence on m_s for masses $m_s \lesssim 20$ keV. An exemplary comparison between the signal associated with the best fit point for $m_s = 60$ eV and the data is shown in Fig. 4.3. This choice of parameters corresponds to $\chi^2_{best} = 38.9$ compared to $\chi^2_{bd} = 47.1$ for the background-only hypothesis. We can see that our results are in good qualitative agreement with those in [245–247] which study a related setup. Next, we confront them with a comprehensive set of complementary experimental constraints.

DM Scattering and Relic Abundance

One of the many advantages of the eDMEFT [9] and the slightly extended eDMEFT frameworks, presented in Sect. 3.3 and Sec. 4.2, accordingly, is that both of them naturally include DM interactions. Hence, the scattering between DM and electrons is possible, and could account to the observed excess (see right panel of Fig. 4.2). In addition, it is also, interesting to check whether the correct relic abundance can be achieved simultaneously with an explanation of the XENON1T excess. These observables are correlated with each other as in the neutrino case, via the mediator couplings to SM fermions.

A naive estimate of the maximum recoil energy possible in non-relativistic DM-electron collisions leads to

$$E_{r,max} = \frac{2\mu_{\chi,e}^2}{m_e} v_{max}^2 \approx 2 \times 10^{-6} m_e, \qquad (4.17)$$
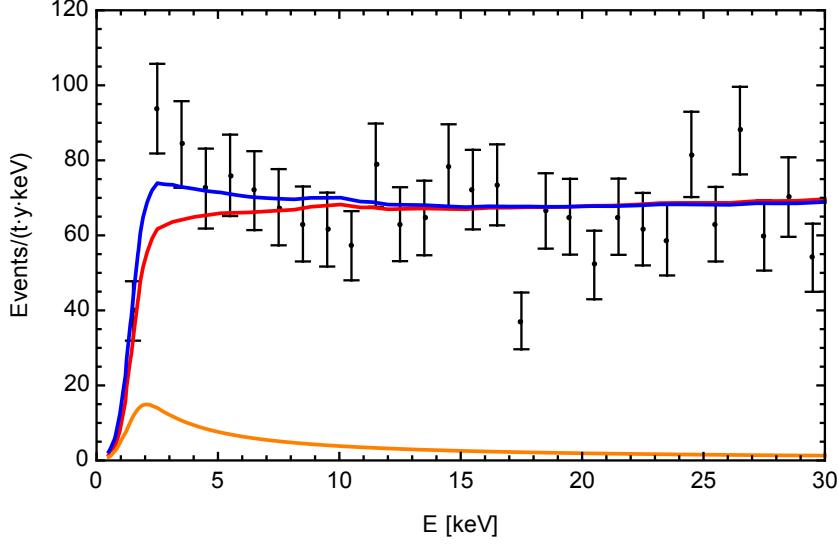
FIGURE 4.3: Comparison between an exemplary differential event rate
for a scalar with $m_s = 60 \, \text{eV}$ and $\sqrt{y_e^s y_\nu^s} = 7.9 \times 10^{-7}$ and the data as
reported by [183]. The full differential event rate is shown in blue while
the pure signal (background) contribution is depicted in orange (red).

where $\mu_{\chi,e}$ is the reduced mass of the system and v the speed of DM. After taking into
account that v is limited by the local escape velocity of our galaxy, $v_{esc} = \mathcal{O}(10^{-3} c)$,
and for $m_{DM} \gg m_e$ this leads to an estimate of $E_{r,max} \approx 1 \, \text{eV}$ and thus well below the
energy scale required to account for the signal. Nevertheless, it is important to note
that the electrons form part of a bound system, the xenon atom. As a consequence, the
momentum of the electron is different from zero and could in principle take an arbitrary
value. The typical momentum of the bound electron is expected to be $\mathcal{O}(\alpha_{em} m_e)$ which
is small but allows for a larger energy transfer in the DM-electron scattering process
[296]. Then, the differential event rate is given by

$$\frac{dR}{dE_r} = \frac{n_{Xe} \rho_\chi}{m_\chi} \frac{d\langle \sigma_{\chi e} \rangle}{dE_r} \tag{4.18}$$

where n_{Xe} is the number of xenon atoms per unit mass in the detector and $\rho_\chi \approx$
$0.3 \, \text{GeV}/\text{cm}^3$ the local DM density. For the velocity averaged differential cross section,
we rely on the results of [297, 298]. In the heavy mediator limit, it can be parametrized
as

$$\frac{d\langle \sigma_{\chi e} \rangle}{dE_r} = \frac{\sigma_{\chi e}}{2 m_e} \int dv \, \frac{f(v)}{v} \int dq \, a_0^2 q K(E_r, q) \,, \tag{4.19}$$

where $\sigma_{\chi e}$ is the cross section for scattering on a free electron with a momentum trans-
fer $a_0^{-1} = \alpha_{em} m_e$, while $f(v)$ denotes the velocity distribution of the DM at Earth. The
atomic physics is encoded in the excitation factor K, originally computed in [297]. In or-
der to estimate the implications of a DM signal, we consider the averaged cross sections
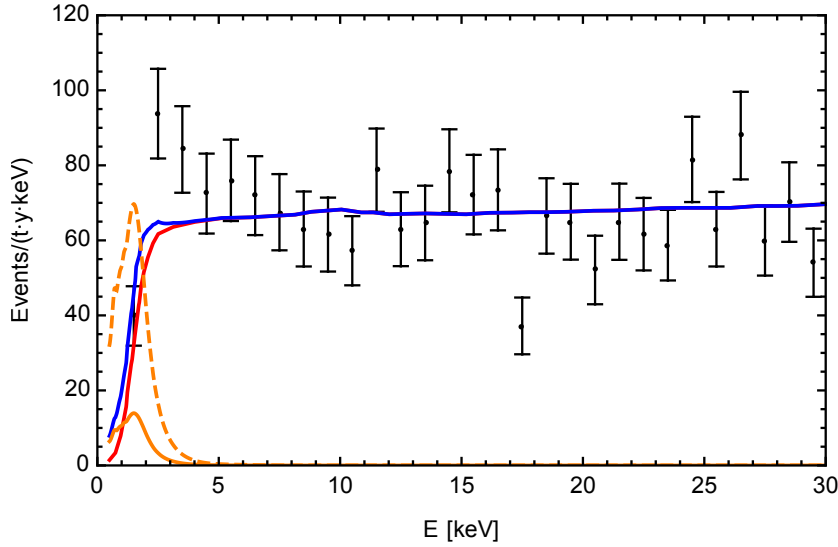
FIGURE 4.4: Comparison between the best fit differential event rate for a
DM particle with $m_\chi = 10\,\text{GeV}$ and $\sigma_{e\chi} = 1.25 \times 10^{-39}\,\text{cm}^2$ and the data.
The style is similar to Fig. 4.3 and for better visibility we also show the
signal rate enhanced by a factor of 5 as an orange dashed line.

reported in [298], and perform a fit to the signal using the same assumptions about the
detector as in the neutrino case. Note that, the case of a light mediator, leads to a much
stronger energy dependence of the signal and is expected to provide a worse fit of the
signal than a heavy mediator.

The best fit recoil rate that we found is depicted in Fig. 4.4, where the correspond-
ing values are $m_\chi = 10\,\text{GeV}$ and $\sigma_{\chi e} \approx 1.25 \times 10^{-39}\,\text{cm}^2$, which could for instance be
explained by an MeV scale mediator with an $\mathcal{O}(1)$ coupling to DM and $y_e^S \approx 10^{-5}$. It
can be seen that, at low energies, the signal (in orange) rises very steeply such that the
peak occurs at approximately 1.5 keV instead of the 2.5 keV needed to reproduce the
data. Nonetheless, it is interesting to note that the fit shows some improvement if a
small DM signal is added, even though, the statistical improvement only amounts to
marginally more than 1σ. Therefore, the DM-electron-scattering hypothesis does not
provide a convincing explanation of the observation and we do not entertain this pos-
sibility further. In reference [253], similar conclusions were reached. To have a better
fit with DM, requires a flatter recoil spectrum. This could for instance be achieved if a
relativistic or semi-relativistic DM sub-population [258,259,262] contribute to the signal
or if the interaction has additional momentum dependence [253].

Regardless of the success of the DM-electron scattering model in fitting the excess, it
is interesting to explore whether the observed DM relic density can be accounted for in
our framework. To this end, we assume the DM production mechanism via freeze-out
(see Sec. 3.2), the main DM annihilation channels are e^+e^- and $\mathcal{S}^2$ final state[1]. Then, the

---

[1]Here we neglect the corresponding contributions involving the light mediator s for simplicity, which
does not lead to qualitative changes.

correct relic abundance can be achieved if the thermally averaged annihilation cross-section is $\mathcal{O}(10^{-26}\,\mathrm{cm}^3\,\mathrm{s}^{-1})$. The cross-section for the e^+e^- channel can be estimated as [12]:

$$\langle \sigma v \rangle_{ee} \approx \frac{1}{8\pi}\,\frac{v^2 v_e^2}{\Lambda^4}\,\frac{(y_\chi^e)^2 (y_e^{\mathcal{S}})^2 m_\chi^2}{(m_S^2 - 4m_\chi^2)^2}\,v_\chi^2$$

$$\approx 10^{-5} \sigma_v^0 \left(\frac{v_e}{5\,\mathrm{GeV}}\right)^2 \left(\frac{1\,\mathrm{GeV}}{m_\chi}\right)^2 \left(\frac{10\,\mathrm{TeV}}{\Lambda}\right)^4 (y_\chi^e)^2 (y_e^{\mathcal{S}})^2 , \qquad (4.20)$$

where v_χ is the DM velocity (the cross-section is p-wave suppressed), while $\sigma_v^0 = 2 \times 10^{-26}\,\mathrm{cm}^3\,\mathrm{s}^{-1}$. A similar estimate for the cross-section $\chi\bar{\chi} \to \bar{\mathcal{S}}\mathcal{S}$ final state reads:

$$\langle \sigma v \rangle (\bar{\chi}\chi \to \bar{\mathcal{S}}\mathcal{S}) \approx 10^{-3}\,\sigma_v^0 \left(\frac{10\,\mathrm{TeV}}{\Lambda}\right)^2 (y_\chi^e)^2. \qquad (4.21)$$

We find that the e^+e^- cross section is too small if the XENON1T excess is explained consistently. However, the S^2 cross section could lead to the correct relic density, under the conditions: Λ is lowered to the TeV scale and $y_\chi^e \gtrsim 1$.

Another possibility to improve the cross sections is considering an alternative production mechanism. In this case, we use the freeze-in mechanism as it is more easily realized within our setup. In this case, the thermal equilibrium has never been realized in the early Universe as $y_\chi^\ell \ll 1$ and the DM interactions are extremely weak. Then the relic density can be built up from a negligible initial value, by $S\bar{S}(s\bar{s}) \to \bar{\chi}\chi$ inverse annihilation processes and, $S \to \bar{\chi}\chi$ decays for sufficiently light DM. Since it is realized via a $D = 5$ operator, the annihilation process leads to a UV dominated rate. Hence the relic density is sensitive to the largest temperature and we need to specify our assumed value for the reheating temperature T_R. In order not to exceed the validity of our EFT we limit ourselves to T_R below the new physics scale Λ.

We compute the relic density with the freeze-in module implemented in the public software micrOMEGAs 5 [299] which takes the full momentum dependence of the annihilation and decay rates into account. In Fig. 4.5, we show the isocontours of $\Omega_\chi h^2 = 0.12$ in the (m_χ, y_χ^e) plane for the two benchmark models described in Sec. 4.4, assuming $y_\chi^\nu = y_\chi^e$. In our computation we have adopted $T_R = 100\,\mathrm{GeV}$. The DM relic density depends, besides the plotted parameters, on m_S and v_e. The values of the latter two parameters are comparable for our benchmarks ($m_S \sim 5\,\mathrm{MeV}$, $v_e \sim 5\,\mathrm{GeV}$), so that the two contours in Fig. 4.5 are rather close to each other and align in the high and low mass limit.

4.4 Terrestrial and Astrophysical Constraints

We continue with the study of the neutrino-scattering case. As additional interactions of scalars with electrons and neutrinos are targets of various experimental searches, we confront the neutrino-electron scattering with several of these constraints. We keep the exploration in two different scenarios: our specific $Z_2^e \times Z_2^\nu$ setup and in a more general
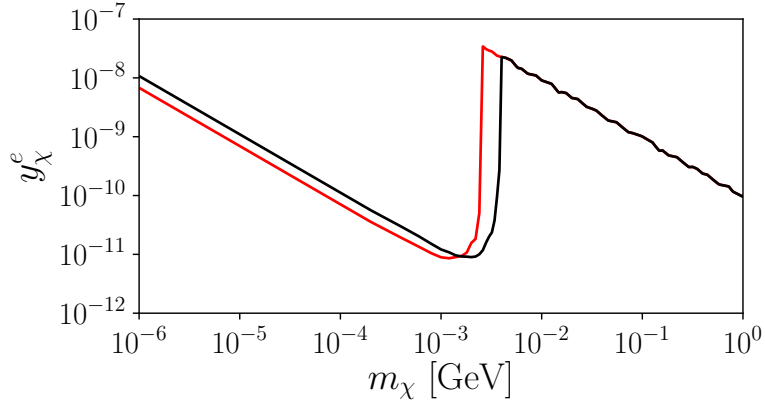
FIGURE 4.5: Isocontours of correct DM relic density assuming production through freeze-in and considering the assignations of model parameters for BM1 (red) and BM2 (black). The reheating temperature T_R has been set to 100 GeV.

subset of eDMEFT operators. The above models are summarized in Figs. 4.6 and 4.7 for the scalar-couplings to electrons and neutrinos, respectively.

Bounds on the Electron-Neutrino Scalar Interaction

There are several experiments studying the neutrino-electron scattering, as it is a key signature for the observation of solar and reactor neutrinos. These experiments probe very similar physics as XENON1T and place an upper bound on the neutrino-electron scattering rate, which is relevant for our study. The reported bounds on new physics that lead to a recoil spectrum peaking at low energies are normally interpreted in terms of a neutrino magnetic moment μ_ν. Nowadays, the best limits come from Borexino [301] and GEMMA [302] standing at $\mu_\nu < 2.9 \times 10^{-11} \mu_B$ with a 90% C.L. This is right on the edge of the values preferred by the XENON1T excess, $\mu_\nu = 1.4 - 2.9 \times 10^{-11} \mu_B$ found by the collaboration in [183], but does not exclude the neutrino magnetic moment interpretation. This observation is particularly relevant for the scenario under consideration featuring a light scalar mediator.

In the energy range of the observed XENON1T signal, the recoil energy distribution of events that are induced by solar or reactor neutrinos interacting via a light scalar ($m_s \lesssim E_r$) or a magnetic moment are essentially indistinguishable. Therefore, an interpretation of the Borexino data in our model will only apply relevant constraints on the upper boundary of the preferred region. Furthermore, as the signal and the expected exclusion are close to each other, the exact position of the upper bound will depend on the details of the experimental data and the statistical procedure, and a naive phenomenological recast is unlikely to allow for a clear comparison. Thus, we refrain from quoting an explicit limit and note that the bound is expected to be closely aligned with the upper edge of the preferred values $\sqrt{y_e^s y_\nu^s}$.
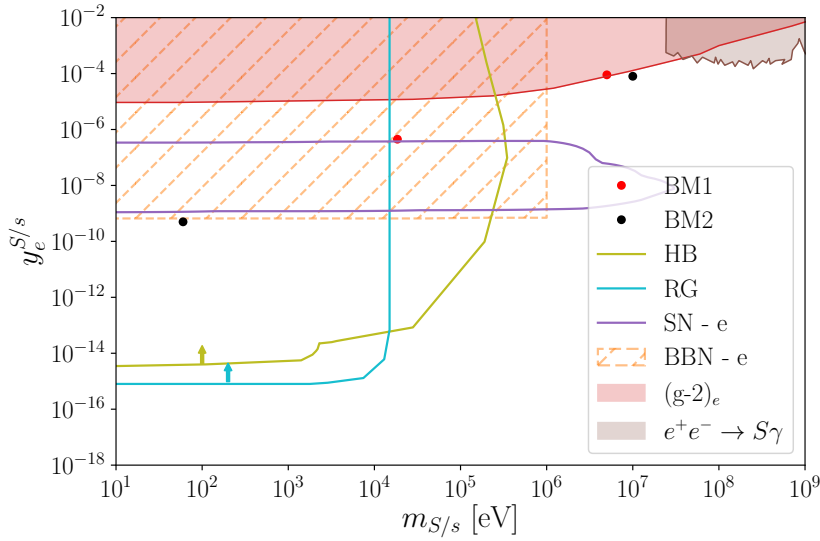
FIGURE 4.6: Constraints in the $m_{S/s} - y_e^{S/s}$-plane from [300] and our own analysis, including our two BM points. For a discussion of the various limits and their shading, see the main text.

Bounds on Electron Couplings

In this case, terrestrial precision experiments are remarkably good at testing couplings between electron and NP states. Particularly, in the mass range of interest, the tighter constraints come from the anomalous magnetic moment of the electron, a_e, as both the experimental measurement and the SM prediction are incredibly precise. At 3σ the deviation of a_e from the SM expectation is limited to $\delta a_e \lesssim 1.4 \times 10^{-12}$ [303, 304]. The new scalars under consideration then contribute [305]

$$\delta a_e^s = \frac{(y_e^s)^2}{4\pi^2} \frac{m_e^2}{m_s^2} I_S\left(\frac{m_e^2}{m_s^2}\right),$$ (4.22)

where the loop function is given by

$$I_S(r) = \int_0^1 dz \frac{z^2(2-z)}{1 - z + z^2 r}.$$ (4.23)

For $m_s \ll m_e$, this leads to $y_e^s \lesssim 10^{-5}$ while the limit relaxes for $m_s \geq m_e$, a similar behaviour is shown in the red area in Fig. 4.6. Softer terrestrial constraints can be derived from e^+e^- colliders through the process $e^+e^- \to \gamma s$ which dominates for $m_s \sim \mathcal{O}(1)$ GeV, see for example [300].

In addition, there are a number of bounds on $y_e^{s,S}$ from astrophysical and cosmological observations. In the energy range where the mediator mass is comparable or smaller than the core temperature of a star, the emission of the scalars can contribute to the energy loss and change the properties and dynamics of these astrophysical systems. In particular, strong limits can be derived from red giants (RG) and horizontal

branch stars (HB). We adopt the results of [300,306] where plasma mixing is considered to be the main production mechanism of the light scalars, for a more recent analysis of the impact of stellar cooling on NP in other models refer to Ref. [307]. In principle, for $m_{s,S} \ll 10$ keV, the RG bound excludes couplings $y_e^s \gtrsim 10^{-15}$ and therefore such a small y_e^s excludes a solar neutrino interpretation of the XENON1T excess for all reasonable values of y_ν^s. The bounds from observations of HB stars are less severe at low masses but take over for $m_{s,S} \gtrsim 10$ keV. However, it is conceivable that these constraints can be circumvented in the presence of additional new physics such as an environment-dependent mass for the scalar similar to the chameleon mechanism considered in cosmology [308,309]. In Ref. [310], a first attempt to perform such a solution for theories that explain the XENON1T excess has been presented, having promising results. Alternatively, y_e^s could depend on the matter background and thus be suppressed in a high density environment such as stellar cores. Therefore, we consider such astrophysical bounds less robust than the direct laboratory bounds discussed before and in consequence draw them as lines in Fig. 4.6, removing the shading from the disfavored regions.

Moving forward, the supernova (SN) SN1987A set another constraint for mediator masses up to $\mathcal{O}(10)$ MeV, as additional light degrees of freedom would cool the SN too rapidly, in opposition to current observations [311]. Due to the very high density of the SN core, the scalar mediator can be trapped before actually leaving the core and as consequence, the limits for higher values of y_e^s vanish (see Fig. 4.6). We consider the limits from [300], where only the resonant production via mixing with the longitudinal component of the photon is included and direct production through Compton scattering or electron-ion recoil is neglected. This is possible for $m_s < w_p \sim 20$ MeV, where w_p is the photon plasma frequency [312]. The trapping regime for resonant production is included by using the balance of production and absorption rate, with the requirement of the scalar to be re-absorbed in a range of $R \approx 10$ km. In this trapping regime, the decay $s \to e^+ e^-$ determines the bound for masses MeV$\leq m_s \leq 30$ MeV.

To finalize the constraints on the electron couplings, we also assume bounds from Big Bang Nucleosynthesis (BBN), for additional light degrees of freedom entering thermal equilibrium with e and γ. On top of an increase of N_{eff}, the entropy release from $e^+ e^-$ annihilation is diluted in that case. This leads to a lower photon temperature during BBN and therefore a higher baryon-to-photon ratio, which causes a decrease of the deuterium abundance [300]. For $m_s \lesssim 1$ MeV,the BBN bound is flat and requires $y_e^s \lesssim 10^{-9}$. Nonetheless, in our specific setup, this robust constraint can be circumvented with a late time phase transitions in the new physics sector. This prevents the mixing of the scalar mediators s and S in the early Universe, removing the coupling y_e^s at the relevant temperatures. More comments on this are in Sec. 4.5.

Bounds on Neutrino Couplings

Let us now discuss all possible constraints on the neutrino scalar coupling. In general, the interaction between NP and neutrinos is harder to test than in the case of electrons,
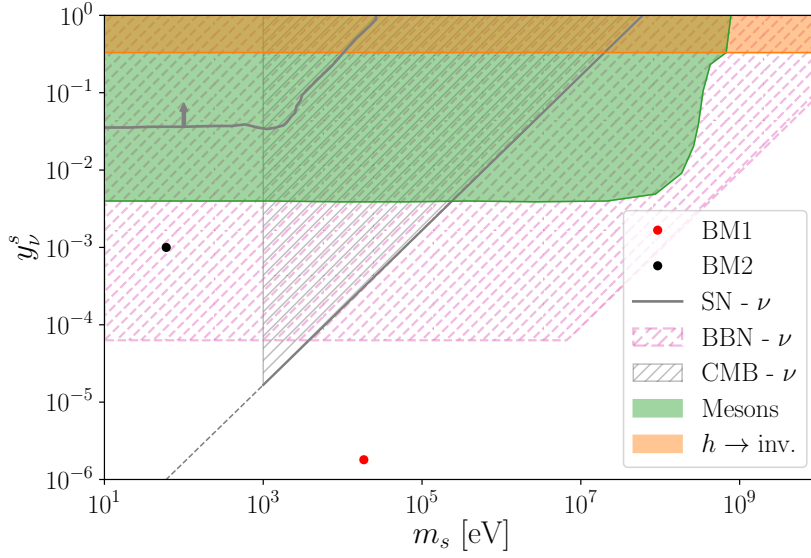
FIGURE 4.7: Constraints in the $m_s - y_\nu^s$-plane including our two BM points. Note that the heavier mediator does not show here as it has a very small coupling.

thus, we expect the bounds to be less constraining. However, robust terrestrial bounds arise from searches for new meson decays such as $K^-/D^-/\pi^- \to e^- s\nu$ [313]. Decays to μ^- can also be considered. In Fig. 4.7, we show the strongest limit of those decay combinations, assuming a flavour universal coupling. In case of flavour non-universality, the bounds for electron couplings are slightly stronger. The tighter bound on y_ν^s comes from the limits on the decay width of Higgs to invisible states via $h \to s\nu\nu$, for mediator masses between $m_h > m_s \gtrsim 1\,\text{GeV}$ [313]. In Fig. 4.6, we use the latest ATLAS result of $\text{BR}(h \to \text{inv.}) < 0.13$ [76,314].

The observation of MeV-scale neutrinos originating from SN1987A constraints the neutrino self-interaction [315]. This is because the scattering of the SN-neutrinos with the CMB-ν via the new mediator shifts their energy to significantly lower values and potentially below the detection threshold. Additionally, the SN neutrinos get deflected which delay their arrival on earth. A first bound was derived in [316], however, we show the one from [315] in Fig. 4.7, where the recent limits on the neutrino masses were used.

The considered model could also have an impact on the amount of radiation in the Universe which can be tested by BBN. Particularly, the right-handed neutrinos are dangerous, as if each of them is fully thermalized, they would contribute $\Delta N_{eff} = 1$ while the upper bound stands at approximately 0.2 [317]. Therefore, the only regions of parameter space allowed by cosmology are those where the right-handed neutrinos do not reach thermal equilibrium before the left-handed ones decouple from the SM bath. Even if the initial population of ν_R is negligible we can produce them in neutrino-antineutrino scattering via s exchange in a t-channel. A good estimate for thermalization can be obtained by requiring that the production rate γ does exceed the Hubble

BM	M_ν	M_e	y_ν^S	y_e^S	Λ	$\lambda_{\nu e}$
BM1	18.5 keV	5 MeV	1×10^{-4}	0.005	10 TeV	3×10^{-4}
BM2	60 eV	10 MeV	0.06	0.005	10 TeV	0.001

TABLE 4.1: Chosen benchmark points to confront our model with the astrophysical and laboratory constraints presented in Sec. 4.4.

rate H before the neutrino decoupling that happens at about $2 - 3$ MeV. In our model, the thermally averaged production rate reads

$$\gamma \approx \langle \sigma v \rangle \times n_\nu \approx \frac{(y_\nu^s)^4}{512\pi} T, \tag{4.24}$$

where n_ν is the equilibrium number density of neutrinos and $\langle \sigma v \rangle$ is the thermally averaged ν_R production cross section. By requiring $\gamma < H$, we find $y_\nu^s \lesssim 6.3 \times 10^{-5}$ for $m_s \ll 2$ MeV, the bound then weakens for larger masses, as depicted in Fig. 4.7. Since the absence of a ν_R bath prevents the direct production of s, its contribution is less pronounced than in the case of electrons. This bound can be avoided by adding another mass term for the right-handed neutrinos, making them too heavy to contribute to N_{eff}. The latter can be realized rather easily in our setup, by just increasing v_ν such as to generate a more sizable Dirac-mass term leading to viable neutrino masses via see-saw suppression in the presence of large Majorana masses for the right-handed neutrinos. This approach would provide a hybrid explanation for the smallness of neutrino masses, however, further details on this are not included in this thesis.

To finalize with the neutrino bounds, there are also constraints coming from the CMB. In this case, if the neutrinos interaction rate is high enough, they cannot be considered as a free-streaming gas. Therefore, the impact of their interactions needs to be included in the Boltzmann equations governing the evolution of the primordial perturbations. For a heavy mediator, this leads to an upper bound on the interaction strength of $(y_\nu^s/m_s)^2 \le (0.06\,\text{GeV})^{-2}$ [318]. This estimate is only valid when $m_s \gg 10$ eV, thus, the limit become unreliable for lower masses, in particular for BM2 while BM1 is outside the limit anyways. Nevertheless, alternative limits on very light mediators are also available [318] but they only become applicable at even smaller masses.

Benchmark Models

To confront our model for the XENON1T excess with the astrophysical and laboratory constraints presented above, we define two different benchmarks (BMs) defined by the independent input parameters depicted in Table 4.1. Both of them delivering a good fit to the anomaly as in Eq. (4.16). While we require roughly natural scales for the model, we are mainly led by the goal to avoid the most severe experimental bounds.

The benchmark points lead to the vevs $(v_\nu, v_e) = (26.5\,\text{keV}, 5.3\,\text{GeV})$ and $(v_\nu, v_e) = (50\,\text{eV}, 5.9\,\text{GeV})$ for BM1 and BM2, respectively. The derived physical couplings for the corresponding mixing angles for each BM, $s_\theta^{\text{BM1}} = -5 \times 10^{-3}$ and $s_\theta^{\text{BM2}} = -6 \times 10^{-6}$,

BM	y_ν^s	y_e^s	y_ν^S	y_e^S
BM1	$1.8{\times}10^{-6}$	$-4.5{\times}10^{-7}$	$8.3{\times}10^{-9}$	$9{\times}10^{-5}$
BM2	0.001	$-5{\times}10^{-10}$	$6{\times}10^{-9}$	$8{\times}10^{-5}$

TABLE 4.2: Derived physical couplings.

are presented in Table 4.2. The couplings associated with BM1 and BM2 are displayed in red and black in the landscape of collected bounds on $y_e^{s/S}$ and y_ν^s in Fig. 4.6 and Fig. 4.7, respectively. For both BMs, we arrive at a prediction for the strength of the anomaly of

$$y_e^s y_\nu^s \approx -(5-7) \times 10^{-13} \,, \tag{4.25}$$

in line with the best-fit value obtained before[2] in Eq. (4.16).

There are two main assumptions, regarding the nature of neutrino masses, that are needed in order to define the aforementioned benchmarks:

1. We assumed an *inverted* neutrino-mass hierarchy, i.e. $m_{\nu_3} \ll m_{\nu_1} \sim m_{\nu_2} \sim 0.05\,\text{eV}$. In this case, the interaction of the lightest neutrino is negligible while both $\nu_{1,2}$ couple to the mediator s with similar strength y_ν^s, see Eq. (4.7). The heaviest neutrinos, $\nu_{1,2}$, couple universally to s and contain almost all the electron-flavour content. As a consequence, no flux from the sun will be lost when considering neutrino-electron scattering in XENON1T and the analysis as described above remains valid.

2. A *normal* hierarchy, i.e. $m_{\nu_1} \sim m_{\nu_2} \sim 0.05\,\text{eV} \ll m_{\nu_3}$, would also be consistent with the same BMs. Here we assume that both chiralities of the heaviest state ν_3 are even under the Z_2^ν symmetry. Therefore, the heaviest state does not couple to s and again, the electron-neutrino content is almost entirely in the universally coupling eigenstates $\nu_{1,2}$.

Let us have some final comments on the chosen benchmarks. The precision bounds for the mediator mass of $m_S \sim 10$ MeV, can be evaded for a value of $v_e > M_e$, somewhat above the electron mass, leading to a coupling of electrons to the heavy mediator of $y_e^S \sim 10^{-4}$ [300]. On the other hand, the coupling to the light s is suppressed in s_θ, pushing the resulting interaction into the window above the SN1987A exclusion region but below the $(g-2)_e$ limit for BM1, while BM2 can even evade BBN constraints without further requirements (at the price of a higher neutrino coupling). The BBN constraint for electrons in BM1 can be avoided via a late phase transition, generating the vev $v_\nu > 0$ below $T \approx 150\,\text{keV}$, as we discuss in Sec 4.5.

---

[2]Moreover, both BMs satisfy the positive-definiteness condition $M_\nu M_e > 2\lambda_{\nu e} v_\nu v_e$, ensuring a proper potential minimum.
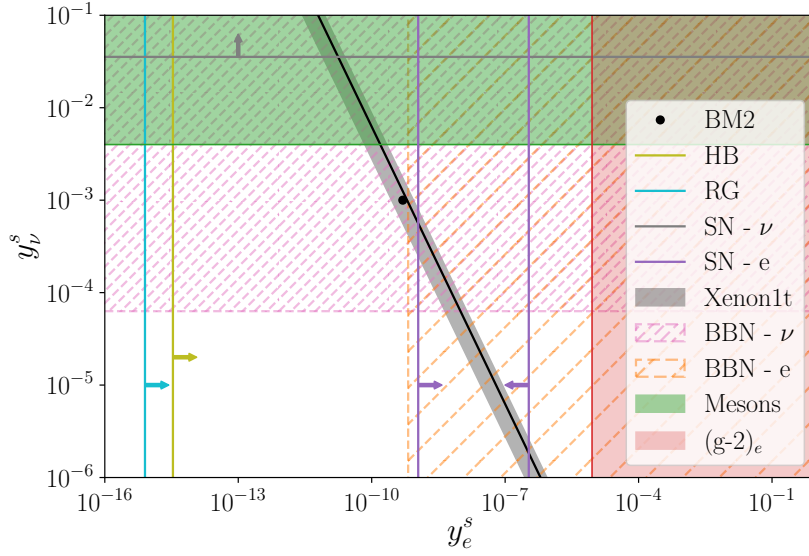
FIGURE 4.8: Constraints in the $y_e^s - y_\nu^s$-plane for a 60 eV mediator (as in BM2) and the 1σ preferred region from our fit to the XENON1T excess. The BBN bound on the electron coupling, indicated by the hatched region, can be circumvented by a late time phase transition.

Free EFT Description

In this rather general description, we confront the EFT resolution to the XENON1T anomaly via scalar couplings to electrons and neutrinos with the constraints discussed above. Here, we just employ the effective Lagrangian (omitting kinetic and potential terms)

$$\mathcal{L}_{\text{eff}} = -\frac{\sqrt{2}}{v} \left[y_\nu^s \, \overline{L}_L^1 H \nu_{1R} \, s + y_e^s \overline{L}_L^1 H e_R \, s + \text{h.c.} \right], \tag{4.26}$$

which can be obtained from Eq. (4.1) by neglecting the second scalar singlet while coupling the remaining one to both, electrons and neutrinos, and removing the Z_2 symmetries as well as the vev of the mediator. In consequence, the only contribution to all fermion masses is through the SM Higgs boson, and $y_{\nu,e}^s$ are now completely free couplings. In particular, Eq. (4.26) corresponds to a subset of operators of the general eDMEFT [9,12].

In Fig. 4.8, we show the constraints and best fit region in the $y_e^s - y_\nu^s$-plane for a mediator mass of 60 eV and in Fig. 4.9 for 20 keV, respectively. For comparison, we also add the coupling values used in the two BMs above.

By looking at Fig. 4.8 and Fig. 4.9, we see two possible regions in the couplings space preferred by the XENON1T fit, that could potentially remain valid, however, both would need extra mechanisms to avoid bounds from BBN in the early universe. The region around $y_e^s \sim \mathcal{O}(10^{-9})$ is excluded by the neutrino BBN bound. As discussed before, this could be avoided by an additional mass terms for the right-handed neutrinos. The other benchmark around $y_e^s \sim \mathcal{O}(10^{-6})$ is under pressure from the electron
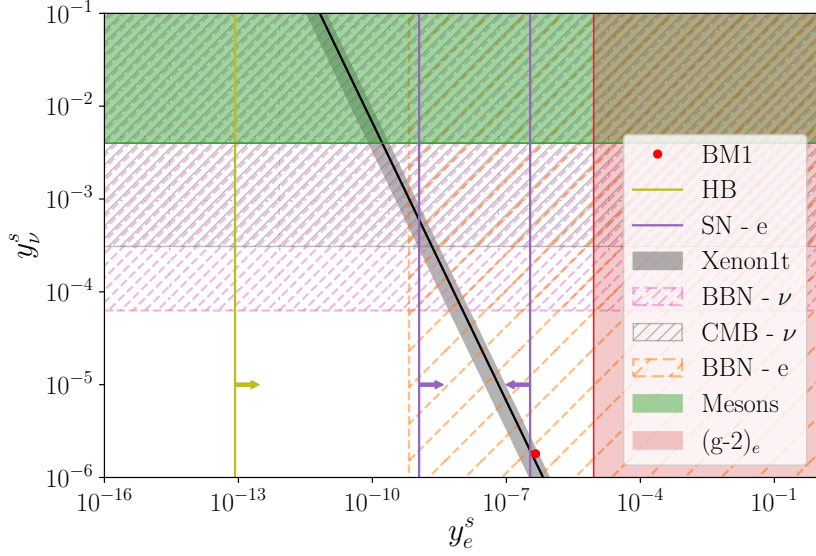
FIGURE 4.9: Constraints in the $y_e^s - y_\nu^s$-plane for a 20 keV mediator (as in BM1) and the 1σ preferred region from our fit to the XENON1T excess. The BBN bound on the electron coupling, indicated by the hatched region, can be circumvented by a late time phase transition.

BBN bound. Nonetheless, as will be shown in the following section, a late phase transition can remove the interaction of the light mediator and electrons during the relevant age of the Universe making this the most promisingly point and potentially viable.

4.5 Avoiding Astrophysical and BBN Bounds

Here we introduce a possible mechanism to ease the astrophysical bounds mentioned above. This is based on a new scalar singlet ϕ with a potential similar to the one employed by [310]. Unlike that work, here we aim to remove the vev of S_ν and not to increase the mass of the offending field. Then, the scalar field couples to the baryons through the $g\phi\overline{N}N$ operator, where g is the coupling between ϕ and the baryons denoted by N. The new mediator also has a four scalar interaction with the light, neutrinophilic scalar S_ν, mediated by $\lambda_{\phi S}$.

The Lagrangian with the relevant terms for this scenario reads

$$\mathcal{L} \supset \frac{1}{2}\left(\partial_\mu\phi\partial^\mu\phi - m_\phi^2\phi^2\right) + g\phi\overline{N}N - \frac{1}{4}\lambda_\phi\phi^4 \qquad (4.27)$$
$$+ \frac{1}{2}\left(\partial_\mu S_\nu\partial^\mu S_\nu - \widetilde{\mu}_\nu^2 S_\nu^2\right) - \frac{1}{4}\lambda_\nu S_\nu^4 - \lambda_{\phi S}\phi^2 S_\nu^2\,,$$

where we have defined the effective mass parameter by $\widetilde{\mu}_\nu^2 \equiv \mu_\nu^2 + 2\lambda_{\nu e}v_e^2$. The Yukaw-like term coupling baryons with the scalar ϕ induces a background dependent contribution to the ϕ potential. In a bath this translates to, $\overline{N}N \to \frac{n_B}{\gamma}$, where $\gamma \approx 1$ in the non-relativistic backgrounds of interest to us.

By assuming $m_\phi^2 > 0$ and neglecting $\lambda_{\phi S}$, the potential develops a vev, $v_\phi \approx g\, n_B / m_\phi^2$, provided that λ_ϕ is small enough. In the case of a non-vanishing $\lambda_{\phi S}$, the vev influences the S_ν sector, transforming the effective $\widetilde{\mu}_\nu^2$ term to $\widetilde{\mu}^2 = \widetilde{\mu}_\nu^2 + 2\lambda_{\phi S}(g n_B / m_\phi^2)^2$. If the new physics contribution exceeds $|\widetilde{\mu}_\nu^2|$, then $\widetilde{\mu}^2 > 0$ making the vev of S_ν disappear. This eliminates the mixing with the scalar S_e shutting off the coupling between s and the electrons that drive the astrophysical constraints.

Even though the aforementioned mechanism looks promising, finding a parameter space where we achieve the desired results, without violating the experimental constraints, would be more advisable. To this end, we provide one working assignment of the couplings and masses that allows to evade the astrophysical bounds for BM2. HB stars possess a central density[3] of about $10^4\,\mathrm{g/cm^3}$ [306] which induces $v_\phi \approx g\, 4 \times 10^{-5}\mathrm{MeV^3}/m_\phi^2$. Choosing $m_\phi = 1\,\mathrm{eV}$ and $g = 10^{-11}$ leads to $v_\phi \approx 400$ eV. Note that the values for m_ϕ and g respect bounds from searches for a fifth force [319]. In our benchmark scenario $|\widetilde{\mu}_\nu| \approx 40\,\mathrm{eV}$ which implies that $\lambda_{\phi S} \approx 0.01$ is sufficient to remove the minimum at non-zero v_ν. In principle, the whole potential should be considered simultaneously and not treated consecutively, however, in this case, v_ϕ exceeds v_ν significantly and thus the expected influence of S_ν on ϕ is small for the values of the coupling at hand. We have checked explicitly that our argument goes through with minimal corrections if the full potential is assumed.

Avoiding BBN Bounds via a Late Phase Transition

As discussed in the previous sections, one of the most problematic bounds for the chosen benchmarks, is the one coming from the BBN. In particular, the benchmark BM1, would be excluded by applying that constraint on the electron coupling. Nonetheless, in this section we demonstrate how our scenario naturally realizes a late Z_2 breaking phase transition, delaying the coupling of the electron to the light mediator until BBN has been completed.

The scalar potential in our original setup, Eq. (4.1), can lead to a rich cosmological history in which the Z_2^ℓ symmetries are broken in a step-wise fashion [320]. For simplicity, we neglect the mixing between scalars S_ν, S_e and the Higgs doublet H by turning $\lambda_{HS_\ell} = 0$. The tree-level scalar potential then reads

$$V_{\text{tree}} = \frac{1}{2}\mu_\nu^2 S_\nu^2 + \frac{1}{2}\mu_e^2 S_e^2 + \lambda_{\nu e} S_\nu^2 S_e^2 + \frac{1}{4}\lambda_\nu S_\nu^4 + \frac{1}{4}\lambda_e S_e^4. \tag{4.28}$$

To study the cosmological evolution of the previous potential, we add the one-loop thermal corrections given by [321]

$$V_{\text{thermal}} = \frac{T^4}{2\pi^2}\left[J_B\left(\frac{m_s^2}{T^2}\right) + J_B\left(\frac{m_S^2}{T^2}\right) \right], \tag{4.29}$$

---

[3]RG stars are even denser and our argument goes through without modification.

where $J_B(\alpha) = \int_0^\infty x^2 \ln(1 - e^{\sqrt{x^2+\alpha}}) dx$ is the thermal correction for bosonic degrees of freedom. Working in the high-temperature limit, the thermal corrections have analytical forms $J_B(\alpha) = -\frac{\pi^4}{45} + \frac{\pi^2}{12}\alpha + O(\alpha^{3/2})$. Since mixing between S_ν and S_e is small, we can take approximately $m_s \approx M_\nu$ and $m_S \approx M_e$. Under these approximations, the critical temperature T_{c2} at which a second minimum with vevs $(\langle S_\nu \rangle, \langle S_e \rangle) = (0, v_e)$ degenerate with the $Z_2^\nu \times Z_2^e$ preserving $(\langle S_\nu \rangle, \langle S_e \rangle) = (0,0)$ forms, is given by

$$T_{c2} = \frac{\sqrt{-12\mu_e^2}}{2\lambda_{ve} + 3\lambda_e}. \tag{4.30}$$

A second phase transition appears once the temperature has dropped to T_{c1} at which a non zero vev of S_ν forms, with

$$T_{c1}^2 = \frac{12(2\lambda_{ve}\mu_e^2 - \lambda_e\mu_\nu^2)}{\lambda_e(2\lambda_{ve} + 3\lambda_\nu) - 2\lambda_{ve}(2\lambda_{ve} + 3\lambda_e)}. \tag{4.31}$$

For BM1, the first phase transition occurs around 500 MeV while the second phase transition occurs at 150 keV. At this temperature most of the photon heating is completed and the electron density has already dropped significantly. Therefore, the thermalization rates start to be exponentially suppressed.

4.6   Current Status of the XENON1T Excess

As the XENON1T excess was reported almost two years ago, it is worth to discuss its current status and refer to Sect. 3.2 of Ref. [322] for the most recent details. The XENON1T collaboration originally reported the analysis of the data taken between the years 2016 and 2018. This showed a low-energy electronic recoil excess below 7 keV and most prominent between 2–3 keV, with a significance of $\sim 3.5\sigma$. The origin of the excess can be rooted to three possibilities: i) a statistical fluctuation, ii) a mismodelled background or iii) a signal of NP. Given the fact that the experiment used an unbinned likelihood analysis and relaying in the $\sim 3.5\sigma$ significance, the former option is the less likely. In the case of background mismodelling, there are certainly many possible backgrounds that could contribute to the excess. One of them is argon as it decays via electron capture and can peak at 2.8 keV, dangerously close to the excess peak. Other backgrounds that could deposit low-energy peaks in the XENON1T excess region are calcium and vanadium peaking at 3.3 keV and 4.5 keV, respectively. However, all the mentioned backgrounds are unlikely to originate the excess, as the uncertainty rate is simply not enough. Interestingly, there is still one background that is considered the most problematic one: tritium. The continuous energy spectrum of the latter, peaks exactly between 2–3 keV. Furthermore, the concentration of tritium that would be required to explain the excess is, in fact, very small, at around 3 atoms per kilogram of xenon. This by its own, could lead to a significance of 3.2σ, requiring further data in order to completely rule out this possibility. The third possible nature of the excess, is a NP signal. The XENON1T collaboration has proposed three possible scenarios: solar axions, bosonic matter or solar neutrinos, favouring the former with a significance of

3.4σ. More theoretical explanations were mentioned through out this chapter. Some of the latest works addressing the XENON1T excess are Refs. [323–327].

So far, there has not been any other independent experiment that scrutinises more on the nature of the excess. Except for the PandaX-II experiment [285] which has reported a consistency of the XENON1T excess with his own data sets. The next-generation xenon experiments could improve the sensitivity, leading to a more accurate results and a possible confirmation of NP. For instance, the upgraded version of XENON1T called XENONnT [328], will feature a sensitive mass of 5.9 tonne liquid xenon, that is a factor of three larger than the current version. This is expected to reduce the total background by a factor of six. Another promising experiment is the LUX-ZEPLIN (LZ) [184], which uses a 7 tonne active mass of liquid xenon. This experiment will focus on seven physical processes: an effective neutrino magnetic moment and an effective neutrino millicharge (both for pp-chain and solar neutrinos), an axion flux generated by the sun, ALPs dark matter, hidden photons, mirror dark matter and leptophilic dark matter. The expected low energy electronic recoil response of LZ to the mentioned scenarios can be found in Ref. [329].

To summarize, the XENON1T excess is a very exciting hint for a possible NP signal. Nevertheless, we still need to wait a few more years in order to fully claim it as a discovery, as with the present data, we do not have certainty on the nature of the excess. The most promising xenon experiments are XENONnT and LZ which will continue searching for DM particles, delivering new data in the future to come.

Chapter 5

Conclusions

The observation, at last, of all particles predicted by the Standard Model (SM), through the discovery of the Higgs boson and the subsequent validation of its properties, in agreement with the SM, so far, ended a many decades chapter in particle physics. As good as it gets, however, other facts, like the poor understanding of the patterns arising from the fermion mixing and mass spectrum, the hierarchy problem, or dark matter (DM), among others, cannot be solely understood by the SM theoretical framework. Therefore, independently of the SM's success, a whole new era has been already opened for particle physics which brings about the existence of new particles and/or dynamics to be unveiled in the upcoming future.

In this thesis, we focused on two particular unexplained observations: DM and the problem of fermion masses. Moreover, motivated by the previous confirmation, of the discovery of a fundamentally looking scalar particle, both conundrums were approached by assuming a multiscalar scenario. Adding scalars to the SM theory can be explored in two ways: renormalizable and non-renormalizable. As a consequence, this document was divided into two parts and ordered correspondingly.

For the first part, in Chapter 2, we devoted ourselves to investigating renormalizable extensions. There, we introduced a second scalar doublet and considered it with the same quantum numbers as the SM Higgs. By it, we were able to address some of the dominant patterns in the fermion masses. Namely, the mass hierarchy between the top quark and the other fermions, or between the third fermion generation and the other two. As both aspects cannot be explained with two Higgs doublets at a time, two new and independent models were proposed and called type-A and B, where either the top quark alone or all third-generation fermions coupled to the doublet with a larger vacuum-expectation-value (vev). This distinction only became possible after implementing a parity symmetry, Z_2, and introducing the *singular alignment ansatz* which allowed us to avoid undesirable flavor-changing-neutral-currents at the tree level. The remaining fermions exclusively acquire their masses through the small vev of the other doublet being produced by the soft-breaking of the parity symmetry. Moreover, within the new types, two naturalness criteria (Dirac and 't Hooft) might be realized in the scalar and/or Yukawa sector. In that sense, we obtained more natural models when compared to those conventional ones (I, II, X, Y).

Phenomenologically speaking, the new types are closely related to the well-known 2HDMs types, I and II. This is a direct consequence of the great similarity between the models when only the heaviest fermions are considered. In return, that allowed us to comprehensively investigate their phenomenological viability and to make use of derived constraints to restrict the parameter space. Nevertheless, the proposed types feature deviations from the conventional ones in channels of the potential reach of the HL-LHC enabling a distinction between them. In particular, strong constraints originate from $b \to s$ flavour violating transitions, requiring the charged scalar mass to be above $600\,\mathrm{GeV}$. Given the phenomenological relevance of the alignment limit, we allowed at most small deviations from it. However, specific signatures can be identified and used to distinguish our models from the conventional ones, namely, i) $h \to \mu^+\mu^-$, ii) $H \to \mu^+\mu^-$, and iii) $h \to J/\psi + \gamma$. With the former decay, it is possible to exclude large values of t_β for type-B, while for type-A most of the range remains consistent with current data. On the other hand, for the latter decay, we found that our two types give the strongest enhancement above the SM value compared to the conventional natural flavor conserving scenarios. Additionally, since the most direct signature of any 2HDM is the detection of the full scalar spectrum, we considered viable decay channels of the heavy CP-even neutral scalar. Specifically, the decay into muon pairs can exclude large values of t_β for Type-A even in the alignment limit.

Overall, the architecture of the two newly proposed types offers new exciting possibilities to construct multi-Higgs models taking the observed hierarchies in the fermion mass spectrum into account and at the same time naturally avoiding dangerous FCNCs. This is certainly an ambitious goal. Many issues should still be addressed to fully understand the pros and cons compared to the well-studied conventional types.

For the second part, we dedicated ourselves to the study of non-renormalizable extensions. In Ch. 3, we built a scenario where the SM is augmented by a real scalar singlet, S, and a fermionic DM, χ. We followed a hybrid approach that adequately combined both the model independence of EFTs, where high dimension operators are suppressed by corresponding powers of a heavy scale Λ, and the virtues of simplified models in which the mediator is explicitly included in a minimal and renormalizable extension, easing its search in colliders. Despite their virtues, both approaches have several drawbacks; for example, the validity of EFTs break at collider energies while simplified models suffer from a model dependence along with occasions where gauge invariance forbids relevant and interesting operators. We thus discussed a minimal yet consistent framework that overcomes the aforementioned shortcomings. This is done through a Lagrangian with operators up to dimension five, in which the new scalar mediator is present in an explicit gauge-invariant way but high dimension operators are suppressed by a new physics scale. This effective approach is called the extended dark matter EFT (eDMEFT). To exemplify it, in Sec. 3.4, we presented a case scenario where we assumed the mediator, as well as the right-handed first fermion generation, to be odd under a Z_2 symmetry. As a consequence, the masses of the up and down quarks and the electron can be generated from the spontaneous breaking of the Z_2 symmetry. We required the mediator to have a small vev of approximately 10 MeV, just enough to generate the mass of the light fermions. As those masses come from

$D = 5$ operators, are thus suppressed by the energy scale $\Lambda \sim 1$ TeV. This approach immediately provides a plausible explanation for the smallness of the first-generation fermion masses. Furthermore, as the setup also includes a DM particle, dimension five operators enabled us to explore the channel $\mathcal{SS} \rightarrow \chi\chi$, where a dijet plus missing-energy-searches were studied.

Our analyses focused on two colliders: the (HL)-LHC and the future experiment CLIC. The final state of the dijet (dilepton) plus missing transverse energy (MET) was $q\bar{q}\chi\chi$ and $e^-e^+\chi\chi$, where $q = u, d$. In both cases, the main background was the same process as before but exchanging $\chi \rightarrow \nu_i$, $i = e, \mu, \tau$. On the dijet plus MET signal, we explored the possibilities where the mediator could be either leptophobic or fully coupled. To perform the analysis, we used the CheckMate software with which we compared our signal with existing ATLAS analyses for mono-jet searches, leading to rather loose bounds, with couplings of $\sim \mathcal{O}(5)$ as depicted in Fig. 3.5. On the other hand, the fully coupled case can translate direct detection limits from the quark sector to the lepton sector. However, we found a very low cross-section due to the large width of S, which strongly depends on the value of the quark and lepton couplings and enters inversely to σ. In addition, with the future CLIC detector, we studied the hadrophobic case, in which the mediator just couples to electrons (positrons). Here we analyzed the signal process with the `MadAnalysis` software noticing a very clear peak-like structure in the kinematic variable m_{e+e-} as shown in Fig. 3.6. By performing a more sophisticated statistical analysis we got tighter constraints where small couplings of $\mathcal{O}(0.5)$ (already in stage I) are allowed. We also studied the conditions for our model to satisfy the DM relic density presented in Fig. 3.8.

Continuing with the eDMEFT approach, in Sec. 3.5, we performed the matching of our current framework with two more-UV-complete theories: 2HDM plus a pseudoscalar mediator and SM plus a vector-like quark (VLQ). The collider studies were discussed in Sec.3.6, where combining the VLQ completion with the 2HDM+S we found a cancellation of the dimension five gluon- and quark-mediator operators, giving place to DD blind regions. We added the scaled projections for the HL-LHC at 2σ and chose a benchmark point in the blind region that could be potentially discovered by the future HL-LHC collider. We also studied the exclusion limits set by the ATLAS experiment and the corresponding HL-LHC projections for mono-jet searches for the c_G^S/Λ coefficient varying the mediator mass and found that the HL-LHC will be able to exclude values smaller than one for such a coupling. Then, we took the aforementioned benchmark and by utilizing the relations obtained when performing the matching, we translated the limit of the gluon coefficient into a limit on the vector-like top-quark coupling. We could not find any viable parameter space in which the 2HDM plus a (pseudo-)scalar leads to an observable LHC signal, and therefore neglected its contribution in the regime where the VLQ becomes relevant. However, when considering the 2HDM plus a scalar mediator, the values on the bottom-Yukawa coupling can be translated into the coupling λ_{S12}. We found that from both the VLQ and 2HDM + S models, with small coefficients coming from the eDMEFT theory ($c_G^S = 0.7$ and $y_b^S = 0.03$), we can obtain $\mathcal{O}(1)$ couplings in the more-UV-complete theories. Moreover, the sign difference between operators create blind regions in which DD effects can be suppressed. It is in a corner of that blind region that we found a suitable value for the eDMEFT

couplings that could be tested in the future HL-LHC collider. By this, we thus showed that a blind-spot region, identified in the EFT, can in fact be achieved in UV complete models with reasonable ($\mathcal{O}(1)$) values for the fundamental couplings and be potentially detectable at HL-LHC.

Given the previously discussed advantages of the eDMEFT framework, in Ch. 4, we investigated the excess in low energy electron recoil events reported by the XENON1T collaboration. We found that conventional DM-electron scattering only allows for a marginally better fit than the background-only hypothesis since the signal spectrum peaks at lower energies than observed experimentally. Therefore, DM does not provide a convincing explanation of the data. However, the new neutrino and electron couplings induced by the neutrino mass mechanism embedded in the model predict a significant neutrino-electron scattering cross-section. Including this interaction in the fit improves it considerably and we found that a light scalar with an average electron-neutrino coupling of $\sqrt{y_e^s y_\nu^s} \approx 7.9 \times 10^{-7}$ is preferred by more than $2\,\sigma$. These observations motivated us to scrutinize the parameter space of the model in more detail and compare it to limits from various other observations. In general, the parameter space that allows for a successful explanation of the XENON1T excess is rather constrained. While limits from terrestrial experiments can be avoided comparatively easily, bounds from cosmology are more constraining. In particular, BBN bounds on a light scalar coupling to electrons are very severe. Interestingly, the model under consideration here naturally allows for a late phase transition in the early Universe which prevents the scalar-electron coupling during BBN. However, in such a scenario additional contributions to the right-handed neutrino masses are required to avoid their thermalization before BBN. Once this is taken into account, we found solutions that comply with cosmological bounds. There remains a strong tension with astrophysical bounds, that rely on stellar cooling arguments. Nevertheless, if we allow for the possibility of additional new physics, these limits can be avoided by a density-dependent contribution to the S_ν potential that suppresses or even removes the mixing with S_e in a high-density environment.

In summary, we conclude that our model, within the eDMEFT framework, presents promising signal channels for both HL-LHC and CLIC, however, the stronger constraints come from future e^+e^- colliders given the mediator is hadrophobic. Furthermore, from the flavour model perspective, we presented a possible explanation for the lightness of the first fermion generation. Additionally, a new physics explanation of the excess is a tantalizing possibility, but in light of stringent constraints from other observations, this potential sign of physics beyond the SM should be taken with a grain of salt. Luckily, the upcoming run of the XENONnT experiment will be able to weigh in on this question shortly and either strengthen the excess or rule it out conclusively.

Chapter 6

Acknowledgments

After finishing this manuscript, I finally had the time to look back on the past few years in Germany; and how wonderful it was to find out that, during this period, I have had amazing people sharing with me this adventure called Ph.D. I would then like to thank those without whom the realization of this thesis would have been impossible.

First of all, I want to deeply thank my supervisor, Dr. Florian Goertz, for accepting me as a master's and later as a Ph.D. student. Thank you for taking the time to explain and discuss physics with me, for always making me feel in a safe space to ask dumb questions and to be allowed to make mistakes. I have grown a lot as a physicist under your guidance and I feel extremely happy for being your student. Additionally, I feel very thankful to you for providing me with a friendly, respectful and supportive atmosphere in your research group and for the constant group meetings that made me feel the pandemic was not an obstacle to keeping the work going.

I would like to thank Prof. Dr. Tilman Plenh, for being my second referee and for all his support during my studies. I feel especially thankful to you for having allowed me to join a machine learning project in your group and for all the advice I got during the postdoc applications.

I am particularly thankful to Valentin Tenorth, for all the fruitful discussions about physics and beyond. Thank you for always being so kind to me, and for having taught me so much about the physics behind all our projects. I am grateful to you for being there every time I had a complaint with MadGraph, joking with you made all the bugs in the code less stressful. I am happy to have found a good friend in you and I am sure our friendship will continue despite the distance or circumstances.

I would like to thank Thomas Hugle for being my python guru, for all the advice and for everything I learned from you about statistics and machine learning, and beyond. I would have liked to have more time to collaborate with you. However, I am happy to have found a friend in you, so I am sure that in one way or another, our paths will cross again.

I feel very grateful to Felix Kling for all the MadMiner discussion we had and for all the advice during the postdoc applications. In addition, I would like to thank Barry Dillon for all the machine learning concepts I have learned from you and for the exciting project we have, and for the many more to come!

My gratitude also goes to Prof. Dr. Monica Dunford and Prof. Dr. Björn Malte Schäfer, for taking the time to be part of my examination committee.

I am also very grateful to Dr. Susanne Westhoff. Thank you for all the help you gave to me, coming to Heidelberg would have been impossible without your support. Additionally, I enjoyed all the lectures and tutorials I did with you and I hope our paths cross again in the future.

I would like to thank Prof. Dr. Stephen Parke for supporting me with my post-doctoral applications and Prof. Dr. Lorenzo Diaz-Cruz for all the support inside and outside physics.

I also thank Anja Berneiser, Britta Schwarz, Anja Kamp, and Elisabeth Miller for helping with all kinds of bureaucracy. A special and huge thanks to Stefanie Kolb, for helping me, with a kind and positive attitude, with all the IT problems that appeared over the past 4 years, I am endlessly grateful to you.

Furthermore, I would like to thank Michelle Guiliano and Denisse Nickerson, for all the coaching and advice I received from you and that made a difference in both my personal and professional life.

Life is much more than just physics, so I would also like to acknowledge all my friends that were there in the last years, and that made my time in Heidelberg quite special. First of all, I would like to thank Ruth Schäfer. Five years have passed since we first met as a fresh master's student and I could already write an entire book about all we have shared. Thank you for being my best friend and for having taught me the deepest meaning of friendship. Now, I am happy to know that even if our title is "friends", what you are to me, is family. I am very excited to discover all we will share in the future to come! Additionally, I am very thankful to Carlos, Barbara, Judith and Christoph. Thank you for being my German family. Christmas days with you were wonderful. I am deeply thankful for all the board games we played together, all the delicious cookies and warm moments; they changed my life.

I am very thankful to Christina Benso, for the kind friendship and for all the tasty food you have prepared for us. I feel grateful for our trip to Italy, you, your family and Cuneo will be always in my heart.

Furthermore, I would like to thank Lisa Baltes. Since the first time we met, I had a very strong and positive impression of you, and I am very happy to have a beautiful friendship with you that I am sure will last for many many years!

To Carlos J., Sven, Lennert, Susan, Simone, Tommi and all my fellows at both, the University and the MPIK.

There is also that kind of friends that come with a different title and I owe them many of the deepest and most meaningful moments of my time in Germany. Martin Smith, thank you for accepting me as a pupil and for helping me discover the world of classical piano, every hour I spent playing music with you was fundamental for the growth I had in the last years. I am deeply grateful to have had the opportunity to listen to you playing, that concert was not only for my mind and emotion but for all my being and will be alive inside of me forever.

Ronald and Carolina, thank you for all the unconditional love you have given and still give me. For listening to me and for all the lectures and advice you have provided to me. But most importantly, thank you for the opportunity to share my experiences

and to always have some words for us, for reminding me about the important things in life, and for accompanying me in my search for a meaningful life.

Jöelle Sintas: Je vous remercie car dans votre présence, dans vos mots et dans vos silences, je trouve un exemple de vie. Merci d'être une boussole dans ma recherche, d'être une ancre quand je suis sur le point de me perdre et d'être l'espoir quand je suis dans les ténèbres.

To all my friends in Bayerdilling, thank you for your presence and influence in my life, you will always live within me. Your search and life inspire and help me to keep going. Additionally, I would like to thank Fernando Saldana, gracias por darme la oportunidad de continuar con mi búsqueda sin importar las condiciones, por siempre escucharme con amor y darme dirección. Mi eterno agradecimiento para ustedes.

Lucile: Dès notre premier cours, j'ai su que je trouverais en toi un très bon ami. Je suis très heureux de vous avoir rencontré et je vous suis profondément reconnaissant pour tout le français que j'ai appris avec vous. Vous avez apporté beaucoup de bonheur à mes journées en Allemagne.

Finally, I want to thank the most important people in my life: my family. Ulises, there is just not enough time nor words that express the endless gratitude I feel towards you. Some of the many things I am grateful for are: all the physics discussions we had and still have, all I have learned from you, the papers we wrote together and all the professional advice you have given me. My time in Germany, my Ph.D., and all I have lived in the past 5 years would have been impossible without your support. But also, I feel immensely grateful to you for being there, every day and night, for really *knowing* me (even better than myself), for listening to me and always saying the words I need to hear, even those that are not spoken. You are my best decision ever, and this life only makes sense if I live it with you. I am grateful for you being a scientific, sensible, loving, smart and strong wonderful man. Thank you for healing my heart and insecurities with your endless patience and love. Being married to you is the biggest adventure of my life and I am very excited for our future together. Te amo con todo lo que soy y con todo lo que pueda llegar a ser.

A mis padres, Rosario y Alfredo. Gracias por apoyarme siempre, con su amor infinito. Gracias por estar ahí en todo momento, por celebrar mis victorias y por abrazarme con amor en mis momentos más difíciles. Su ejemplo de lucha y superación ha sido una fuente constante de inspiración en mi vida, y es un motor que me impulsa a volar alto y sin miedo. ¡Me siento inmensamente agradecida por todas las bienvenidas a México que siempre son de otro mundo! Por su amor desmesurado. Gracias por darme la vida y los valores necesarios, para salir al mundo con la seguridad y la confianza para ser capaz de lograr lo imposible. En definitiva, no hubiera sido posible llegar tan lejos, sin su apoyo incondicional, desde mi primer día en este mundo. Agradezco a la vida por tenerlos como mis padres, y este logro es por y para ustedes también. Los amo profundamente.

A mi hermano, Alfredo. Las palabras no hacen justicia para expresar lo que siento por ti. Eres mi primer mejor amigo, mi confidente, mi compañero de clases virtuales, mi segundo padre y mi primer gran maestro. Gracias por estar en mi vida, por darme tanta fortaleza, por enseñarme a luchar por mis sueños hasta hacerlos realidad y nunca

conformarme. Gracias por querer conocerme y siempre interesarte en mí, por lo que soy y por lo que amo. Gracias por siempre hacerme sentir que estás cerca, sin importar la distancia física, tu amor me abraza constantemente. Eres un gran ejemplo en mi vida y me siento muy feliz por saber que eres mi aliado en este mundo. Te amo con todo mi ser y deseo profundamente seguir compartiendo el resto de mi vida contigo.

A Raquel. Gracias por ser parte de la familia, por recibirnos siempre con amor y calidez y por compartir multiples aventuras con nosotros. Gracias por escucharnos a Uli y a mí, por platicar y siempre contagiarnos de alegría y buen humor. Me siento inmensamente feliz y agradecida, por saberte parte tanto de la vida de mi hermano como de la mía. ¡Deseo sigamos compartiendo muchos momentos juntos! ¡Tu nombre ya está en mi corazón!

A mi Abu, Angélica, gracias por ser el pilar de la familia, por enseñarme uno de los amores más grandes y profundos que existen; y por siempre estar ahí para mí en la forma de un abrazo, una palabra, una historia, una comida, un recuerdo. Eres una guerrera, abuelita, te admiro muchísimo y te amo con todo mi corazón.

A mi familia: Karina, Ariana, Memo, Gerardo, Lorena, Sofi, Majo, Montse, Isabel, Poncho y mis maravillosos sobrinos Grecia, Ameli, Itan y Alex. Gracias por ser el piso firme sobre el cual he construido todo lo que soy. Gracias por enseñarme el significado de ser una familia y por todos los momentos que hemos pasado juntos y han forjado quien soy y quien quiero ser. Los amo inmensamente y nunca podré estar más agradecida con la vida, por haberme dado una familia tan hermosa y unida como la mía. Gracias por estar siempre ahí, en todos los momentos de mi vida. Los amo profundamente y siempre están en mi pensamiento y en mi corazón.

A Michelle Saldana y Michael Liebel, gracias por ser parte de nuestras vidas, por siempre estar ahí para escucharnos, por consentirnos, por bromear y por su presencia. Mich, gracias por ser la primera en conocer nuestro mundo. Agradezco por todos los momentos y aventuras que hemos pasado juntos y espero seguir siendo parte de su vida y ustedes de la mía. Los amo.

Luk aka el misifis, thank you for giving me lots of moments of joy and love, I am learning so much from you, and I am deeply thankful for your presence in my life.

At last, I am thankful to myself for having come so far and for keeping going.

Appendix A

Flavour in the SM

We present here a brief overview of flavour physics in the SM. Specifically, we focus on the fermion masses and mixing. We recall for completeness that the SM is a relativistic quantum field theory whose Lagrangian is intentionally made invariant under the local symmetry group $SU(3)_c \times SU(2)_L \times U(1)_Y$, where the subscripts c, L and Y stand for color, left-handedness and hypercharge, respectively. The SM fermion content with the respective gauge charges is shown in Table A.1. Note that as the massive nature of neutrinos is outside the scope of this thesis it is not considered in the following discussion.

A.1 Fermion Masses

Let us start from the scenario where the Yukawa interactions with the SM Higgs boson are not present in the SM Lagrangian. As a consequence, all the fermions would be massless and a global flavour symmetry would appear

$$U(3)_{L_L} \times U(3)_{Q_L} \times U(3)_{e_R} \times U(3)_{u_R} \times U(3)_{d_R} \, . \tag{A.1}$$

By bringing back the Yukawa terms, this global symmetry group gets broken to baryon and three lepton flavour numbers, $U(1)_B \times U(1)_e \times U(1)_\mu \times U(1)_\tau$. The masses of the SM fermions can arise after the EWSB.

The Yukawa Lagrangian reads

$$\mathcal{L}_{Yuk} = \mathbf{Y}_u^{ij} \bar{Q}_L^i \widetilde{\Phi} u_R^j + \mathbf{Y}_d^{ij} \bar{Q}_L^i \Phi d_R^j + \mathbf{Y}_e^{ij} \bar{L}_L^i \Phi e_R^j + h.c. \, . \tag{A.2}$$

Here $\mathbf{Y}_{u,e,d}$ are the Yukawa matrices for the corresponding fermion type, ij represent the matrix element and Φ is the scalar doublet (see Eq. 2.7). Note that neutrinos do not appear in the Yukawa Lagrangian as they do not have a right-handed partner. This is why, by construction, neutrinos are massless particles in the SM.

The corresponding mass matrices for each fermion type read

$$\mathbf{M}_f = \frac{v}{\sqrt{2}} \mathbf{Y}_f \, , \tag{A.3}$$

where $v = 246$ GeV is the Higgs vev and sets the EW scale. In general, as the mass matrices are complex they require a bi-unitary transformation for their diagonalization.

	$SU(3)_c$	$SU(2)_L$	$U(1)_Y$
$L_L = \begin{pmatrix} \nu_L^i \\ \ell_L^i \end{pmatrix}$	1	2	-1/2
$Q_L = \begin{pmatrix} u_L^i \\ d_L^i \end{pmatrix}$	3	2	1/6
e_R, μ_R, τ_R	1	1	-1
u_R, c_R, t_R	3	1	2/3
d_R, s_R, b_R	3	1	-1/3

TABLE A.1: SM fermion content and charge distribution under the SM gauge group. Here the L_L are the the left-handed lepton doublets and Q_L are the left-handed quark doublets where $i = 1, 2, 3$.

The value of all the measured fermion masses and Yukawa couplings are depicted in Table A.2. It is clear that the only $\mathcal{O}(1)$ Yukawa coupling is the one from the top quark. The fermion masses can be divided into four different scales:

- $\mathcal{O}(10^0)$ MeV for $\{e, u, d\}$,

- $\mathcal{O}(10^2)$ MeV for $\{\mu, s\}$,

- $\mathcal{O}(10^3)$ MeV for $\{\tau, c, b\}$,

- $\mathcal{O}(10^5)$ MeV for the top quark.

These various scales suggest a possible underlining mechanism behind it. There have been many ideas discussed in the literature which try to explain the fermion mass hierarchies [8, 46, 330–335].

We remark that in this thesis, we mainly focus on only three aspects of the fermion masses and treat them separately by a very specific model:

- $m_t \gg m_f$,

- $m_3^f \gg m_2^f, m_1^f$ with $f = q_u, q_d, \ell$,

- $m_3^f, m_2^f \gg m_1^f$ with $f = q_u, q_d, \ell$.

A.2   Fermion Mixing

Let us now explore the fermion mixing by starting with the gauge couplings. The gauge Lagrangian reads

$$\mathcal{L}_{gauge} = \sum_j i\overline{\psi}_j \gamma_\mu D^\mu \psi_j \tag{A.4}$$

	Mass [MeV]	Yukawa coupling
e	0.511	3×10^{-6}
μ	105.6	6×10^{-4}
τ	1776.86 ± 0.12	10^{-2}
u	$2.3^{+0.7}_{-0.5}$	10^{-5}
d	$4.8^{+0.5}_{-0.3}$	2×10^{-5}
s	95 ± 5	5×10^{-4}
c	1275 ± 25	7×10^{-3}
b	4180 ± 30	2×10^{-2}
t	$(173.21 \pm 0.51) \times 10^3$	1

TABLE A.2: Masses and Yukawa couplings for the SM fermions.

where $\psi_j = \{Q_L, L_L, u_R, d_R, e_R\}$ and the covariant derivative D^μ is defined as

$$D^\mu = \partial^\mu + ig_s G_a^\mu T_a + ig_w W_b^\mu \tau_b + ig' B^\mu Y. \tag{A.5}$$

Here G_a^μ are the eight gluons ($a = 1, ...8$) and $T_a = \lambda_a/2$ are the $SU(3)$ generators or Gell-Mann matrices acting on the colour triplets. The three weak interaction bosons are denoted as W_b^μ, $\tau_a = \sigma_a/2$ are the Pauli matrices acting on fermion doublets and $b = 1, 2, 3$. Lastly, B^μ is the hypercharge boson and Y is the corresponding $U(1)_Y$ charge.

Quark Sector

By replacing the covariant derivative in the gauge Lagrangian, we can now study, for example, the left-handed quark gauge interactions

$$\mathcal{L}_{gauge}^{Q_L} = i\overline{Q}_L^i \gamma_\mu \left(\partial^\mu + ig_s G_a^\mu \frac{\lambda_a}{2} + ig_w W_b^\mu \frac{\sigma_b}{2} + \frac{ig'}{6} B^\mu \right) Q_L^i. \tag{A.6}$$

Note that the gauge interactions are unchanged by linear unitary transformations such as $\psi_{L(R)} \to \mathbf{V}_{\psi L(R)} \psi_{L(R)}$. After EWSB and the diagonalization of the Yukawa matrices $\mathbf{Y}_{\text{diag}}^u = \mathbf{V}_{uL}^\dagger \mathbf{Y}^u \mathbf{V}_{uR}$ and $\mathbf{Y}_{\text{diag}}^d = \mathbf{V}_{dL}^\dagger \mathbf{Y}^d \mathbf{V}_{dR}$, the gauge Lagrangian can be written as

$$\mathcal{L}_{gauge}^{Q_L} \supset \frac{g}{\sqrt{2}} (\bar{u}_L \mathbf{V}_{uL}^\dagger \mathbf{V}_{dL} \gamma^\mu W_\mu^+ d_L + \bar{d}_L \mathbf{V}_{dL}^\dagger \mathbf{V}_{uL} \gamma^\mu W_\mu^- u_L) \tag{A.7}$$

$$+ \frac{g}{c_w} \left[\bar{u}_L \gamma^\mu (\frac{1}{2} - \frac{2}{3} \sin^2 \theta_W) u_L + ... \right] Z_\mu^0. \tag{A.8}$$

where $\sin \theta_W = g'/\sqrt{g^2 + g'^2}$ and Z^0 is the weak neutral boson. We can conclude from here two interesting facts: i) the interactions with the weak neutral boson are flavor diagonal and ii) the interactions with the charge bosons $W^\pm$ are parametrized by the unitary matrix $\mathbf{V} = \mathbf{V}_{uL}^\dagger \mathbf{V}_{dL}$. The quark mixing matrix is called the Cabibbo-Kobayashi-Maskawa matrix (CKM) and implies flavour transitions among the left-handed up and down quarks.

The CKM matrix elements have been measured and they are [336]

$$|\mathbf{V}_{CKM}| \equiv \begin{pmatrix} V_{ud} & V_{us} & V_{ub} \\ V_{cd} & V_{cs} & V_{cb} \\ V_{td} & V_{ts} & V_{tb} \end{pmatrix} = \begin{pmatrix} 0.97445 & 0.22458 & 0.00364 \\ 0.22442 & 0.97358 & 0.04217 \\ 0.00897 & 0.04137 & 0.999104 \end{pmatrix}. \tag{A.9}$$

It is interesting to note how the elements of the CKM matrix show a strong hierarchy among them

$$|\mathbf{V}_{CKM}| \sim \begin{pmatrix} \epsilon^0 & \epsilon^1 & \epsilon^3 \\ \epsilon^1 & \epsilon^0 & \epsilon^2 \\ \epsilon^3 & \epsilon^2 & \epsilon^0 \end{pmatrix}, \tag{A.10}$$

where $\epsilon \sim 10^{-1}$. There is also a physical parameter composed by elements of the CKM matrix called the Jarlskog invariant defined by $J = Im(V_{ud}V_{cd}^*V_{cb}V_{ub}^*)$ with a value of $J_{CKM} = (3.18 \pm 0.15) \times 10^{-5}$ [336].

Let us know do a quick counting on the physical parameter in the quark sector. On the one side, from the two Yukawa matrices $\mathbf{Y}_u$ and $\mathbf{Y}_d$ we obtain $2 \times 9 + 2 \times 9 = 36$ arbitrary parameters. Note that 18 are magnitudes while the other half are complex phases. On the other hand, after the Yukawas break the quark global symmetry, $U(3)_{Q_L} \times U(3)_{u_R} \times U(3)_{d_R} \to U(1)_B$ where $U(1)$ is the baryon number symmetry. We then get $(9 \times 9 \times 9) - 1 = 26$ broken generators. Realize how each one of them can be employed to move to another basis without changing the theory. Their presence comes through two three-dimensional unitary matrices and one three-dimensional special unitary matrix. All the freedom contained in these matrices is characterized by 26 (9 magnitudes and 17 complex phases) parameters to be chosen such that the initial arbitrariness is reduced to its least amount. Combining the two results, we are left with only $36 - 26 = 10$ physical parameters [337]. More precisely, $18 - 9 = 9$ magnitudes and $18 - 17 = 1$ complex phase. Now, from those 10 parameters, 6 can be assigned to the quark masses and, therefore, the CKM has 4 physical parameters that can be expressed as 3 angles and 1 phase.

At this point, we can also mention something about the discrete symmetries in the SM [338]: parity (P), time reversal (T) and charge conjugation (C). The strong interactions conserve C and P separately whereas the weak interactions violate C and P. When analysing CP invariance, we notice that the only source of CP violation in the SM quark sector comes through the CKM phase δ. It enters in the Jarlskog invariant as $J = c_{12}c_{23}c_{13}^2 s_{12}s_{23}s_{13}s_\delta$ where $c_{ij} = \cos(\theta)_{ij}$ and $s_{ij} = \sin(\theta)_{ij}$. It has been noted that to obtain CP violation in the weak interactions we require some conditions to be satisfied, for example, the Jarlskog invariant should be different from zero ($J \neq 0$) implying non-vanishing angles and non-vanishing phase in the CKM matrix. In addition we should have non-degenerate masses, i.e. $m_1^f \neq m_2^f \neq m_3^f$ with $f = q_u, q_d$.

Leptonic Sector

The flavour structure of the lepton sector in the SM can be analyzed similarly to the quark sector. If we assume neutrinos to be massless, the only relevant particle content

would then be $L_L^{iT} = (\nu_L^i, \ell_L^i)^T$, ℓ_R^i where $\ell^i = e, \mu, \tau$. In the mass basis of the charged leptons, the charged weak interactions of the leptons are given by

$$\mathcal{L}_{gauge} \supset \frac{g}{\sqrt{2}} \bar{\nu}_L \mathbf{V}_{eL}^\dagger \gamma^\mu W_\mu^+ e_L + \text{h.c.} . \tag{A.11}$$

In the case of massless neutrinos, the charged lepton transformation can be absorbed by the neutrino left-handed field and as a consequence there is no lepton mixing. For massive neutrinos, an independent transformation is required to bring them to the mass basis, and the flavour mixing among left-handed leptons becomes physical,

$$\mathcal{L}_{gauge} \supset \frac{g}{\sqrt{2}} \bar{\nu}_L \mathbf{V}_{eL}^\dagger \mathbf{V}_{\nu L} \gamma^\mu W_\mu^+ e_L + \text{h.c.} , \tag{A.12}$$

where $\mathbf{V}_{eL}^\dagger \mathbf{V}_{\nu L}$ is called the Pontecorvo–Maki–Nakagawa–Sakata (PMNS) matrix, and it has at 3σ the values [339]

$$\mathbf{U}_{PMNS} \equiv \begin{pmatrix} U_{e1} & U_{e2} & U_{e3} \\ U_{\mu 1} & U_{\mu 2} & U_{\mu 3} \\ U_{\tau 1} & U_{\tau 2} & U_{\tau 3} \end{pmatrix} = \begin{pmatrix} 0.801 \to 0.845 & 0.513 \to 0.579 & 0.144 \to 0.156 \\ 0.244 \to 0.499 & 0.505 \to 0.693 & 0.631 \to 0.768 \\ 0.272 \to 0.518 & 0.471 \to 0.669 & 0.623 \to 0.761 \end{pmatrix} . \tag{A.13}$$

In this case, the Jarlskog invariant at 1σ is $J_{PMNS} = -(0.0329 \pm 0.0007)$ [339]. Similar to the CKM matrix, the PMNS matrix can be parametrized by 3 angles and 1 phase as long as neutrinos are Dirac particles. If instead neutrinos are of Majorana nature, the lepton sector acquires two additional phases. We will not discuss the neutrino nature as it is beyond the interest of this thesis. For further information in flavour physics, we refer the reader to Refs. [337, 340–350].

Appendix B

EFT Examples

We present here three bottom-up EFT examples that are commonly used. The first and most common one is the SMEFT. The second one is the basis of the eDMEFT as it presents the general EFT theory for DM. Lastly, the third one is more QCD focused.

B.1 Standard Model EFT (SMEFT)

Quoting the theorem of modesty *"no quantum field theory is ever complete at arbitrarily high energies"* [106], we can interpret the SM as an EFT from other more-UV-complete theories where the energy $\Lambda \gg$ EW scale. Then, the SMEFT provides a very powerful framework for analyzing many LHC and other NP searches [95, 351]. To this end, additional high-energy gauge-invariant interactions of the SM fields are introduced via effective operators. Remarkably, at D = 5 only the Weinberg-operator $\mathcal{O}_W = (LH)^2$ arises, which violates lepton number by two units and gives rise to a Majorana mass-term for neutrinos after EWSB [352]. In this case, the suppression scale can be related to the mass of right-handed neutrinos.

There are 2499 dimension-6 possible operators $\mathcal{O}_i$ of the SMEFT Lagrangian [353, 354]:

$$\mathcal{L}_{SMEFT} \supset \mathcal{L}_{SM} + \frac{g_0}{\Lambda} \mathcal{O}_W + \sum_{i=1}^{2499} \frac{g_i \mathcal{O}_i}{\Lambda^2} \, . \tag{B.1}$$

It is clearly impractical to include 2499 parameters. Therefore, further assumptions, for example, on the flavour structure of the operators involving fermions are needed in order to simplify the SMEFT Lagrangian. For example, assuming baryon-number conservation, to forbid strongly constrained proton decays, and flavor-universality to circumvent bounds from flavour physics, the list drops down to only 59 independent operators that can be given in different bases [80, 110]. At higher dimension, the number of operators grows rapidly [355, 356].

B.2 Dark Matter EFT (DMEFT)

In this scenario, the SM particles are connected with the dark sector through a set of non-renormalizable operators, parametrized by the SM fermions, a DM particle (χ)

and one effective scale (Λ). The first relevant operators arise at $D = 6$ for fermionic DM, and are commonly written in the broken phase, but can also be constructed such as to respect the SM gauge symmetries. While SM fermions are often the only particles considered, the SM gauge bosons could also have interactions with the DM fermions, and appear at $D = 7$ operators, see e.g. in [357–360]. The effective Lagrangian up to dimension 6 can be written as [361–367]

$$\mathcal{L}_{DMEFT} = \sum_{i,j} \sum_{f} \frac{g_{ij}^{f}(\bar{f}\Gamma_{i}^{f}f)(\bar{\chi}\Gamma_{j}^{\chi}\chi)}{\Lambda^2} + ... \tag{B.2}$$

where the sum runs over all fermions $f = u, d, s, c, b, t, e, \mu, \tau$. The gamma matrices are defined as $\Gamma^{f} = \{1, \gamma_5, \gamma_\mu, \gamma_5\gamma_\mu, \sigma_{\mu\nu}\}$ and $\Gamma^{\chi} = \{\Gamma^{f}, \gamma_5\sigma_{\mu\nu}\}$. These are chosen appropriately to form valid combinations of bilinear operators. Note that the DMEFT Lagrangian is described by the DM mass and the Wilson coefficients, g_{ij}^{f}. The imprint of gauge symmetry reflects itself in the scaling of the coefficients, which for scalar operators takes the form (acknowledging that gauge symmetry could be restored by inserting an additional Higgs field) [368]

$$g_{ij}^{f} = \frac{g_{ij}^{f}m_f}{\Lambda}. \tag{B.3}$$

The DMEFT approach has been used and it is very successful on setting bounds that are model independent. Moreover, this perspective has the attribute of providing correlation between several experiments. While this framework was originally constructed for comparison of all DM searches, people realized its questionable validity, since the energy of the processes is often around the limit on Λ, and thus is not used so extensively anymore [174, 361, 369–375]. However, in DD experiments the recoil energy is much smaller ($\sim$ keV), and DMEFTs are still used to calculate collision rates and set bounds on the allowed interaction strength. All of this is done in a model independent way. As the aforementioned calculations are performed at the nuclear scale, quarks interactions are replaced by nucleons. Furthermore, the heavy SM fields are integrated out, and the non-relativistic limit is taken [376–382].

B.3   Soft Collinear Effective Theory (SCET)

The SCET [383–385] is a theory that includes both soft (low energy) particles and collinear (high energy) particles travelling in the same direction at a given process. In other words, SCET is an effective theory for highly energetic quarks interacting with collinear and/or soft gluons. In order to write the most general Lagrangian, we first need to divide the QCD fields into two components $q_n = \psi_n(x) + \Sigma_n(x)$, where

$$\psi_n(x) = \frac{\not{n}\not{\bar{n}}}{4}q_n(x) \quad \text{and} \quad \Sigma_n(x) = \frac{\not{\bar{n}}\not{n}}{4}q_n(x) \tag{B.4}$$

where $n, \bar{n}$ are light-like vectors in light-cone basis and $n \cdot \bar{n} = 2$. Then one can study the equation of motion for Σ_n that can be integrated out due to the fact that its degrees of freedom are far off-shell. At leading order the Lagrangian reads [106]

$$\mathcal{L}_{SCET} = \overline{\psi}_n(x) \left[in \cdot D + i\slashed{D} \frac{1}{i\bar{n} \cdot D} i\slashed{D} \right] \frac{\overline{\slashed{n}}}{2} \psi_n \, . \tag{B.5}$$

The procedure for writing the heavy quarks EFT (HQEFT) Lagrangian is similar as in SCEFT, and is therefore not mentioned here, however, you can find details about that framework in Refs. [106, 386, 387].

Appendix C

Statistical Analysis

We discuss here the details about the statistics used in the CLIC analysis in Sec. 3.13.

C.1 Likelihood Function

To derive the exclusion regions, we start with the binned Likelihood function. This expresses how likely is a statistical parameter with respect to a set of observables [388]. We use a similar Likelihood as the one in CheckMate [171]. For the number of events n_i in the i-th bin, the function reads

$$L(\mu, \theta_S, \theta_B) = \prod_i \frac{[\phi(\mu, \theta_S, \theta_B)]^{n_i}}{n_i!} e^{-\phi(\mu, \theta_S, \theta_B)} e^{-\theta_S^2/2 - \theta_B^S/2} \,, \tag{C.1}$$

with

$$\phi(\mu, \theta_S, \theta_B) \;=\; \mu S e^{\sigma_S \theta_S} \;+\; B e^{\sigma_B \theta_B} \tag{C.2}$$

and

$$\sigma_S = \frac{\Delta S}{S} \,, \quad \sigma_B = \frac{\Delta B}{B} \,. \tag{C.3}$$

Here, S and B, are the predicted numbers of signal and background events, respectively, while $\theta_{S,B}$ are nuisance parameters incorporating the corresponding uncertainties ΔS and ΔB. The variation of the signal strength with the input parameters, given in Sec. 3.4, is parameterized by the signal-strength modifier μ, which is normalized for fixed y_e^S/Λ and fixed masses such that $\mu = (y_\chi^S/\Lambda)^2$. Finally, the last exponential in Eq. (C.1) is required to ensure a good behaviour in the distribution, i.e. no negative values.

For testing the compatibility of different values for μ with data, we need a profile likelihood ratio [388], in this case we use

$$\tilde{\lambda}(\mu) = \begin{cases} \frac{L(\mu, \hat{\hat{\theta}}_S(\mu), \hat{\hat{\theta}}_B(\mu))}{L(\hat{\mu}, \hat{\theta}_S, \hat{\theta}_B)} & \hat{\mu} \geq 0 \,, \\[12pt] \frac{L(\mu, \hat{\hat{\theta}}_S(\mu), \hat{\hat{\theta}}_B(\mu))}{L(0, \hat{\hat{\theta}}_S(0), \hat{\hat{\theta}}_B(0))} & \hat{\mu} < 0 \,, \end{cases} \tag{C.4}$$

where $\hat{\hat{\theta}}_S(\mu), \hat{\hat{\theta}}_B(\mu)$ maximize the Likelihood L for the given value of μ, while $\hat{\mu}, \hat{\theta}_S, \hat{\theta}_B$ are called *unconditional Maximum Likelihood estimators* and correspond to the global maximum, appearing in the denominator Here, the lower case accounts for the fact that we can only have a positive signal contribution.

Finally, for the numerical analysis, we used by convenience the test statistics [388]

$$\tilde{q}_\mu = \begin{cases} -2\ln \tilde{\lambda}(\mu) & \hat{\mu} \leq \mu \\ 0 & \hat{\mu} > \mu \end{cases} \tag{C.5}$$

for setting upper limits (with higher values corresponding to less compatibility), we use the python package `iminuit` [389].

C.2 p-Value

The p-value gives an insight into the statistical significance. It measures the possibility that a difference could have happened by random events. Additionally, the p-value is related to the confident level (CL) of a measurement as it represents the part of the distribution that is not excluded. For example, a p-value of 0.32 would represent a 68% CL (1σ), while a p-value of 0.05 a 95% CL (2σ). Then, to set the limits in the current model at CLIC we quantify the agreement between the background only and the signal hypothesis μ. In the following we assume $\mu = 0$, i.e. we expect to see background only, and derive corresponding projected experimental exclusion regions on μ.

In general, the $p-$value used for $\mu > 0$, leading to a certain $\tilde{q}_{\mu,obs}$ is

$$p_\mu = \int_{\tilde{q}_{\mu,obs}}^\infty f(\tilde{q}_\mu|\mu)d\tilde{q}_\mu \tag{C.6}$$

where $f(\tilde{q}_\mu|\mu')$ is the probability density function (pdf) of $\tilde{q}_\mu$ under the assumption that the data is distributed according to a true $\mu = \mu'$, while the subscript in the first argument denotes the hypothesis being tested[1]. As we want to derive the *expected* upper limits from future experiments (i.e. we do not know $\tilde{q}_{\mu,obs}$) and assuming no signal to be present, we will use the median value of the corresponding distribution, $f(\tilde{q}_\mu|0)$, for $\tilde{q}_{\mu,obs}$. Finally, working at the 95% CL, we will solve for the value of μ that leads to $p_\mu = 0.05$.

To avoid a large number of Monte Carlo simulations when computing the distributions $f(\tilde{q}_\mu|\mu')$, we use the asymptotic formulas given in [388]. Those are valid for a sufficiently high number of events in each bin, which is fulfilled in our case. While in the case $\mu' = \mu$, $f(\tilde{q}_\mu|\mu)$ is given by a simple half-chi-square distribution, we use the so-called Asimov data set [388][2] for obtaining the median of $\tilde{q}_\mu$ according to $f(\tilde{q}_\mu|0)$, where all estimators obtain their true values. This data set can be approximated via large

---

[1]In fact, this quantifies the probability that, given the true signal strength μ, we will observe a value of $\tilde{q}_\mu$ as large as $\tilde{q}_{\mu,obs}$ (or larger).

[2]The Asimov data set is such that all observed quantities are set equal to their expected values, with all the statistic fluctuations suppressed.

Monte Carlo simulations. Here we assume that our initial sets are large enough and use the fitted distributions as Asimov data. With this, the corresponding likelihood-function and test statistics can be evaluated, which are denoted by $\mathcal{L}_A$ and $q_{\mu,A}$. The variance, from which $f(\widetilde{q}_\mu|0)$ can be obtained, is then simply given by $\sigma_A^2 = \frac{\mu^2}{q_{\mu,A}}$, assuming background-only hypothesis [388]. In practice, we can however just use the Asimov value $q_{\mu,A}$ for the median of $[\widetilde{q}_\mu|0]$, according to [388], and therefore the expected $p-$value for a signal hypothesis becomes

$$p_\mu = 1 - \Phi\left(\sqrt{q_{\mu,A}}\right), \tag{C.7}$$

with Φ the cumulative Gaussian distribution. In the end, p_μ is evaluated for varying μ in order to find $p_\mu = 0.05$.

Bibliography

[1] S. Chatrchyan, V. Khachatryan, A.M. Sirunyan, and et al. Observation of a new boson at a mass of 125 gev with the cms experiment at the lhc. Physics Letters B, 716(1):30–61, Sep 2012.

[2] G. Aad, T. Abajyan, B. Abbott, J. Abdallah, and et al. Observation of a new particle in the search for the standard model higgs boson with the atlas detector at the lhc. Physics Letters B, 716(1):1–29, Sep 2012.

[3] Steven Weinberg. The Problem of Mass. Trans. New York Acad. Sci., 38:185–201, 1977.

[4] Andrea De Simone and Thomas Jacques. Simplified models vs. effective field theory approaches in dark matter searches. Eur. Phys. J. C, 76(7):367, 2016.

[5] Giuseppe Carleo, Ignacio Cirac, Kyle Cranmer, Laurent Daudet, Maria Schuld, Naftali Tishby, Leslie Vogt-Maranto, and Lenka Zdeborová. Machine learning and the physical sciences. Reviews of Modern Physics, 91(4), Dec 2019.

[6] Pankaj Mehta, Marin Bukov, Ching-Hao Wang, Alexandre G.R. Day, Clint Richardson, Charles K. Fisher, and David J. Schwab. A high-bias, low-variance introduction to machine learning for physicists. Physics Reports, 810:1–124, May 2019.

[7] J. L. Diaz-Cruz, U. J. Saldana-Salazar, K. M. Tame-Narvaez, and V. T. Tenorth. Natural 2HDMs without FCNCs. Phys. Rev. D, 104(3):035018, 2021.

[8] Werner Rodejohann and Ulises Saldaña Salazar. Multi-Higgs-Doublet Models and Singular Alignment. JHEP, 07:036, 2019.

[9] Tommi Alanne and Florian Goertz. Extended Dark Matter EFT. Eur. Phys. J. C, 80(5):446, 2020.

[10] Florian Goertz, Karla Tame-Narvaez, and Valentin Titus Tenorth. Di-jet/e^+e^-+ MET to Probe Z_2-Odd Mediators to the Dark Sector. Eur. Phys. J. C, 79(10):860, 2019.

[11] M. Aicheler, P.N. Burrows, N. Catalan Lasheras, R. Corsini, M. Draper, J. Osborne, D. Schulte, S. Stapnes, and M.J. Stuart. The Compact Linear Collider (CLIC) – Project Implementation Plan. CERN Yellow Reports: Monographs. Mar 2019. 247 p.

[12] Tommi Alanne, Giorgio Arcadi, Florian Goertz, Valentin Tenorth, and Stefan Vogl. Model-independent constraints with extended dark matter EFT. JHEP, 10:172, 2020.

[13] Stephyn Vogl Florian Goertz, Karla Tame-Narvaez. Work in preparation.

[14] E. Aprile, J. Aalbers, F. Agostini, M. Alfonsi, L. Althueser, F.D. Amaro, V.C. Antochi, E. Angelino, J.R. Angevaare, F. Arneodo, D. Barge, L. Baudis, B. Bauermeister, L. Bellagamba, and et. all. Excess electronic recoil events in xenon1t. Physical Review D, 102(7), Oct 2020.

[15] E. A. Paschos. Diagonal Neutral Currents. Phys. Rev. D, 15:1966, 1977.

[16] Sheldon L. Glashow and Steven Weinberg. Natural Conservation Laws for Neutral Currents. Phys. Rev. D, 15:1958, 1977.

[17] Michael Dine. Naturalness Under Stress. Ann. Rev. Nucl. Part. Sci., 65:43–62, 2015.

[18] Csaba Csáki and Philip Tanedo. Beyond the Standard Model. In 2013 European School of High-Energy Physics, pages 169–268, 2015.

[19] Anson Hook. Naturalness without new particles. JHEP, 04:048, 2021.

[20] Gia Dvali. Cosmological Relaxation of Higgs Mass Before and After LHC and Naturalness. 8 2019.

[21] Goran Senjanović. Natural Philosophy versus Philosophy of Naturalness. Mod. Phys. Lett. A, 35(18):2030006, 2020.

[22] Paul A. M. Dirac. New basis for cosmology. Proc. Roy. Soc. Lond. A, 165:199–208, 1938.

[23] Gerard 't Hooft. Naturalness, chiral symmetry, and spontaneous chiral symmetry breaking. NATO Sci. Ser. B, 59:135–157, 1980.

[24] Brian Batell, Matthew Low, Ethan T. Neil, and Christopher B. Verhaaren. Review of Neutral Naturalness. In 2022 Snowmass Summer Study, 3 2022.

[25] Nathaniel Craig. Naturalness and Top-Down BSM Lecture 1. In MITP Summer School 2018, 2018.

[26] Porter Williams. Two notions of naturalness. Foundations of Physics, 49(9):1022–1050, dec 2018.

[27] RENATA JORA, SALAH NASRI, and JOSEPH SCHECHTER. NATURALNESS IN a SIMPLE TWO HIGGS DOUBLET MODEL. International Journal of Modern Physics A, 28(12):1350036, may 2013.

[28] P. M. Ferreira and B. L. Gonçalves. Stability of neutral minima against charge breaking in the Higgs triplet model. JHEP, 02:182, 2020.

[29] Michael S. Chanowitz and Mitchell Golden. Higgs Boson Triplets With M (*W*) = M (*Z*) cos $\theta \omega$. Phys. Lett. B, 165:105–108, 1985.

[30] Marc Sher. Electroweak Higgs Potentials and Vacuum Stability. Phys. Rept., 179:273–418, 1989.

[31] J. F. Gunion, R. Vega, and J. Wudka. Higgs triplets in the standard model. Phys. Rev. D, 42:1673–1691, 1990.

[32] M. Tanabashi et al. Review of Particle Physics. Phys. Rev. D, 98(3):030001, 2018.

[33] Gautam Bhattacharyya and Dipankar Das. Scalar sector of two-Higgs-doublet models: A minireview. Pramana, 87(3):40, 2016.

[34] G. C. Branco, P. M. Ferreira, L. Lavoura, M. N. Rebelo, Marc Sher, and Joao P. Silva. Theory and phenomenology of two-Higgs-doublet models. Phys. Rept., 516:1–102, 2012.

[35] K. G. Klimenko. On Necessary and Sufficient Conditions for Some Higgs Potentials to Be Bounded From Below. Theor. Math. Phys., 62:58–65, 1985.

[36] M. Maniatis, A. von Manteuffel, O. Nachtmann, and F. Nagel. Stability and symmetry breaking in the general two-Higgs-doublet model. Eur. Phys. J. C, 48:805–823, 2006.

[37] P. M. Ferreira, R. Santos, and A. Barroso. Stability of the tree-level vacuum in two Higgs doublet models against charge or CP spontaneous violation. Phys. Lett. B, 603:219–229, 2004. [Erratum: Phys.Lett.B 629, 114–114 (2005)].

[38] P. M. Ferreira and D. R. T. Jones. Bounds on scalar masses in two Higgs doublet models. JHEP, 08:069, 2009.

[39] Rikard Enberg, Johan Rathsman, and Glenn Wouda. Higgs properties in a broken Inert Doublet Model. JHEP, 08:079, 2013. [Erratum: JHEP 01, 087 (2015)].

[40] Abdesslam Arhrib, Yue-Lin Sming Tsai, Qiang Yuan, and Tzu-Chiang Yuan. An Updated Analysis of Inert Higgs Doublet Model in light of the Recent Results from LUX, PLANCK, AMS-02 and LHC. JCAP, 06:030, 2014.

[41] S. L. Glashow, J. Iliopoulos, and L. Maiani. Weak Interactions with Lepton-Hadron Symmetry. Phys. Rev. D, 2:1285–1292, 1970.

[42] J. Lorenzo Díaz-Cruz. The Higgs profile in the standard model and beyond. Rev. Mex. Fis., 65(5):419–439, 2019.

[43] T. P. Cheng and Marc Sher. Mass Matrix Ansatz and Flavor Nonconservation in Models with Multiple Higgs Doublets. Phys. Rev. D, 35:3484, 1987.

[44] Antonio Pich and Paula Tuzon. Yukawa Alignment in the Two-Higgs-Doublet Model. Phys. Rev. D, 80:091702, 2009.

[45] Ana Peñuelas and Antonio Pich. Flavour alignment in multi-Higgs-doublet models. JHEP, 12:084, 2017.

[46] Rafael A. Porto and A. Zee. The Private Higgs. Phys. Lett. B, 666:491–495, 2008.

[47] Pere Arnan, Damir Bečirević, Federico Mescia, and Olcyr Sumensari. Two Higgs doublet models and $b \to s$ exclusive decays. Eur. Phys. J. C, 77(11):796, 2017.

[48] Giorgio Arcadi, Abdelhak Djouadi, and Martti Raidal. Dark Matter through the Higgs portal. Phys. Rept., 842:1–180.

[49] F. Arco, S. Heinemeyer, and M. J. Herrero. Exploring sizable triple Higgs couplings in the 2HDM. Eur. Phys. J. C, 80(9):884, 2020.

[50] John F. Gunion and Howard E. Haber. The CP conserving two Higgs doublet model: The Approach to the decoupling limit. Phys. Rev. D, 67:075019, 2003.

[51] Andrew G. Akeroyd, Abdesslam Arhrib, and El-Mokhtar Naimi. Note on tree level unitarity in the general two Higgs doublet model. Phys. Lett. B, 490:119–124, 2000.

[52] A. Barroso, P. M. Ferreira, I. P. Ivanov, and Rui Santos. Metastability bounds on the two Higgs doublet model. JHEP, 06:045, 2013.

[53] Alexander L. Kagan, Gilad Perez, Tomer Volansky, and Jure Zupan. General Minimal Flavor Violation. Phys. Rev. D, 80:076002, 2009.

[54] Andrzej J. Buras, Maria Valentina Carlucci, Stefania Gori, and Gino Isidori. Higgs-mediated FCNCs: Natural Flavour Conservation vs. Minimal Flavour Violation. JHEP, 10:009, 2010.

[55] L. J. Hall and L. Randall. Weak-scale effective supersymmetry. Phys. Rev. Lett., 65:2939–2942, Dec 1990.

[56] G. D'Ambrosio, G. F. Giudice, G. Isidori, and A. Strumia. Minimal flavor violation: An Effective field theory approach. Nucl. Phys. B, 645:155–187, 2002.

[57] A. J. Buras, P. Gambino, M. Gorbahn, S. Jager, and L. Silvestrini. Universal unitarity triangle and physics beyond the standard model. Phys. Lett. B, 500:161–167, 2001.

[58] Ivo de Medeiros Varzielas. Family symmetries and alignment in multi-Higgs doublet models. Phys. Lett. B, 701:597–600, 2011.

[59] H. Serodio. Yukawa Alignment in a Multi Higgs Doublet Model: An effective approach. Phys. Lett. B, 700:133–138, 2011.

[60] Lawrence J. Hall, Hitoshi Murayama, and Neal Weiner. Neutrino mass anarchy. Phys. Rev. Lett., 84:2572–2575, 2000.

[61] A. E. Cárcamo Hernández, C. O. Dib, and U. J. Saldaña Salazar. When $\tan \beta$ meets all the mixing angles. Phys. Lett. B, 809:135750, 2020.

[62] F. J. Botella, G. C. Branco, M. N. Rebelo, and J. I. Silva-Marcos. What if the masses of the first two quark families are not generated by the standard model Higgs boson? Phys. Rev. D, 94(11):115031, 2016.

[63] S. Centelles Chuliá, W. Rodejohann, and U. J. Saldaña Salazar. Two-Higgs-doublet models with a flavored $\mathbb{Z}_2$ symmetry. Phys. Rev. D, 101(3):035013, 2020.

[64] Shao-Ping Li, Xin-Qiang Li, Yuan-Yuan Li, Ya-Dong Yang, and Xin Zhang. Power-aligned 2HDM: a correlative perspective on $(g - 2)_{e,\mu}$. JHEP, 01:034, 2021.

[65] Geoffrey T. Bodwin, Frank Petriello, Stoyan Stoynev, and Mayda Velasco. Higgs boson decays to quarkonia and the $H\bar{c}c$ coupling. Phys. Rev. D, 88(5):053003, 2013.

[66] Ilaria Brivio, Florian Goertz, and Gino Isidori. Probing the Charm Quark Yukawa Coupling in Higgs+Charm Production. Phys. Rev. Lett., 115(21):211801, 2015.

[67] Albert M Sirunyan et al. Combined measurements of Higgs boson couplings in proton–proton collisions at $\sqrt{s} = 13$ TeV. Eur. Phys. J. C, 79(5):421, 2019.

[68] Albert M Sirunyan et al. Search for MSSM Higgs bosons decaying to $\mu + \mu -$ in proton-proton collisions at s=13TeV. Phys. Lett. B, 798:134992, 2019.

[69] Georges Aad et al. Combined measurements of Higgs boson production and decay using up to 80 fb^{-1} of proton-proton collision data at $\sqrt{s} = 13$ TeV collected with the ATLAS experiment. Phys. Rev. D, 101(1):012002, 2020.

[70] Felix Kling, Shufang Su, and Wei Su. 2HDM Neutral Scalars under the LHC. JHEP, 06:163, 2020.

[71] Abdelhak Djouadi. The Anatomy of electro-weak symmetry breaking. I: The Higgs boson in the standard model. Phys. Rept., 457:1–216, 2008.

[72] Abdelhak Djouadi. The Anatomy of electro-weak symmetry breaking. II. The Higgs bosons in the minimal supersymmetric model. Phys. Rept., 459:1–241, 2008.

[73] Albert M Sirunyan et al. Measurements of the Higgs boson width and anomalous HVV couplings from on-shell and off-shell production in the four-lepton final state. Phys. Rev. D, 99(11):112003, 2019.

[74] M. A. Arroyo-Ureña and J. Lorenzo Diaz-Cruz. Hidden Signals of New Physics within the Yukawa Couplings of the Higgs boson. Phys. Lett. B, 810:135799, 2020.

[75] Albert M Sirunyan et al. Evidence for Higgs boson decay to a pair of muons. JHEP, 01:148, 2021.

[76] Search for invisible Higgs boson decays with vector boson fusion signatures with the ATLAS detector using an integrated luminosity of 139 fb^{-1}. 4 2020.

[77] M. Aaboud et al. Search for scalar resonances decaying into $\mu^+\mu^-$ in events with and without b-tagged jets produced in proton-proton collisions at $\sqrt{s} = 13$ TeV with the ATLAS detector. JHEP, 07:117, 2019.

[78] J. M. Gerard and M. Herquet. A Twisted custodial symmetry in the two-Higgs-doublet model. Phys. Rev. Lett., 98:251802, 2007.

[79] Simon de Visscher, Jean-Marc Gerard, Michel Herquet, Vincent Lemaitre, and Fabio Maltoni. Unconventional phenomenology of a minimal two-Higgs-doublet model. JHEP, 08:042, 2009.

[80] B. Grzadkowski, M. Maniatis, and Jose Wudka. The bilinear formalism and the custodial symmetry in the two-Higgs-doublet model. JHEP, 11:030, 2011.

[81] Mikolaj Misiak and Matthias Steinhauser. Weak radiative decays of the B meson and bounds on $M_{H^\pm}$ in the Two-Higgs-Doublet Model. Eur. Phys. J. C, 77(3):201, 2017.

[82] A. Abdesselam et al. Measurement of the inclusive $B \rightarrow X_{s+d}\gamma$ branching fraction, photon energy spectrum and HQE parameters. In 38th International Conference on High Energy Physics, 8 2016.

[83] Jorge de Blas, Otto Eberhardt, and Claudius Krause. Current and Future Constraints on Higgs Couplings in the Nonlinear Effective Theory. JHEP, 07:048, 2018.

[84] Felix Kling, Jose Miguel No, and Shufang Su. Anatomy of Exotic Higgs Decays in 2HDM. JHEP, 09:093, 2016.

[85] Measurement of Higgs boson decay to a pair of muons in proton-proton collisions at $\sqrt{s} = 13$ TeV. 2020.

[86] Nina M. Coyle, Carlos E. M. Wagner, and Viska Wei. Bounding the charm Yukawa coupling. Phys. Rev. D, 100(7):073013, 2019.

[87] D. de Florian et al. Handbook of LHC Higgs Cross Sections: 4. Deciphering the Nature of the Higgs Sector. 2/2017, 10 2016.

[88] Philip Bechtle, Cristin Chall, Martin King, Michael Kraemer, Peter Maettig, and Michael Stoeltzner. Bottoms up: Standard model effective field theory from a model perspective, 2022.

[89] Howard Georgi. An Effective Field Theory for Heavy Quarks at Low-energies. Phys. Lett. B, 240:447–450, 1990.

[90] H. Georgi. Effective field theory. Ann. Rev. Nucl. Part. Sci., 43:209–252, 1993.

[91] A. V. Manohar. Effective field theories. Lect. Notes Phys., 479:311–362, 1997.

[92] Antonio Pich. Effective field theory: Course. In Les Houches Summer School in Theoretical Physics, Session 68: Probing the SM ..., pages 949–1049, 6 1998.

[93] Matthias Neubert. Effective field theory and heavy quark physics. Physics In D 4 Tasi 2004, Jul 2006.

[94] Howard Georgi, Greg Kestin, and Aqil Sajjad. Towards an effective field theory on the light-shell. Journal of High Energy Physics, 2016(3), Mar 2016.

[95] Ilaria Brivio and Michael Trott. The Standard Model as an Effective Field Theory. Phys. Rept., 793:1–98, 2019.

[96] Riccardo Penco. An introduction to effective field theories, 2020.

[97] Markus A. Luty. Naive dimensional analysis and supersymmetry. Physical Review D, 57(3):1531–1538, Feb 1998.

[98] Roberto Contino, Adam Falkowski, Florian Goertz, Christophe Grojean, and Francesco Riva. On the validity of the effective field theory approach to sm precision tests. Journal of High Energy Physics, 2016(7), Jul 2016.

[99] Aneesh V. Manohar. Effective field theories. Lecture Notes in Physics, page 311–362.

[100] Aneesh V. Manohar. Introduction to effective field theories, 2018.

[101] Ira Z. Rothstein. Tasi lectures on effective field theories, 2004.

[102] Joseph Polchinski. Effective field theory and the fermi surface, 1999.

[103] Witold Skiba. Tasi lectures on effective field theory and precision electroweak measurements, 2010.

[104] David B. Kaplan. Five lectures on effective field theory, 2005.

[105] A. Pich. Effective field theory, 1998.

[106] Matthias Neubert. Les houches lectures on renormalization theory and effective field theories, 2020.

[107] Florian Goertz. Warped extra dimensions: Flavor, precision tests and higgs physics, 2011.

[108] Upalaparna Banerjee, Joydeep Chakrabortty, Suraj Prakash, Shakeel Ur Rahaman, and Michael Spannowsky. Effective Operator Bases for Beyond Standard Model Scenarios: An EFT compendium for discoveries. JHEP, 01:028, 2021.

[109] Roberto Contino, Margherita Ghezzi, Christophe Grojean, Margarete Muhlleitner, and Michael Spira. Effective Lagrangian for a light Higgs-like scalar. JHEP, 07:035, 2013.

[110] Rodrigo Alonso, Elizabeth E. Jenkins, Aneesh V. Manohar, and Michael Trott. Renormalization Group Evolution of the Standard Model Dimension Six Operators III: Gauge Coupling Dependence and Phenomenology. JHEP, 04:159, 2014.

[111] Adam Falkowski and Adam Falkowski. Higgs Basis: Proposal for an EFT basis choice for LHC HXSWG. Mar 2015.

[112] John Ellis, Christopher W. Murphy, Verónica Sanz, and Tevong You. Updated Global SMEFT Fit to Higgs, Diboson and Electroweak Data. JHEP, 06:146, 2018.

[113] J. H. Oort. The force exerted by the stellar system in the direction perpendicular to the galactic plane and some related problems. , 6:249, August 1932.

[114] F. Zwicky. Die Rotverschiebung von extragalaktischen Nebeln. Helvetica Physica Acta, 6:110–127, January 1933.

[115] Sidney van den Bergh. The early history of dark matter. Publications of the Astronomical Society of the Pacific, 111(760):657–660, Jun 1999.

[116] E. Komatsu, K. M. Smith, J. Dunkley, C. L. Bennett, B. Gold, G. Hinshaw, N. Jarosik, D. Larson, M. R. Nolta, L. Page, D. N. Spergel, M. Halpern, R. S. Hill, A. Kogut, M. Limon, S. S. Meyer, N. Odegard, G. S. Tucker, J. L. Weiland, E. Wollack, and E. L. Wright. Seven-year wilkinson microwave anisotropy probe (wmap) observations: Cosmological interpretation. The Astrophysical Journal Supplement Series, 192(2):18, Jan 2011.

[117] D. N. Spergel, L. Verde, H. V. Peiris, E. Komatsu, M. R. Nolta, C. L. Bennett, M. Halpern, G. Hinshaw, N. Jarosik, A. Kogut, M. Limon, S. S. Meyer, L. Page, G. S. Tucker, J. L. Weiland, E. Wollack, and E. L. Wright. First-year wilkinson microwave anisotropy probe (wmap) observations: Determination of cosmological parameters. The Astrophysical Journal Supplement Series, 148(1):175–194, Sep 2003.

[118] P. A. R. Ade, N. Aghanim, M. I. R. Alves, C. Armitage-Caplan, M. Arnaud, M. Ashdown, F. Atrio-Barandela, J. Aumont, H. Aussel, C. Baccigalupi, A. J. Banday, R. B. Barreiro, and et al. Planck2013 results. i. overview of products and scientific results. Astronomy Astrophysics, 571:A1, Oct 2014.

[119] N. Aghanim, Y. Akrami, F. Arroja, M. Ashdown, J. Aumont, C. Baccigalupi, M. Ballardini, A. J. Banday, R. B. Barreiro, N. Bartolo, S. Basak, R. Battye, and et al. Planck2018 results. Astronomy Astrophysics, 641:A1, Sep 2020.

[120] F. Zwicky. On the Masses of Nebulae and of Clusters of Nebulae. , 86:217, October 1937.

[121] Vera C. Rubin, W. Kent Ford, Jr., and Norbert Thonnard. Extended rotation curves of high-luminosity spiral galaxies. IV. Systematic dynamical properties, Sa through Sc. Astrophys. J. Lett., 225:L107–L111, 1978.

[122] K. G. Begeman, A. H. Broeils, and R. H. Sanders. Extended rotation curves of spiral galaxies : dark haloes and modified dynamics. , 249:523, April 1991.

[123] Douglas Clowe, Maruša Bradač, Anthony H. Gonzalez, Maxim Markevitch, Scott W. Randall, Christine Jones, and Dennis Zaritsky. A direct empirical proof of the existence of dark matter. The Astrophysical Journal, 648(2):L109–L113, Aug 2006.

[124] David Harvey, Richard Massey, Thomas Kitching, Andy Taylor, and Eric Tittley. The nongravitational interactions of dark matter in colliding galaxy clusters. Science, 347(6229):1462–1465, Mar 2015.

[125] Matthew Colless, Bruce A. Peterson, Carole Jackson, John A. Peacock, Shaun Cole, Peder Norberg, Ivan K. Baldry, Carlton M. Baugh, Joss Bland-Hawthorn, Terry Bridges, Russell Cannon, Chris Collins, Warrick Couch, Nicholas Cross, Gavin Dalton, Roberto De Propris, Simon P. Driver, George Efstathiou, Richard S. Ellis, Carlos S. Frenk, Karl Glazebrook, Ofer Lahav, Ian Lewis, Stuart Lumsden, Steve Maddox, Darren Madgwick, Will Sutherland, and Keith Taylor. The 2df galaxy redshift survey: Final data release, 2003.

[126] Lauren Anderson, Éric Aubourg, Stephen Bailey, Florian Beutler, Vaishali Bhardwaj, Michael Blanton, Adam S. Bolton, J. Brinkmann, Joel R. Brownstein, Angela Burden, Chia-Hsun Chuang, Antonio J. Cuesta, Kyle S. Dawson, and et al. The clustering of galaxies in the sdss-iii baryon oscillation spectroscopic survey: baryon acoustic oscillations in the data releases 10 and 11 galaxy samples. Monthly Notices of the Royal Astronomical Society, 441(1):24–62, Apr 2014.

[127] Volker Springel, Rüdiger Pakmor, Annalisa Pillepich, Rainer Weinberger, Dylan Nelson, Lars Hernquist, Mark Vogelsberger, Shy Genel, Paul Torrey, Federico Marinacci, and Jill Naiman. First results from the illustristng simulations: matter and galaxy clustering. Monthly Notices of the Royal Astronomical Society, 475(1):676–698, Dec 2017.

[128] Leonard S. Kisslinger and Debasish Das. A brief review of dark matter. International Journal of Modern Physics A, 34(27):1930013, sep 2019.

[129] A. Arbey and F. Mahmoudi. Dark matter and the early universe: A review. Progress in Particle and Nuclear Physics, page 103865, apr 2021.

[130] Martin Bauer and Tilman Plehn. Yet Another Introduction to Dark Matter: The Particle Physics Approach, volume 959 of Lecture Notes in Physics. Springer, 2019.

[131] Annika H. G. Peter. Dark matter: A brief review, 2012.

[132] B. J. Carr, Kazunori Kohri, Yuuiti Sendouda, and Jun'ichi Yokoyama. New cosmological constraints on primordial black holes. Phys. Rev. D, 81:104019, 2010.

[133] Maxim Pospelov, Adam Ritz, and Mikhail B. Voloshin. Secluded WIMP Dark Matter. Phys. Lett. B, 662:53–61, 2008.

[134] Teresa Marrodán Undagoitia and Ludwig Rauch. Dark matter direct-detection experiments. Journal of Physics G: Nuclear and Particle Physics, 43(1):013001, Dec 2015.

[135] Marc Schumann. Direct detection of wimp dark matter: concepts and status. Journal of Physics G: Nuclear and Particle Physics, 46(10):103003, Aug 2019.

[136] E. Aprile, J. Aalbers, F. Agostini, M. Alfonsi, L. Althueser, F.D. Amaro, M. Anthony, F. Arneodo, L. Baudis, B. Bauermeister, M.L. Benabderrahmane, T. Berger, P.A. Breur, and et al. Dark matter search results from a one ton-year exposure of xenon1t. Physical Review Letters, 121(11), Sep 2018.

[137] Xiangyi Cui, Abdusalam Abdukerim, Wei Chen, Xun Chen, Yunhua Chen, Binbin Dong, Deqing Fang, Changbo Fu, Karl Giboni, Franco Giuliani, Linhui Gu, Yikun Gu, Xuyuan Guo, and et al. Dark matter results from 54-ton-day exposure of pandax-ii experiment. Physical Review Letters, 119(18), Oct 2017.

[138] D.S. Akerib, S. Alsum, H.M. Araújo, X. Bai, A.J. Bailey, J. Balajthy, P. Beltrame, E.P. Bernard, A. Bernstein, T.P. Biesiadzinski, E.M. Boulton, R. Bramante, P. Brás, and et al. Results from a search for dark matter in the complete lux exposure. Physical Review Letters, 118(2), Jan 2017.

[139] Rebecca K. Leane. Indirect detection of dark matter in the galaxy, 2020.

[140] Jennifer M. Gaskins. A review of indirect searches for particle dark matter. Contemporary Physics, 57(4):496–525, Jun 2016.

[141] Louis E. Strigari. Galactic searches for dark matter. Physics Reports, 531(1):1–88, Oct 2013.

[142] Emma Tolley. Dark Matter searches with Mono-X signatures at the ATLAS experiment. PoS, DIS2016:107, 2016.

[143] S. Chatrchyan et al. The CMS Experiment at the CERN LHC. JINST, 3:S08004, 2008.

[144] Johan Alwall, Philip C. Schuster, and Natalia Toro. Simplified models for a first characterization of new physics at the lhc. Physical Review D, 79(7), Apr 2009.

[145] Nima Arkani-Hamed, Bruce Knuteson, Stephen Mrenna, Philip Schuster, Jesse Thaler, Natalia Toro, and Lian-Tao Wang. Marmoset: The path from lhc data to the new standard model via on-shell effective theories, 2007.

[146] Daniele Alves, Nima Arkani-Hamed, Sanjay Arora, Yang Bai, Matthew Baumgart, Joshua Berger, Matthew Buckley, Bart Butler, Spencer Chang, Hsin-Chia Cheng, Clifford Cheung, R Sekhar Chivukula, Won Sang Cho, and et al. Simplified models for lhc new physics searches. Journal of Physics G: Nuclear and Particle Physics, 39(10):105005, Sep 2012.

[147] C.D. McCoy and Michela Massimi. Simplified models: A different perspective on models as mediators. European Journal for Philosophy of Science, 8, 02 2017.

[148] Andrea De Simone and Thomas Jacques. Simplified models vs. effective field theory approaches in dark matter searches. The European Physical Journal C, 76(7), Jul 2016.

[149] Jory Sonneveld. Limits and fits from simplified models, 2015.

[150] Jalal Abdallah, Henrique Araujo, Alexandre Arbey, Adi Ashkenazi, Alexander Belyaev, Joshua Berger, Celine Boehm, Antonio Boveia, Amelia Brennan, Jim Brooke, Oliver Buchmueller, Matthew Buckley, Giorgio Busoni, and et al. Simplified models for dark matter searches at the lhc. Physics of the Dark Universe, 9-10:8–23, Sep 2015.

[151] Enrico Morgante. Simplified dark matter models, 2018.

[152] Christoph Borschensky, Gabriele Coniglio, and Barbara Jäger. Dark matter pair production in the MSSM and in simplified dark matter models at the LHC. Eur. Phys. J. C, 79(5):428, 2019.

[153] Nicole F. Bell, Giorgio Busoni, and Isaac W. Sanderson. Two higgs doublet dark matter portal. Journal of Cosmology and Astroparticle Physics, 2018(01):015–015, Jan 2018.

[154] Jalal Abdallah, Henrique Araujo, Alexandre Arbey, Adi Ashkenazi, Alexander Belyaev, Joshua Berger, Celine Boehm, Antonio Boveia, Amelia Brennan, Jim Brooke, Oliver Buchmueller, Matthew Buckley, Giorgio Busoni, and et al. Simplified models for dark matter searches at the lhc. Physics of the Dark Universe, 9-10:8–23, Sep 2015.

[155] Matthew R. Buckley, David Feld, and Dorival Gonçalves. Scalar simplified models for dark matter. Physical Review D, 91(1), Jan 2015.

[156] Jessica Goodman, Masahiro Ibe, Arvind Rajaraman, William Shepherd, Tim M. P. Tait, and Hai-Bo Yu. Constraints on dark matter from colliders. Physical Review D, 82(11), Dec 2010.

[157] Maria Beltrán, Dan Hooper, Edward W. Kolb, Zosia A. C. Krusberg, and Tim M. P. Tait. Maverick dark matter at colliders. Journal of High Energy Physics, 2010(9), Sep 2010.

[158] William Shepherd, Tim M. P. Tait, and Gabrijela Zaharijas. Bound states of weakly interacting dark matter. Physical Review D, 79(5), Mar 2009.

[159] Duarte Azevedo, Mateusz Duch, Bohdan Grzadkowski, Da Huang, Michal Iglicki, and Rui Santos. Testing scalar versus vector dark matter. Phys. Rev. D, 99(1):015017, 2019.

[160] Tommi Alanne, Giorgio Arcadi, Florian Goertz, Valentin Tenorth, and Stefan Vogl. Model-independent constraints with extended dark matter eft. Journal of High Energy Physics, 2020(10), Oct 2020.

[161] Michael A. Fedderke, Jing-Yuan Chen, Edward W. Kolb, and Lian-Tao Wang. The Fermionic Dark Matter Higgs Portal: an effective field theory approach. JHEP, 08:122, 2014.

[162] Céline Degrande, Claude Duhr, Benjamin Fuks, David Grellscheid, Olivier Mattelaer, and Thomas Reiter. Ufo – the universal feynrules output. Computer Physics Communications, 183(6):1201–1214, Jun 2012.

[163] Neil Christensen, Priscila de Aquino, Celine Degrande, Claude Duhr, Benjamin Fuks, Michel Herquet, Fabio Maltoni, and Steffen Schumann. A comprehensive approach to new physics simulations. The European Physical Journal C, 71(2), Feb 2011.

[164] Adam Alloul, Neil D. Christensen, Céline Degrande, Claude Duhr, and Benjamin Fuks. Feynrules 2.0 — a complete toolbox for tree-level phenomenology. Computer Physics Communications, 185(8):2250–2300, Aug 2014.

[165] Johan Alwall, Michel Herquet, Fabio Maltoni, Olivier Mattelaer, and Tim Stelzer. Madgraph 5: going beyond. Journal of High Energy Physics, 2011(6), Jun 2011.

[166] J. Alwall, R. Frederix, S. Frixione, V. Hirschi, F. Maltoni, O. Mattelaer, H.-S. Shao, T. Stelzer, P. Torrielli, and M. Zaro. The automated computation of tree-level and next-to-leading order differential cross sections, and their matching to parton shower simulations. Journal of High Energy Physics, 2014(7), Jul 2014.

[167] J. de Favereau, C. Delaere, P. Demin, A. Giammanco, V. Lemaître, A. Mertens, and M. Selvaggi. Delphes 3: a modular framework for fast simulation of a generic collider experiment. Journal of High Energy Physics, 2014(2), Feb 2014.

[168] Torbjörn Sjöstrand, Stefan Ask, Jesper R. Christiansen, Richard Corke, Nishita Desai, Philip Ilten, Stephen Mrenna, Stefan Prestel, Christine O. Rasmussen, and Peter Z. Skands. An introduction to pythia 8.2. Computer Physics Communications, 191:159–177, Jun 2015.

[169] Yu Jiang, Vivek Natarajan, Xinlei Chen, Marcus Rohrbach, Dhruv Batra, and Devi Parikh. Pythia v0.1: the winning entry to the vqa challenge 2018, 2018.

[170] Manuel Drees, Herbi Dreiner, Jong Soo Kim, Daniel Schmeier, and Jamie Tattersall. Checkmate: Confronting your favourite new physics model with lhc data, 2014.

[171] Daniel Dercks, Nishita Desai, Jong Soo Kim, Krzysztof Rolbiecki, Jamie Tattersall, and Torsten Weber. Checkmate 2: From the model to the limit. Computer Physics Communications, 221:383–418, Dec 2017.

[172] M. Aaboud, G. Aad, B. Abbott, O. Abdinov, B. Abeloos, S. H. Abidi, O. S. AbouZeid, N. L. Abraham, H. Abramowicz, H. Abreu, R. Abreu, Y. Abulaiti, B. S. Acharya, S. Adachi, and L. et.all Adamczyk. Search for dark matter and other new phenomena in events with an energetic jet and large missing transverse momentum using the atlas detector. Journal of High Energy Physics, 2018(1), Jan 2018.

[173] M. Aaboud, G. Aad, B. Abbott, O. Abdinov, B. Abeloos, S.H. Abidi, O.S. AbouZeid, N.L. Abraham, H. Abramowicz, H. Abreu, R. Abreu, Y. Abulaiti, B.S. Acharya, S. Adachi, and month=Jun Adamczyk, L. et.all year=2018. Search for squarks and gluinos in final states with jets and missing transverse momentum using 36fb1 of s=13tev pp collision data with the atlas detector. Physical Review D, 97(11).

[174] Giorgio Busoni, Andrea De Simone, Enrico Morgante, and Antonio Riotto. On the Validity of the Effective Field Theory for Dark Matter Searches at the LHC. Phys. Lett., B728:412–421, 2014.

[175] Enrico Morgante. On the validity of the effective field theory for dark matter searches at the LHC. Nuovo Cim., C38(1):32, 2015.

[176] G. Aad, B. Abbott, D.C. Abbott, O. Abdinov, A. Abed Abud, K. Abeling, D.K. Abhayasinghe, S.H. Abidi, O.S. AbouZeid, and N.L. Abraham. Search for high-mass dilepton resonances using 139 fb1 of pp collision data collected at s=13 tev with the atlas detector. Physics Letters B, 796:68–87, Sep 2019.

[177] ATLAS Collaboration. Extrapolation of E_T^{miss}+ jet search results to an integrated luminosity of 300 fb^{-1} and 3000 fb^{-1}. (ATL-PHYS-PUB-2018-043), Dec 2018.

[178] Abdelhak Djouadi. The anatomy of electroweak symmetry breaking. Physics Reports, 457(1–4):1–216, Feb 2008.

[179] M. Aaboud, G. Aad, B. Abbott, O. Abdinov, B. Abeloos, S.H. Abidi, O.S. AbouZeid, N.L. Abraham, H. Abramowicz, H. Abreu, R. Abreu, Y. Abulaiti, B.S. Acharya, S. Adachi, and L. Adamczyk. Search for new phenomena in high-mass diphoton final states using 37 fb1 of proton–proton collisions collected at s=13 tev with the atlas detector. Physics Letters B, 775:105–125, Dec 2017.

[180] Eric Conte, Béranger Dumont, Benjamin Fuks, and Chris Wymant. Designing and recasting lhc analyses with madanalysis 5. The European Physical Journal C, 74(10), Oct 2014.

[181] Eric Conte and Benjamin Fuks. Confronting new physics theories to lhc data with madanalysis 5. International Journal of Modern Physics A, 33(28):1830027, Oct 2018.

[182] G. Belanger, F. Boudjema, and A. Pukhov. micromegas : a code for the calculation of dark matter properties in generic models of particle interaction, 2014.

[183] XENON Collaboration, Elena Aprile, J. Aalbers, F. Agostini, Matteo Alfonsi, F. Amaro, Mouliere Anthony, B. Antunes, F. Arneodo, M. Balata, P. Barrow, L. Baudis, B. Bauermeister, M. L. Benabderrahmane, T. Berger, Amos Breskin, P. Breur, Andrew Brown, Ethan Brown, and Yi Zhang. The xenon1t dark matter experiment. The European Physical Journal C, 77, 08 2017.

[184] B. J. Mount, S. Hans, R. Rosero, M. Yeh, C. Chan, R. J. Gaitskell, D. Q. Huang, J. Makkinje, D. C. Malling, M. Pangilinan, C. A. Rhyne, W. C. Taylor, J. R. Verbus, Y. D. Kim, H. S. Lee, J. Lee, D. S. Leonard, J. Li, J. Belle, and eprint=1703.09144 archivePrefix=arXiv primaryClass=physics.ins-det et. all, year=2017. Lux-zeplin (lz) technical design report.

[185] J. Aalbers, F. Agostini, M. Alfonsi, F.D. Amaro, C. Amsler, E. Aprile, L. Arazi, F. Arneodo, P. Barrow, and L. et. all. Baudis. Darwin: towards the ultimate dark matter detector. Journal of Cosmology and Astroparticle Physics, 2016(11):017–017, Nov 2016.

[186] Brian Henning, Xiaochuan Lu, and Hitoshi Murayama. One-loop Matching and Running with Covariant Derivative Expansion. JHEP, 01:123, 2018.

[187] M. K. Gaillard. The Effective One Loop Lagrangian With Derivative Couplings. Nucl. Phys. B, 268:669–692, 1986.

[188] Oren Cheyette. Effective Action for the Standard Model With Large Higgs Mass. Nucl. Phys. B, 297:183–204, 1988.

[189] Aleksandra Drozd, John Ellis, Jérémie Quevillon, and Tevong You. The Universal One-Loop Effective Action. JHEP, 03:180, 2016.

[190] Sebastian A. R. Ellis, Jérémie Quevillon, Tevong You, and Zhengkang Zhang. Extending the Universal One-Loop Effective Action: Heavy-Light Coefficients. JHEP, 08:054, 2017.

[191] Brian Henning, Xiaochuan Lu, and Hitoshi Murayama. How to use the Standard Model effective field theory. JHEP, 01:023, 2016.

[192] Minyuan Jiang, Nathaniel Craig, Ying-Ying Li, and Dave Sutherland. Complete one-loop matching for a singlet scalar in the Standard Model EFT. JHEP, 02:031, 2019. [Erratum: JHEP 01, 135 (2021)].

[193] Giorgio Arcadi, Giorgio Busoni, Thomas Hugle, and Valentin Titus Tenorth. Comparing 2HDM + Scalar and Pseudoscalar Simplified Models at LHC. JHEP, 06:098, 2020.

[194] Jose Miguel No. Looking through the pseudoscalar portal into dark matter: Novel mono-Higgs and mono-Z signatures at the LHC. Phys. Rev. D, 93(3):031701, 2016.

[195] Martin Bauer, Ulrich Haisch, and Felix Kahlhoefer. Simplified dark matter models with two Higgs doublets: I. Pseudoscalar mediators. JHEP, 05:138, 2017.

[196] Howard E. Haber and Oscar Stål. New LHC benchmarks for the $\mathcal{CP}$ -conserving two-Higgs-doublet model. Eur. Phys. J. C, 75(10):491, 2015. [Erratum: Eur.Phys.J.C 76, 312 (2016)].

[197] P. S. Bhupal Dev and Apostolos Pilaftsis. Maximally Symmetric Two Higgs Doublet Model with Natural Standard Model Alignment. JHEP, 12:024, 2014. [Erratum: JHEP 11, 147 (2015)].

[198] Hermès Bélusca-Maïto, Adam Falkowski, Duarte Fontes, Jorge C. Romão, and João P. Silva. Higgs EFT for 2HDM and beyond. Eur. Phys. J. C, 77(3):176, 2017.

[199] Nicole F. Bell, Giorgio Busoni, and Isaac W. Sanderson. Self-consistent Dark Matter Simplified Models with an s-channel scalar mediator. JCAP, 03:015, 2017.

[200] Nicole F. Bell, Giorgio Busoni, and Isaac W. Sanderson. Two Higgs Doublet Dark Matter Portal. JCAP, 01:015, 2018.

[201] Stefan von Buddenbrock, Alan S. Cornell, Elie D. R. Iarilala, Mukesh Kumar, Bruce Mellado, Xifeng Ruan, and Esra Mohammed Shrif. Constraints on a 2HDM with a singlet scalar and implications in the search for heavy bosons at the LHC. J. Phys. G, 46(11):115001, 2019.

[202] Sebastian Baum and Nausheen R. Shah. Benchmark Suggestions for Resonant Double Higgs Production at the LHC for Extended Higgs Sectors. 4 2019.

[203] F. del Aguila, L. Ametller, Gordon L. Kane, and J. Vidal. Vector Like Fermion and Standard Higgs Production at Hadron Colliders. Nucl. Phys. B, 334:1–23, 1990.

[204] Cesar Bonilla, A. E. Cárcamo Hernández, João Gonçalves, Felipe F. Freitas, António P. Morais, and R. Pasechnik. Collider signatures of vector-like fermions from a flavor symmetric model. JHEP, 01:154, 2022.

[205] G. Barenboim, F. J. Botella, and O. Vives. Constraining Models with Vector - Like Fermions from FCNC in K and B Physics. Nucl. Phys. B, 613:285–305, 2001.

[206] G. Cynolter and E. Lendvai. Electroweak Precision Constraints on Vector-like Fermions. Eur. Phys. J. C, 58:463–469, 2008.

[207] Koji Ishiwata, Zoltan Ligeti, and Mark B. Wise. New Vector-Like Fermions and Flavor Physics. JHEP, 10:027, 2015.

[208] J. A. Aguilar-Saavedra, R. Benbrik, S. Heinemeyer, and M. Pérez-Victoria. Handbook of vectorlike quarks: Mixing and single production. Phys. Rev. D, 88(9):094010, 2013.

[209] Albert M Sirunyan et al. Search for vector-like T and B quark pairs in final states with leptons at $\sqrt{s} = 13$ TeV. JHEP, 08:177, 2018.

[210] Salvatore Rappoccio. The experimental status of direct searches for exotic physics beyond the standard model at the Large Hadron Collider. Rev. Phys., 4:100027, 2019.

[211] Morad Aaboud et al. Combination of the searches for pair-produced vector-like partners of the third-generation quarks at $\sqrt{s} = 13$ TeV with the ATLAS detector. Phys. Rev. Lett., 121(21):211801, 2018.

[212] Georges Aad et al. Search for new phenomena in events with an energetic jet and missing transverse momentum in pp collisions at $\sqrt{s}$ =13 TeV with the ATLAS detector. Phys. Rev. D, 103(11):112006, 2021.

[213] Armen Tumasyan et al. Search for new particles in events with energetic jets and large missing transverse momentum in proton-proton collisions at $\sqrt{s} = 13$ TeV. JHEP, 11:153, 2021.

[214] Mathieu Buchkremer, Giacomo Cacciapaglia, Aldo Deandrea, and Luca Panizzi. Model Independent Framework for Searches of Top Partners. Nucl. Phys. B, 876:376–417, 2013.

[215] Giacomo Cacciapaglia, Aldo Deandrea, Daisuke Harada, and Yasuhiro Okada. Bounds and Decays of New Heavy Vector-like Top Partners. JHEP, 11:159, 2010.

[216] Giacomo Cacciapaglia, Aldo Deandrea, Luca Panizzi, Naveen Gaur, Daisuke Harada, and Yasuhiro Okada. Heavy Vector-like Top Partners at the LHC and flavour constraints. JHEP, 03:070, 2012.

[217] Clifford Cheung, Lawrence J. Hall, David Pinner, and Joshua T. Ruderman. Prospects and Blind Spots for Neutralino Dark Matter. JHEP, 05:100, 2013.

[218] Peisi Huang and Carlos E. M. Wagner. Blind Spots for neutralino Dark Matter in the MSSM with an intermediate m_A. Phys. Rev. D, 90(1):015018, 2014.

[219] Asher Berlin, Stefania Gori, Tongyan Lin, and Lian-Tao Wang. Pseudoscalar Portal Dark Matter. Phys. Rev. D, 92:015005, 2015.

[220] Arghya Choudhury, Kamila Kowalska, Leszek Roszkowski, Enrico Maria Sessolo, and Andrew J. Williams. Blind Spots for Direct Detection with Simplified DM Models and the LHC. Universe, 3(2):41, 2017.

[221] Search for dark matter and other new phenomena in events with an energetic jet and large missing transverse momentum using the ATLAS detector. Technical report, CERN, Geneva, Jul 2017. All figures including auxiliary figures are available at https://atlas.web.cern.ch/Atlas/GROUPS/PHYSICS/CONFNOTES/ATLAS-CONF-2017-060.

[222] Search for new phenomena in events with jets and missing transverse momentum in p p collisions at $\sqrt{s} = 13$ TeV with the ATLAS detector. 8 2020.

[223] Teresa Marrodán Undagoitia and Ludwig Rauch. Dark matter direct-detection experiments. J. Phys. G, 43(1):013001, 2016.

[224] Julien Billard, Mark Boulay, Susana Cebrián, Laura Covi, Giuliana Fiorillo, Anne Green, Joachim Kopp, Béla Majorovits, Kimberly Palladino, Federica Petricca, Leszek Roszkowski, and Marc Schumann. Direct detection of dark matter – appec committee report, 2021.

[225] K. Fushimi et al. Dark matter search with high purity NaI(Tl) scintillator. 6 2021.

[226] S K Kim, H J Kim, and Y D Kim. Scintillator-based detectors for dark matter searches i. New Journal of Physics, 12(7):075003, jul 2010.

[227] R. Bernabei et al. First results from DAMA/LIBRA and the combined results with DAMA/NaI. Eur. Phys. J. C, 56:333–355, 2008.

[228] R. Bernabei et al. Dama/nai results. In 39th Rencontres de Moriond on Electroweak Interactions and Unified Theories, pages 378–386, 5 2004.

[229] R. Bernabei et al. The dark matter: DAMA/LIBRA and its perspectives. In 16th Marcel Grossmann Meeting on Recent Developments in Theoretical and ..., 10 2021.

[230] N. J. C. Spooner et al. NaI dark matter limits and the NAIAD array - a detector with improved sensitivity to WIMPs using unencapsulated NaI. Phys. Lett. B, 473:330–336, 2000.

[231] J. Amaré et al. First Results on Dark Matter Annual Modulation from the ANAIS-112 Experiment. Phys. Rev. Lett., 123(3):031301, 2019.

[232] C. E. Aalseth et al. CoGeNT: A Search for Low-Mass Dark Matter using p-type Point Contact Germanium Detectors. Phys. Rev. D, 88:012002, 2013.

[233] Rouven Essig, Marivi Fernandez-Serra, Jeremy Mardon, Adrian Soto, Tomer Volansky, and Tien-Tien Yu. Direct Detection of sub-GeV Dark Matter with Semiconductor Targets. JHEP, 05:046, 2016.

[234] S. Roth, C. Ciemniak, C. Coppi, F. v. Feilitzsch, A. Gütlein, C. Isaila, J. C. Lanfranchi, S. Pfister, W. Potzel, and W. Westphal. Cryogenic Composite Detectors for the Dark Matter Experiments CRESST and EURECA. Opt. Mater., 31:1415–1420, 2009.

[235] S. Roth, C. Ciemniak, C. Coppi, F. v. Feilitzsch, A. Gutlein, C. Isaila, J. C. Lanfranchi, S. Pfister, W. Potzel, and W. Westphal. Thermal detector model for cryogenic composite detectors for the dark matter experiments CRESST and EURECA. J. Phys. Conf. Ser., 136:042085, 2008.

[236] F. Petricca et al. New results on low-mass dark matter from the CRESST-II experiment. J. Phys. Conf. Ser., 718(4):042044, 2016.

[237] G. Angloher et al. Limits on WIMP dark matter using scintillating CaWO$_4$ cryogenic detectors with active background suppression. Astropart. Phys., 23:325–339, 2005.

[238] G. Angloher et al. The COSINUS project - perspectives of a NaI scintillating calorimeter for dark matter search. Eur. Phys. J. C, 76(8):441, 2016.

[239] D. S. Akerib et al. First results from the LUX dark matter experiment at the Sanford Underground Research Facility. Phys. Rev. Lett., 112:091303, 2014.

[240] T. J. Sumner. The ZEPLIN III dark matter project. New Astron. Rev., 49:277–281, 2005.

[241] V. N. Lebedenko et al. Result from the First Science Run of the ZEPLIN-III Dark Matter Search Experiment. Phys. Rev. D, 80:052010, 2009.

[242] K. Abe et al. XMASS detector. Nucl. Instrum. Meth. A, 716:78–85, 2013.

[243] J. Aalbers et al. DARWIN: towards the ultimate dark matter detector. JCAP, 11:017, 2016.

[244] Marc Schumann. Dark Matter Search with liquid Noble Gases. 6 2012.

[245] Celine Boehm, David G. Cerdeno, Malcolm Fairbairn, Pedro A. N. Machado, and Aaron C. Vincent. Light new physics in XENON1T. Phys. Rev. D, 102:115013, 2020.

[246] D. Aristizabal Sierra, V. De Romeri, L. J. Flores, and D. K. Papoulias. Light vector mediators facing XENON1T data. Phys. Lett. B, 809:135681, 2020.

[247] Amir N. Khan. Can Nonstandard Neutrino Interactions explain the XENON1T spectral excess? Phys. Lett. B, 809:135782, 2020.

[248] Shao-Feng Ge, Pedro Pasquini, and Jie Sheng. Solar neutrino scattering with electron into massive sterile neutrino. Phys. Lett. B, 810:135787, 2020.

[249] Wei Chao, Yu Gao, and Ming jie Jin. Pseudo-Dirac Dark Matter in XENON1T. 6 2020.

[250] Yugen Lin, Yu Gao, and Tianjun Li. Lepton Number Violating Electron Recoils at XENON1T and PANDAX by the $U(1)_{B-L}$ Model with Non-Standard Interactions. 6 2020.

[251] Fuminobu Takahashi, Masaki Yamada, and Wen Yin. XENON1T Excess from Anomaly-Free Axionlike Dark Matter and Its Implications for Stellar Cooling Anomaly. Phys. Rev. Lett., 125(16):161801, 2020.

[252] Gonzalo Alonso-Álvarez, Fatih Ertas, Joerg Jaeckel, Felix Kahlhoefer, and Lennert J. Thormaehlen. Hidden Photon Dark Matter in the Light of XENON1T and Stellar Cooling. JCAP, 11:029, 2020.

[253] Itay M. Bloch, Andrea Caputo, Rouven Essig, Diego Redigolo, Mukul Sholapurkar, and Tomer Volansky. Exploring new physics with O(keV) electron recoils in direct detection experiments. JHEP, 01:178, 2021.

[254] Nobuchika Okada, Satomi Okada, Digesh Raut, and Qaisar Shafi. Dark matter Z' and XENON1T excess from $U(1)_X$ extended standard model. Phys. Lett. B, 810:135785, 2020.

[255] Hong-Jian He, Yu-Chen Wang, and Jiaming Zheng. EFT Approach of Inelastic Dark Matter for Xenon Electron Recoil Detection. JCAP, 01:042, 2021.

[256] Manfred Lindner, Yann Mambrini, Téssio B. de Melo, and Farinaldo S. Queiroz. XENON1T anomaly: A light Z' from a Two Higgs Doublet Model. Phys. Lett. B, 811:135972, 2020.

[257] Andreas Bally, Sudip Jana, and Andreas Trautner. Neutrino self-interactions and XENON1T electron recoil excess. Phys. Rev. Lett., 125(16):161802, 2020.

[258] Kristjan Kannike, Martti Raidal, Hardi Veermäe, Alessandro Strumia, and Daniele Teresi. Dark Matter and the XENON1T electron recoil excess. Phys. Rev. D, 102(9):095002, 2020.

[259] Bartosz Fornal, Pearl Sandick, Jing Shu, Meng Su, and Yue Zhao. Boosted Dark Matter Interpretation of the XENON1T Excess. Phys. Rev. Lett., 125(16):161804, 2020.

[260] Liangliang Su, Wenyu Wang, Lei Wu, Jin Min Yang, and Bin Zhu. Atmospheric Dark Matter and Xenon1T Excess. Phys. Rev. D, 102(11):115028, 2020.

[261] Qing-Hong Cao, Ran Ding, and Qian-Fei Xiang. Searching for sub-MeV boosted dark matter from xenon electron direct detection. Chin. Phys. C, 45(4):045002, 2021.

[262] Haider Alhazmi, Doojin Kim, Kyoungchul Kong, Gopolang Mohlabeng, Jong-Chul Park, and Seodong Shin. Implications of the XENON1T Excess on the Dark Matter Interpretation. JHEP, 05:055, 2021.

[263] Luca Di Luzio, Marco Fedele, Maurizio Giannotti, Federico Mescia, and Enrico Nardi. Solar axions cannot explain the XENON1T excess. Phys. Rev. Lett., 125(13):131804, 2020.

[264] Keisuke Harigaya, Yuichiro Nakai, and Motoo Suzuki. Inelastic Dark Matter Electron Scattering and the XENON1T Excess. Phys. Lett. B, 809:135729, 2020.

[265] Nicole F. Bell, James B. Dent, Bhaskar Dutta, Sumit Ghosh, Jason Kumar, and Jayden L. Newstead. Explaining the XENON1T excess with Luminous Dark Matter. Phys. Rev. Lett., 125(16):161803, 2020.

[266] Hyun Min Lee. Exothermic dark matter for XENON1T excess. JHEP, 01:019, 2021.

[267] Joseph Bramante and Ningqiang Song. Electric But Not Eclectic: Thermal Relic Dark Matter for the XENON1T Excess. Phys. Rev. Lett., 125(16):161805, 2020.

[268] Seungwon Baek, Jongkuk Kim, and P. Ko. XENON1T excess in local Z_2 DM models with light dark sector. Phys. Lett. B, 810:135848, 2020.

[269] K. S. Babu, Sudip Jana, and Manfred Lindner. Large Neutrino Magnetic Moments in the Light of Recent Experiments. JHEP, 10:040, 2020.

[270] Ian M. Shoemaker, Yu-Dai Tsai, and Jason Wyenberg. Active-to-sterile neutrino dipole portal and the XENON1T excess. Phys. Rev. D, 104(11):115026, 2021.

[271] O. G. Miranda, D. K. Papoulias, M. Tórtola, and J. W. F. Valle. XENON1T signal from transition neutrino magnetic moments. Phys. Lett. B, 808:135685, 2020.

[272] David McKeen, Maxim Pospelov, and Nirmal Raj. Hydrogen Portal to Exotic Radioactivity. Phys. Rev. Lett., 125(23):231803, 2020.

[273] Lei Zu, Guan-Wen Yuan, Lei Feng, and Yi-Zhong Fan. Mirror Dark Matter and Electronic Recoil Events in XENON1T. Nucl. Phys. B, 965:115369, 2021.

[274] Yongsoo Jho, Jong-Chul Park, Seong Chan Park, and Po-Yan Tseng. Leptonic New Force and Cosmic-ray Boosted Dark Matter for the XENON1T Excess. Phys. Lett. B, 811:135863, 2020.

[275] P. Ko and Yong Tang. Semi-annihilating Z_3 dark matter for XENON1T excess. Phys. Lett. B, 815:136181, 2021.

[276] Chengfeng Cai, Hong Hao Zhang, Mads T. Frandsen, Martin Rosenlyst, and Giacomo Cacciapaglia. XENON1T solar axion and the Higgs boson emerging from the dark. Phys. Rev. D, 102(7):075018, 2020.

[277] Giorgio Arcadi, Andreas Bally, Florian Goertz, Karla Tame-Narvaez, Valentin Tenorth, and Stefan Vogl. EFT interpretation of XENON1T electron recoil excess: Neutrinos and dark matter. Phys. Rev. D, 103(2):023024, 2021.

[278] Sunny Vagnozzi, Luca Visinelli, Philippe Brax, Anne-Christine Davis, and Jeremy Sakstein. Direct detection of dark energy: The xenon1t excess and future prospects. Physical Review D, 104(6), Sep 2021.

[279] Dario Buttazzo, Paolo Panci, Daniele Teresi, and Robert Ziegler. Xenon1t excess from electron recoils of non-relativistic dark matter. Physics Letters B, 817:136310, 2021.

[280] So Chigusa, Motoi Endo, and Kazunori Kohri. Constraints on electron-scattering interpretation of XENON1t excess. Journal of Cosmology and Astroparticle Physics, 2020(10):035–035, oct 2020.

[281] R. Primulando, J. Julio, and P. Uttayarat. Collider constraints on a dark matter interpretation of the xenon1t excess. The European Physical Journal C, 80(11), Nov 2020.

[282] P. Ko and Yong Tang. Semi-annihilating z3 dark matter for xenon1t excess. Physics Letters B, 815:136181, 2021.

[283] Ujjal Kumar Dey, Tarak Nath Maity, and Tirtha Sankar Ray. Prospects of migdal effect in the explanation of xenon1t electron recoil excess. Physics Letters B, 811:135900, 2020.

[284] Astronomy Now. Scientists ponder inconclusive data from dark matter experiment. Astronomy Now, the UK's Best Astronomy Magazine., 2020.

[285] Andi Tan et al. Dark Matter Results from First 98.7 Days of Data from the PandaX-II Experiment. Phys. Rev. Lett., 117(12):121303, 2016.

[286] HongGuang Zhang, Abdusalam Abdukerim, Wei Chen, Xun Chen, YunHua Chen, XiangYi Cui, BinBin Dong, DeQing Fang, ChangBo Fu, Karl Giboni, Franco Giuliani, LinHui Gu, XuYuan Guo, ZhiFan Guo, Ke Han, ChangDa He, Sheng-Ming He, Di Huang, XingTao Huang, Zhou Huang, Peng Ji, XiangDong Ji, YongLin Ju, ShaoLi Li, Yao Li, Heng Lin, HuaXuan Liu, JiangLai Liu, YuGang Ma, YaJun Mao, KaiXiang Ni, JinHua Ning, XiangXiang Ren, Fang Shi, AnDi Tan, AnQing Wang, Cheng Wang, HongWei Wang, Meng Wang, QiuHong Wang, SiGuang Wang, XiuLi Wang, XuMing Wang, Zhou Wang, MengMeng Wu, ShiYong Wu, JingKai Xia, MengJiao Xiao, PengWei Xie, BinBin Yan, JiJun Yang, Yong Yang, ChunXu Yu, JuMin Yuan, JianFeng Yue, Dan Zhang, Tao Zhang, Li Zhao, QiBin Zheng, JiFang Zhou, Ning Zhou, and XiaoPeng Zhou. Dark matter direct search sensitivity of the pandax-4t experiment. Science China Physics, Mechanics Astronomy, 62(3), Aug 2018.

[287] E. Aprile, J. Aalbers, F. Agostini, M. Alfonsi, L. Althueser, F.D. Amaro, V.C. Antochi, E. Angelino, J.R. Angevaare, F. Arneodo, D. Barge, L. Baudis, B. Bauer-meister, L. Bellagamba, M.L. Benabderrahmane, T. Berger, A. Brown, and et. all. Projected wimp sensitivity of the xenonnt dark matter experiment. Journal of Cosmology and Astroparticle Physics, 2020(11):031–031, Nov 2020.

[288] D.S. Akerib, C.W. Akerlof, D.Yu. Akimov, A. Alquahtani, S.K. Alsum, T.J. Anderson, N. Angelides, H.M. Araújo, A. Arbuckle, J.E. Armstrong, M. Arthurs, H. Auyeung, X. Bai, A.J. Bailey, J. Balajthy, S. Balashov, J. Bang, M.J. Barry, J. Barthel, D. Bauer, P. Bauer, A. Baxter, J. Belle, P. Beltrame, J. Bensinger, T. Benson, E.P. Bernard, A. Bernstein, A. Bhatti, A. Biekert, T.P. Biesiadzinski, B. Birrittella, K.E. Boast, A.I. Bolozdynya, E.M. Boulton, B. Boxer, R. Bramante, S. Branson, P. Brás, M. Breidenbach, J.H. Buckley, V.V. Bugaev, R. Bunker, S. Burdin, J.K. Busenitz, J.S. Campbell, C. Carels, D.L. Carlsmith, B. Carlson, M.C. Carmona-Benitez, M. Cascella, C. Chan, J.J. Cherwinka, A.A. Chiller, C. Chiller, N.I. Chott, A. Cole, J. Coleman, D. Colling, R.A. Conley, A. Cottle, R. Coughlen, W.W. Craddock, D. Curran, A. Currie, J.E. Cutter, and J.P. da Cunha. The lux-zeplin (lz) experiment. Nuclear Instruments and Methods in Physics Research Section A: Accelerators, Spectrometers, Detectors and Associated Equipment, 953:163047, 2020.

[289] John Ellis, Andrew Fowlie, Luca Marzola, and Martti Raidal. Statistical analyses of higgs- and z -portal dark matter models. Physical Review D, 97(11), Jun 2018.

[290] Michael A. Fedderke, Jing-Yuan Chen, Edward W. Kolb, and Lian-Tao Wang. The fermionic dark matter higgs portal: an effective field theory approach. Journal of High Energy Physics, 2014(8), Aug 2014.

[291] David G. Cerdeño, Malcolm Fairbairn, Thomas Jubb, Pedro A. N. Machado, Aaron C. Vincent, and Céline Bœhm. Physics from solar neutrinos in dark matter direct detection experiments. JHEP, 05:118, 2016. [Erratum: JHEP 09, 048 (2016)].

[292] Edoardo Vitagliano, Irene Tamborra, and Georg Raffelt. Grand Unified Neutrino Spectrum at Earth: Sources and Spectral Components. Rev. Mod. Phys., 92:45006, 2020.

[293] John N. Bahcall. Gallium solar neutrino experiments: Absorption cross-sections, neutrino spectra, and predicted event rates. Phys. Rev. C, 56:3391–3409, 1997.

[294] E. Aprile et al. Excess electronic recoil events in XENON1T. Phys. Rev. D, 102(7):072004, 2020.

[295] E. Aprile et al. Observation of two-neutrino double electron capture in ^{124}Xe with XENON1T. Nature, 568(7753):532–535, 2019.

[296] B. M. Roberts, V. V. Flambaum, and G. F. Gribakin. Ionization of atoms by slow heavy particles, including dark matter. Phys. Rev. Lett., 116(2):023201, 2016.

[297] B. M. Roberts, V. A. Dzuba, V. V. Flambaum, M. Pospelov, and Y. V. Stadnik. Dark matter scattering on electrons: Accurate calculations of atomic excitations and implications for the DAMA signal. Phys. Rev. D, 93(11):115037, 2016.

[298] B. M. Roberts and V. V. Flambaum. Electron-interacting dark matter: Implications from DAMA/LIBRA-phase2 and prospects for liquid xenon detectors and NaI detectors. Phys. Rev. D, 100(6):063017, 2019.

[299] Geneviève Bélanger, Fawzi Boudjema, Andreas Goudelis, Alexander Pukhov, and Bryan Zaldivar. micrOMEGAs5.0 : Freeze-in. Comput. Phys. Commun., 231:173–186, 2018.

[300] Simon Knapen, Tongyan Lin, and Kathryn M. Zurek. Light Dark Matter: Models and Constraints. Phys. Rev. D, 96(11):115021, 2017.

[301] M. Agostini et al. Limiting neutrino magnetic moments with Borexino Phase-II solar neutrino data. Phys. Rev. D, 96(9):091103, 2017.

[302] A. G. Beda, V. B. Brudanin, V. G. Egorov, D. V. Medvedev, V. S. Pogosov, M. V. Shirchenko, and A. S. Starostin. The results of search for the neutrino magnetic moment in GEMMA experiment. Adv. High Energy Phys., 2012:350150, 2012.

[303] D. Hanneke, S. Fogwell, and G. Gabrielse. New Measurement of the Electron Magnetic Moment and the Fine Structure Constant. Phys. Rev. Lett., 100:120801, 2008.

[304] G. F. Giudice, P. Paradisi, and M. Passera. Testing new physics with the electron g-2. JHEP, 11:113, 2012.

[305] R. Jackiw and Steven Weinberg. Weak interaction corrections to the muon magnetic moment and to muonic atom energy levels. Phys. Rev. D, 5:2396–2398, 1972.

[306] Edward Hardy and Robert Lasenby. Stellar cooling bounds on new light particles: plasma mixing effects. JHEP, 02:033, 2017.

[307] Francesco Capozzi and Georg Raffelt. Axion and neutrino bounds improved with new calibrations of the tip of the red-giant branch using geometric distance determinations. Phys. Rev. D, 102(8):083007, 2020.

[308] Justin Khoury and Amanda Weltman. Chameleon fields: Awaiting surprises for tests of gravity in space. Phys. Rev. Lett., 93:171104, 2004.

[309] Austin Joyce, Bhuvnesh Jain, Justin Khoury, and Mark Trodden. Beyond the Cosmological Standard Model. Phys. Rept., 568:1–98, 2015.

[310] William DeRocco, Peter W. Graham, and Surjeet Rajendran. Exploring the robustness of stellar cooling constraints on light particles. Phys. Rev. D, 102(7):075015, 2020.

[311] G. G. Raffelt. Stars as laboratories for fundamental physics: The astrophysics of neutrinos, axions, and other weakly interacting particles. 5 1996.

[312] Chien-Yi Chen, Jonathan Kozaczuk, and Yi-Ming Zhong. Exploring leptophilic dark matter with NA64-μ. JHEP, 10:154, 2018.

[313] Jeffrey M. Berryman, André De Gouvêa, Kevin J. Kelly, and Yue Zhang. Lepton-Number-Charged Scalars and Neutrino Beamstrahlung. Phys. Rev. D, 97(7):075030, 2018.

[314] Andreas Albert. Searches for invisible Higgs decays at the LHC. PoS, LHCP2021:076, 2021.

[315] Shashank Shalgar, Irene Tamborra, and Mauricio Bustamante. Core-collapse supernovae stymie secret neutrino interactions. Phys. Rev. D, 103(12):123008, 2021.

[316] Edward W. Kolb and Michael S. Turner. Supernova SN 1987a and the Secret Interactions of Neutrinos. Phys. Rev. D, 36:2895, 1987.

[317] Richard H. Cyburt, Brian D. Fields, Keith A. Olive, and Tsung-Han Yeh. Big Bang Nucleosynthesis: 2015. Rev. Mod. Phys., 88:015004, 2016.

[318] Maria Archidiacono and Steen Hannestad. Updated constraints on non-standard neutrino interactions from Planck. JCAP, 07:046, 2014.

[319] Hannah Banks and Matthew Mccullough. Charting the Fifth Force Landscape. Phys. Rev. D, 103(7):075018, 2021.

[320] Marcela Carena, Zhen Liu, and Yikun Wang. Electroweak phase transition with spontaneous Z_2-breaking. JHEP, 08:107, 2020.

[321] Mariano Quiros. Finite temperature field theory and phase transitions. In ICTP Summer School in High-Energy Physics and Cosmology, pages 187–259, 1 1999.

[322] Rebecca K. Leane et al. Snowmass2021 Cosmic Frontier White Paper: Puzzling Excesses in Dark Matter Searches and How to Resolve Them. In 2022 Snowmass Summer Study, 3 2022.

[323] P. Ko, Chih-Ting Lu, and Ui Min. Crossing two-component dark matter models and implications for 511 keV γ-ray and XENON1T excesses. 2 2022.

[324] Shao-Feng Ge, Pedro Pasquini, and Jie Sheng. Solar Active-Sterile Neutrino Conversion with Atomic Effects at Dark Matter Direct Detection Experiments. 12 2021.

[325] Orlando Luongo, Nicola Marcantognini, and Marco Muccino. Unifying baryogenesis with dark matter production. 12 2021.

[326] C. D. Froggatt and H. B. Nielsen. Atomic Size Pearls being Dark Matter giving Electron Signal. In 24th Workshop on What Comes Beyond the Standard Models?, 3 2022.

[327] Viacheslav Khruschov and Sergey Fomichev. Oscillations of Active Neutrinos at Short Baseline in the Model with Three Decaying Sterile Neutrinos. Universe, 8(2):97, 2022.

[328] E. Aprile et al. Projected WIMP sensitivity of the XENONnT dark matter experiment. JCAP, 11:031, 2020.

[329] D. S. Akerib et al. Projected sensitivities of the LUX-ZEPLIN experiment to new physics via low-energy electron recoils. Phys. Rev. D, 104(9):092009, 2021.

[330] C. D. Froggatt and Holger Bech Nielsen. Hierarchy of Quark Masses, Cabibbo Angles and CP Violation. Nucl. Phys. B, 147:277–298, 1979.

[331] Rabindra N. Mohapatra. Gauge Model for Chiral Symmetry Breaking and Muon electron Mass Ratio. Phys. Rev. D, 9:3461, 1974.

[332] B. S. Balakrishna, A. L. Kagan, and R. N. Mohapatra. Quark Mixings and Mass Hierarchy From Radiative Corrections. Phys. Lett. B, 205:345–352, 1988.

[333] Francesca Borzumati, Glennys R. Farrar, Nir Polonsky, and Scott D. Thomas. Soft Yukawa couplings in supersymmetric theories. Nucl. Phys. B, 555:53–115, 1999.

[334] Nima Arkani-Hamed, Hsin-Chia Cheng, and L. J. Hall. A Supersymmetric theory of flavor with radiative fermion masses. Phys. Rev. D, 54:2242–2260, 1996.

[335] Christopher T. Hill, Pedro A. N. Machado, Anders E. Thomsen, and Jessica Turner. Scalar Democracy. Phys. Rev. D, 100(1):015015, 2019.

[336] P.A. Zyla et al. Review of Particle Physics. PTEP, 2020(8):083C01, 2020. and 2021 update.

[337] Yuval Grossman. Introduction to flavor physics. In 2009 European School of High-Energy Physics, pages 111–144, 2010.

[338] R. D. Peccei. Discrete and global symmetries in particle physics. Lect. Notes Phys., 521:1–50, 1999.

[339] Ivan Esteban, M. C. Gonzalez-Garcia, Michele Maltoni, Thomas Schwetz, and Albert Zhou. The fate of hints: updated global analysis of three-flavor neutrino oscillations. JHEP, 09:178, 2020.

[340] C. Giganti, S. Lavignac, and M. Zito. Neutrino oscillations: The rise of the PMNS paradigm. Progress in Particle and Nuclear Physics, 98:1–54, jan 2018.

[341] Michael J. Baker, José Bordes, Hong-Mo Chan, and Sheung Tsun Tsou. On the Corner Elements of the CKM and PMNS Matrices. EPL, 102(4):41001, 2013.

[342] Enrique Fernandez-Martinez. PMNS matrix elements without assuming unitarity. Nucl. Phys. B Proc. Suppl., 168:366–368, 2007.

[343] Stefan Floerchinger and Jan-Markus Schwindt. Neutrino flavor-mass uncertainty relations and an entanglement-assisted determination of the PMNS matrix. Phys. Rev. D, 102(9):093001, 2020.

[344] U. J. Saldana-Salazar and K. M. Tame-Narvaez. The mass ratios parametrization. Int. J. Mod. Phys. A, 34(01):1950007, 2019.

[345] Christopher T. Sachrajda. Flavor physics. In The 1997 European School of High-Energy Physics, pages 150–189, 1 1998.

[346] J. F. Kamenik. Flavour Physics and CP Violation. In 2014 European School of High-Energy Physics, pages 79–94, 2016.

[347] Yosef Nir. Flavor physics and new physics. In 9th Baikal Summer School on Physics of Elementary Particles and Astrophysics, 2009.

[348] Gilad Perez. Brief Introduction to Flavor Physics. 11 2009.

[349] Ferruccio Feruglio. Flavour Physics 1. PoS, CORFU2014:016, 2015.

[350] Monika Blanke. Flavour Physics from Present to Future Colliders. In Strong dynamics for physics within and beyond the Standard Model at LHC ..., pages 116–123, 2019.

[351] Matthias Neubert. Renormalization Theory and Effective Field Theories. 1 2019.

[352] Steven Weinberg. Baryon and Lepton Nonconserving Processes. Phys. Rev. Lett., 43:1566–1570, 1979.

[353] W. Buchmuller and D. Wyler. Effective Lagrangian Analysis of New Interactions and Flavor Conservation. Nucl. Phys. B, 268:621–653, 1986.

[354] John Ellis. SMEFT Constraints on New Physics beyond the Standard Model. In Beyond Standard Model: From Theory to Experiment, 5 2021.

[355] Brian Henning, Xiaochuan Lu, Tom Melia, and Hitoshi Murayama. 2, 84, 30, 993, 560, 15456, 11962, 261485, ...: Higher dimension operators in the SM EFT. JHEP, 08:016, 2017. [Erratum: JHEP 09, 019 (2019)].

[356] Coenraad B. Marinissen, Rudi Rahn, and Wouter J. Waalewijn. ..., 83106786, 114382724, 1509048322, 2343463290, 27410087742, ... efficient Hilbert series for effective theories. Phys. Lett. B, 808:135632, 2020.

[357] Daniel Abercrombie et al. Dark Matter benchmark models for early LHC Run-2 Searches: Report of the ATLAS/CMS Dark Matter Forum. Phys. Dark Univ., 27:100371, 2020.

[358] R. C. Cotta, J. L. Hewett, M. P. Le, and T. G. Rizzo. Bounds on Dark Matter Interactions with Electroweak Gauge Bosons. Phys. Rev. D, 88:116009, 2013.

[359] Andreas Crivellin, Ulrich Haisch, and Anthony Hibbs. LHC constraints on gauge boson couplings to dark matter. Phys. Rev. D, 91:074028, 2015.

[360] Linda M. Carpenter, Andrew Nelson, Chase Shimmin, Tim M. P. Tait, and Daniel Whiteson. Collider searches for dark matter in events with a Z boson and missing energy. Phys. Rev. D, 87(7):074005, 2013.

[361] Yang Bai, Patrick J. Fox, and Roni Harnik. The Tevatron at the Frontier of Dark Matter Direct Detection. JHEP, 12:048, 2010.

[362] Jessica Goodman, Masahiro Ibe, Arvind Rajaraman, William Shepherd, Tim M. P. Tait, and Hai-Bo Yu. Constraints on Light Majorana dark Matter from Colliders. Phys. Lett. B, 695:185–188, 2011.

[363] William Shepherd, Tim M. P. Tait, and Gabrijela Zaharijas. Bound states of weakly interacting dark matter. Phys. Rev. D, 79:055022, 2009.

[364] Maria Beltran, Dan Hooper, Edward W. Kolb, and Zosia C. Krusberg. Deducing the nature of dark matter from direct and indirect detection experiments in the absence of collider signatures of new physics. Phys. Rev. D, 80:043509, 2009.

[365] Maria Beltran, Dan Hooper, Edward W. Kolb, Zosia A. C. Krusberg, and Tim M. P. Tait. Maverick dark matter at colliders. JHEP, 09:037, 2010.

[366] Qing-Hong Cao, Chuan-Ren Chen, Chong Sheng Li, and Hao Zhang. Effective Dark Matter Model: Relic density, CDMS II, Fermi LAT and LHC. JHEP, 08:018, 2011.

[367] Jessica Goodman, Masahiro Ibe, Arvind Rajaraman, William Shepherd, Tim M. P. Tait, and Hai-Bo Yu. Constraints on Dark Matter from Colliders. Phys. Rev. D, 82:116010, 2010.

[368] Nicole F. Bell, Yi Cai, James B. Dent, Rebecca K. Leane, and Thomas J. Weiler. Dark matter at the LHC: Effective field theories and gauge invariance. Phys. Rev. D, 92(5):053008, 2015.

[369] Martin Bauer, Anja Butter, Nishita Desai, Juan Gonzalez-Fraile, and Tilman Plehn. Validity of dark matter effective theory. Phys. Rev. D, 95(7):075036, 2017.

[370] Davide Racco, Andrea Wulzer, and Fabio Zwirner. Robust collider limits on heavy-mediator Dark Matter. JHEP, 05:009, 2015.

[371] Giorgio Busoni, Andrea De Simone, Thomas Jacques, Enrico Morgante, and Antonio Riotto. On the Validity of the Effective Field Theory for Dark Matter Searches at the LHC Part III: Analysis for the *t*-channel. JCAP, 09:022, 2014.

[372] Giorgio Busoni, Andrea De Simone, Johanna Gramling, Enrico Morgante, and Antonio Riotto. On the Validity of the Effective Field Theory for Dark Matter Searches at the LHC, Part II: Complete Analysis for the *s*-channel. JCAP, 06:060, 2014.

[373] O. Buchmueller, Matthew J. Dolan, and Christopher McCabe. Beyond Effective Field Theory for Dark Matter Searches at the LHC. JHEP, 01:025, 2014.

[374] Ian M. Shoemaker and Luca Vecchi. Unitarity and Monojet Bounds on Models for DAMA, CoGeNT, and CRESST-II. Phys. Rev. D, 86:015023, 2012.

[375] Patrick J. Fox, Roni Harnik, Joachim Kopp, and Yuhsin Tsai. LEP Shines Light on Dark Matter. Phys. Rev. D, 84:014028, 2011.

[376] Fady Bishara, Joachim Brod, Benjamin Grinstein, and Jure Zupan. Renormalization Group Effects in Dark Matter Interactions. JHEP, 03:089, 2020.

[377] Fady Bishara, Joachim Brod, Benjamin Grinstein, and Jure Zupan. From quarks to nucleons in dark matter direct detection. JHEP, 11:059, 2017.

[378] Nikhil Anand, A. Liam Fitzpatrick, and W. C. Haxton. Weakly interacting massive particle-nucleus elastic scattering response. Phys. Rev. C, 89(6):065501, 2014.

[379] Richard J. Hill and Mikhail P. Solon. Standard Model anatomy of WIMP dark matter direct detection II: QCD analysis and hadronic matrix elements. Phys. Rev. D, 91:043505, 2015.

[380] James B. Dent, Lawrence M. Krauss, Jayden L. Newstead, and Subir Sabharwal. General analysis of direct dark matter detection: From microphysics to observational signatures. Phys. Rev. D, 92(6):063515, 2015.

[381] A. Liam Fitzpatrick, Wick Haxton, Emanuel Katz, Nicholas Lubbers, and Yiming Xu. Model Independent Direct Detection Analyses. 11 2012.

[382] A. Liam Fitzpatrick, Wick Haxton, Emanuel Katz, Nicholas Lubbers, and Yiming Xu. The Effective Field Theory of Dark Matter Direct Detection. JCAP, 02:004, 2013.

[383] Christian W. Bauer, Sean Fleming, Dan Pirjol, and Iain W. Stewart. An effective field theory for collinear and soft gluons: Heavy to light decays. Phys. Rev. D, 63:114020, May 2001.

[384] M. Beneke, A. P. Chapovsky, M. Diehl, and T. Feldmann. Soft collinear effective theory and heavy to light currents beyond leading power. Nucl. Phys. B, 643:431–476, 2002.

[385] Junegone Chay, Chul Kim, and Adam K. Leibovich. Quark mass effects in the soft-collinear effective theory and anti-B —> X(s gamma) in the endpoint region. Phys. Rev. D, 72:014010, 2005.

[386] Y. L. Wu, Y. A. Yan, M. Zhong, Y. B. Zuo, and W. Y. Wang. HQEFT as a large component QCD and comments on the incompleteness of HQET. Mod. Phys. Lett. A, 18:1303–1316, 2003.

[387] F. Berto and M. A. Sanchis-Lozano. Extended HQEFT Lagrangian and currents. Nucl. Phys. B Proc. Suppl., 93:212–215, 2001.

[388] Glen Cowan, Kyle Cranmer, Eilam Gross, and Ofer Vitells. Asymptotic formulae for likelihood-based tests of new physics. Eur. Phys. J. C, 71:1554, 2011. [Erratum: Eur.Phys.J.C 73, 2501 (2013)].

[389] Hans Dembinski and Piti Ongmongkolkul et al. scikit-hep/iminuit. Dec 2020.